Endoplasmic Reticulum Resident Chaperones and their Implications in Health and Disease

STEVEN JAMES BELL

Endoplasmic Reticulum Resident Chaperones and their Implications in Health and Disease

Steven James Bell

2022

A thesis submitted for the degree of Doctor of Philosophy

Department of Biosciences
Durham University

Abstract

The endoplasmic reticulum (ER) is a key organelle in the eukaryotic cell and is responsible for protein folding and quality control, mediated by protein chaperones. It is also home to the oxidoreductase system which is required for disulphide bond formation and is the main theme of this thesis. Two of the vital proteins in the ER-localised oxidoreductase system are protein disulphide isomerase (PDI) and endoplasmic reticulum oxidoreductase 1 α (Ero1α). These proteins work alongside other specialist PDI family members such as anterior gradient 2 (AGR2). This thesis examines the role of both PDI and AGR2 in protein quality control, together with important clients such as collagen, a major component of the extracellular matrix (ECM) and a secreted product of fibroblast cells present in the skin. The role of AGR2 in oesophageal cancer was explored, with data dependant acquisition (DDA) mass spectrometry (MS) used to identify novel interacting partners of AGR2. AGR2 was found to be over expressed in certain oesophageal cell lines and key interacting partners such as MUC5AC and SQSTM1 were identified. Research was undertaken in this thesis to compare the effectiveness and application of the reducing agent dithiobutylamine (DTBA) to biological systems and how this reducing agent affects the cellular proteome and the redox state of PDI. Live cell imaging was used to see how the structure of the ER was affected by reductive stress. Data independent acquisition (DIA) MS was used to identify new molecular players in the cellular response to reductive stress, in the response to PDI inhibitors, in the response to growth factors (PDGF) and in the response to skin bioactives (e.g. niacinamide). Taken together, these analyses lay the foundations for understanding new mechanistic control points in the quality control of protein secretion and homeostasis

Table of Contents

Table of figures

Table of tables

Table of abbreviations

- ADP – Adenosine diphosphate
- AGR – Anterior gradient
- AGR2 – Anterior gradient 2
- ALDH – Aldehyde dehydrogenase
- ANOVA – Analysis of variance
- ANXA2- Annexin 2
- APS – Ammonium persulphate
- AREG – Amphiregulin
- ATF6 – Activating transcription factor 6
- ATP – Adenosine triphosphate
- BiP – Binding immunoglobulin protein
- BSA – Bovine serum albumin
- CC – Cole Carpenters syndrome
- Cdk1 – Cyclin dependent kinase 1
- CEPT – Diacylglycerol choline ethanolamine phosphotransferase
- CHOP – C/EBP homologous protein
- CNX – Calnexin
- Col – Collagen
- COPD – Chronic obstructive pulmonary disease
- COPII – Coat protein complex II
- CRT – Calreticulin
- DDA – Data dependant acquisition
- DGPCho – Phosphatidylcholine
- DIA – Data independent acquisition
- DMEM – Dulbecco's Modified Eagle Medium
- DNA – Deoxyribonucleic acid
- DTBA – Dithiobutylamine
- DTE – Dithioerythritol
- DTT – Dithiothreitol
- ECL – Enhanced chemiluminescence
- ECM – Extracellular matrix
- eIF2α – Eukaryotic translation initiation factor 2α
- EMT – Epithelial to mesenchymal transition
- ER – Endoplasmic reticulum
- ERAD – ER associated degradation
- ERGIC – ER-Golgi compartment
- Ero1α – Endoplasmic reticulum oxidoreductase 1 α
- ERP – Endoplasmic reticulum resident protein
- ESI – Electrospray ionisation
- FAD – Flavin adenine dinucleotide
- FASP – Filter aided sample preparation
- FBS – Foetal bovine serum
- FDR – False discovery rate

- FLOT1 – Flotillin 1
- FT-MS – Fourier transform ion cyclotron
- GADD34 – Growth arrest DNA damage-inducible 34
- GAGs – Glycosaminoglycans
- GAMPO – Goat anti-rabbit peroxidase
- GERD – Gastro oesophageal reflux disease
- GET – Guided entry of tail-anchored proteins
- GI – Gastrointestinal
- GO – Gene ontology
- GPX1 – Glutathione peroxidase 1
- GRP – Glucose regulated protein
- GSH – Glutathione
- GSSG – Glutathione disulphide
- GTP – Guanosine triphosphate
- H&E – Haematoxylin and Eosin
- H_2O_2 – Hydrogen peroxide
- HIF – Hypoxia inducible factor
- Hsp – Heat shock protein
- INM – Inner nuclear membrane
- IP – Immunoprecipitation
- IRE1 – Inositol requiring enzyme 1
- LB – Lysogeny Broth
- LC – Liquid chromatography
- LC-MS/MS – Liquid chromatography tandem mass spectrometry
- LDL-R – Low density lipoprotein receptor
- m/z – Mass to charge ratio
- *m/z* – Mass to charge ratio
- mAb – Monoclonal antibody
- MALDI – Matrix-assisted laser desorption/ionisation
- MEM – Modified Eagle Medium
- MMP – Matrix metalloproteinase
- mNG – mNeonGreen
- MS – Mass spectrometry
- MUC – Mucin
- NAD^+ - Nicotinamide adenine dinucleotide
- NADPH – Nicotinamide adenine dinucleotide phosphate
- NAPRT – Nicotintinate phosphoribosyltransferase
- NE – Nuclear envelope
- NEFs – Nucleotide exchange factors
- NEM – N-ethylmaleimide
- NMR – Nuclear magnetic resonance
- NR – Non-reducing
- OES – Oesophageal
- ONM – Outer nuclear membrane
- P- – Phosphorylated

- P&G – Proctor and Gamble
- P4H – Prolyl 4-hydroxylase
- pAb – Polyclonal antibody
- PAGE – Polyacrylamide gel electrophoresis
- PARP – Poly-ADP-ribose polymerase
- PBS – Phospho-buffered saline
- PDCD4 – Programmed cell death 4
- PDGF – Platelet derived growth factor
- PDGFR – Platelet derived growth factor receptor
- PDI – Protein disulphide isomerase
- PERK – Protein kinase (PKR)-like ER kinase
- PFA – Paraformaldehyde
- PKR – Protein tyrosine kinase receptor
- PPIs – Proton pump inhibitors
- PrxIV – Peroxiredoxin 4
- PTM – Post translational modification
- PVDF – Polyvinylidene difluoride
- QTOF – Quadrupole time-of-flight
- R – Reducing
- RNA – Ribonucleic acid
- ROS – Reactive oxygen species
- S1P – Site 1 protease
- S2P – Site 2 protease
- SARPO – Swine anti-rabbit peroxidase
- SDS – Sodium dodecyl sulphate
- SERCA – Sarco/ER calcium ATPase
- SFM – Serum free medium
- SND – SRP independent targeting
- SOD – Super oxide dismutase
- SORT1 – Sortilin 1
- SQSTM1 - Sequestosome 1
- SRP – Signal recognition particle
- SWATH – Sequential window acquisition of all theoretical fragment ion spectra
- TBS – Tris-buffered saline
- TBS-T – Tris buffered saline with tween
- TEMED – N,N,N’,N’-Tetramethylethylenediamine
- TGF-β – Transforming growth factor β
- TMED2 – Transmembrane P24 trafficking protein 2
- TOF – Time of flight
- TRC40 – Transmembrane recognition complex of 40 kDa
- Tx100 – Triton X-100
- UGGT – UDP-glucose glycoprotein-glucosyltransferase
- UPR – Unfolded protein response
- UV – Ultraviolet
- WB – Western blot

- WT – Wild type
- XBP1 – X-box binding protein 1
- YAP1 – Yes-associated protein 1
- β-ME – β-mercaptoethanol

Acknowledgements

Firstly, I would like to thank my supervisor Adam Benham for the opportunity to undertake this PhD and for all the guidance and support he has offered myself over the past 4/5 years even when times were tough during the COVID pandemic. I thank Adrian Brown in the proteomic facility for his work to support this thesis, the SWATH-MS data would not be possible without his help. Thank you to my thesis committee for their help during my PhD. Thank you to my funding body BBSRC and my industrial partner P&G, without them the PhD would not have been possible.

Secondly, I would like to thank all the members of lab 8 for all the help and friendship that has been offered over the years. Thank you especially to Naomi whose help with the proteomics and R coding saved me many painful hours of manual data analysis. Also thank you to Max who I have known for many years and has always been happy to answer any questions I have asked him.

Thank you to my family for their support during my PhD especially my mum and sister for their unwavering love, support, and encouragement throughout this time. I wouldn't be where I am today without you.

Finally, thank you to my girlfriend Hetty for the words of love, support, and for having faith in me during my write up.

1 Introduction

1.1 Endoplasmic reticulum

Biochemistry involves studying molecules that are required for the process of life. These can be macromolecules such as nucleic acids and proteins. Metabolites are also studied such as glucose and glycerol, these metabolites are transformed in various biological processes. Living organisms contain deoxyribonucleic acid (DNA) which stores the genetic information that codes for protein synthesis. Proteins are macromolecules made up of 20 amino acids which are crucial in many biological processes. Living things on Earth are thought to have a common ancestor due to similarities in biological processes between certain biochemical processes. The three groups are named Eukarya (eukaryotes), Bacteria and Archaea. Eukaryotes, including multicellular organisms such as yeast and humans, they contain a nucleus inside their cell. Prokaryotes refers to organisms like bacteria which lack a nucleus inside the cell (Berg, Tymoczko, Gatto, *et al.* 2019). This thesis will focus on Eukaryotes and how their proteins are processed and folded.

The endoplasmic reticulum (ER) is the largest organelle present in the mammalian cell. It is a perinuclear organelle which is dynamic and has many functions in the cell, these include protein synthesis, protein folding, protein transport, lipid metabolism and calcium storage. The structure of the ER is a single continuous membrane which forms a large network containing domains with varying structures and functions. Two major domains make up the ER, they are named the nuclear envelope (NE) and the peripheral ER. The NE is present at the centre of the cell and is comprised of two flat ER membrane bilayers, these two bilayers are stacked and make up the inner nuclear membrane (INM) and outer nuclear membrane (ONM). The shape of the NE is maintained with various forces such as, INM proteins binding to lamin and chromatin, proteins that link the INM and ONM, nuclear pores and the

cytoskeleton. The peripheral ER expands from the ONM at the NE and reaches into the cytosol, forming dynamic tubules and cisternal sheets. Different cell types exhibit different ER shapes. Those cell types which are predisposed to more protein secretion, such as pancreatic cells, have more cisternal sheets. Whereas muscle cells which require more calcium modulation have more dynamic tubules (Westrate, Lee, Prinz, *et al.* 2015). Historically, the ER has been subdivided into the rough ER and the smooth ER. The rough ER is so named because it consists of flattened cisternae which has many ribosomes on the cytoplasmic surface of the ER. It assists in the secretion and folding of secretory and membrane proteins. The smooth ER is made up of tubules and does not contain any surface features. The smooth ER is involved in the synthesis of various steroids, phospholipids, lipids, and it is the storage site for calcium within cells. The smooth ERs functions tend to be more prominent in cells where an enhanced smooth ER is needed (Breen & Draper 2008).

The ER contains a high concentration of calcium inside its lumen (between 100-800 μM). Calcium constantly leaks out of the ER into the surrounding cytoplasm. The higher calcium concentration inside of ER is maintained by the active transport of the sarco/ER calcium ATPase (SERCA) (Moore, Chen, Knapp, *et al.* 1975). The high level of calcium in the ER is necessary as chaperones in the ER depend on calcium for protein folding and maturation. Some of the chaperones which bind the calcium in the ER are BiP, calreticulin and GRP94 who are thought to bind the calcium at doublets and triplets of acidic amino acids as these chaperones do not possess an acidic C-terminus (Meldolesi & Pozzan 1998). Most lipid synthesis in the ER occurs in the endomembrane compartment, which includes the ER and Golgi apparatus. The ER is the main site for the synthesis of sterols and phospholipids which make up the cellular membrane. An example of lipid synthesis in the ER is of phosphatidylcholine (DGPCho), which is the most abundant glycerophospholipid present in

mammalian cells. It is formed in the Kennedy pathway which involves diacylglycerol choline ethanolamine phosphotransferase (CEPT) to take diacylglycerol and incorporate it into DGPCho (Fagone & Jackowski 2009).

Protein folding starts when mRNA is translated by ribosomes into a polypeptide chain. This chain must then be correctly folded within the ER before it is able to perform its function within the cell or be excreted. For proteins to perform their functions they must first fold into a distinct 3D arrangement and this arrangement must be held whilst the protein undergoes its functions within or outside the cell. There are two key views which are applied to the protein folding problem. The first is Levinthal's paradox, which states that a polypeptide chain has a large number of possible conformations so if a protein was to achieve its correctly folded configuration by testing all possibly conformations, then it would require an extremely long time to find the correct conformation. This does not occur, therefore he suggested that there are other stable amino acids which help form nucleation points (Rooman, Dehouck, Kwasigroch, *et al.* 2012). The second view is Anfinsen's dogma which was developed in 1973 and states that the amino acid sequence determines the native state of the protein, and it will fold into the most thermodynamically stable conformation based on the solvents that surround it (Anfinsen 1973). A large body of evidence suggests that hydrophobic interactions play a major part in protein folding and folding initiation sites arise from hydrophobic interactions (Dyson, Wright & Scheraga 2006). The hydrophobic residues of amino acids are in the core of the protein where they are protected by the hydrophilic residues on the outside of the protein. There are other interactions which help stabilise a proteins native structure, they include hydrogen bonds, van der Waals forces, disulphide bridges and ionic interactions (Dill, Ozkan, Shell, *et al.* 2008). Chaperones are also present in the ER to assist in protein

folding as proteins fold the chaperones to protect the exposed hydrophobic sites, and this prevents protein aggregation from occurring (Kim, Hipp, Bracher, *et al.* 2013).

1.1.1 Protein folding in the ER

Redox stands for reduction-oxidation and it is a chemical reaction which involves the change in an oxidation state of a substrate. Both reduction and oxidation must happen in a redox reaction, and redox reactions also occur in other biological pathways, including photosynthesis and respiration. Redox balance in the ER is also very important in protein folding as it is required for the formation of disulphide bonds. Proteins that are destined to be secreted tend to have more disulphide bonds than those which remain in the cytosol. The chaperones present in the cytosol have differing functions that may not detect misfolded proteins as efficiently as those in the ER. Therefore, it is important that the secreted proteins are folded and checked correctly before they leave the ER as there is little capacity for proteins to be repaired after secretion (Dobson 2003). The ER is specialised to allow for the formation and rearrangement of disulphides and this redox balance in the ER lumen allows for oxidation and reduction of disulphides (Ellgaard 2004).

Many proteins are co-translationally targeted to the ER via signal sequences. These sequences are usually found on the first 25 amino acids of the protein (Petersen, Brunak, von Heijne, *et al.* 2011). The signal sequence is composed of an N-domain (amino-terminal basic domain), a H-domain (middle hydrophobic domain) and a C-domain (polar domain which contains the cleavage site) (Hegde & Bernstein 2006). This sequence is recognised by the signal recognition particle (SRP). The SRP is formed of six polypeptides (P19, P54, P9/P14 and P68/P72) and a 7S SRP ribonucleic acid (RNA) (Saraogi & Shan 2011). The SRP binds to the signal sequence which emerges from the ribosome, and this will slow chain elongation (Walter & Blobel 1982). Lakkaraju et al., showed that the delay in peptide elongation is

necessary to prevent translation of secretory proteins to the wrong cellular compartment. When this delay was removed, they observed inefficient protein targeting of the preproteins, which lead to defects in secretion of proteins and reduced cell growth (Lakkaraju, Mary, Scherrer, *et al.* 2008).

The translation of the nascent peptide does not continue until SRP binds to the SRP receptor which is present on the ER membrane. The SRP receptor is held into place on the ER membrane by its β subunit and the α subunit interacts with P54 on the SRP (Saraogi & Shan 2011). Guanosine triphosphate (GTP) hydrolysis then removes the SRP to recruit other nascent polypeptides for protein folding. When SRP binds to the SRP receptor the 60S subunit of the ribosome is positioned so it is above the translocon of the ER. The translocon translocates the native polypeptide structure into the ER lumen. The translocon is comprised of three subunits Sec61α, β, and γ and it is gated by binding immunoglobulin protein (BiP/grp78) which keeps the ER barrier function (Alder, Shen, Brodsky, *et al.* 2005). The signal peptide is removed from the newly synthesised protein by signal peptidase, this occurs as the protein enters the ER lumen (Jackson & Blobel 1977). There are other pathways that can also target proteins to the ER, including the guided entry of tail-anchored proteins (GET) pathway in yeast, (transmembrane recognition complex of 40 kDa in mammals (TRC40)) and the SRP independent targeting pathway (SND). The TRC40 is used to deliver tail anchored (TA) proteins to the ER. Around 5% of membrane proteins have a tag on their C-terminus the called the tail anchor and they are key to cellular processes such as membrane fusion and vesicle trafficking (Hegde & Keenan 2011). TRC40 binds to these TA proteins post-translationally and delivers them to the ER as soon as they are released from the ribosome (Favaloro, Spasic, Schwappach, *et al.* 2008). The substrate is loaded onto TCR40 by SGTA and the heterotrimeric BAG6 complex. After TRC40 has had the substrate loaded it is then inserted into the ER by the

heterodimeric ER membrane receptor complex WRB-CAML (Casson, McKenna, Haßdenteufel, *et al.* 2017). Loss of the WRB subunit has been shown to affect the delivery of TA proteins to the ER only slightly. This suggests that *in vivo* other mechanisms may exists which target TA to the ER (Rivera-Monroy, Musiol, Unthan-Fechner, *et al.* 2016). Studies in yeast have revealed a third conserved pathway which targets proteins to the ER which is the SND pathway. This pathway is composed of three components, SND1 which is associated with the ribosome, SND2 and SND3 which both form a complex with Sec61, and this allows for the insertion of the substrate into the ER. This pathway can recruit membrane proteins to the ER that do not depend on SRP or TCR40 pathways of ER delivery (Aviram, Ast, Costa, *et al.* 2016). In conventional ER protein targeting, folding occurs cotranslationally/translocationally as soon as the peptide chain enters the ER lumen. The two-domain polypeptide domains begin to fold by sequential and co-translational folding (Netzer & Hartl 1997). Most proteins are also modified by N-linked glycans where these glycans improve kinetics and the thermodynamics of folding (Hanson, Culyba, Hsu, *et al.* 2009). Disulphide bonds also begin to form; this and other folding is assisted by the recruitment of chaperones. They prevent misfolding and aggregation of the nascent proteins being made. Classic chaperones such as those from the heat shock protein 70 (Hsp70) and Hsp90 family assist in general protein folding (both in the ER and cytoplasm) whereas more specialised lectin chaperones (calnexin and calreticulin) assist with the N-linked glycans.

1.1.2 Classic chaperones in the ER

The classic chaperones are one of the major families of chaperones located in the ER. They are generally found in all cellular locations, and they work by binding directly to the polypeptide chain. Both the Hsp70 and Hsp90 families of chaperones are present in the ER exemplified by BiP/GRP78 and GRP94. Chaperones tend to identify and then bind to proteins

which are immature, aberrant, or predisposed to aggregating. They identify these proteins as the proteins usually contain an exposed hydrophobic segment which is usually buried in the core of the protein. Their binding is regulated by various cofactors and adenine-nucleotide binding. They have a diverse range of functions in the ER.

The Hsp70 family of chaperones all contain three key domains, a 44 kDa N-terminal ATPase domain, a 15 kDa substrate binding domain, and a 10 kDa C-terminal lid (Sousa & Lafer 2006). Hsp70 functions by first binding to the substrate and then energy from adenosine triphosphate (ATP) hydrolysis further influences substrate binding (Jeung-Hoi & McKay 1994). When ATP is bound, the lid remains open, and the substrates have a low affinity for the peptide binding domain and this causes a high on/off rate to occur. When a substrate binds to Hsp70, it stimulates ATP hydrolysis and the lid clamps down on the substrate (Jordan & McMacken 1995). When adenosine diphosphate (ADP) is bound to Hsp70 there is a high affinity of the interaction between the substrate and peptide binding domain and the on/off rate is low (Russell, Karzai, Mehl, *et al.* 1999). When ADP is eventually released Hsp70 then rebinds ATP, the lid opens and the peptide is released (Mayer, Schröder, Rüdiger, *et al.* 2000). Other co-factors as well as peptides stimulate the ATPase cycle, they are Hsp40s and nucleotide exchange factors (NEFs) (Cheetham & Caplan 1998). The Hsp40s help stimulate ATP hydrolysis whereas, the NEFs help in the release of ADP (Alberti, Esser & Höhfeld 2003). One of the major Hsp70 chaperones is BiP (GRP78), it has a wide range of functions in the ER such as acting as a rachet to facilitate translocation of nascent chains in the ER lumen and preventing them from going back into the cytosol (Matlack, Misselwitz, Plath, *et al.* 1999). It assists in protein folding and oligomerisation (Haas & Wabl 1983), prevents non-native protein aggregation (Puig & Gilbert 1994), it is involved in calcium homeostatsis in the ER (Lièvremont, Rizzuto, Hendershot, *et al.* 1997), and it can also target terminally misfolded

proteins for ER associated degradation (ERAD) BiP is also involved in regulating the UPR through IRE1 (Cabral, Liu, Moremen, *et al.* 2002).

The Hsp90 family of chaperones also uses ATP binding and ATP hydrolysis to facilitate in the binding and release of substrates. Hsp90 contains a 25 kDa N-terminal ATP binding domain, a middle domain and a 12 kDa C-terminal domain. The Hsp90 chaperones target specific proteins that are near the end of their folding process. They tend to hold proteins or interact with them in a conformation which allows for the client protein to interact with other proteins (Zhao & Houry 2011). An example of an ER resident Hsp90 is glucose-regulated protein 94 (GRP94) which resides in the lumen of the ER. Although GRP94 itself is not an oxidoreductase all of its client proteins such as major histocompatibility complex (MHC) class II, insulin like growth factor and toll like receptors contain disulphide bonds (Marzec, Eletto & Argon 2012). Hsp90 has also been shown to be involved in evolution by selecting for traits in certain organisms. Rohner et al., found that the cavefish *Astyanax mexicanus* has standing eye variation in surface populations which is phenotypically masked by Hsp90. A reduced-eye phenotype can be obtained by inhibition of Hsp90. If the surface-dwelling fish are grown in conditions similar to those found in caves the phenotypic variation is unmasked, this also occurs with Hsp90 inhibition. This work was the first to show evidence of Hsp90 affecting morphological evolution in the wild (Rohner, Jarosz, Kowalko, *et al.* 2013). Hsp90 is also found to be involved in cancer progression. In breast cancer the overexpression of Hsp90 has been shown to lead to poorer prognosis. The overexpression of Hsps in cancer is most likely due to the fact they are cytoprotective to the stresses that occur in a tumour microenvironment such as hypoxia, acidosis, and lack of nutrients. One of the main targets of Hsp90 during cancer is the SRC tyrosine kinase. This kinase can become oncogenic due to mutations such as truncation of the C-terminus of the kinase (Fabio Falsone, Leptihn, Osterauer, *et al.* 2004).

The C-terminus contains the regulatory domain of SRC tyrosine kinase which interacts with the SH2 domain on the protein and causes repression of the kinase activity. The loss of the regulatory domain causes SRC tyrosine kinase to be constituently active but it is not conformationally stable. This unstable form of the SRC tyrosine kinase receptor displays a close physical association with Hsp90 unlike its normal form which usually requires reduced interaction with Hsp90 for its maturation and function (Whitesell & Lindquist 2005). Eccles et al., developed NVP-AUY922, which is a Hsp90 inhibitor, and found that the drug inhibited growth in tumour xenografts - for example the growth of the breast tumour BT474 was reduced by 21% when compared to the control. This inhibitor was thought to inhibit cytostasis, apoptosis, invasion and angiogenesis which inhibited tumour growth and metastasis (Eccles, Massey, Raynaud, *et al.* 2008).

1.1.3 Lectin chaperones

Lectin chaperones such as calnexin (CNX, membrane bound) and calreticulin (CRT, soluble) bind to glycoproteins which contain a monoglucosylated carbohydrate. As the new protein enters the ER lumen they are usually modified by N-linked glycans, especially if they are to become a secretory protein. The glucose from the N-linked glycans is removed by glucosidases I and II (Parodi 2003). The protein now has a monoglucosylated N-linked glycan and is recognised by CRT and CNX which then go on to fold and release the protein if it is correctly folded. If the N-glycosylated protein cannot be folded UDP-glucose glycoprotein-glucosyltransferase (UGGT) another ER resident protein is recruited to catalyse the transfer of glucose from UDP-glucose to a mannose residue on the N-glycan chain (Sousa, Ferrero-Garcia & Parodi 1992). This reglucosylation will generate a new N-linked glycan which

provides a new binding site for CNX and CRT, allowing re-folding, which repeats until correct folding is accomplished (Taylor, Thibault, Tessier, *et al.* 2003). ERP57 is also present in the CNX and CRT system. ERP57 is a PDI family member that contains two thioredoxin motifs and catalyses disulphide bond formation of the glycoproteins and this encourages the protein to fold in its native state (Molinari & Helenius 1999). ERP57 is thought to achieve this by docking with the extended proline rich arm present in both CNX and CRT after both CNX and CRT have interacted with their substrates (Michalak, Parker & Opas 2002).

1.1.4 Chaperones in disease

Chaperones play a key role in protecting against disease. An example is chaperones involvement in protecting neural cells from many pathogenic factors such as neurodegeneration. Some examples of these neurodegenerative diseases are Alzheimer's disease, Parkinson's disease, amyotrophic lateral sclerosis, and Huntington's disease. These diseases arise from the formation of oligomers or amyloidogenic aggregates caused by mutant proteins. These aggregated proteins have been found to also appear in the extracellular space which can affect the viability of nearby cells (Lim & Yue 2015). Hsp70, together with DNAJ, has been shown to bind and inhibit the growth of aggregates in Huntington's disease (Labbadia, Novoselov, Bett, *et al.* 2012). Other chaperones such as Hsc70 cognate chaperone, DNAJA and the Hsp110 family have been shown to bind to α-synuclein amyloids, which converts them into their non-toxic monomers (Gao, Carroni, Nussbaum-Krammer, *et al.* 2015).

1.1.5 Disulphide bond formation in the ER

One of the key bonds which increases the stability of a protein is the disulphide bond. It is a characteristic addition to proteins that enter the secretory pathway as it allows the secretory

proteins to be more stable when exposed to the extracellular milieu or when these proteins are recycled through the acidic endocytic compartments. Disulphide bond formation occurs as soon as the protein enters the ER. The formation of the secondary structure as the polypeptide chain collapses brings the cysteine residues close enough together to allow for the formation of disulphides (Figure 1.1).

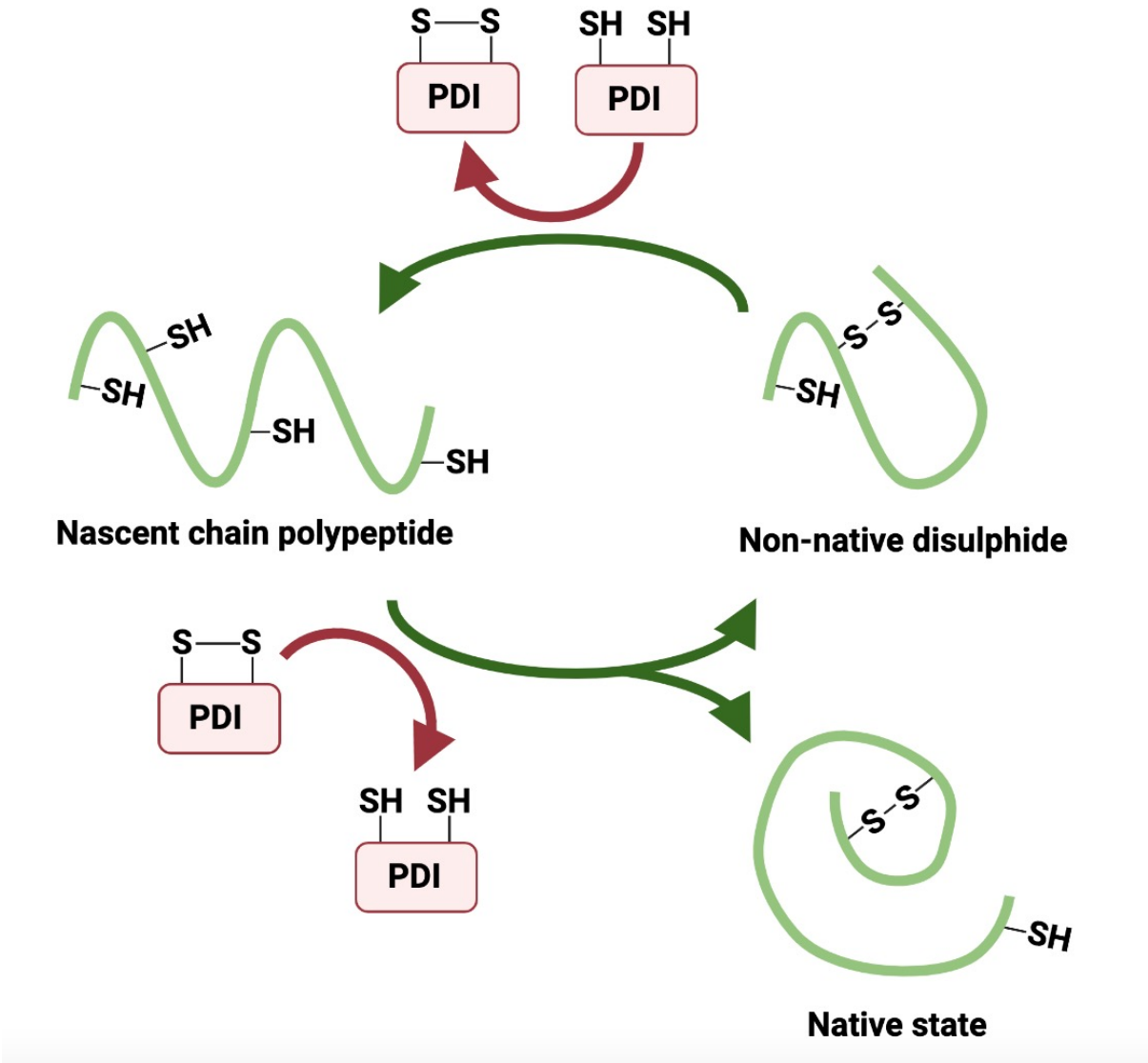

Figure 1.1: Disulphide bonds that occur in protein folding. PDI is a key protein that assists in the formation and breakage of disulphide bonds in proteins Figure adapted from (Bulleid 2012).

Correct oxidative protein folding only occurs when enzymes are present which can introduce the disulphide bond between two close cysteine residues. The enzymes also reduce disulphides that occur during folding but are not present in the final native structure of the protein (Jansens, van Duijn & Braakman 2002). Anfinsen also noticed an enzyme from bovine liver microsomes that catalyses disulphide interchange in the ER. The re-arrangement of disulphides occurs if low levels of mercaptoethanol is present (Fuchs, de Lorenzo & Anfinsen 1967). If a protein does not fold correctly, it is likely to be degraded in the cytoplasm but its disulphides still need to be removed before it passes through the ER membrane into the cytosol. This function has been found to be performed by ERdj5 which has reductase activity and cleaves the disulphide bonds (Ushioda, Hoseki, Araki, *et al.* 2008). Reduction and oxidation pathways are present in the ER to ensure the formation of native disulphides and for the breakdown of non-native disulphides.

The PDI family of enzymes are key to the formation of disulphide bonds, and they exchange disulphides with their substrate proteins (Table 1.1).

Table 1.1: The human family of protein disulphide isomerase proteins. AA stands for amino acid Table adapted from (Benham 2012).

Name	Domain arrangement	Active site sequence	Residue length in AA
PDI (PDIA1)	abb'xa'	CGHC, CHGC	508
PDIp (PDIA2)	abb'xa'	CGHC, CTHC	525
ERP57 (PDIA3)	abb'xa'	CGHC, CHGC	505
ERP72 (PDIA4)	a^{o}abb'xa'	CGHC, CHGC, CGHC	645
PDIR (PDIA5)	ba^{o}aa'	CSMC, CGHC, CPHC	519
P5 (PDIA6)	aa'b	CGHC, CHGC	440
PDILT	abb'xa'	SKQS, SKKC	584
ERdJ5	Jabbaaa	CSHC, CPPC, CHPC, CGPC	793
ERp44	abb'	CRFS	406
ERp46	a^{o}aa'	CGHC, CGHC, CGHC	432
ERp18	a	CGAC	172
ERp27	bb'	N/A	273
Erp29	b'D	N/A	261
TMX	a	CPAC	280
TMX2	a	SNDC	296
TMX3	abb'	CGHC	454
TMX4	a	CPSC	349
TMX5	a	CRFS	360
hAG2 (AGR2)	a	CPHS	175
hAG3 (AGR3)	a	CQYS	166
ERp90	Trx1-5	N/A	825

It was first noticed by two groups, the first of which observed that the rat liver contained a system which rapidly accelerated the conversion of reduced bovine pancreatic RNase to its enzymatically active form (Goldberger, Epstein & Anfinsen 1963). Straub et al., also saw reactivation of reduced ribonuclease after the addition of pigeon and chicken pancreas (Venetianer & Straub 1963). PDI is a 55 kDa protein which exists in the majority of mammalian

tissues. It contains a C-terminal KDEL motif which keeps PDI in the ER although PDI has also been detected in the cytosol and extracellularly (Yoshimori, Semba, Takemoto, *et al.* 1990). A structural domain of PDI which is shared throughout most of its family is the thioredoxin domains, of which there are four in PDI (Kemmink, Darby, Dijkstrat, *et al.* 1997). Two of the domains are the catalytic domains a and a' which are separated by two non-catalytic domains b and b'. There is also an X linker region which caps the hydrophobic pocket present on the b' domain and this regulates ligand binding and homodimerisation of PDI (Wang, Chen, Wang, *et al.* 2010). Wang et al., have identified the crystal structure of mammalian PDI (Figure 1.2). Both active sites of PDI contain a CXXC motif, in the case of PDI it is a CGHC motif (Figure 1.2) with a labile disulphide bond. PDI has a higher reduction potential than that of the client proteins (-180 mV); this means PDI can easily donate its disulphide to a protein with a reduced SH group (Hatahet & Ruddock 2009).

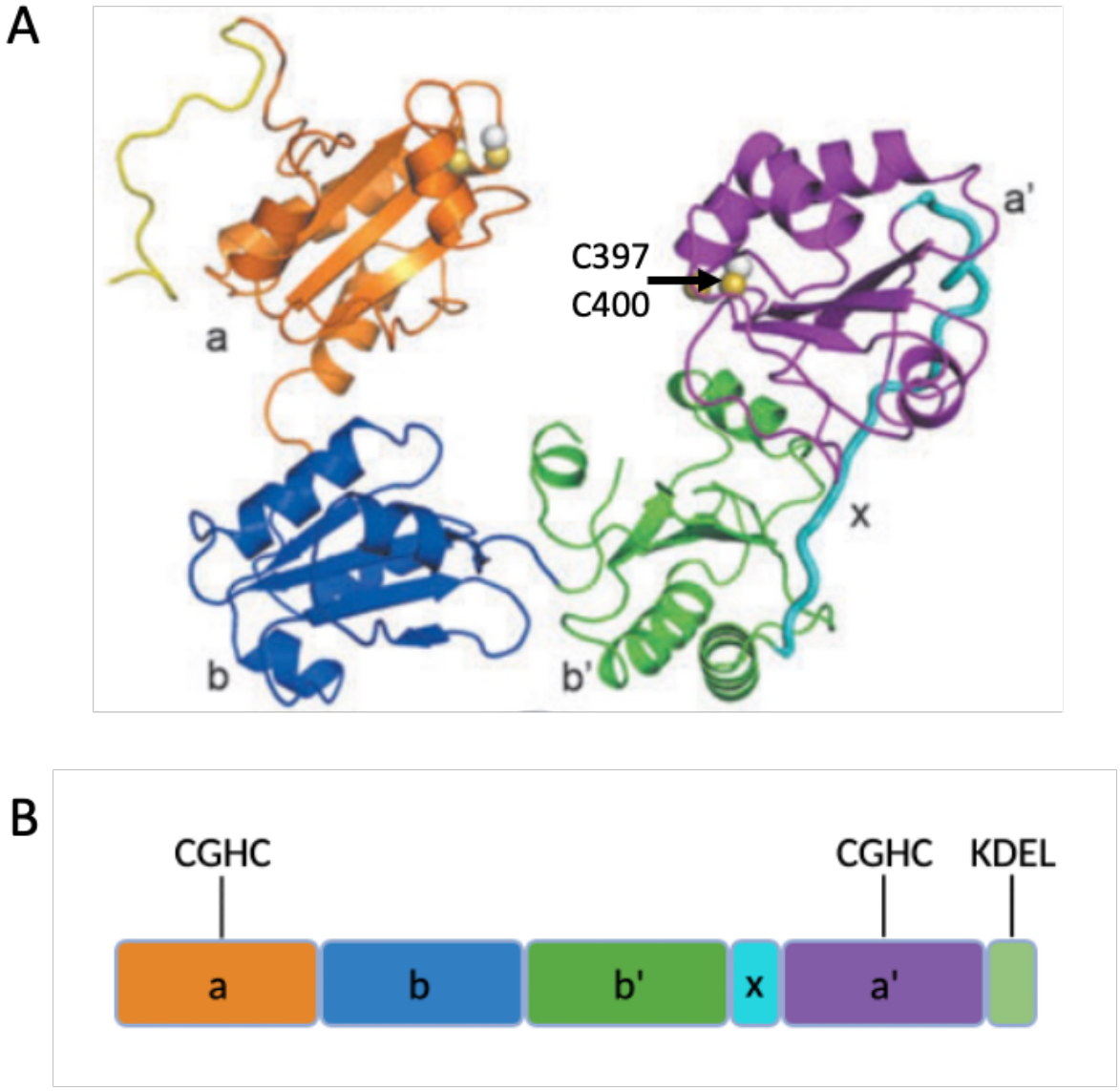

Figure 1.2: (A) Ribbon diagram of the crystal structure of mammalian PDI as viewed from the front of the protein. Image taken from (Wang, Li, Ren, *et al.* 2013). (B) Diagram of PDI domain structure. PDI contains two active site domains (a, a') and two non-catalytic domains (b, b') the x separates b' and a'. The C-terminal possesses a KDEL sequence for ER retention.

On the back of a number of NMR structure of PDI domains, the crystal structure of yeast PDI was solved by Tian et al., and they established that the thioredoxin domains of PDI form a twisted U shape. Both a and a' are located at the top of the U opposite of each other, b and b' are located at the bottom of the U in an area which contains hydrophobic residues. The interior of the U structure of PDI is hydrophobic, and it was suggested that it binds to

hydrophobic residues of unfolded proteins. This explains why PDI is also involved in chaperone functions in proteins which do not contain a disulphide bond (Cai, Wang & Tsou 1994; Tian, Xiang, Noiva, *et al.* 2006). In the U shape of the PDI structure, the major binding site for proteins is the b' domain, as shown via nuclear magnetic resonance (NMR) studies which looked at the binding of RNase to PDI (Denisov, Määttänen, Dabrowski, *et al.* 2009). Between helices α1 and α3 there is a large hydrophobic space which contains various side chains. The b'x domain of PDI interact with each other to affect substrate binding to PDI. The x domain is able to cap a hydrophobic spot on the b' domain and this prevents substrate binding to PDI (Nguyen, Wallis, Howard, *et al.* 2008). Even though the b' domain is key for the binding of proteins the other regions are still required for substrate binding, the a' region has been shown to bind misfolded proteins in conjunction with b' (Klappa, Ruddock, Darby, *et al.* 1998). PDI is able to catalyse three reactions which are: oxidation, reduction and isomerisation reactions (Figure 1.1). The oxidation reaction occurs when a dithiol on a protein or peptide substrate is oxidised to a disulphide by PDI losing a disulphide from its active site. When this oxidation occurs *in vitro* glutathione disulphide (GSSG) is used to reoxidise PDI and GSSG is changed to glutathione (GSH) (Chakravarthi, Jessop & Bulleid 2006). When GSSG is not present PDI can reduce a disulphide in one protein and form a disulphide in another. Reduction reactions occur when a disulphide on a protein or peptide substrate is reduced and PDI gains a disulphide in its active site. *In vitro* GSH or dithiothreitol (DTT) is used to reduce PDI. Isomerisation occurs when the disulphides or thiols which are on proteins or peptide substrates are readjusted and a different disulphide bonding pattern occurs, this does not cause a change in the active site of PDI (Hatahet & Ruddock 2009).

GSH is a small thiol antioxidant present in mammalian cells, with the ER containing 15 mM of GSH (Montero, Tachibana, Rahr Winther, *et al.* 2013). The ratio of the reduced form

of GSH to the oxidised form of GSSG is thought to be a measure of oxidative stress. In healthy tissue, GSH is mainly in the reduced form. GSSG is converted to GSH by reduced nicotinamide adenine dinucleotide phosphate (NADPH), and this is catalysed by glutathione reductase (Couto, Malys, Gaskell, *et al.* 2013). The reduced form of GSH is thought to assist with the reduction of PDI by acting as a terminal electron acceptor (Kojer & Riemer 2014). Research by Tsunoda et al., suggests that this may not be the case and there may still be other electron donors which can assist in maintaining the reductive capacity of the ER. They found the maturation of the low-density lipoprotein receptor (LDL-R), which requires reduced PDI to mature, was not affected by the depletion of GSH. The depletion of GSH also did not affect the UPR which would be expected if the lack of glutathione caused a build-up of unfolded proteins (Tsunoda, Avezov, Zyryanova, *et al.* 2014).

Ero1 was first characterised in yeast in 1998 by two groups who found it to be essential in the formation of disulphides in PDIp (Pollard, Travers & Weissman 1998; Frand & Kaiser 1998). Mammalian cells contain two Ero1 proteins: Ero1α, expressed ubiquitously in all tissues and Ero1β, which is expressed in specific tissues such as the pancreas and testis (Pagani, Fabbri, Benedetti, *et al.* 2000; Cabibbo, Pagani, Fabbri, *et al.* 2000). Ero1 is a flavoenzyme, because it uses flavin adenine dinucleotide (FAD) as a cofactor to transfer electrons from PDI to oxygen, generating H_2O_2 as a by-product (Tu & Weissman 2002). Inaba et al., discovered the crystal structure of Ero1α and this allowed for the elucidation of how Ero1α interacts with PDI (Figure 1.3). Ero1α interacts with PDI at the b' domain of PDI with hydrophobic and electrostatic interactions. It is thought that Phe240, Phe249 and Phe304 in the b' domain of PDI form non-covalent bonds with the β-hairpin in ero1α (Inaba, Masui, Iida, et al. 2010). Also, Val101 and Trp272 of Ero1α are needed for Ero1α-PDI formation. They position the Cys397 and Cys400 active cysteines of PDI near the disulphide bonded cysteines

in the shuttle loop of Ero1α and allow for disulphide exchange to occur (Zhang, Li, Zhang, *et al.* 2019).

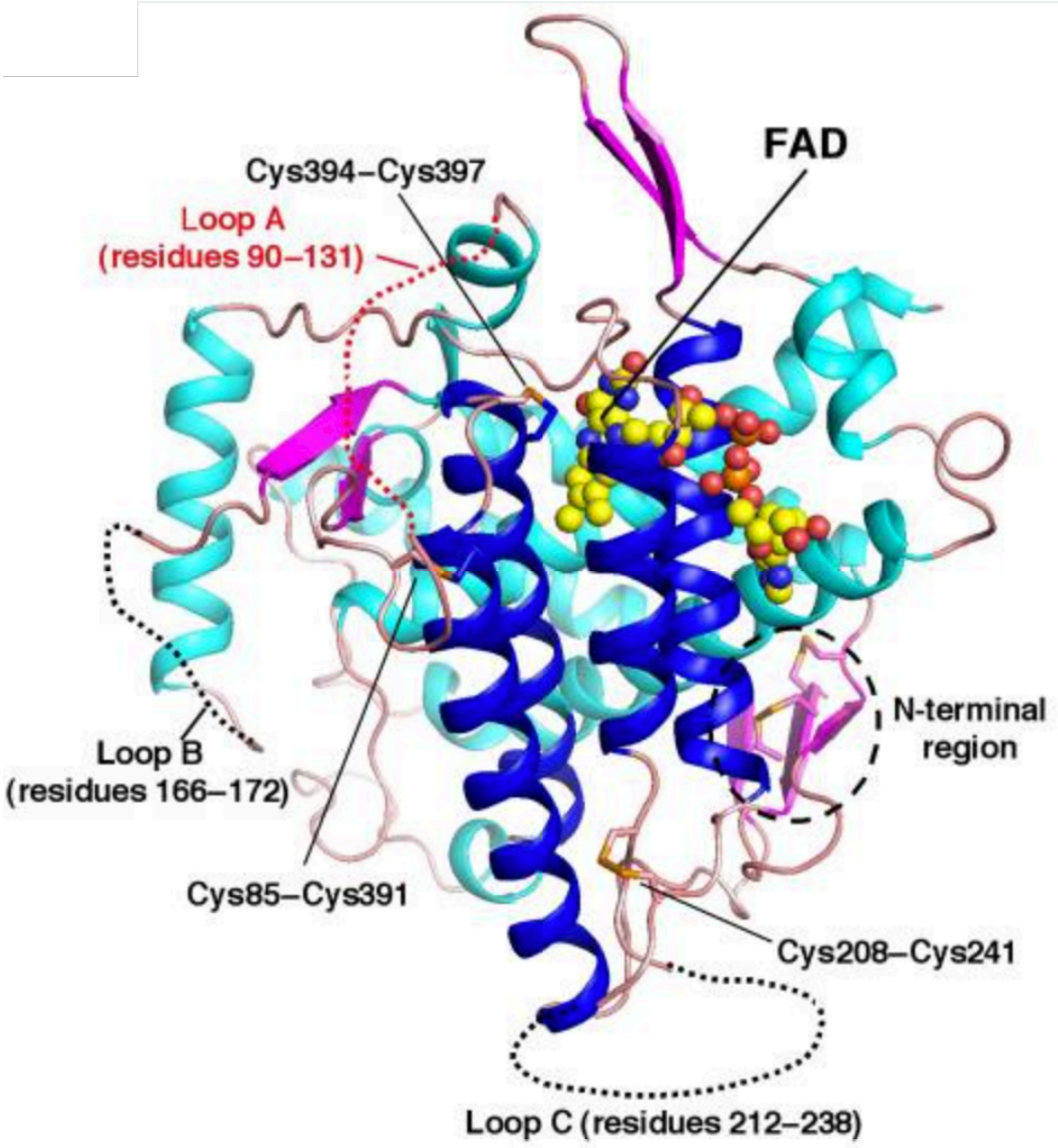

Figure 1.3: Ribbon diagram of the crystal structure of Ero1α. The lack of electron density prevented some of the loops from being modelled so they are represented by the dotted lines. Image taken from (Inaba, Masui, Iida, et al. 2010).

Ero1α has a collection of cysteines which are involved in the active site of Ero1α, namely Cys394 and Cys397. Ero1α has two active sites, the inner and outer active site. The outer active site is made up of a pair of cysteines which are attached to an unstructured flexible

loop these cysteines are termed shuttle cysteines. The inner active site is made up of two cysteines which are present in a CXXC motif and are close to the FAD cofactor (Inaba, Masui, Iida, et al. 2010).

The process of disulphide bond formation requires PDI to work with the Ero1 family of proteins (Figure 1.4). An electron transport chain is formed between PDI and Ero1 and the electrons are passed onto oxygen. PDI accepts electrons from the from the protein PDI is bound to and this oxidises the active site cysteines of PDI. The flexible loop cysteines directly accept the electrons from PDI. The electrons are transferred from the outer active site to the cysteines in the inner active site, the electrons are then passed onto FAD reducing it to $FADH_2$. $FADH_2$ then reacts with molecular oxygen to form H_2O_2 and Ero1 can catalyse another reaction (Bulleid 2012; Inaba, Masui, Iida, et al. 2010).

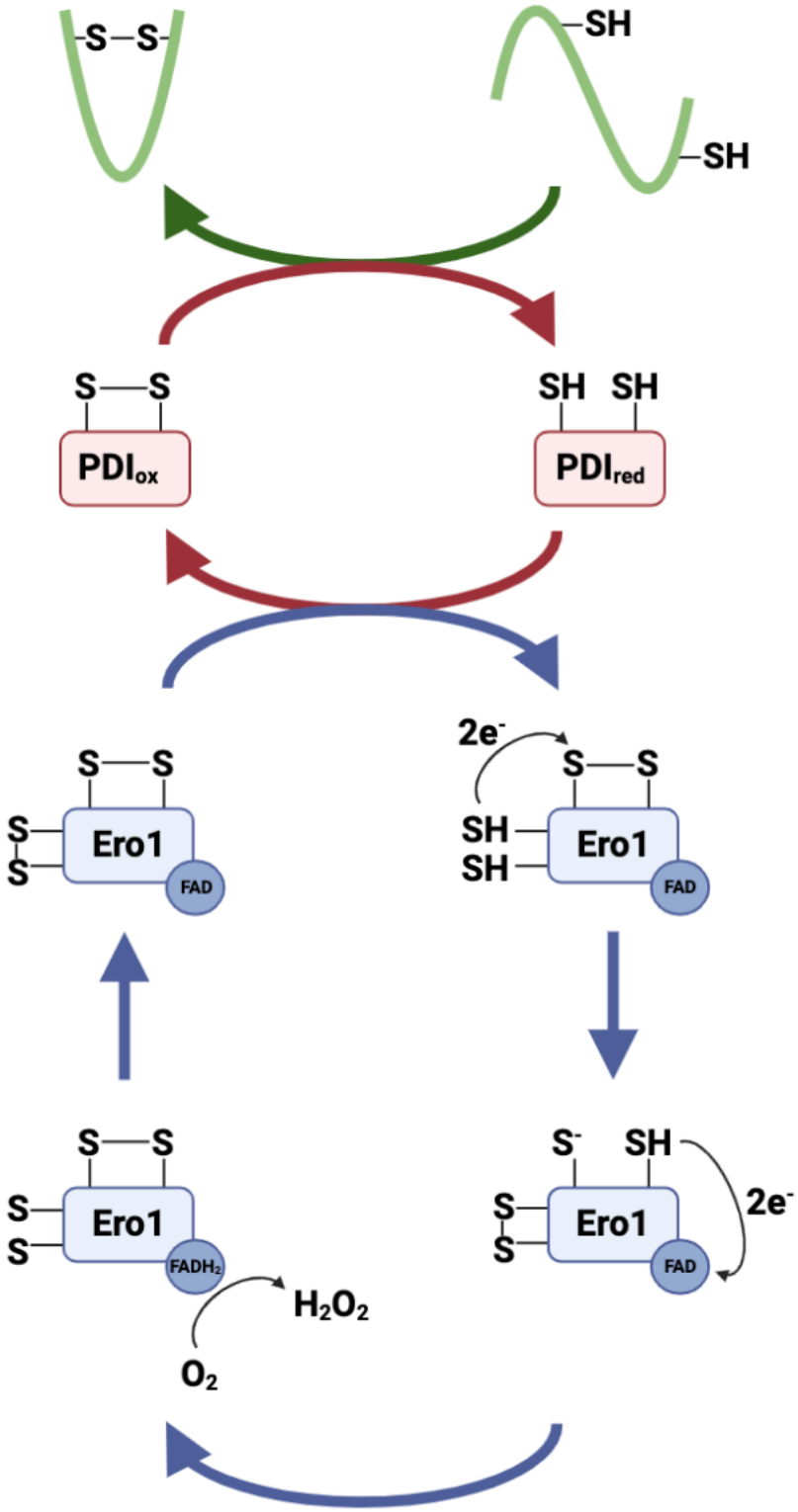

Figure 1.4: Disulphide bond formation with PDI and Ero1. PDI catalyses the formation of disulphide bonds in the ER. Ero1 is present to refresh PDI for the formation of more disulphide bonds. It does this by using oxygen as an electron acceptor. Figure adapted from (Bulleid 2012).

To prevent the over production of H_2O_2, the activity of Ero1 must be regulated. Ero1 has non-catalytic cysteine residues which restricts movement in the outer active site Cys94, Cys99 and Cys131, which prevents disulphide exchange occurring at the inner active site (Appenzeller-Herzog, Riemer, Christensen, *et al.* 2008). Reduction of the regulatory disulphides in Ero1 needs to take place before transfer of electrons between the active site can occur again. One theory is that PDI regulates Ero1 activity by reducing the regulatory disulphides when the majority of the PDI in the ER is reduced. The disulphides are reformed when there is a majority oxidised PDI in the ER (Kim, Sideris, Sevier, *et al.* 2012). Zito et al., showed that in mammalian cells which had an Ero1 deficiency there was only a small decrease in disulphide bond formation. Transgenic mouse embryonic fibroblasts lacking Ero1 and had peroxiredoxin 4 (PrxIV) died. Ectopic PrxIV rescued this loss of Ero1 (Zito, Melo, Yang, *et al.* 2010). PrxIV uses H_2O_2 as an electron acceptor, meaning an interchain disulphide bond between Cys124 and Cys245 in PrxIV can then be reduced by PDI (Tavender, Springate & Bulleid 2010).

1.1.6 Protein quality control and degradation

A large number of proteins that enter the ER fail to reach the native state required for proper function in the cell. These misfolded proteins may occur due to various factors such as mutations, insufficiency of a binding partner or a shortage of chaperones to assist in folding. The misfolded proteins are kept in the ER and eventually are processed through ER-associated protein degradation (ERAD). ERAD can also target proteins which have been properly folded to their native state. An example of a properly folded protein which is targeted by ERAD is the degradation of the substrate 3-hydroxyl-3-methylglutaryl acetyl-coenzyme-A reductase (HMGR) which is involved in sterol biosynthesis. ERAD is used to degrade HMGR as a feedback

inhibition system to ensure sterol homeostasis takes place. This also occurs with squalene monooxygenase (SQLE) as accumulation of sterol metabolites is toxic for cells (Foresti, Ruggiano, Hannibal-Bach, *et al.* 2013).

ERAD degradation occurs when misfolding is detected by lectin chaperone family members such as CNX and CRT. The misfolded substrate must be retrotranslocated, so part of the protein now faces the cytoplasm. The misfolded protein is then modified, with a 76 AA peptide called ubiquitin is added. The ubiquitin on the misfolded protein is recognised by p97 a member of the AAA-ATPase family which utilises ATP to deliver the misfolded protein to the proteasome (Rabinovich, Kerem, Fröhlich, *et al.* 2002). The polyubiquitinated proteins are recognised and degraded by the 26S proteasome. 26S is a multicatalytic protease, the misfolded proteins are transported to a chamber where tryptic, chymotryptic and caspase-like proteolytic activates reside (Finley 2009). The presence of proteasomes outside the ER membrane binds misfolded proteins which are retrotranslocated to the ERAD system to ensure the misfolded proteins are efficiently degraded.

Some alternative modes of degradation are also used in the ER there are two which are used to clear procollagen aggregates. The first is autophagic elimination of collagen Brodsky et al., found that procollagen was degraded in the lysosome via the autophagy pathway but not via ERAD. They used rapamycin to enhance autophagic activity and found that this increased the rate of procollagen clearance. This clearance by autophagy which is normally a cytoplasmic process is thought to occur because of ER stress, the expansion of the ER and upregulation of autophagic components push the ER to start degrading misfolded proteins with autophagy (Ishida, Yamamoto, Kitamura, *et al.* 2009). The second involves CNX interacting with the ER-phagy receptor named FAM134B. CNX is able to recognise ER luminal misfolded procollagens, CNX then goes on to interact with FAM134B. FAM134B then

proceeds to bind to LC3 which is an autophagosome membrane associated protein, this delivers a part of the ER which contains CNX and the misfolded procollagen for degradation (Forrester, Leonibus, Grumati, *et al.* 2019).

1.1.7 ER stress and the unfolded protein response

ER stress occurs when the ER is exposed to conditions which perturb the normal state. The research focus in this field has primarily been on how ER stress is caused by disruptions in protein folding, although aberrations in lipid metabolism can also cause ER stress but this area is less well understood. Kozutsumi et al., expressed wild type and mutant forms of the influenza virus haemagglutinin and found that it induced the synthesis of GRP78 and GRP94 which are stress proteins (Kozutsumi, Segal, Normington, *et al.* 1988). The ER uses two main mechanisms to try and reduce the ER stress on the cell to prevent apoptosis. It first upregulates the number of chaperones and foldases in the ER, doing so increases the physical size of the ER and its folding capacity. The ERs other mechanism is to shut down protein synthesis by stopping transcription and translation of new proteins (Harding, Zhang & Ron 1999; Pakula, Laxell, Huuskonen, *et al.* 2003). It also clears unfolded proteins through the ERAD system. If these two systems are unable to restore the folding capacity of the ER and alleviate ER stress, then the cell undergoes apoptosis to remove itself from the surrounding healthy cells. There are three main branches of the unfolded protein response (UPR), which work in parallel in higher eukaryotic cells. Each contains a different transmembrane ER signalling component; inositol requiring enzyme (IRE1), double-stranded RNA-activated protein kinase (PKR)-like ER kinase (PERK) and activating transcription factor 6 (ATF6) (Ron & Walter 2007).

ATF6 is a transcription factor but is synthesised as a transmembrane protein that sits on the ER membrane. It stays in the ER membrane until there is an accumulation of unfolded proteins, when this occurs it is pinched off the ER where it is deposited into a transport vesicle and delivered to the Golgi apparatus (Brown & Goldstein 1999). At the Golgi there are two proteases that receive ATF6, site-1-protease (S1P) and site-2-protease (S2P). S1P removes the luminal domain of ATF6 and S2P removes the transmembrane anchor (Ye, Rawson, Komuro, *et al.* 2000). The cytosolic part of ATF6 then proceeds to the nucleus where UPR genes are activated such as BiP and GRP94 (Walter & Ron 2011) (Figure 1.5).

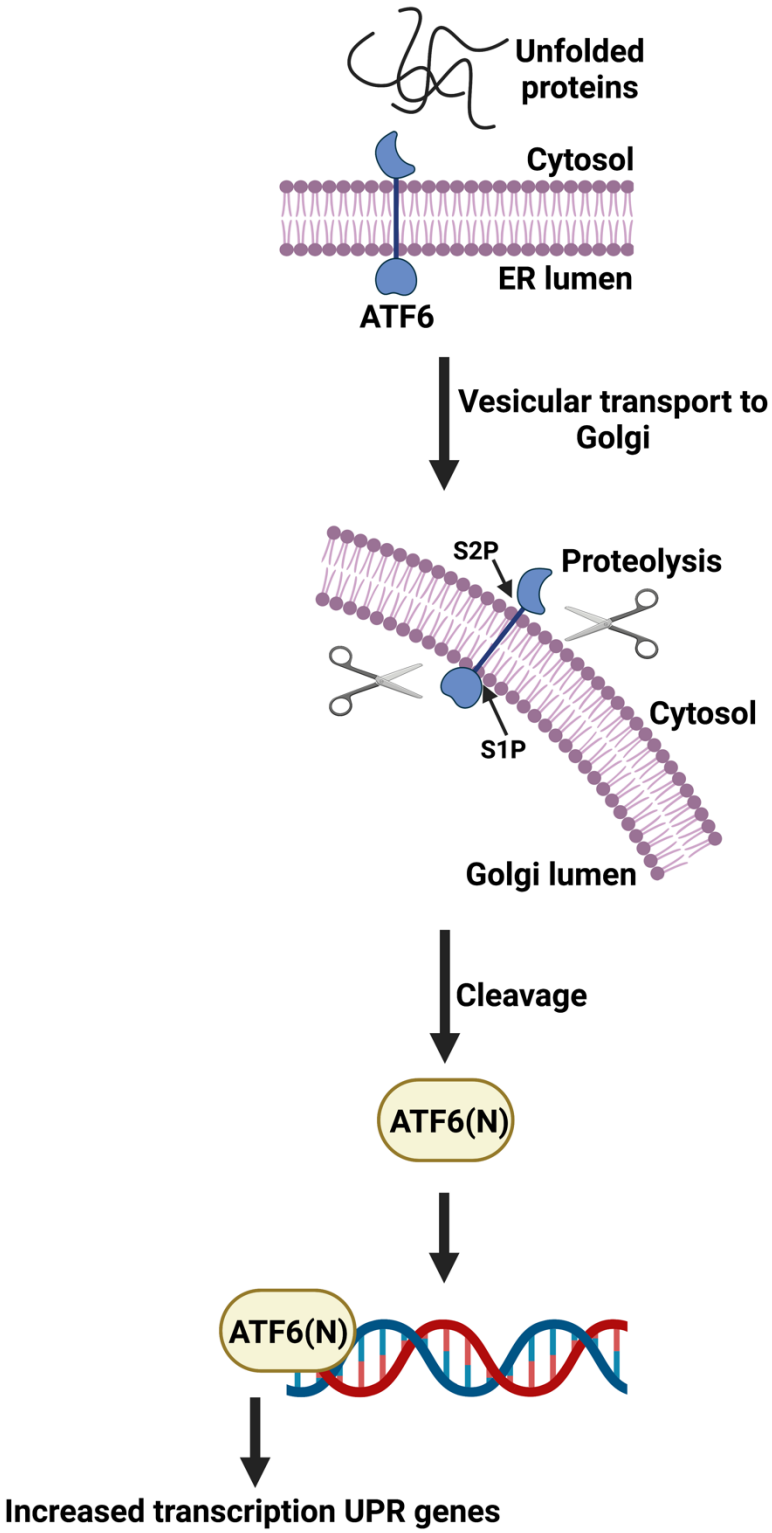

Figure 1.5: The ATF6 pathway of the UPR. During ER stress ATF6 is transported to the Golgi where the luminal and transmembrane domains are removed. The cytosolic domain then proceeds to the nucleus where UPR genes are activated. Figure adapted from (Walter & Ron 2011).

PERK is an ER-resident transmembrane kinase. When it senses ER stress it oligomerises and then phosphorylates itself and as it phosphorylates itself it also phosphorylates eukaryotic translation initiation factor 2α (eIF2α). The phosphorylation of eIF2α prevents mRNA translation which reduces the number of proteins entering the ER. One mRNA which is still translated even during eIF2α phosphorylation is ATF4. ATF4 then proceeds to upregulate two genes which are transcription factor C/EBP homologous protein (CHOP) and growth arrest DNA damage-inducible 34 (GADD34) (Figure 1.6). GADD34 is involved in a negative feedback loop where it encodes a regulatory subunit induced by PERK. PERK goes on to dephosphorylate eIF2α and this allows the protein transcription to reoccur (Tsaytler, Harding, Ron, *et al.* 2011). CHOP is also a transcription factor involved in the UPR, but it controls factors that regulate apoptosis (Marciniak, Yun, Oyadomari, *et al.* 2004). CHOP and GADD34 work synergistically: low levels of ER stress will cause PERK to protect the cell but if there is too much ER stress, PERK is able to cause apoptosis and in turn cell death, one way PERK can do this is by increasing the global protein synthesis in the cell and this causes proteotoxicity.

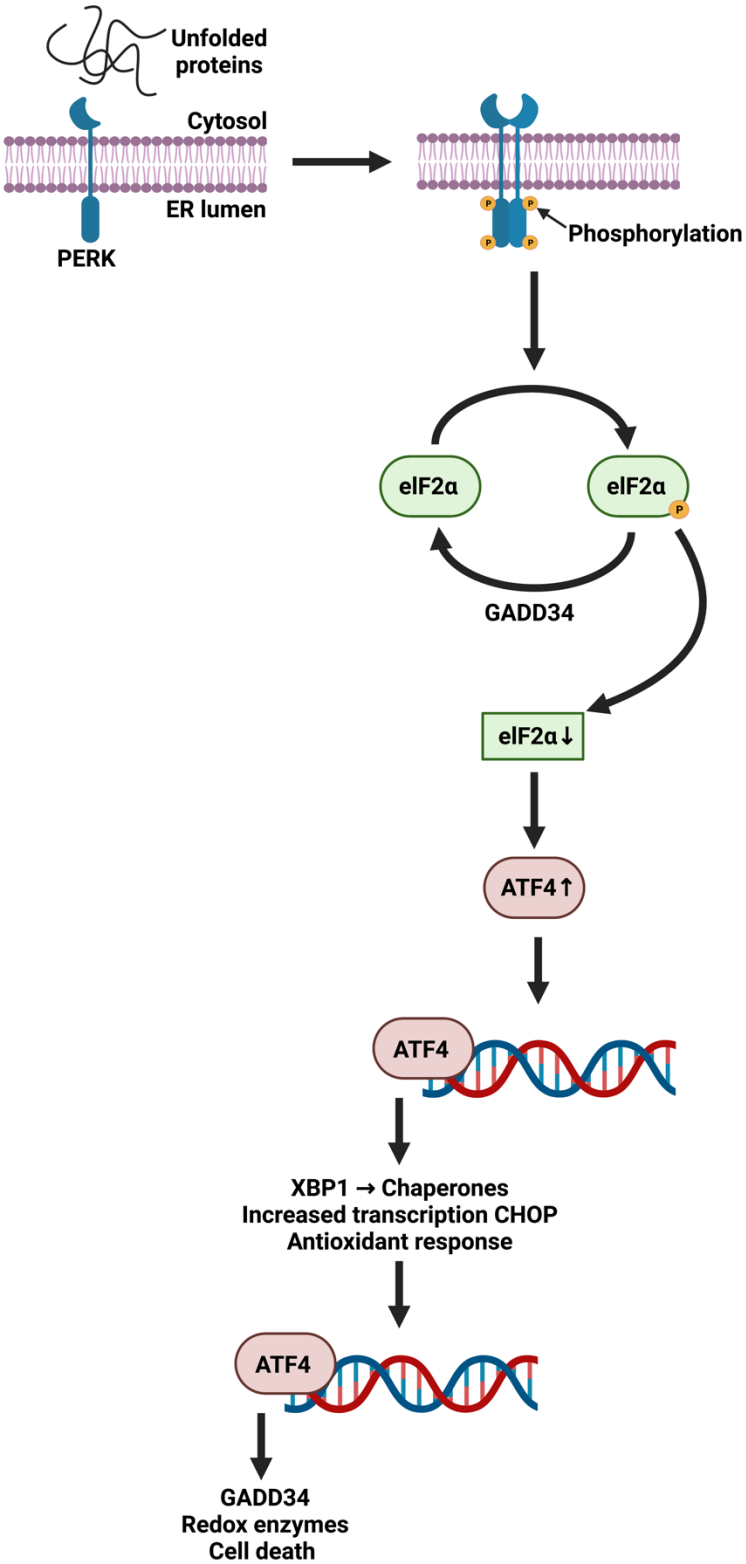

Figure 1.6: The PERK pathway of the UPR. ER stress causes dimerisation and autophosphorylation of the cytosolic domain of PERK. PERK then goes to phosphorylate eIF2α causing a reduction in protein synthesis which causes an increase in translation of ATF4. ATF4 goes on to promote transcription of UPR proteins CHOP and GADD34. Figure adapted from (Walter & Ron 2011).

The final branch of the UPR is IRE1. IRE1 is a bifunctional transmembrane kinase and endonuclease which uses nonconventional mRNA splicing; it is nonconventional due to the fact spliceosomes are not involved. When IRE1 detects unfolded proteins, it becomes oligomerised and autophosphorylated (like PERK) at the ER membrane. Autophosphorylated activated IRE1 cleaves X-box binding protein 1 (XBP1). IRE1 removes the intron from XBP1, and the exons are ligated together with tRNA in yeast (this enzyme is not currently known in mammalian cells), creating the activated transcription factor, spliced XBP1. Spliced XBP1 then migrates to the nucleus to upregulate the production of chaperones and ERAD associated proteins (Yoshida, Matsui, Yamamoto, *et al.* 2001) (Figure 1.7).

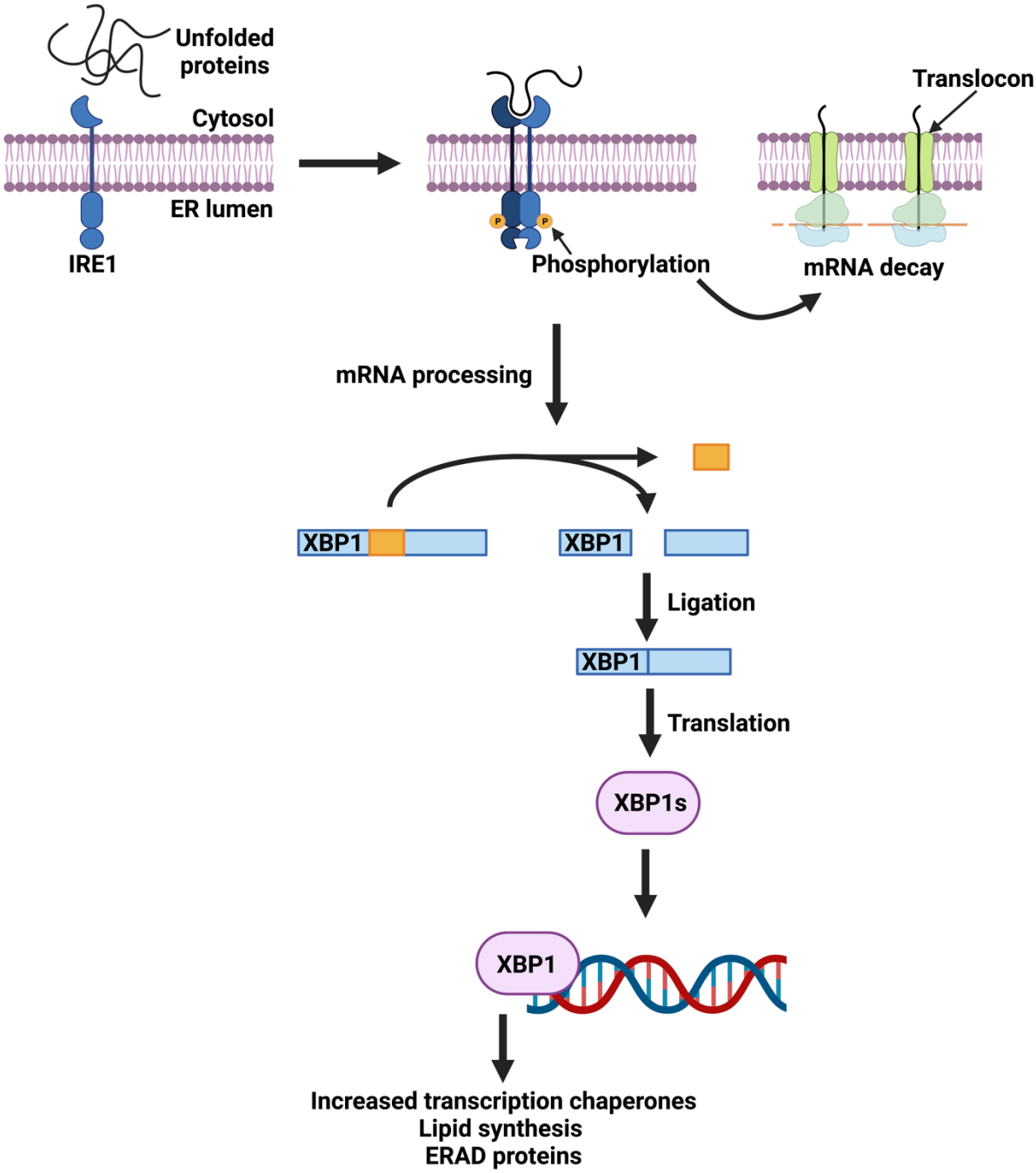

Figure 1.7: The IRE1 pathway in the UPR. ER stress leads to the oligomerisation, autophosphorylation and activates the cytosolic RNase domain of IRE1. This causes XBP1 to be spliced causing XBP1 to move to the nucleus which leads to upregulation of chaperones and ERAD associated proteins. Figure adapted from (Walter & Ron 2011).

If the activation of these three pathways of the UPR is effective, then the cell is able to restore ER homeostasis and the cell will most likely survive. If the ER is unable to attain homeostasis, then the cell is likely to be removed by apoptosis.

1.2 Proteomics importance and methodology

A key technique used to generate data in this thesis is mass spectrometry and its application to proteomics. Proteomics is defined as the study of the proteome; this is the protein accompaniment of the genome. The genome of a cell does not vary as much between each cell, however, there is a large amount of variation in the proteome. Proteins in a cell can vary in different forms such as having a post-translational modification (PTM) can affect the protein's structure or function and is usually influenced by various stimuli. An example of a PTM is phosphorylation which can affect many processes such as cellular growth, apoptosis and it has impact in signal transduction pathways. Phosphorylation usually occurs on the serine, threonine, or tyrosine residues on proteins, but has recently been shown to be more widespread than previously thought. Hardman et al., used an unbiased phosphopeptide enrichment approach which was based on strong anion exchange chromatography coupled with MS based phosphoproteomics and found that histidine, arginine, lysine, aspartate, glutamine, and cysteine could become phosphorylated (Hardman, Perkins, Brownridge, *et al.* 2019). Mass spectrometry has increased the understanding of the proteome by observing protein interactions, protein expression and PTMs on proteins. There are various MS techniques available with each more suited to a different application (Han, Aslanian & Yates 2008). In this thesis, "bottom-up" proteomics has been employed. This process involves breaking up a protein into peptides with enzymatic digestion, the peptides are then analysed by MS and the protein is built back up via informatic techniques so the structure and characteristics can be analysed (Gundry, White, Murray, *et al.* 2009). It is important that the enzyme used for digestion (e.g., trypsin) has a known cleavage site and the frequency of the cut is known. The cleavage site for trypsin is the peptide bond between the carboxyl group of

arginine or lysine and the amino group of the adjacent amino acid (Simpson 2006). The choice of protein-digesting enzyme is important due to the fact proteomics analysis involves comparing the mass of the peptides obtained from MS to the predicted mass of peptides which is obtained from the proteins sequence. This comparison is usually performed *in silico* and allows for the protein to be built up from overlapping peptides.

The measurements of the mass to charge ratio (*m/z*) for MS have to be performed on the gas phase of the ionised sample. A mass spectrometer is made up of an ion source, a mass analyser which measures the *m/z* of the sample and a detector which measures the numbers of ions present at each *m/z* value. The two most common techniques used to ionise the protein samples are electrospray ionisation (ESI) and matrix-assisted laser desorption/ionisation (MALDI). ESI involves ionising the sample from solution, so it is usually paired with tools that separate liquids best such as chromatographic separation tools (Fenn, Mann, Meng, *et al.* 1989). MALDI uses laser pulses to sublimate and then ionise the samples from a dry crystalline matrix (Karas & Hillenkamp 1988). ESI is more suited to complex samples in integrated liquid chromatography systems (LC-MS) whereas, MALDI is more suited for analysis of simple samples. There are four mass analysers currently used in MS; the ion trap, time-of-flight (TOF), quadrupole and Fourier transform ion cyclotron (FT-MS), with each analyser having its own advantages and disadvantages. For protein analysis and PTM analysis a technique called tandem MS (MS/MS) is used. MS/MS can be performed by combining different analysers, either triple quadrupole (QQQ) or quadrupole-TOF (Q-TOF). In MS/MS the mass spectrometer first measures all ions hitting the detector that fall between a certain *m/z* range. After this, a single ion/peptide is isolated and given energy by collision-induced dissociation, this ion/peptide is fragmented, and the masses of the newly generated fragments are recorded. The first ion generated is known as the precursor/parent ion (MS1)

and the fragments generated from it are known as the product/daughter ions (MS2). As certain rules exist in the amino acid sequence which cause the peptides to be broken in a specific way these fragments can be used to identify the structure of the protein. Only two peptides are usually needed to detect a singular protein in a mixture of many proteins (Lovric 2011).

Analysis of the results can involve two methods namely data-dependant acquisition (DDA) and data independent acquisition (DIA). DDA involves selecting the most intense peptides in the first stage of MS/MS these are then further fragmented as described earlier and the resulting fragments are searched in a database. DIA involves focusing on a smaller window either of ions that enter the mass spectrometer at a given time or looking at a window of *m/z* and fragmenting all of the precursors in that window. A variant of DIA and one that was used to generate the data in this thesis is sequential window acquisition of all theoretical mass spectra (SWATH-MS). SWATH-MS works by recording the entire set of the peptide ions without any preselecting. The MS2 scans are repeatedly recorded through an entire chromatographic gradient. All of the ions that fall within a set mass range are recorded in an unbiased fashion. The resulting fragment ions are analysed for their intensity which allows for protein quantification. Some advantages of using SWATH-MS are that the results have greater reproducibility, broader coverage and the ability to detect low abundance proteins that may otherwise be missed (Ludwig, Gillet, Rosenberger, *et al.* 2018; Chen, Zhang, Fernie, *et al.* 2021). Some examples of how these techniques have been used to answer biological questions are the use of quantification of protein interactomes, in the development of disease biomarkers, to reveal how certain organisms respond to stress and to look at proteostasis in fibroblasts from individuals with Down's syndrome (Liu, Borel, Li, *et al.* 2017; Xiao, Duan, Lin, *et al.* 2018; Martins-Marques, Anjo, Pereira, *et al.* 2015; Gao, Wang, Sang, *et al.* 2017).

1.3 Thesis aims

Although a lot is known about the roles chaperones play in health and disease, there is still plenty to be elucidated. There is currently little knowledge of how the cellular redox balance and protein homeostasis is influenced by reducing agents or how collagen folding can be restored following redox perturbations in different cell types. In this thesis, various hypothesis were explored to examine the role of oxidoreductases and their response to ER stress. A list of aims are presented below.

- To determine the effect of novel reducing agents *in vitro* and how they affect oxidoreductase complexes (Chapter 3).
- To analyse the effect of reductive stress on the proteome of HT1080 cells (Chapter 3).
- To investigate anterior gradient 2 (AGR2) interactions and expression in oesophageal cancer in cell lines and human tissue (Chapter 4).
- To investigate the effect of PDGF on the expression of lamin A/C in BJ fibroblasts and its effect on lamin phosphorylation (Chapter 5).
- To look at the protective effects of niacinamide against oxidative stress in BJ fibroblasts by using proteomics to study the changes in the BJ fibroblast proteome (Chapter 5).
- To optimise imaging methods for HT1080 cells transfected with mNeonGreen reporter proteins (Chapter 6).
- To establish whether transfected mNeonGreenCol1α is being correctly folded and processed in HT1080 cells (Chapter 6).
- To observe the interacting partners of mNeonGreen Col1α in transfected HT1080 cells (Chapter 6).

2 Materials and Methods

2.1 Cell culture

All cell lines were grown in a humidified incubator at 37 °C and 5% CO_2 (Binder). The cell lines were subcultured twice a week in T75 flasks (TPP, 90076). Cell culture was performed in sterile conditions in a CL2 flow hood (SteriGUARD, The Baker company, Sanford, Maine 04073 USA). HT1080 cells (ATCC® CCL-121™) were grown in Dulbecco's Modified Eagle's Medium (DMEM, Gibco, 41965-062). The medium was supplemented with 100 units ml^{-1} penicillin and 100 µg ml^{-1} streptomycin (Gibco, 15140-122), Glutamax (Gibco, 35050-061) and 8% foetal bovine serum (FBS, Sigma, F7524). BJ fibroblast cells (ATCC® CRL-2522™) were grown in Modified Eagle's Medium (MEM, Gibco, 41966-052), the medium was supplemented with 100 units ml^{-1} penicillin and 100 µg ml^{-1} Streptomycin, Glutamax and 10% FBS. The oesophageal cells OE19 (ECACC, 96071721) and OE33 (ECACC, 96070808) were grown in Roswell Park Memorial Institute (RPMI) 1640 (Gibco, 21875-091). The medium was supplemented with 100 units ml^{-1} penicillin and 100 µg ml^{-1} Streptomycin, Glutamax and 8% FBS.

Fresh media was first warmed in a water bath to 37 °C. The spent media was removed from the flask and the OE cells were washed twice in 6 ml of sterile phosphate buffered saline (PBS; 2.67 mM KCl, 1.47 mM KH_2PO_4, 138 mM NaCl, 8.10 mM Na_2HPO_4-$7H_2O$, 14190-250). 1 ml of 0.05% trypsin (Gibco, 15400-054) was applied to the cells, then 0.5 ml of the trypsin was removed. The cells were left in a 37 °C incubator for 5 minutes. In a new sterile T75 flask, sufficient fresh media was added for the required dilution (e.g. 5 ml for a 1:2 passage for the BJ fibroblasts and 9 ml for a 1:10 passage for the HT1080, OE19 and OE33 cells). After the cells were trypsinised, a single cell suspension was created by adding media to the flask (10 ml for a T75 flask) and pipetting to mix the cells. The cells were added to the T75 flasks which

contained fresh media (5 ml for a 1:2 passage for the BJ fibroblasts and 1 ml for a 1:10 passage for the HT1080, OE19 and OE33 cells) and mixed by pipetting.

2.2 Transfection

HT1080 cells were grown in 6 cm dishes until they reached 70% confluency. For transfections with the jetPEI® transfection kit (VWR, 101-10N), 5 µg of the required plasmid was diluted in 150 mM NaCl to a final volume of 250 µl and the solution was vortexed briefly before being centrifuged at 16,000 g for 1 minute at 4 °C. Two µl of jetPEI® reagent was diluted in 150 mM NaCl to a final volume of 250 µl, this was also briefly vortexed before being centrifuged at 16,000 g for 1 minute at 4 °C. The jetPEI® solution was added to the DNA solution. This was vortexed and centrifuged at 16,000 g for 1 minute at 4 °C briefly. The mixture was incubated for 30 minutes at room temperature (RT). Next 500 µl of the jetPEI® mixture was added to the HT1080 cells grown in the 6 cm dishes in complete media. The plates were gently swirled to mix the reagent with the media. After 24 hours of transfection, the cells were either taken for lysis or immunofluorescence (IF).

2.3 Cell lysis

Prior to lysis, cells were washed twice with PBS and then placed on ice after the PBS was removed. Cells were lysed with MNT lysis buffer (20 mM MES (M8250), 30 mM Tris-HCl (T3253), 100 mM NaCl (S7653), pH 7.4, with 1% v/v Triton X-100 (X100) and protease inhibitor (PI, Sigma, 2 mM AEBSF, 0.3 µM Aprotinin, 116 µM Bestatin, 14 µM E-64, 1 µM Leupeptin, 1 mM EDTA, P2714) was used when cytosolic and ER proteins needed to be solubilised. Cell lysis volumes were adjusted according to culture conditions. For example, 300 µl of lysis buffer was added to a 6 cm dish (TPP, 93060T) which contained approximately 3.2×10^6 cells. The HT1080 cells were left on ice for 1 minute and then lysed with a cell scraper (Fisher,

11587692). The lysate was then transferred to a 1.5 ml microcentrifuge tube and then centrifuged at 16,100 g at 4 ^{o}C for 10 minutes to remove nuclei. The supernatant was transferred to a new microcentrifuge tube. The lysates were flash frozen in liquid nitrogen and were then either used fresh or transferred to a -20 ^{o}C freezer for storage.

For BJF lysis, radioimmunoprecipitation assay (RIPA) buffer (1% v/v Triton X-100 (X100), 50 mM Tris HCl (T3253), pH 8, 150 mM NaCl (S7653), 0.5% w/v Na-deoxycholate (D6750), 0.1% w/v sodium dodecyl sulphate (SDS, 74255) was used. This buffer also contained PI and 1x phosSTOP (made from a 10x stock of 1 tablet in 1 ml dH_2O; Roche, 04906845001). Next 300 µl of RIPA lysis buffer was left on the BJF for 5 minutes at RT. The lysates were again centrifuged at 16,100 g at 4 ^{o}C for 10 minutes. The pellets of cellular debris were discarded, and the supernatant transferred to a new 1.5 ml microcentrifuge tube. The lysates were flash frozen in liquid nitrogen and were then transferred to a -20 ^{o}C freezer for storage.

2.4 BCA assay

The Pierce™ Bicinchoninic acid (BCA) protein assay kit (Thermofisher, 23225) was used to determine protein concentration for the lysates that were generated. The microplate procedure was used, and this involved making standards from a 2 mg ml^{-1} stock of bovine serum albumin (BSA) in PBS. 25 µl of each standard and sample was pipetted in duplicate into a 96 well plate (Sarstedt, 83.3924). Next 200 µl of working reagent was pipetted into each well with standard or lysate and left to incubate at 37 ^{o}C for 30 minutes. The plate was read at 570 nm in a microplate reader (BioTek ELX800). The standards were used to plot a standard curve of protein concentration against absorbance. The curve was used to determine the protein concentration of the lysates.

2.5 SDS PAGE

Samples were made by adding variable quantities of lysate to 2×, 4× or 5× Laemmli sample buffer (2× sample buffer contained; 65.8 mM Tris-HCl, pH 6.8, 26.3% (w/v) glycerol, 2.1% SDS and 0.01% bromophenol blue (Biorad, #1610737)). For certain samples, 50 mM DTT was added to the Laemmli buffer to reduce disulphide bonds. Samples were boiled at 95 ^{o}C for 5 minutes, then spun down for 5 minutes at 16,100 g. Either 8% or 10% polyacrylamide gels were used to run the samples, (resolving gel: 40% acrylamide (Severn Biotech, 20-3600-10), 0.375 M Tris (pH 8.8), 0.1% SDS (Sigma, 74225), 0.1% APS (Sigma, A3678) and 0.04% N,N,N',N'-tetramethylethylenediamine (TEMED; Sigma, T9281); stacking gel: 5% acrylamide, 0.125M Tris (pH 6.8), 0.1% SDS, 0.075% APS, 0.1% TEMED). The running section of the gel was cast in a Hoefer gel caster and left to polymerise for 40 minutes with 0.5 ml water to cover the gel. The water was then removed, and the stacking gel was added along with a 10 or 15 well comb. The gel was left to polymerise for 20 minutes. After polymerisation, the samples in Laemmli sample buffer were loaded next to a protein marker (Bio-Rad, 1610374). The samples in the gel were run at 50 mA for about an hour in a mighty small II mini vertical electrophoresis unit (Hoefer, SE250) and then either stained with Coomassie blue or taken for western blotting.

2.6 Gel staining

Gels were fixed in fixing solution (7% acetic acid and 40% methanol in dH_2O) for 10 minutes. The solution was removed and then the Coomassie stain was poured on the gel (80% Brilliant blue G-colloidal concentrate (Sigma, B2025) and 20% methanol. The gel was left to stain overnight on a rocker. The first destain solution (25% methanol and 10% acetic acid fill in dH_2O) was left on for 10 minutes. The first destain was poured off and a second destain (25%

methanol in dH_2O) was added and left on whilst the gel was rocking until the majority of the background staining had disappeared. The gel was then scanned, and an image saved on a computer.

2.7 Western blotting

The proteins on the gel were transferred onto polyvinylidene difluoride (PVDF) membranes (Millipore, 10344661). The membranes were activated in methanol for 20 seconds before being placed in transfer buffer (25 mM Tris-Base, 190 mM glycine and 20% methanol). Transfer was carried out for 2 hours at 150 mA or at 30 V overnight, at RT or 4 ^{o}C respectively. After transfer, the membranes were blocked in 5% milk dissolved in Tris buffered saline with Tween (TBS-T; 10 mM Tris-Base, 70 mM NaCl, 1.34 mM KCl pH 9-9.4 and 0.1% Tween) overnight at 4 ^{o}C or for 1 hour at room temperature. The membrane was incubated with a suitable primary antibody at the optimal concentration in 1 ml of 5% milk and 2 ml of TBS-T (Section 2.18). The membranes were then washed in TBS-T 5 times. The initial wash was manually shaken and then poured out; the other 4 washes were for 5 minutes each on a rotator. After this step, secondary antibody incubation was performed with either goat anti-mouse peroxidase (GAMPO, DAKO, P0447) or swine anti-rabbit peroxidase (SARPO, DAKO, P0217), diluted to 1:3000 in the milk/TBS-T mix described earlier and left on a rocker or rotator for 1 hour. The membranes were then washed again 5 times in TBS-T. 500 µl of enhanced chemiluminescence (ECL, GE, RPN2232) solution (250 µl of luminol and 250 µl of peroxide solution) was added to the membrane to visualise the protein bands. The membranes were dabbed to remove excess ECL and put in fresh saran wrap (Sarogold, FIL1040). The membranes were exposed to photographic film (Thermofisher, 34091) in a light-proof cassette in a dark room and then developed in an X-ray developer machine

(XOMAT).

2.8 Immunofluorescence

Cells were grown on 13 mm glass coverslips (VWR, 631-1578) overnight in 6 cm dishes with complete media to allow adherence to the coverslips. The coverslips were then washed three times for 5 minutes each with PBS++ (PBS with 1 mM $CaCl_2$ and 0.5 mM $MgCl_2$, Gibco, 14040174). After the washes, the cells were fixed in 4% PFA (paraformaldehyde, Agar scientific, AGR1026) for 10 minutes at RT. An alternate fixative (cytoskeleton fixative) was also used, this consisted of 3.7% PFA, 0.02% glutaraldehyde, 50 mM PIPES pH 6.8, 5 mM EGTA, 2 mM $MgSO_4$ and 0.5% triton X-100. The cells were washed twice again for 5 minutes each in PBS++. To permeabilise the cells 0.1% Triton x100 was added for 10 minutes at RT. After permeabilisation the cells were washed three times for 5 minutes each. The coverslips were inverted and blocked in 50 µl 2% BSA in PBS (Sigma, A4503) on parafilm (FIL1022) for 30 minutes at RT or overnight at 4 ^{o}C. The coverslips were incubated in 50 µl of the specified primary antibody, diluted to the required concentration in the BSA mixture that was used for blocking for either 2 hours at RT or overnight at 4 ^{o}C in a humidity chamber. The coverslips were returned to the 6 cm dishes and washed three times for 5 minutes each in PBS++. The coverslips were again inverted onto parafilm containing 50 µl of the appropriate secondary antibody at a 1:500 concentration for 1 hour at RT. Whilst protecting the coverslips from light, they were washed three times for 5 minutes each with PBS++ in the 6 cm dishes. The coverslips were inverted onto 50 µl of DAPI dissolved in PBS with sodium azide (40 ng ml^{-1}, Sigma, D9542) for 10 minutes to visualise nuclei. After this step, the coverslips were dipped in PBS++ to wash off the excess DAPI and mounted onto microscope slides (VWR, 631-1551) with 5 µl of soft set or hard set Vectashield (Vector, H-1400, H-1700). The coverslips were

then sealed with nail varnish. The slides were imaged on a Zeiss 800 or 880 confocal microscope. After imaging Fiji (ImageJ) or Zen blue was used to export the images as .tiff files.

2.9 Bacterial growth and lysis

Bacterial transformation was performed with plasmid cDNAs with DH5α *E. coli* bacteria as the host. 1 µg of plasmid in an Eppendorf tube was incubated for 1 minute at 42 °C. Next, 50 µl of competent bacteria were added and the mixture was incubated at 42 °C for another minute, to heat shock the bacteria. The primed bacteria were added to 900 µl lysogeny broth (LB, Fisher Scientific, 1426-500) media and incubated at 37 °C for 45 minutes. After incubation, the bacteria were pelleted by centrifugation at 218 g for 1 minute. The bacterial pellet was resuspended in 100 µl of LB media and spread onto LB agar plates supplemented with 100 µg ml^{-1} ampicillin. The plates were inverted and left to grow overnight in a 37 °C incubator.

A single colony of the bacteria expressing the required plasmid was picked from a previously prepared plate that was inoculated with 100 µg ml^{-1} ampicillin (Sigma, A9518) from a 100 mg ml^{-1} ampicillin stock. The colony was then dispersed into 3 ml of autoclaved LB containing 100 µg ml^{-1} ampicillin in a 13 ml conical tube (Sarstedt, 62.515.006). The tube was placed in an incubator at 37 °C for 8 hours with vigorous shaking (200 rpm). The starter culture was then added to a conical flask containing 150 ml of the LB Broth with 100 µg ml^{-1} ampicillin and grown for 12 hours in a 37 °C incubator with vigorous shaking (200 rpm). After growth, the culture was separated into three 50 ml falcon tubes (Sarsdedt, 62.547.254) and spun down in a centrifuge (Sigma) at 4 °C and 6,000 g for 15 minutes. After discarding the supernatant some of the pellets were frozen at -20 °C to be processed later and some were lysed for plasmid purification with the Qiagen Maxiprep kit (Qiagen, 12162) explained in section 2.10. At the

end of plasmid extraction, the DNA pellet was dissolved in 1x TE buffer (10 mM Tris pH 8, (Sigma Aldrich, T1503), 1 mM EDTA (ThermoScientific, AM9260G). The dissolved plasmid DNA was then transferred to a clean 1.5 ml microcentrifuge tube (Starlab, S1615-5500). The concentration of the dissolved plasmid was measured with a NanoDrop 1000 Spectrophotometer (ThermoScientific). After the concentration was determined the plasmid was stored at -20 ^{o}C until needed for transfection.

2.10 Qiagen plasmid extraction

This protocol was undertaken with the Qiagen plasmid maxi kit. The bacterial culture was pelleted by centrifugation at 6,000 g for 15 minutes at 4 ^{o}C. The supernatant was then poured off and the pellet was resuspended in 10 ml of buffer P1. Next buffer P2 was added and the solutions were mixed by inverting 4-6 times and then incubated at RT for 5 minutes. LyseBlue was present in buffer P1 turning the solution blue. To this mix pre-chilled buffer P3 was added, this was mixed by inverting 4-6 times or until the solution turned colourless and then left to incubate on ice for 20 minutes. The solution was centrifuged at 20,000 g for 30 minutes at 4 ^{o}C, the supernatant was poured off and recentrifuged at 20,000 g for 15 minutes at 4 ^{o}C. A Qiagen-tip 500 was equilibrated by pouring 10 ml buffer QBT and allowing the buffer to enter the resin by gravity flow. The supernatant from earlier was poured into the column and entered the resin by gravity flow. The Qiagen-tip was washed with 30 ml buffer QC twice and moved through the tip by gravity flow. The DNA was eluted with the addition of 15 ml buffer QF into a clean 50 ml falcon tube. DNA precipitation was accomplished by adding 10.5 ml RT isopropanol (VWR, 20880.320) and mixing. The DNA was pelleted by centrifugation at 15,000 g for 30 minutes at 4 ^{o}C and the supernatant was carefully decanted as to not disturb the pellet. The DNA pellet was washed with 5 ml RT 70% ethanol and re-pelleted by centrifugation

at 15,000 g for 10 minutes at 4 °C and the supernatant was carefully decanted. The pellet was air-dried for 10 minutes, and the pellet was then dissolved in 100 µl of TE buffer at pH 8.0. This was then stored at -20 °C for further use.

2.11 Insulin reduction assay

For this assay, human insulin (Sigma, I9278) at a concentration of 1.7 mM was incubated with various concentrations of DTT (0 mM, 1 mM, 5 mM and 10 mM) and dithiobutylamine (DTBA, Sigma, 774405, 1 µM, 1 mM, 5 mM and 10 mM). The assay was prepared on a 96 well plate with three repeats of each sample. The plate was read on a 96 well plate reader (Thermofisher Multiskan™ FC) with readings taken every 5 minutes at 650 nm. The absorbance was then plotted on a graph against time. A 1-way ANOVA with a Dunnett's multiple comparison post ad-hoc test was performed to analyse the data.

2.12 Spinning disk microscopy

Live cell imaging was carried out to explore the effect of DTBA and other reducing agents on the ER HT1080 cells. HT1080 cells were grown on 35 mm µ-dishes with glass bottoms (Ibidi, 81158). ER tracker green, ER tracker blue or Mitotracker red (Invitrogen Thermofisher, E34251, E12353 and M7512) were added to the cells for an hour before treatment at 1:1000, 1:800 and 1:2000 respectively. The cells were then treated with 1 mM DTT, 0.1 mM DTBA or untreated and the cells were imaged for 6 hours, with images being taken every minute for ER tracker blue and green. For Mitotracker red, the cells were imaged for 3 hours with images being taken every minute. An Andor Revolution XD spinning disk confocal microscope with an Olympus 60× UPlanApo lens was used to take the images. After imaging Fiji was used to export the images as movies.

2.13 Scratch wound assay

Human BJ fibroblasts were seeded onto a 6-well plate (Greiner, 657160) which had been pre-treated with 10 µg ml^{-1} Fibronectin (Sigma, F1141) and grown to confluency. The cells were serum starved for 24 hours, and the bottom of each well was scratched 3 times with a pipette tip (0.2 ml) to create an area free of cells. After washing twice with PBS, the cells were incubated in culture media containing the following treatments: 5 mM DTT, 10 ng PDGF (Gibco, PHG0044). After 10 minutes of DTT treatment, the cells were washed and fresh serum free media (SFM) was added containing 10 ng PDGF. Cell migration was recorded with a Zeiss Cell Observer for 24 hours with images being taken every 30 minutes. The cells were kept at 37 °C and 5% CO_2 during image capture. Migration was quantified by both counting how many cells passed a reference point after 10 hours and by calculating the percentage of cells in the field of view that had passed the reference point after 10 hours. A 1-way ANOVA with a Dunnett's multiple comparison test was conducted in Prism 8 to assess statistical significance.

2.14 Immunoprecipitation

A 100 µl suspension of protein A sepharose beads in lysis buffer were incubated with the required primary antibody (Section 2.18) for 1 hour at 4 °C. The supernatant was removed, and 500 µl MNT lysis buffer was added to wash the beads. The beads were then centrifuged at 4,000 g for 1 minute at 4 °C and this wash was repeated twice. After washing the antibody bound beads, 150 µl of lysate was incubated with the beads for the required antibody-dependant time period. After incubation the beads were centrifuged, and the unbound lysate proteins were removed. The remaining beads were resuspended in MNT lysis buffer and the wash was repeated 4 times. The beads were resuspended in elution buffer (50 mM NH_4HCO_3, 50 mM DTT, 1% SDS) or 2× sample buffer and boiled at 95 °C for 5 minutes to elute the

proteins. The samples were either analysed by SDS-PAGE and Western blotting or were digested with filter aided sample preparation (FASP) and analysed by mass spectrometry.

2.15 FASP

FASP was performed with the Expedeon FASP kit (Expedeon Ltd, 44255). 30 µl or 0.4 mg of the eluted protein was first reduced with the addition of 0.05 ml of 100 µl DTT and then mixed with 200 µl of urea solution before loading onto a filter membrane. The sample was pipetted onto the filter and then spun at 14,000 g for 15 minutes. The urea wash was repeated twice. The reduced disulphide bonds in the samples were alkylated by the addition of 10 µl 10× iodoacetamide solution with 90 µl of urea solution and were left to incubate for 20 minutes in the dark. The iodoacetamide solution was removed by centrifugation at 14,000 g for 10 minutes. After this step, the samples were washed three times in urea solution and three times in 50 mM ammonium bicarbonate solution. The samples were then incubated with a 1:100 enzyme-to-protein ratio of mass spectrometry grade trypsin (Promega, V528A) for 4-18 hours at 37 ^{o}C. The spin filters which contained the digested peptides were transferred to new collection tubes. The peptides were collected with two washes of 40 µl 50 mM ammonium bicarbonate and one wash with 50 mM sodium chloride to inhibit any remaining trypsin activity.

2.16 Mass spectrometry analysis

Sample fractions which contained 5 µg peptides were analysed using an ekspert™ nanoLC 425 with low micro gradient flow module (Eksigent) attached to a quadrupole Time-Of-Flight (QTOF) mass analyser (TripleTOF 6600, SCIEX) connected to a DuoSpray source (SCIEX) and a 50-micron ESI electrode (Eksigent). The samples were loaded and then washed on a TriArt C18 Capillary guard column 1/32”, 5µm, 5 x 0.5mm trap column (YMC) and online

chromatographic separation performed over 57 minutes on a TriArt C18 Capillary column 1/32", 12 nm, S-3 µm, 150 x 0.3 mm (YMC) at a flow rate of 5 µl minute^{-1} with a linear gradient of 3-32% acetonitrile, 0.1% formic acid over 43 minutes, then to 80% acetonitrile, 0.1% formic acid over 2 minutes, held for 3 minutes before returning to 3% acetonitrile, 0.1% formic acid and re-equilibrated. Analyst software (version 1.7.1, Applied Biosystems) was used to acquire the MS and MS/MS data.

2.17 Data independent acquisition (DIA)

Samples to be analysed by SWATH were spiked with iRT peptides (Biognosys) at a ratio of 1 µg protein to 0.1 µl 10 x RT peptide mix. Protein identifications were acquired by comparing spectra against the panhuman 10000 protein 2014 spectral library in PeakView version 2.2 with SWATH acquisition microapp version 2.0 (Rosenberger, Koh, Guo, *et al.* 2014). Chromatographic retention time calibration was performed using iRT peptides, and SWATH data processing was carried out with the filters: 300 peptides per protein, 5 transitions per peptide, 95% peptide confidence threshold, 1% false discovery rate threshold and XIC width 75 ppm. Additional analysis was performed using MarkerView 1.2.1 before data was exported to Microsoft Excel and R to generate graphs and figures.

2.18 Antibodies

All the antibodies used were commercially available apart from the polyclonal anti-PDI. The polyclonal anti-sera against PDI was generated by immunising rabbits with a purified rat PDI protein preparation as described by Benham et al. The experimental conditions for the antibodies are described in the table below (table 2.1).

Table 2.1: Antibodies

Antibody	Species raised in	Application	Dilution (WB/IF)	Supplier and catalogue number
β-actin	Mouse mAb	WB	1:10000	Abcam #8224
PDI	Rabbit pAb	WB	1:1000	Benham laboratory (Benham et al., 2000)
P4HB	Mouse mAb	WB/IF	1:5000/1:100	Abcam #2792
GAPDH	Mouse mAb	WB	1:10000	Proteintech #60004-1-Ig
Ero1α	Rabbit pAb	WB	1:200	Santa Cruz H-90
AGR2	Rabbit pAb	WB/IF/IHC	1:1000/1:200/:800	Cell Signalling Technology® #DV92F
BiP	Rabbit pAb	WB	1:1000	Cell Signalling Technology® #3183
ERP44	Rabbit mAb	WB	1:1000	Cell Signalling Technology® #3798
Calnexin	Rabbit pAb	WB	1:1000	Gift from Prof. Masuru Okabe, Osaka University
SQSTM1/p62	Rabbit pAb	WB/IHC	1:1000/1:200	Cell Signalling Technology® #5114
AGR2	Rabbit mAb	WB	1:5000	Abcam #76473
MUC-5AC	Rabbit mAb	WB/IF/IHC	1:10000/1:250/1:500	Abcam #198294
ERP29	Rabbit pAb	WB	1:1000	Abcam #11420
PrxIV	Mouse mAb	WB/IF/IHC	1:2000/1:200/1:250	Abcam #16943
ALDH3A1	Rabbit pAb	IF	1:100	Proteintech #15578-1-AP
GM130	Mouse mAb	IF	1:200	BD Biosciences #610823
αTubulin	Rabbit pAb	IF	1 μg ml^{-1}	Abcam #4074
Collagen I	Goat pAb	WB/IF	1:1000/1:200	Southern Biotech #1310-01
mNeonGreen	Mouse mAb	IF	1:500	ChromoTek 32f6
P4HA1	Rabbit pAb	IF	1:100	Proteintech #12658-1-AP
ERGIC-53	Rabbit pAb	IF	1:100	Proteintech #13364-1-AP
Phospho-Lamin A/C (Ser22)	Rabbit mAb	IF	1:100	Cell Signalling Technology® #D2B2E
JOL2 (Lamin A/C)	Mouse mAb	IF/WB	1:100/1:50	(Dryer at al., 1997)
Spartin SPG20	Rabbit pAb	WB	1:1000	Proteintech #13791-1-AP
Vimentin V9	Mouse mAb	IF	1:100	Sigma #V63889
Sortillin/NT3	Rabbit pAb	WB	1:1000	Abcam #16640

3 The effect of reductive stress on the proteome of HT1080 cells

3.1 Introduction

In this chapter, the application of reducing agents and in particular a novel reducing agent dithiobutylamine (DTBA) were used *in vitro.* The speed of action of DTBA versus another reducing agent, DTT, was explored to find out if the newer reducing agent could be used at lower concentrations to achieve a similar affect. The effect of reducing agents on the complexes of oxidoreductases such as PDI interacting with Ero1α and how the reduction and oxidation states of Ero1α are affected was also investigated. SWATH proteomics was also undertaken to establish the effect that DTT and DTBA had on the proteome of HT1080 cells. The effect of reducing stress on mammalian cells is a less explored area of biology so by using proteomics and the reducing agents further mechanistic insights into biological processes can be gained in this area.

Reducing agents are used in a wide variety of biological applications. Reducing agents are used to reduce disulphide bonds *in vitro*, to analyse protein folding in cells and to stabilise free thiols in proteins and peptides (Wingfield 2001). There are a wide variety of reducing agents currently in use as molecular tools: monothiols, such as $\beta_2$mercaptoethanol and glutathione, and dithiols, such as DTT (Cleland 1963) and DTBA (Lukesh, Palte & Raines 2012), which will be discussed in this chapter.

The majority of reducing agents are based on thiols; they can reduce specific disulphide bonds in a relatively fast manner (half-life of 2 hr). The process of a thiol-disulphide exchange occurs upon the reaction of a thiol (RSH) with a disulphide (R'SSR'), which then forms a new disulphide (RSSR') and a thiol (R'SH). The new thiol comes from the original disulphide (Singh & Whitesides 1993):

$$RSH + R'SSR' \rightleftarrows RSSR' + HSR'$$

The thiol-disulphide exchange reaction occurs via means of a S_N2 nucleophilic substitution where a cleavage occurs, and a covalent S-S bond is formed. The active nucleophile is the thiolate anion (RS^-). If the reaction is too acidic, the reaction will be stopped (Benesch & Benesch 2002) as the acid quenches the thiolate anion causing it to become the thiol (RSH) which is not active. Thiol-disulphide interchange occurs via a nucleophilic attack of the thiolate anion along the S-S bond of the disulphide. This occurs when the thiolate is present, and the most electrophilic sulphur on the disulphide or the least acidic sulphur undergoes a nucleophilic attack, after which the most acidic thiol is liberated. The rate constant of this reaction is affected by many factors such as pK_a and steric hindrances that may occur in the disulphide. Increasing the pK_a of the thiols increases the nucleophilicity of the thiolate anions and this in turn increases the rate constant. The optimal rate constant occurs when the pK_a value is the same as the pH of the solution. Steric hinderance can happen if there are too many thiols present, which can occur when a third thiol is introduced. This happens because the orbital that overlaps the central sulphur decreases and the energy of the intermediate reaction increases (Antonino Fava, Iliceto, Camera, *et al.* 1957). Some proteins have thiol groups which are hard to access due to steric effects, hydrophobicity, and charge-charge repulsion. The solvent in which the reaction takes place also affects the rate that the exchange occurs, because S_N2 reactions favour an aprotic environment and the polar protic solvents have a greater stabilising effect on the reactants versus the transition state complexes, which increases the activation energy. The reaction rate of thiol-disulphide interchange reactions was found to be three orders of magnitude faster in aprotic solvents compared to in water (Singh & Whitesides 1990).

Monothiols are commonly used in the laboratory and in living organisms to reduce disulphide bonds. As mentioned previously, glutathione, a Glu-Cys-Gly tripeptide, is involved in keeping the sulphydryl groups of some proteins in their reduced form. In the laboratory, the most common monothiol reducing agent is β-mercaptoethanol (β-ME). The hydroxyl group on β-ME allows it to be soluble in water and reduces the volatility of the molecule (nevertheless it is still foul smelling) (Wingfield 2001). The pKa of β-ME is 9.5 and, because it is a monothiol, two molecules are needed to allow the reaction to proceed; to prevent the reaction from ceasing, excess reducing agent is added.

$$R'SSR' + 2(HOCH_2CH_2SH) \rightleftarrows 2(R'SH) + HOCH_2CH_2S - SCH_2CH_2OH$$

For more efficient reduction of disulphide bonds, a dithiol was created in 1963 by W.W. Cleland (Cleland 1963). He synthesised a reducing agent which featured a sterically stable cyclic disulphide; this permits two products to form from one reactant which would then cause the reaction to be displaced to the right, even in dilute solutions. Unlike β-ME, less of the reducing agent is needed to reduce disulphide bonds. W.W Cleland created two isomers from 2,3-dihydroxy-1,4-dithiobutane, DTT which is the threo isomer and dithioerythritol (DTE) which is the erythro isomer. Subsequently, DTBA has been adopted as a versatile reducing agent (Figure 3.1).

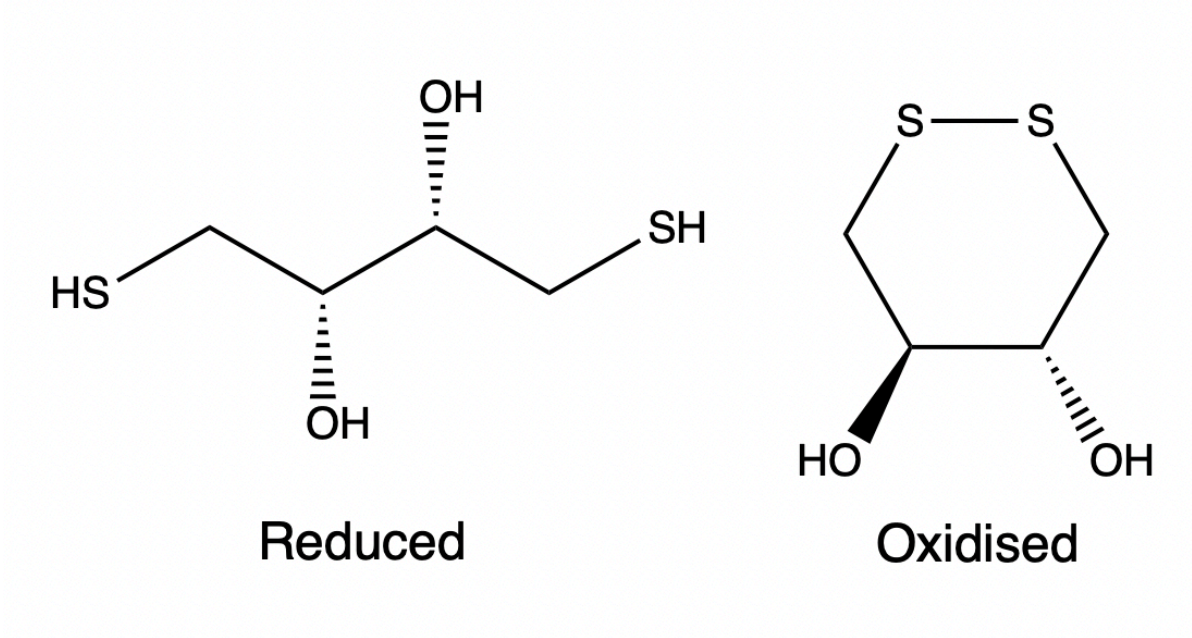

Figure 3.1: Reduced and oxidised form of DTT.

DTT is a water-soluble white solid which is less odorous than β-ME. The redox potential of DTT is -0.332 v at pH 7 and -0.366 v at pH 8.1 and its pKa is 8.3 and 9.5. This is a lower pKa compared to β-ME (pKa 9.5), meaning that a lower concentration is needed to reduce the same amount of disulphide (Jocelyn 1987). The lower concentration of DTT required to reduce a disulphide is also due to the cyclic oxidised product that is formed, its stability causes the equilibrium to move right and prevents the need of excess reducing agent such as with β-ME. The reducing capacity of DTT increases in the pH range 7 to 9.5 and the reaction can be quenched by acidification (<pH 3) (Wingfield 2001). DTT has limitations, as some intact proteins are usually only partially reduced by DTT because of the hydrophobicity of the DTT it may not be able to penetrate the protein. To bypass this, DTT is used alongside a denaturant such as SDS. Another limitation of DTT is the fact it has a very short half-life when in solution: at pH 7.5 its half-life is 10 hr, but this drops to 1.4 hr at pH 8.5 compared to 10 hr and 4 hr respectively of β-ME. To combat air oxidation, solutions of DTT should be prepared freshly before use (Stevens, Stevens & Price 1983).

Due to the limitations of DTT, alternative reducing agents have been developed to reduce disulphides in an efficient manner at a neutral pH and with a reducing potential that is similar to DTT. Lukesh et al developed a new reducing agent from aspartic acid (2S)-2-amino-1,4-dimercaptobutane (DTBA, Figure 3.2).

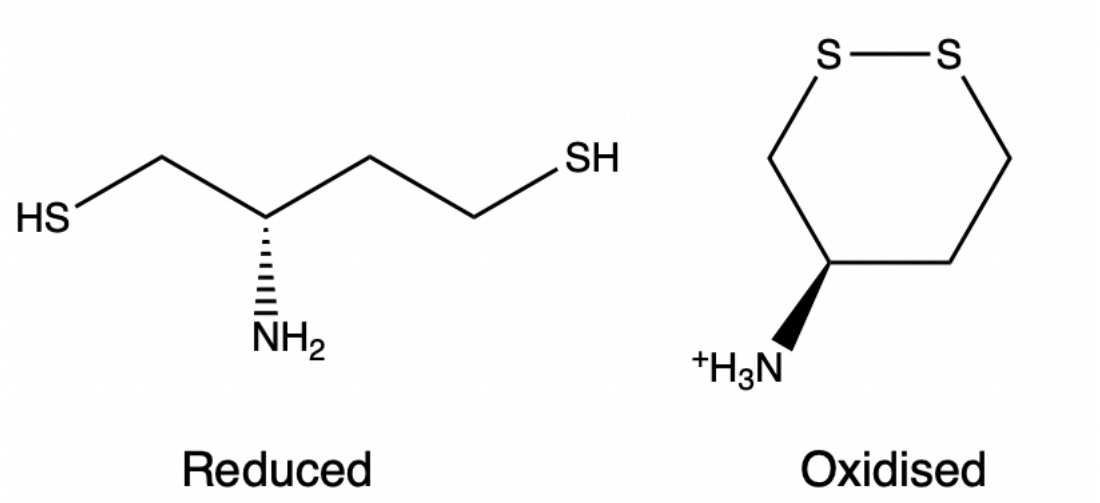

Figure 3.2: Reduced and oxidised forms of DTBA

DTBA is a nearly odourless white solid that has high solubility in water. The pKa values of 8.2 and 9.3, are both roughly one unit lower than those in DTT, and the lower pKa values are most likely due to the protonated amine group which exert strong Coulombic and inductive effects. The higher acidity of the thiols makes DTBA more suitable for certain applications than DTT where the pH is lower than 7.4, such as in certain cellular compartments like the Golgi (Adamczyk, Bal & Krężel 2015). The reduction potential of oxidised DTBA is -0.317 V and even though this is marginally less than DTT, Lukesh et al., showed that DTBA can reduce the disulphide bonds in oxidised β-ME 3.5 times faster at pH 7 than DTT is able to. DTBA also reduces oxidised glutathione 5.2 times faster than DTT at pH 7 (Lukesh, Palte & Raines 2012). Another advantage of DTBA is that the amine group allows for easy separation of DTBA by

cation exchange. The amine group in DTBA also brings some disadvantage to DTBA as it is unable to reduce certain disulphide bonds due to unfavourable Coulombic interactions (Lukesh, Wallin & Raines 2014). It also has been shown to have a high affinity to metal ions such as Zn^{2+} which means it may not be as useful when used to reduce metalloproteins, but it could be instead used in competition studies with metalloproteins (Adamczyk, Bal & Krężel 2015). DTBA is also a more expensive chemical to manufacture and purchase than DTT.

This chapter will explore the suitability of DTBA for biological applications. The ability of DTBA to reduce proteins *in vitro* and *in vivo* will be assessed and the capacity for DTBA to probe the redox system in the ER (PDI and Ero1α) will be tested. Quantitative proteomics will be used to observe how the proteome of HT1080 cells is affected by DTBA treatment, to see whether DTBA has the potential to be used as a tool to identify key proteins or protein groups involved in redox stress responses in the cell.

3.2 DTBA can reduce insulin and bovine serum albumin *in vitro* and is able to affect oxidative refolding in cells

Initial experiments were performed to evaluate the usefulness of DTBA as a reducing agent. To see how well DTBA performs as a reducing agent *in vitro*, an insulin reduction assay was performed. The assay involves reducing insulin cleaving the two interchain disulphide bridges, causing a white precipitate to form from the B chain as it is insoluble. The turbidity of the insoluble B chain can be measured with a spectrophotometer at 650 nm (Holmgren 1979). DTBA (10 mM) was able to fully reduce 1.7 mM insulin in the assay. In the same timeframe, an equivalent concentration of 10 mM DTT was unable to reduce insulin (Figure 1A). Similarly to the 10 mM DTBA, even 5 mM DTBA was able to reduce insulin before 10 mM DTT and 5 mM DTT, suggesting that even at lower concentrations DTBA is a faster reducing agent. As DTT is commonly used to reduce proteins analysed by SDS-PAGE, the suitability of DTBA in

SDS-PAGE was also investigated. Varying concentrations of DTBA were mixed with 100 µM albumin in sample buffer. These samples were then run on an SDS-PAGE gel with a 50 µM DTT-reduced sample as a loading control (Figure 1B). After electrophoresis, the gels were stained with Coomassie blue, and the reduction and oxidation states of the albumin protein were analysed. As little as 5 µM DTBA could reduce the albumin in the sample, and this experiment also showed DTBA to be compatible with Tris-Glycine-SDS electrophoresis buffers.

As DTBA was shown to reduce disulphide bonds *in vitro* successfully at low concentrations the next step was to see if it also reduced proteins successfully *in vivo.* PDI can create disulphide dependant complexes with many client proteins such as Ero1α, an ER-localised oxidoreductase (Benham, van Lith, Sitia, *et al.* 2013). Adding reducing agents such as DTT to the culture medium of the cells can cause the PDI disulphide-dependant complexes to become reduced. Replacing the media containing DTT with fresh media and allowing the cells to recover lets the complexes become re-oxidised and return to equilibrium. To investigate how DTBA performed in this assay, 1 mM DTBA was compared to 1 mM DTT. The reductants were added to the media of HT1080 cells for 10 min. This was then replaced with fresh media and the cells were allowed to recover for 0, 5, 10 and 20 min. The cells were lysed with NEM to trap the disulphide bonds and the samples were run on an SDS-PAGE gel under non-reducing (Figure 1C) and reducing (50 mM DTT added to the samples, Figure 1D) conditions, and this was followed by western blotting with an anti PDI antibody. DTT and DTBA were both able to reduce the disulphide-dependant complexes present but had no effect on the mobility of the PDI monomers (Figure 3.3C lanes 5 and 9). After replacing the media with fresh media, the more oxidised (faster running) complexes were re-established (Figure 3.3C lanes 6-8 and 10-12). As shown in the reducing gel, there was no change in the

PDI monomer due to the lack of long-distance disulphide bonds in the protein. For both experiments, actin was used as a loading control. Both the *in vitro* and *in vivo* experiments show that DTBA is a capable reducing agent that is reversible and can reduce disulphide bonds in living cells at the same or lower concentrations as DTT.

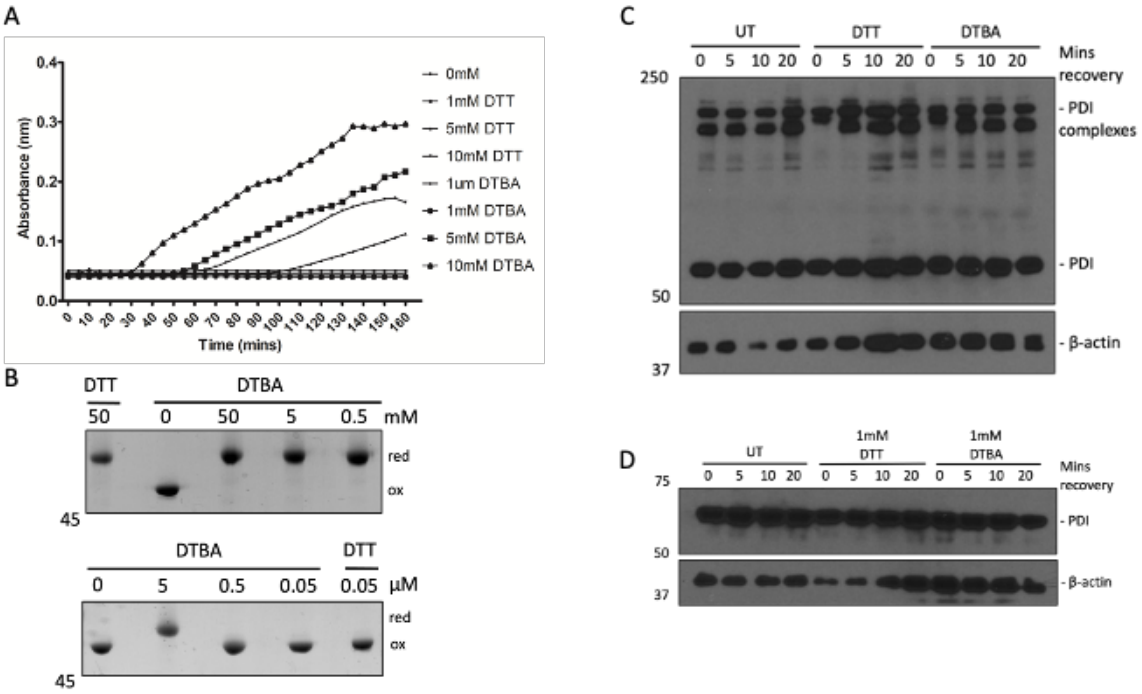

Figure 3.3: *In vitro* reduction of proteins by DTBA. (A) Reduction of 1.7 mM insulin by 0-10 mM DTBA and DTT was measured at OD 650 nm. DTBA reduces insulin more effectively than DTT. (B) Albumin mixed with Laemmli sample buffer containing 5-500 µM DTBA was analysed by SDS-PAGE and Coomassie Blue staining. 50 mM DTT was used as a control for reduction. Red = reduced albumin; ox = oxidised albumin. (C, D) HT1080 cells were untreated or treated for 10 min with medium containing 1 mM DTT or 1 mM DTBA, washed and "chased" for 0, 5, 10 or 20 min. Cell lysates were analysed by SDS-PAGE and WB under non-reducing (C) or reducing (D) conditions for PDI and β-actin expression (control). Both DTT and DTBA reduce disulphide dependent PDI complex that reoxidises within 5 min of recovery. kD markers are indicated on the left (B, C and D).

3.3 Reducing conditions caused by DTT and DTBA induce ER remodelling

As DTT can cause reductive ER stress in cellular systems, the question was asked if DTBA is also able to cause reductive stress and at what concentrations it is able to do this (Rand & Grant 2006). HT1080 cells were stained with one of three organelle trackers: ER tracker green, ER tracker blue or mitotracker red to visualise the difference between DTT and DTBA treatment. The HT1080 cells were stained with one of the tracker dyes, treated +/- 0.1 mM DTBA or +/- 1 mM DTT and live cell imaged on a spinning disk microscope. Because DTBA is a more effective reducing agent, a lower concentration used for these experiments. Both

reducing agents were able to elicit a response in the HT1080 cells whilst having minimal cell rounding. Shortly after the cells were exposed to DTBA, ER tracker green relocated from the ER to the cellular membrane (Figure 3.4 C, D). No effect was seen in the mitochondrial distribution (Figure 3.4 I, J) after DTBA treatment. No relocation of ER tracker green was observed in the control treated cells. However, dye relocalisation was observed in the cells treated with DTT, nothing that the higher concentration of DTT and the laser exposure from the microscope at higher imaging frequencies negatively affected the cells adhesion. No dye redistribution was observed in the cells stained with ER tracker blue (Figure 3.5). The difference in distribution of the two ER tracker dyes is due to the fact they both target different parts of the ER. ER tracker green is a BODIPY labelled glibenclamide dye which targets the sulfonylurea receptors and ER tracker blue targets lipids present in the ER, although the lipid specificity of ER tracker blue is not known (Zünkler, Wos-Maganga & Panten 2004). The results indicate that reducing agents such as DTT and DTBA can affect ER membrane protein localisation but not the lipids in the ER or mitochondria. It may be possible to use BODIPY labelled glibenclamides for redox stress labelling. In the future it would be advantageous to test this dye with other reducing agents such as β-ME to see if a similar effect is observed. It would also be advantageous to treat HT1080 cells with DTT and DTBA for a period and then replace the media with fresh media and image the cells after a recovery period in live cell imaging.

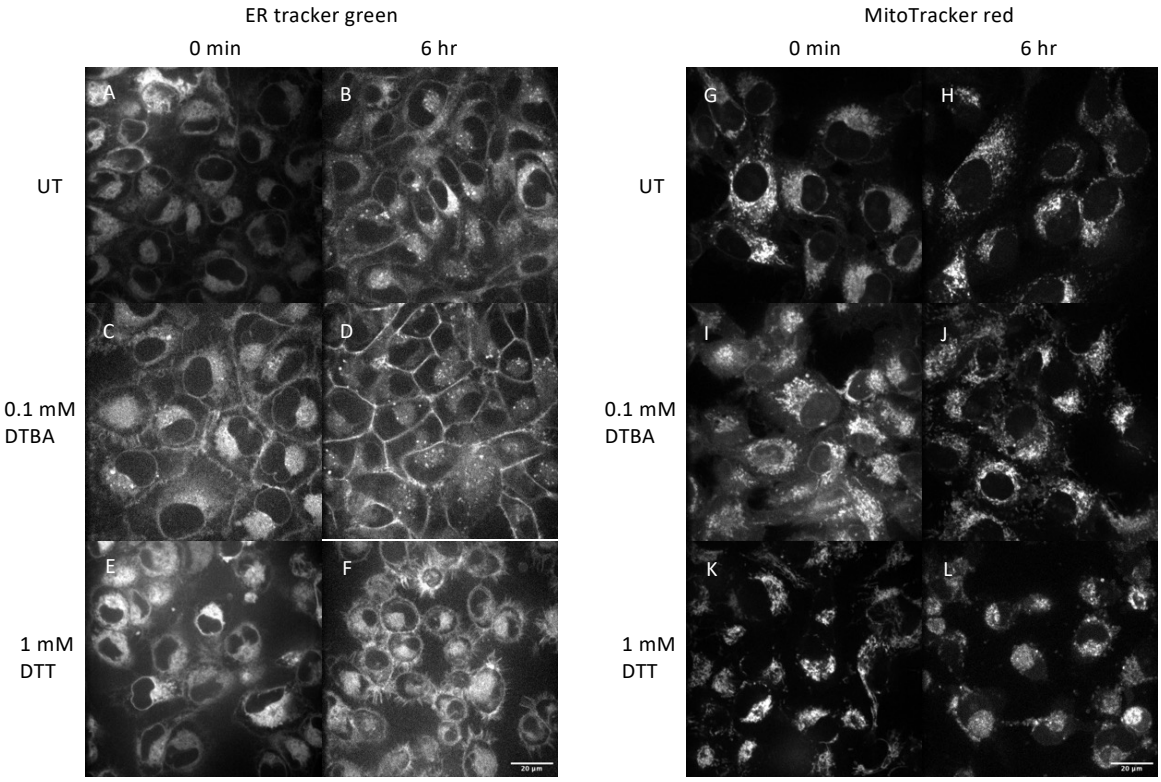

Figure 3.4: Live cell imaging of reductively challenged HT1080 cells. HT1080 cells were incubated with ER-Tracker green (panels A, B, C, D, E, F) or MitoTracker red (panels G, H, I, J, K, L), and untreated treated (A, B, G, H), treated with 0.1 mM DTBA (C, D, I, J) or 1 mM DTT (E, F, K, L). Images were taken at 0 min and after 6 hr. Redistribution of ER tracker green occurred upon reductive stress (panels F and J). UT = untreated; scale bar = 20 µM.

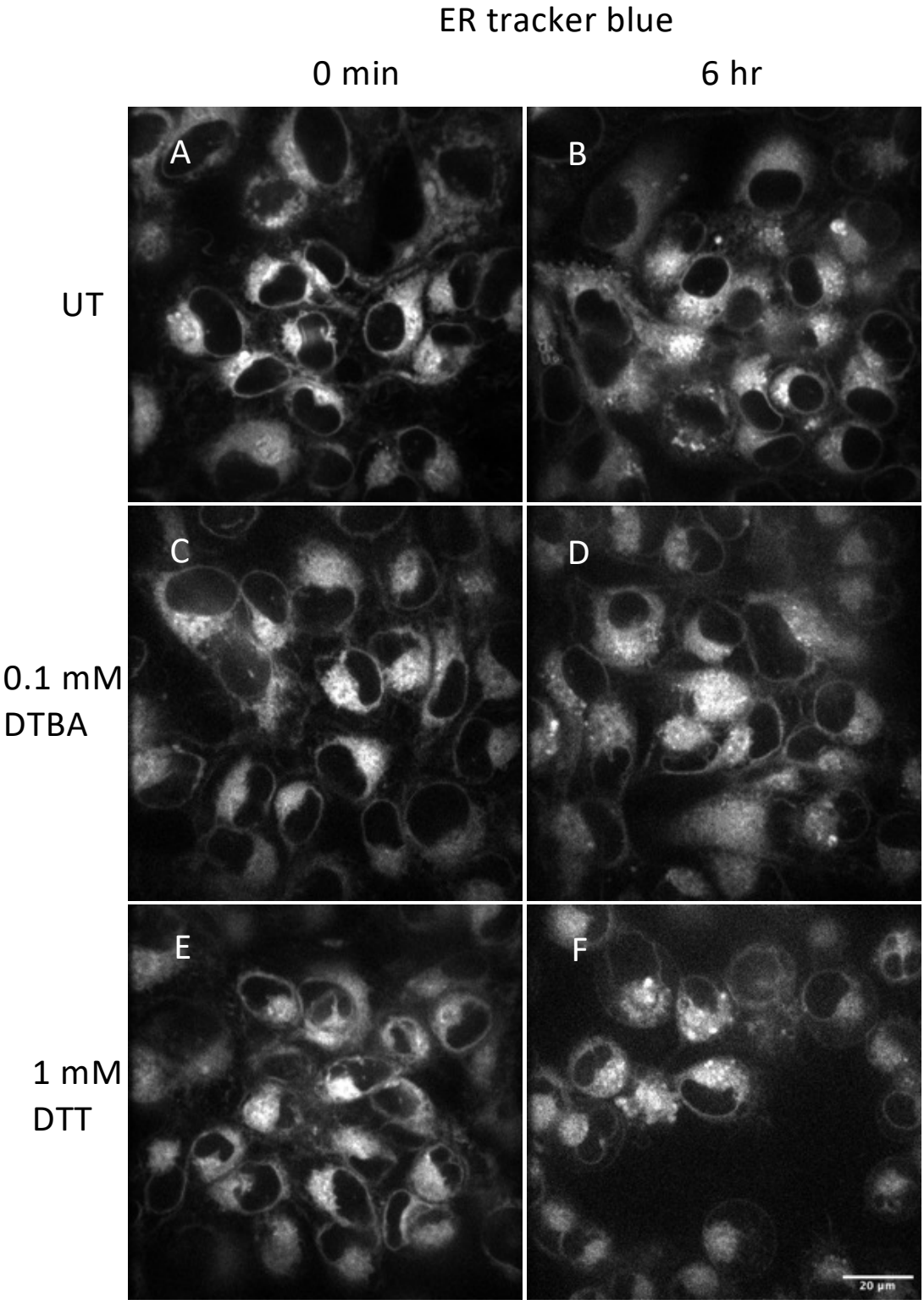

Figure 3.5: Live cell imaging of the ER in reductively challenged HT1080 cells. HT1080 cells were incubated with ER-Tracker blue and mock treated (A-B), treated with 0.1 mM DTBA (C-D) or 1 mM DTT (E-F). Images were taken at 0 min and after 6 hr. There was no redistribution of ER-Tracker™ blue upon treatment (panels D and F). UT = untreated; scale bar = 20 µM.

3.4 Quantitative DIA proteomics of HT1080 cells subjected to 1 mM DTBA

Several environmental stresses (osmotic, hypoxic and pH stress) can cause a shift in the redox balance of the cell. This can create reactive oxygen species (ROS) such as the hydroxyl radical and hydrogen peroxide in the cell and lead to cell stress. This cellular stress can affect the cells proteome in various ways such as protein post translational modifications (PTM) either directly or indirectly with ROS interaction. Some examples of these PTM are S-nitrosylation and carbonylation (McDonagh 2017). Investigating how the proteome is affected by reductive stress may also provide some insight into alterations in protein trafficking that might explain the live cell imaging results (Figure 3.4, 3.5). To test the effect of DTBA treatment on the HT1080 cells, they were treated +/- 1 mM DTBA for 0 or 1 hr, lysed and then analysed by DIA MS (Figure 3.6A). The advantage of using DIA MS and analysing the data with SWATH is that label free quantification of proteins in the cell can be performed. Around 4000 proteins were identified by SWATH from the HT1080 cells treated +/- 1 mM DTBA, and of these 4000 there were 24 significant hits (FDR adjusted $p<0.05$). Of these 24 proteins, 13 were upregulated (Table 3.1) and 11 were downregulated (Table 3.2) by 2-fold when cells were treated with DTBA (Figure 3.6C). Of the key proteins up and down regulated, at least 10 of the 24 identified are involved in cytoskeletal and organelle organisation (Figure 3.6C). To confirm the mass spectrometry results, spartin was analysed by western blotting (Figure 3.6B). Consistent with the proteomic results, spartin levels were lower in DTBA treated cells than the control and actin blot.

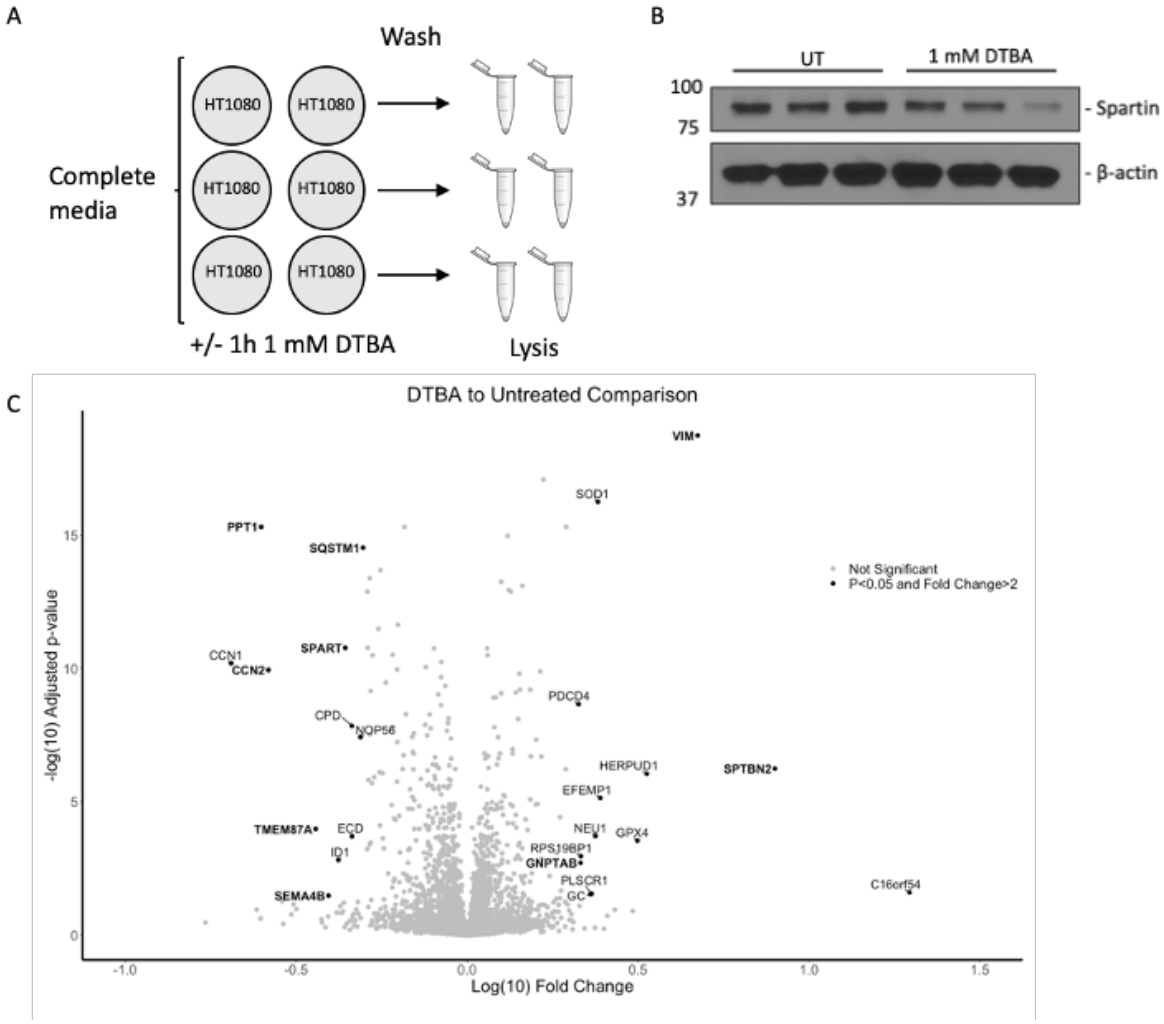

Figure 3.6: DIA proteomic analysis of HT1080 cells subjected to DTBA. (A) Schematic. Lysates from 6 biological repeats for each state were trypsinised and used for MS analysis with 3 technical injections for each. (B) Three independent lysates from cells treated +/- 1 mM DTBA for 1 hr were analysed by SDS-PAGE and WB. Spartin decreased after 1 hr treatment with 1 mM DTBA; β-actin was used as a loading control. (C) Protein identification and relative quantification was achieved using SWATH acquisition on a TripleTOF 6600 (SCIEX). Proteins with a significant (FDR-adjusted $p<0.05$) and fold change > 2 are labelled on the volcano plot. Proteins in bold are involved in trafficking and cytoskeletal organisation.

Table 3.1: Proteins significantly increased >2-fold by 1 mM DTBA.

Gene Name	P value	Fold change	Log fold change	GO Function
C16orf54	0.025	19.67	1.29	NA
SPTBN2	5.76E-07	7.94	0.90	Actin cytoskeleton organisation
VIM	1.87E-19	4.72	0.67	Intermediate filament organisation
HERPUD1	9.00E-07	3.35	0.53	Transmembrane transporter targeting
GPX4	0.0003	3.15	0.50	Response to oxidative stress
EFEMP1	7.22E-06	2.45	0.39	Epidermal growth factor receptor signalling pathway
SOD1	5.76E-17	2.41	0.38	Response to superoxide
NEU1	0.0002	2.37	0.38	Oligosaccharide catabolic process
PLSCR1	0.028	2.31	0.36	Apoptotic process
GC	0.029	2.29	0.36	Vitamin transport
RPS19BP1	0.001	2.15	0.33	NA
GNPTAB	0.002	2.15	0.33	Lysosome organisation
PDCD4	2.20E-09	2.12	0.33	Apoptotic process

Table 3.2: Proteins significantly decreased >2-fold by 1 mM DTBA.

Gene Name	P value	Fold change	Log fold change	GO Function
SQSTM1	3.00E-15	0.50	-0.30	Autophagy
NOP56	3.78E-08	0.49	-0.31	rRNA processing
ECD	0.0002	0.46	-0.34	mRNA processing
CPD	1.45E-08	0.46	-0.34	Protein processing
SPART	1.72E-11	0.44	-0.36	Cell division
ID1	0.0015	0.42	-0.38	Cell differentiation
SEMA4B	0.0334	0.39	-0.41	Positive regulation of cell migration
TMEM87A	0.0001	0.36	-0.44	Retrograde transport, endosome to Golgi
CCN2	1.15E-10	0.26	-0.58	Cell adhesion
PPT1	4.99E-16	0.25	-0.60	Lipid catabolic process
CCN1	6.43E-11	0.20	-0.69	Cell adhesion

3.5 Restructuring of the cytoskeletal network in HT1080 cells after DTBA induced reductive stress

One of the proteins with a high fold change and significance was vimentin (P value 1.87×10^{-19}, fold change 4.72). The proteomic results suggested that 1 mM DTBA treatment affected the cellular cytoskeleton. To validate the proteomic results, HT1080 cells were treated +/- 1 mM DTBA for 10 min or 1 hr and then fixed and stained for confocal microscopy. After treatment, the cells remained attached to the coverslips, and overall nuclear and ER structures were unaffected by the DTBA treatment, indicating that the cells remained viable. The DAPI stain remained nuclear and the PDI stain remained perinuclear, suggesting there has been no redistribution of PDI in the ER and that KDEL sequence function was unaffected. Vimentin showed marked changes after treatment with DTBA for 10 min and further changes

after 1 hr treatment. When compared to the control (Figure 3.7A) there is an increase in the appearance of longitudinal stress fibres (Figure 3.7C).

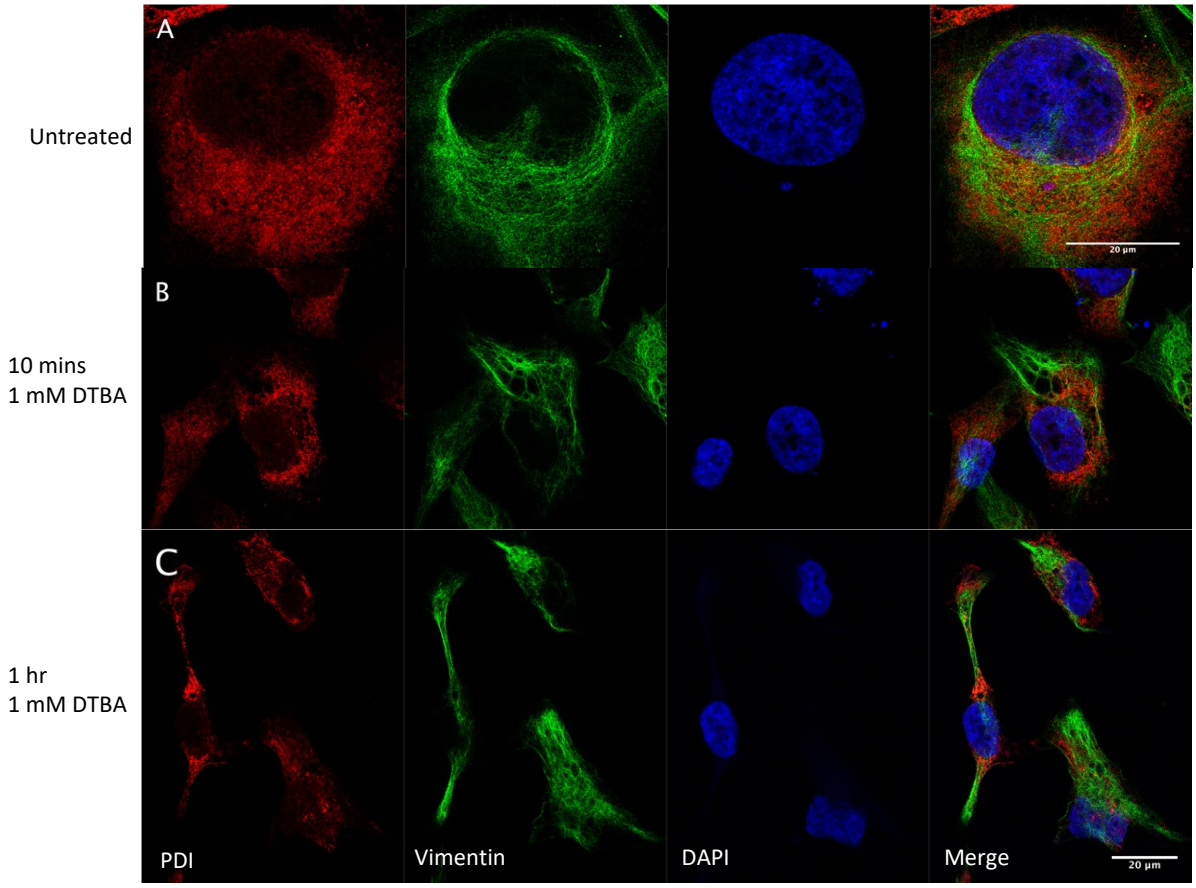

Figure 3.7: Reorganisation of vimentin after DTBA-induced reductive stress. HT1080 cells were (A) untreated, (B) treated with 1 mM DTBA for 10 min or (C) treated with 1 mM DTBA for 1 hr, prior to fixing and staining for vimentin and PDI. DAPI was used to stain the nucleus. Confocal microscopy showed that PDI remained ER localised whereas vimentin stress fibres were prominent after DTBA treatment. NT = not treated. Images were taken on a Zeiss 800 confocal microscope at 63x.

3.6 Lower concentrations of DTBA are able to affect oxidative refolding in HT1080 cells

As DTBA has been shown to be a stronger reducing agent than DTT, the next experiment was performed to show that a lower concentration than 1 mM, DTBA can still reduce disulphide-bonded protein complexes *in vivo*. Similarly to before (Figure 3.1C), HT1080 cells were treated with 5 µM and 100 µM DTBA; and 5 µM, 100 µM and 5 mM DTT for 10 min, lysed and run on a SDS-PAGE gel under non-reducing (Figure 3.8A) and reducing conditions (Figure 3.8B). As before, 100 µM DTBA was able to reduce the PDI and Ero1α complexes in

the non-reducing gel. DTBA also had no effect on the PDI or Ero1α monomer as shown in the reducing gel. β-actin was used as a loading control for both experiments. This experiment shows that DTBA is capable of reduction in living cells at even lower concentrations than previously shown.

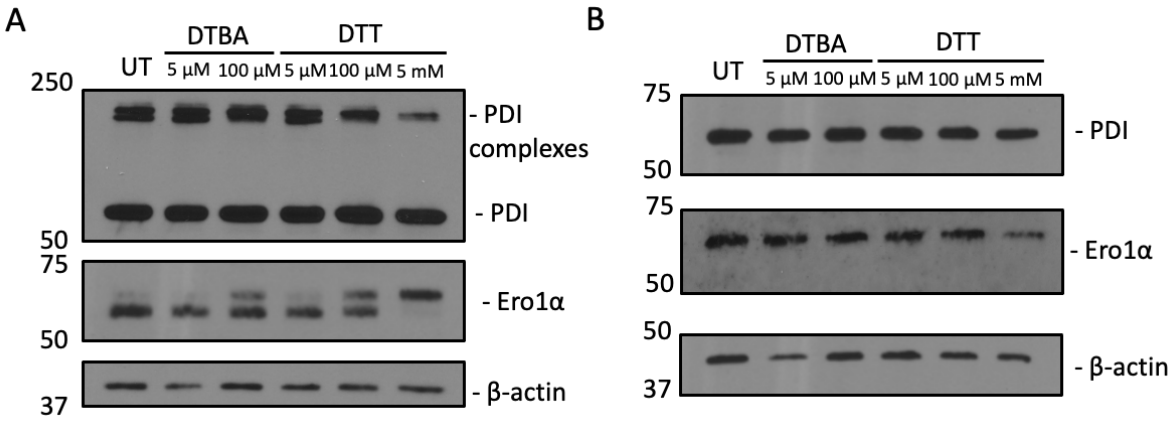

Figure 3.8: *In vitro* reduction of protein complexes by DTBA and DTT with NEM. HT1080 cells were treated with 5, 100 µm DTBA/DTT and 5 mM DTT for 10 min. The cell lysates were analysed with SDS-PAGE and WB under non-reducing (A) and reducing (B) conditions. The blots were blotted with Ero1α, PDI and β-actin was used as a loading control. Treatment with 100 µm DTBA and DTT caused a loss of PDI complex formation similarly with the 5 mM treatment of DTT.

3.7 Quantitative DIA proteomics of HT1080 cells subjected to 100 µM DTBA

As 100 µM DTBA was able to affect the biology of HT1080 cells, a SWATH experiment was performed once again to find out if 100 µM DTBA and a longer time of treatment would affect the homeostasis of the HT1080 cells proteome. HT1080 cells were treated +/- 100 µM DTBA for 1 hr or overnight, lysed and analysed by DIA MS (Figure 3.9). Approximately 5000 proteins were identified in SWATH when comparing +/- DTBA for 1 hr (Figure 3.10A) and when comparing +/- DTBA overnight (Figure 3.10B).

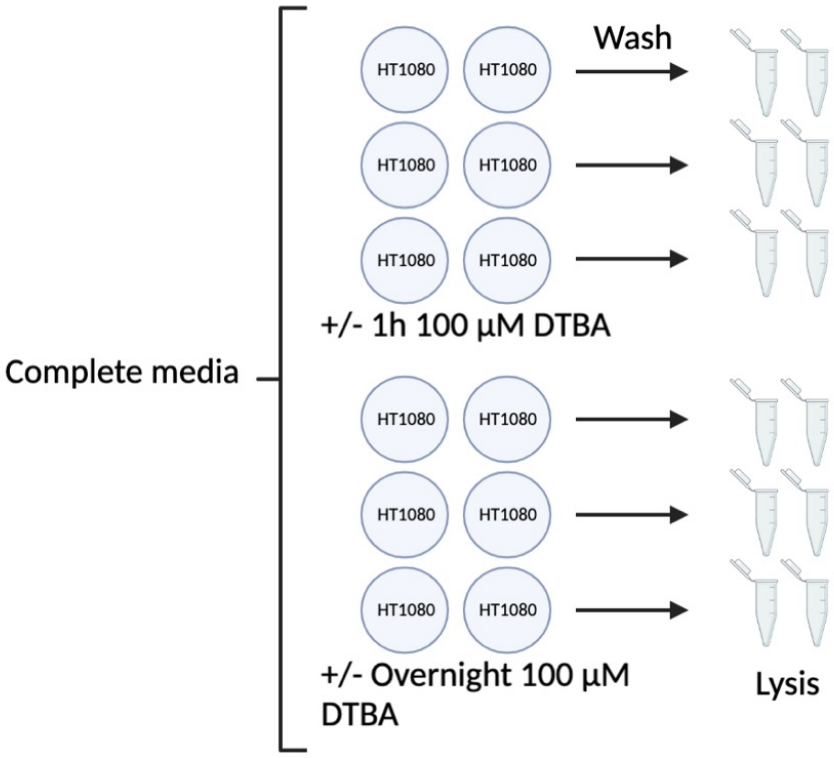

Figure 3.9: DIA proteomic analysis of HT1080 cells subjected to DTBA. Schematic. Lysates from 6 biological repeats for each state were trypsinised and used for MS analysis with 3 technical injections for each.

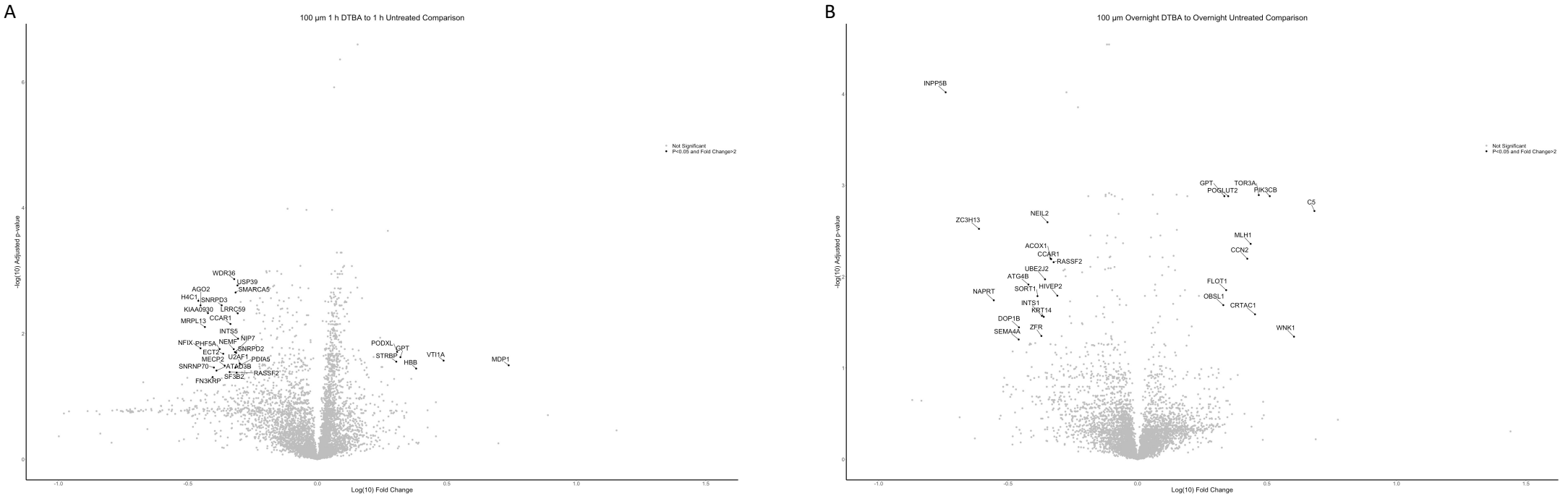

Figure 3.10: DIA proteomic analysis of HT1080 cells treated with a 100 µM concentration of DTBA. HT1080 cells were treated +/- 100 µM DTBA for either 1 hr or overnight. The lysates from 12 biological repeats were used for MS analysis with 3 technical injections for each. Protein identification and relative quantification was achieved using SWATH acquisition on a TripleTOF 6600 (SCIEX). Proteins with a significant (FDR-adjusted $p<0.05$) and fold change > 2 are labelled on the volcano plot. (A) 100 µM DTBA for 1 hr vs untreated 1 hr. (B) 100 µM DTBA overnight vs untreated overnight.

Of these 5000 proteins in the +/- 100 µM DTBA 1 hr comparison, there were 31 proteins with a significant negative or positive fold change (FDR adjusted $P<0.05$) (Table 3.3). Of these 31 proteins, there were 6 proteins upregulated and 25 which were downregulated (Figure 3.11).

Table 3.3: Proteins significantly increased or decreased >2-fold by 100 µm DTBA for 1 hr.

Gene Name	Fold change	P value	Log fold change	GO Function
MDP1	5.479	0.032	0.739	NA
VTI1A	3.071	0.027	0.487	Autophagy
HBB	2.406	0.036	0.381	Oxygen transport
GPT	2.092	0.024	0.321	Response to starvation
PODXL	2.032	0.020	0.308	Cell adhesion
STRBP	2.016	0.028	0.305	Mechanosensory behaviour
U2AF1	0.501	0.030	-0.300	mRNA processing
INTS5	0.494	0.012	-0.307	snRNA processing
LRRC59	0.492	0.005	-0.308	Signal transduction
USP39	0.49	0.002	-0.309	Cell cycle
SF3B2	0.488	0.042	-0.312	mRNA processing
SNRPD2	0.485	0.020	-0.314	RNA splicing
SMARCA5	0.483	0.002	-0.316	DNA repair
PDIA5	0.482	0.035	-0.317	Protein folding
NIP7	0.480	0.020	-0.318	Ribosome assembly
WDR36	0.477	0.001	-0.321	rRNA processing
NEMF	0.475	0.020	-0.323	Nuclear export
CCAR1	0.461	0.007	-0.336	Cell cycle
RASSF2	0.458	0.041	-0.339	Cell cycle
MECP2	0.438	0.032	-0.358	Protein localisation
ECT2	0.433	0.021	-0.364	Cell differentiation
SNRPD3	0.427	0.004	-0.370	RNA splicing
PHF5A	0.419	0.018	-0.378	mRNA splicing, via spliceosome
ATAD3B	0.407	0.039	-0.390	Mitochondrial organisation
SNRNP70	0.398	0.035	-0.400	mRNA splicing, via spliceosome
FN3KRP	0.394	0.049	-0.405	Phosphorylation
KIAA0930	0.378	0.005	-0.423	NA
MRPL13	0.368	0.008	-0.435	Translation
AGO2	0.354	0.004	-0.452	Translation
NFIX	0.354	0.017	-0.452	DNA replication
H4C1	0.347	0.003	-0.461	Nucleosome assembly

In the +/- 100 µM DTBA treatment overnight, there were 27 significant proteins (FDR adjusted P<0.05) (Table 3.4). Of these 27 proteins, that were identified, 11 were upregulated and 16 were downregulated.

Table 3.4: Proteins significantly increased or decreased >2-fold by 100 µm DTBA overnight.

Gene Name	Fold change	P value	Log fold change	Go Function
C5	4.819	0.002	0.683	Complement activation
WNK1	4.019	0.045	0.604	Ion homeostasis
PIK3CB	3.240	0.001	0.511	Autophagy
TOR3A	2.938	0.001	0.468	NA
CRTAC1	2.842	0.025	0.454	Axonal fasciculation
MLH1	2.733	0.004	0.437	Mismatch repair
CCN2	2.653	0.006	0.424	Cell adhesion
POGLUT2	2.239	0.001	0.350	Protein O-linked glycosylation via serine
FLOT1	2.199	0.014	0.342	Protein localisation to plasma membrane
GPT	2.164	0.001	0.335	Biosynthetic process
OBSL1	2.144	0.021	0.331	Cytoskeletal organisation
HIVEP2	0.490	0.016	-0.310	Regulation of transcription by RNA polymerase II
RASSF2	0.474	0.007	-0.324	Cell cycle
CCAR1	0.464	0.006	-0.334	Cell cycle
ACOX1	0.461	0.006	-0.336	Fatty acid oxidation
NEIL2	0.449	0.003	-0.348	Base-excision repair
UBE2J2	0.439	0.011	-0.357	Protein polyubiquitination
KRT14	0.434	0.028	-0.362	Ageing
INTS1	0.427	0.027	-0.370	Inner cell mass proliferation
ZFR	0.425	0.045	-0.372	NA
SORT1	0.411	0.016	-0.387	Endocytosis
ATG4B	0.379	0.012	-0.422	Autophagy
DOP1B	0.348	0.036	-0.458	Protein transport
SEMA4A	0.347	0.049	-0.459	Regulation of cell shape
NAPRT	0.278	0.018	-0.556	Response to oxidative stress
ZC3H13	0.244	0.003	-0.613	mRNA processing
INPP5B	0.181	9.56E-05	-0.741	Regulation of protein processing

One of the main groups of proteins that were affected with 100 µM DTBA treatment were those involved in vesicle transport such as sortilin 1 (SORT1). To validate the MS results, SORT1 was analysed by western blotting. Consistent with the proteomic data, (Figure 3.10), SORT1 decreased after DTBA treatment (Figure 3.11).

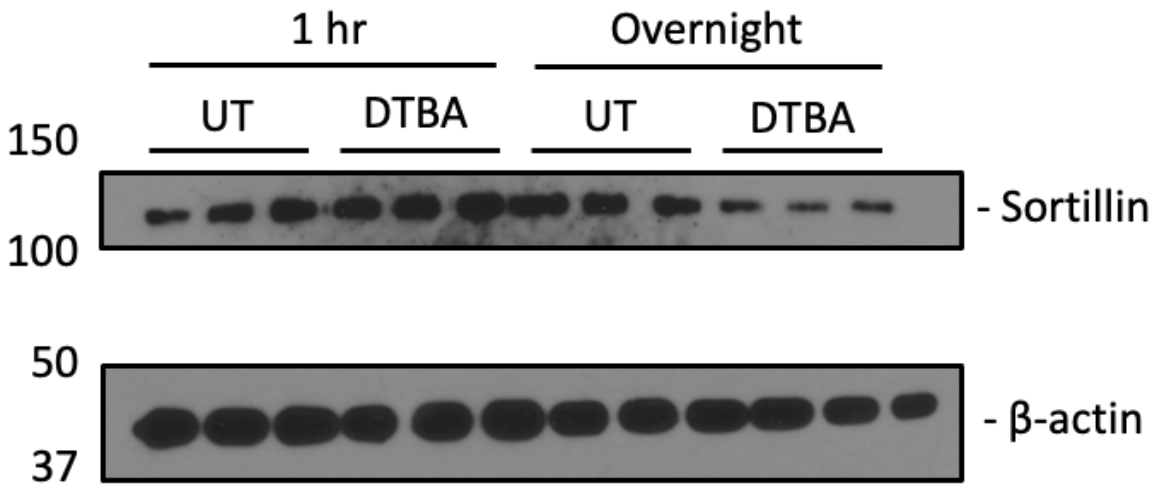

Figure 3.11: WB analysis of Sortillin changing in 100 µM DTBA SWATH analysis. Three independent lysates from cells treated +/- 100 µM DTBA for 1 hr or overnight were analysed by SDS-PAGE and WB. β-actin was used as a loading control.

To establish if a longer exposure of DTBA treatment affects the cell's proteome, the significant proteins in both the +/- 100 µM 1 hr DTBA treatment and the +/- 100 µM overnight DTBA treatment were taken and analysed with an R script which takes the gene name and finds the GO ID for the respective protein (Figure 3.12, 3.13). These data were then plotted on graphs which display the biological processes (Figure 3.12A, 3.13A), the molecular function (Figure 3.12B, 3.13B) and cellular compartment (Figure 3.12C, 3.13C). When comparing the information from both treatment times overall, there were not large differences. However, in the overnight treatment there were more signalling and localisation identifiers apparent. This data suggests that the HT1080 cells are still affected by 100 µM DTBA treatment whether it is 1 hr or overnight, but a different subset of proteins is affected. Whereas with the 1 mM

DTBA treatment the cellular cytoskeleton was largely affected, when the concentration of DTBA is reduced to 100 µM the cellular vesicle transport becomes affected.

A

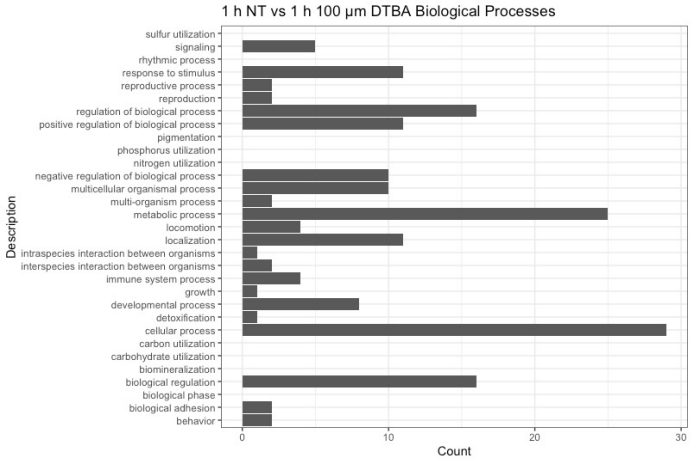

B

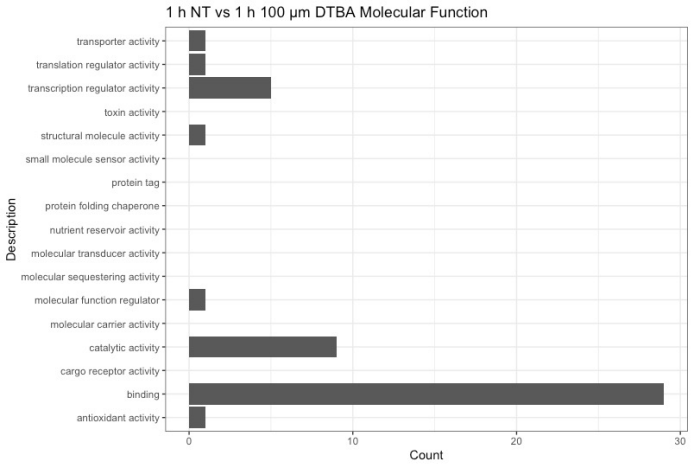

C

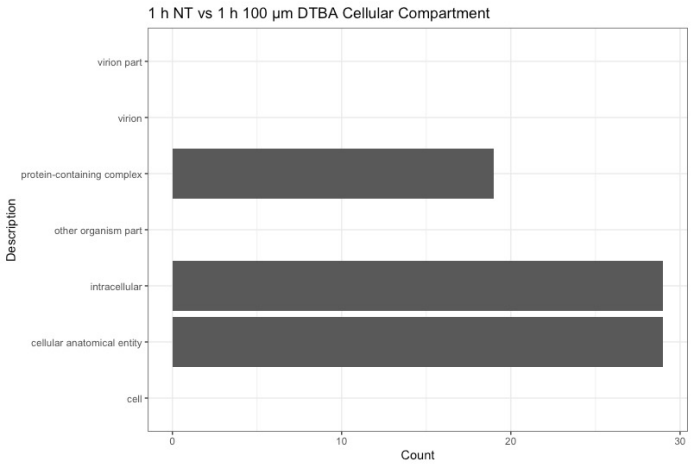

Figure 3.12: GO analysis of proteomic data from SWATH of HT1080 cells treated +/- 100 µM DTBA for 1 hr. The significant (FDR-adjusted $p<0.05$) SWATH data with a fold change > 2 was converted to GO terms in R. These were then plotted based on (A) biological processes, (B) molecular function and (C) cellular compartment.

A

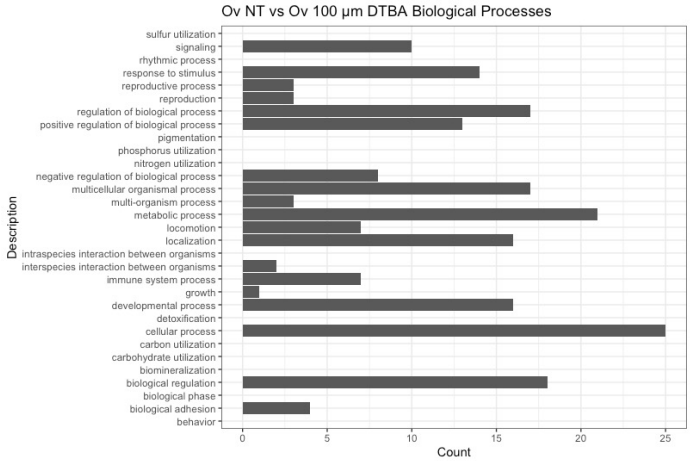

B

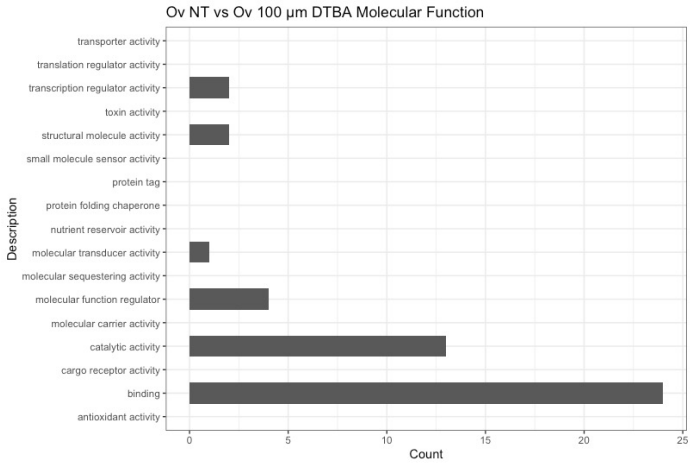

C

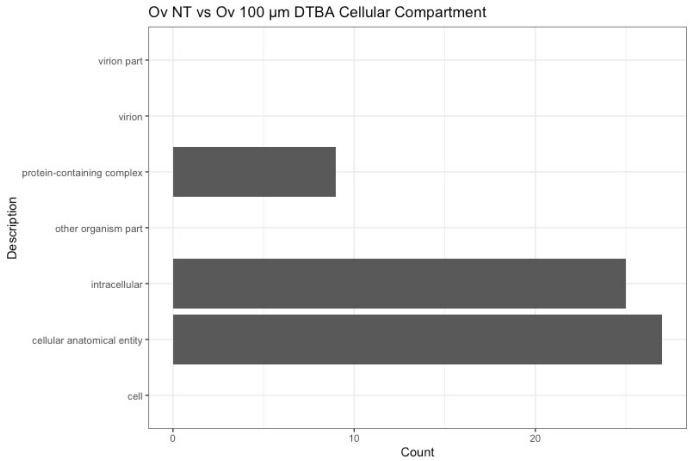

Figure 3.13: GO analysis of proteomic data from SWATH of HT1080 cells treated +/- 100 µM DTBA overnight. The significant (FDR-adjusted $p<0.05$) SWATH data with a fold change > 2 was converted to GO terms in R. These were then plotted based on (A) biological processes, (B) molecular function and (C) cellular compartment.

In summary DTBA has been shown to be a potent reducing agent and is suitable for a range of biological applications (Figure 3.3). It has also shown to be suitable for live cell imaging redox studies and exhibits less cellular toxicity than DTT (Figure 3.4). Using DIA to analyse various concentrations of DTBA treatment to HT1080 cells has identified key pathways affected by reductive stress such as the cellular cytoskeleton and vesicle transport within the cells. Future experiments would involve further analysis and validation of the proteomic results using western blotting and immunofluorescence to observe how other identified proteins are affected by the DTBA treatment.

3.8 Discussion and conclusion

The results in this chapter identify novel redox responsive proteins that increase and decrease after cells experience reductive stress induced by DTBA (Figure 3.6). Some of the proteins that change are those involved in proteostasis, protein trafficking and cytoskeletal organisation. One of the key proteins which saw a fold change increase of 4.72 when compared to the untreated after 1 mM DTBA treatment was vimentin, where changes in the organisation of vimentin were also observed by IF (Figure 3.7). Other work has shown that C328 is targeted by oxidative modifications such as glutathionylation, nitrosylation or carbonylation and is key for vimentin network reorganisation as it is involved in vimentin subunit exchange. Similarly to the work presented in this chapter, when vimentin is exposed to oxidative stress it causes the remodelling of vimentin networks present in the cell (Mónico, Duarte, Pajares, *et al.* 2019; Pérez-Sala, Oeste, Martínez, *et al.* 2015). Other intracellular organisational proteins were also affected when treated with 1 mM DTBA such as the spectrin SPTBN2 which associates with the Golgi and is involved in vesicular membrane skeletons, it is thought to assist in the post-Golgi transport of trafficking vesicles (Stankewich, Tse, Peters, *et al.* 1998). The other protein

is TMEM87A which mediates endosome to Golgi retrograde and anterograde transport (Hirata, Fujita, Nakamura, *et al.* 2015). After treatment with 100 µM DTBA a wider set of redox responsive proteins were observed to change. Although this work was very preliminary, proteins which were involved in vesicle transport were identified to change after the addition of the lower concentration of DTBA (Table 3.4). One of these proteins was SORT1 which was shown to be downregulated after DTBA treatment and saw a fold change decrease of 0.41 (Figure 3.11). SORT1 is a type I membrane glycoprotein involved in vacuolar protein sorting (Petersen, Nielsent, Nykjaer, *et al.* 1997). Another protein which was observed to be upregulated after 100 µM DTBA treatment was FLOT1 which saw a fold change of 2.21 when compared to the non-treated samples, this protein is involved in vesicle trafficking and cell morphology and can localise to the caveola (Bickel, Scherer, Schnitzer, *et al.* 1997). The changes in protein levels after two different DTBA treatments agrees with previous work which shows that redox stress can affect cells differently, thus changing the concentration of the reducing agent varies the amount of stress a cell experiences (Murray, Whitfield, Trinklein, *et al.* 2004). Different cell types also are affected by reductive stress differently, for example collagen levels were observed to be sensitive to reductive stress in fibroblasts which are professional architects of ECM deposition (Carne, Bell, Brown, *et al.* 2019).

When analysing how ER resident proteins were affected by DTBA treatment, it was observed that PDI (an ER resident chaperone), the mitochondria and ER tracker blue localisation was unaffected by DTBA treatment (Figure 3.4, 3.5 and 3.7). These results showed that the KDEL retention mechanism for PDI remained functional, as was the integrity of the ER membrane. Similar results have been observed when HEPG2 cells were treated with 2 mM DTT. In this case, soluble secreted proteins were retained in the ER when disulphide bonds were unable to be formed (Lodish & Kong 1993). This did not occur in the ER tracker green

stained cells, where the fluorescent glibenclamide was observed to be redistributed from the ER membrane to the plasma membrane of the HT1080 cells (Figure 3.4). This suggests that reducing agents may causes receptors such as the sulfonylurea receptor (SUR1, which is the target of glibenclamide) to no longer be retained in the ER. One possibility is that SUR1 can be retained in the ER by a disulphide bond, and that the treatment with DTT and DTBA causes this disulphide bond to be reduced, allowing release to the plasma membrane (Fukuda, Aguilar-Bryan, Vaxillaire, *et al.* 2011).

The data presented in this chapter shows that DTBA is a suitable alternative to DTT in a range of biological applications such as reducing samples for WB analysis, and it can be used at lower concentrations (Figure 3.4). Since the intracellular levels of DTBA in the cells is unknown, the concentration at which DTBA becomes toxic to cells can only be establish empirically. The use of DIA MS has allowed for the analysis of the redox proteome for further downstream study into how reducing stress affects HT1080 cells. Finally, the work on the glibenclamide dye and sulfonylurea receptor will allow further work into studying genes and finding drugs which are involved in protein trafficking in diabetes as sulfonylurea receptors are involved in insulin exocytosis.

4 Studying the AGR2 interactome reveals novel interacting partners of AGR2

4.1 Introduction

In this chapter, the PDI family member AGR2 was investigated in mucus producing oesophageal cells. Studies in this chapter included observing how AGR2 varies between different immortalised oesophageal cell types and how AGR2 maps to different stages of cancer. The interaction partners of AGR2 were also investigated to determine if there were any novel targets for manipulating AGR2 in protein quality control.

AGR2 is a 19 kDa protein that is a member of the PDI family. It was first discovered in *Xenopus laevis* and was named XAG-2. In the African clawed frog, it regulates dorsoanterior ectodermal fate and it is required for the formation of the cement gland (Aberger, Weidinger, Grunz, *et al.* 1998). Ivanova et al also showed that AGR genes play a critical role in the limb regeneration of salamanders and AGR2 was shown to be involved in the limb and tail regeneration of frog tadpoles (Ivanova, Tereshina, Ermakova, *et al.* 2013). The mammalian homolog of XAG-2 was cloned from murine intestinal goblet cells, was initially named gob-4 and also was also found to be involved in mucus secretion (Komiya, Tanigawa & Hirohashi 1999).

The properties of the mucus secreted by goblet cells are a result of glycoproteins called mucins. They are heterogeneous, highly glycosylated and have a high molecular weight (Messina, O'Riordan & Smaldone 1991). Approximately twenty mucin genes have been identified and they are separated into two categories: membrane bound or secreted mucins. The polymeric mucins (MUC2, MUC5AC, MUC5B and MUC6) are present within a cluster of the human chromosome 11p15. They have a complex multidomain peptide structure which is essential to their function (Figure 4.1).

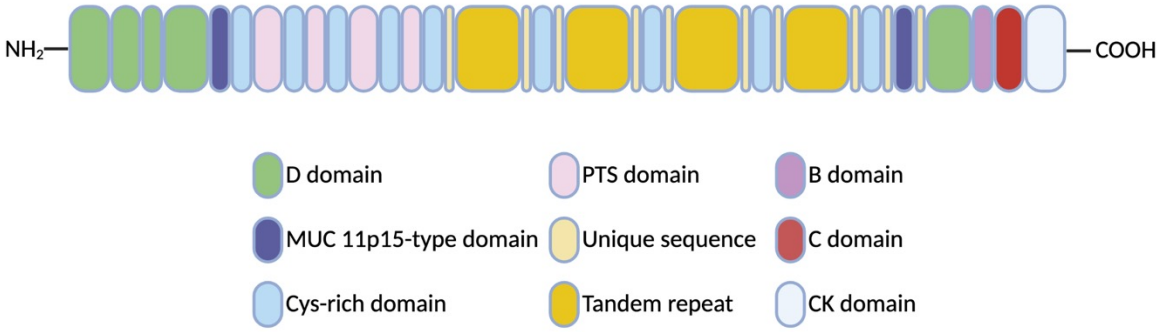

Figure 4.1: Schematic of MUC5AC molecule. It is made up of a MUC protein backbone which has O-glycans attached. They normally have NH_2-terminal domain and a COOH-terminal domain. The O-glycans are attached to threonines or serines. Diagram was adapted from (Lillehoj, Kato, Lu, *et al.* 2013).

These mucins are cysteine rich and contain von Willebrand factor (vWf)-like D domains which are located at the N and C terminus of the mucin, allowing for mucin dimerisation and polymerisation (Rose & Voynow 2006). The disulphide bonded polymers formed can be 2-50 mDa and 0.5-10 µM in length (Thornton & Sheehan 2004). MUC5AC is the main mucin that is relevant to the results presented in this chapter, so it is the focus of this introduction. MUC5AC has been detected in human airways with the main expression being in goblet cells in the tracheal and bronchial epithelium (Porchet, Pigny, Buisine, *et al.* 1995). When MUC5AC is knocked out in mice they have normal mucociliary transport and defence against bacteria (Roy, Livraghi-Butrico, Fletcher, et al. 2014). In MUC5AC deficient mice, mucus plugging was significantly reduced compared to the WT after being exposed to an allergen and the mucin-deficient mice had less chance of airway hyperreactivity (Evans, Raclawska, Ttofali, *et al.* 2015). MUC5AC is expressed in abnormal amounts in various cancers; although poorly understood, and its expression levels have been shown to indicate the prognosis for certain cancers such as gastric and pancreatic. In gastric cancer low MUC5AC expression and survival was found to be significant (P=0.031), a linear relationship was shown between low MUC5AC

expression and a shorter survival (≤5%, 64.6 ± 2.5 months; 5-25%, 67.8 ± 2.3 months; and ≥25%, 72.4 ± 1.8 months) (Kim, Kwon, Shin, *et al.* 2014).

AGR2 expression was shown to be highest in the gastrointestinal tract, genitourinary tract, and respiratory epithelia from a proteomic study of human tissue (Fagerberg, Hallstrom, Oksvold, *et al.* 2014). AGR2 is important in gastro-intestinal biology, as shown when a mouse model (which was deficient in AGR2 due to a gene knockout) developed colitis, because there was a lack of mucus production (Park, Zhen, Verhaeghe, et al. 2009). The lack of AGR2 expression was also found to cause hyperplasia and defective lineage maturation of the glandular stomach cells in a mouse model (Gupta, Wodziak, Tun, *et al.* 2013), showing that AGR2 is necessary for glandular stomach cell proliferation.

As previously mentioned, AGR2 is a member of the PDI superfamily and as such is mainly expressed in the ER. Like other PDI family members, AGR2 possesses an ER retention sequence but unlike other PDI family members it is a carboxyterminal KTEL motif and not a KDEL motif (Gupta, Dong & Lowe 2012). It also possesses a thioredoxin like domain which unlike most other PDI members is a CXXS domain rather than a CXXC motif (Figure 4.2).

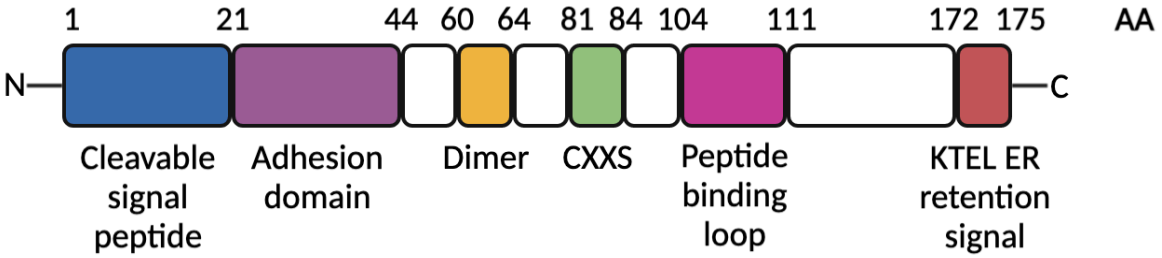

Figure 4.2: AGR2 protein structure. The functional domains are represented by the coloured boxes and their amino acids are labelled (figure adapted from (Delom, Mohtar, Hupp, *et al.* 2020).

The N-terminal region of AGR2 is unfolded (residues 21-40), which was shown through nuclear magnetic resonance (NMR) (Patel, Clarke, Barraclough, et al. 2013). The N-terminal

region is involved in promoting cell adhesion; in this capacity it is thought to attach to the substratum, dimerise, then interacting with possible cell surface targets such as dystroglycan (Delom, Mohtar, Hupp, *et al.* 2020). AGR2 can form homodimers with the motif EALYK at positions E60, Y63 and K64. A salt bridge between E60 and K64 is formed between the two AGR2 proteins in a reverse parallel arrangement which stabilises the homodimer. The dimerisation site of AGR2 is not close to the active cysteine in the CSSX motif (C81). On its own AGR2 has diminished redox capacity and as such can only perform isomerisation due to only having one active cysteine but this may be equivalent to CXXC thioredoxin domains in other PDI family members when AGR2 forms a dimer (Patel, Clarke, Barraclough, et al. 2013). Ryu et al, also showed that AGR2 can form a homodimer with C81 in the CXXS motif as the dimers were lost when C81 was substituted for a serine (Ryu, Park, Lee, *et al.* 2013). The NH_2 terminal region of AGR2 is also purported to be involved in dimerisation as deleting this region causes AGR2 to form more stable homodimers (Gray, Murray, Nowicki, *et al.* 2013). AGR2 resides in a monomer to homodimer equilibrium, with a K_d of 8.83 μM (Patel, Clarke, Barraclough, et al. 2013) in physiological conditions the homodimer may be the more prevalent form. Disruptions of this equilibrium could be an indication of ER proteostasis imbalance (Maurel, Obacz, Avril, *et al.* 2019). It has been shown that AGR2 can respond to bunder cancerous conditions such as increased metabolic activity, increased signalling and mitochondrial dysfunction, the ER becomes more oxidative due to the increase in ROS within the cell (Liou & Storz 2010). The imbalance of the redox environment in the ER may affect the AGR2 monomer and homodimer equilibrium which could lead to AGR2 contributing to oncogenic factors as described below.

AGR2 can activate the UPR when it homodimerises, which along with the increased expression of AGR2 contributes to the pro-inflammatory response, and the homodimer may

be used as a sensor that leads to ER proteostasis (Salmans, Zhao & Andersen 2013; Maurel, Obacz, Avril, *et al.* 2019). Maurel et al., showed that transmembrane P24 trafficking protein 2 (TMED2) was a specific client that enhanced AGR2 homodimerization, and that upon ER stress TMED2 and AGR2 disassociate. The interaction between AGR2 and TMED2 occurred on the K66 and Y111 amino acid residues of AGR2 (Maurel, Obacz, Avril, *et al.* 2019). Knocking AGR2 down has been shown to inhibit the protein degradation process in the ER and diminish the ER stress response (Higa, Mulot, Delom, *et al.* 2011). Another way in which AGR2 can activate the ER stress response is by AGR2 dimerising and then binding with other chaperones such as heat shock protein A5 (HSPA5) and this causes activation of the UPR (Ryu, Park, Lee, *et al.* 2013).

AGR2 has been shown to be overexpressed in many cancers such as breast, lung, and oesophageal cancers (Fritzsche, Dahl, Dankof, *et al.* 2007; Fritzsche, Dahl, Pahl, *et al.* 2006; Worfolk, Bell, Simpson, *et al.* 2019). AGR2 appears to be involved in signal transduction pathways in the cancers it is overexpressed in. It can be secreted as extracellular AGR2 (eAGR2) and causes pro-oncogenic gain of function mutations in the surrounding tumour environment (Fessart, Domblides, Avril, *et al.* 2016). AGR2 can affect cellular proliferation in cancers as it interacts with numerous pathways such as yes-associated protein 1 (YAP-1) and amphiregulin (AREG). These two proteins interact with the Hippo signalling pathway and epidermal growth factor receptor (EGFR) respectively which promotes growth in cells present in adenocarcinoma tumours (Dong, Gupta, Pai, *et al.* 2011). In breast cancer, AGR2 is able to cause lung tumour cells to proliferate by repressing the tumour suppressor p21 (CIP1). This may occur by AGR2 interacting with the ubiquitin/proteasome system as this is how p21 is degraded (Fessart, de Barbeyrac, Boutin, *et al.* 2021). AGR2 also has been shown to contribute to breast cancer chemoresistance, which occurs when AGR2 interacts with HIF-1α. AGR2

binds to HIF-1α and stabilises it, reducing proteasomal degradation and leading to hypoxia induced doxorubicin resistance (Li, Zhu, Hu, *et al.* 2015).

AGR2 is also involved in oesophageal adenocarcinoma and Barrett's oesophagus (Pohler, Craig, Cotton, *et al.* 2004; Worfolk, Bell, Simpson, *et al.* 2019). Oesophageal adenocarcinoma is preceded by changes in the epithelium of the oesophagus. These changes involve metaplasia and dysplasia of the epithelial tissue. The normal stratified squamous epithelium transdifferentiates to small intestinal epithelium with the presence of mucinous goblet cells (Maley & Rustgi 2006). This change is thought to occur due to the cells having to respond to gastro oesophageal reflux disease (GERD), where contents of the stomach and duodenum are refluxed into the oesophageal tract (Pohler, Craig, Cotton, *et al.* 2004). Although Barrett's oesophagus does not always precede oesophageal adenocarcinoma the risk of this occurring when Barrett's is present is 30 to 125-fold higher (Walch, Zitzelsberger, Bink, *et al.* 2000). Pohler et al., found that AGR2 was a key protein upregulated in Barrett's epithelium; they also found that AGR2 attenuated the tumour suppressor P53 activity and supressed P53 after phosphorylation. This suggests that AGR2 is an inhibitor of the P53 pathway and may be a factor which affects the patient's response to acid-reflux (Pohler, Craig, Cotton, *et al.* 2004). In oesophageal adenocarcinoma AGR2 was found to increase colony formation and transformation. Conversely, when AGR2 was knocked down the colony formation was inhibited, suggesting that in oesophageal tissue AGR2 supports the adenocarcinoma growth (Wang, Hao & Lowe 2008).

This chapter will further explore the AGR2 interactome in Barrett's and oesophageal adenocarcinoma by using the oesophageal cell lines OE19 and OE33. This interactome was explored by using an alkylation trapping approach and downstream mass spectrometry analysis to identify any novel potential partners in both cells and human biopsy tissue. The

proteins interacting with AGR2 may be used as biomarkers or therapeutic targets in oesophageal adenocarcinoma.

4.2 AGR2 expression is upregulated in OE19 cells

ER chaperones can be upregulated in certain cancers such as oesophageal adenocarcinomas. The upregulation of chaperones in cancer cells is due to the increased folding demand as cancer cells frequently have a higher level of protein translation (Calderwood & Murshid 2017). The ER is important in protein folding and modification where chaperones play a large part in helping proteins achieve their functional conformation. Dysregulation of the ER chaperones may cause an increase in secretion of proteins that aid in cancer metastasis (Chen & Cubillos-Ruiz 2020). Previous work in the Benham laboratory has shown that the ER oxidoreductase Ero1α is upregulated in oesophageal adenocarcinoma cells, Barrett's epithelium, and oesophageal adenocarcinoma (Battle, Gunasekara, Watson, *et al.* 2013). In this chapter, the work was extended to examine the role of the PDI homolog AGR2 in gastro-intestinal cancer. The oesophageal adenocarcinoma lines OE19 and OE33 were used in this study because they are oesophageal cancer cell lines at differing stages of the cancer, OE19 cells are from a stage 3 tumour whereas OE33 cells are from a stage 2A tumour (Rockett, Larkin, Darnton, *et al.* 1997). Protein lysates were analysed with SDS-PAGE and western blotting to investigate the expression levels of a selection of ER chaperones. This allowed key chaperones which are altered in the cells lines to be identified and evaluated for further study (Figure 4.3). The majority of the ER chaperones and folding factors tested had consistent expression levels between the two cell lines, such as PDI, calnexin and PrxIV. However, there was a slight increase in the expression level of ERP29 in the OE19 cells. AGR2 was expressed

very strongly in western blotting in the OE19 cells but was almost undetectable in the OE33 cells. This is consistent with the role of AGR2 as an upregulated chaperone in cancers.

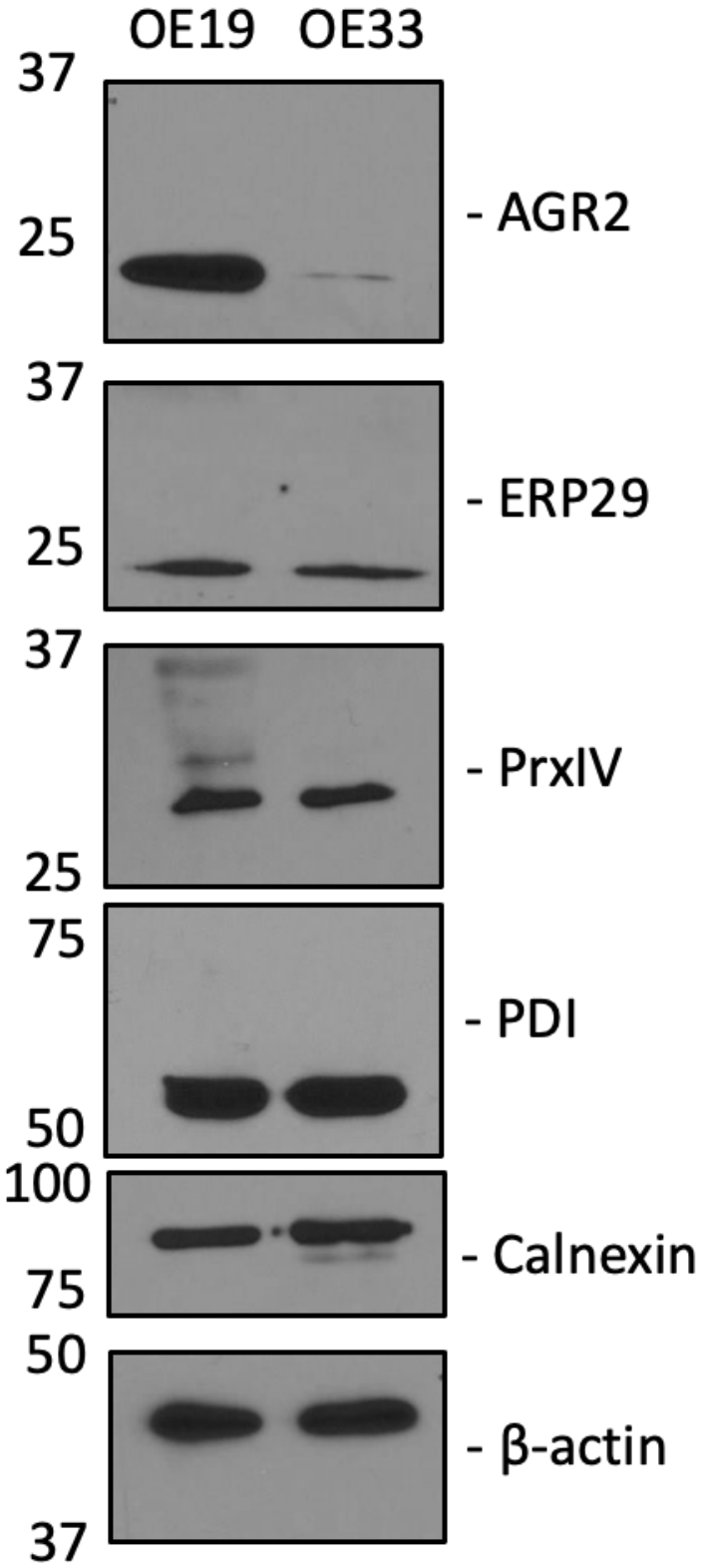

Figure 4.3: AGR2 is expressed in OE19 cells but not in OE33 cells. OE19 and OE33 cell lysates were analysed by reducing SDS-PAGE and WB with antibodies against ER chaperones AGR2 (D9V2F), PrxIV, ERp29, PDI and calnexin (CNX). β-actin was used as a loading control.

4.3 Using proteomics to analyse the AGR2 interactome

Published and background work from the group has shown that under oxidising conditions, redox-dependant AGR2 complexes are formed in the cell (Worfolk, Bell, Simpson, *et al.* 2019). To investigate the interacting partners of AGR2, OE19 and OE33 cells were lysed and treated +/- NEM to alkylate the proteins and prevent post-lysis disulphide exchange. After this, the lysates were IPed with an AGR2 antibody, eluted, trypsin digested and then analysed with DDA MS to identify co-IPing proteins. The significant proteins (more than two unique peptide hits with $P<0.05$) that were identified are presented (Table 4.1, 4.2, 4.3 and 4.4; see discussion for further expansion), with the non-specific binding partners removed by comparison to a database containing common non-specific proteins (Nesvizhskii 2015). The identified proteins present were judged to be significant when Mascot and ProteinPilot analysis showed that there were two or more peptide matches at a 95% confidence interval. High peptide coverage for AGR2 was shown in the OE19 cells which corroborates the western blot data (Figure 4.3). Other key known interacting partners with AGR2 such as MUC5B were identified in the OE19 cells. A new novel interaction between AGR2 and SQSTM1 was identified in the OE19 cells. The OE33 cells revealed an interaction with ALDH3A1 but as they express AGR2 at such low levels this interaction was not followed up. These results confirm and extend the previous data that AGR2 interacts with MUC5B and with SQSTM1 (Worfolk, Bell, Simpson, *et al.* 2019).

Table 4.1: Major proteins that interact with AGR2 identified by mass spectrometry in OE19 cells without the presence of NEM.

Gene Name	Peptides (95%)	%Cov	%Cov (50)	%Cov (95)	GO Function
AGR2	20	46.28	46.28	36.17	Mucus secretion
SQSTM1	3	21.36	18.18	9.091	Autophagy
PKM	2	10.92	9.228	3.578	Glycolysis
MUC5B	2	4.165	2.447	1.284	ECM constituent
APOD	2	15.34	11.64	11.64	Lipid binding
AKR1C1	2	5.882	5.882	5.882	Aldoketo reductase
AKR1C2	2	5.882	5.882	5.882	Aldoketo reductase
AKR1C3	2	5.882	5.882	5.882	Aldoketo reductase
AKR1C4	2	5.882	5.882	5.882	Aldoketo reductase

Table 4.2: Major proteins that interact with AGR2 identified by mass spectrometry in OE19 cells with the presence of NEM.

Gene Name	Peptides (95%)	%Cov	%Cov (50)	%Cov (95)	GO Function
AGR2	34	56.57	56.57	46.86	Mucus secretion

Table 4.3: Major proteins that interact with AGR2 identified by mass spectrometry in OE33 cells without the presence of NEM.

Gene Name	Peptides (95%)	%Cov	%Cov (50)	%Cov (95)	GO Function
AHNAK2	16	22.23	16.88	12.7	Regulation of RNA splicing
AGR2	14	49.14	38.86	34.29	Mucus secretion
ENO1	7	32.03	26.73	16.36	Glycolytic process
PKM	6	21.09	13.75	12.05	Glycolysis
LDHB	5	25.45	20.36	17.66	Metabolism
LDHA	4	23.19	17.17	14.46	Metabolism
ALDH3A1	3	18.75	7.617	7.617	Aging
S100A7	3	36.63	36.63	23.76	Calcium binding; proliferation
FASN	3	3.863	2.429	1.235	Fatty acid synthesis
XRCC5	3	4.235	4.235	4.235	DNA repair
GPI	2	6.631	6.631	6.631	Glycolysis
S100A8	2	27.96	27.96	19.35	Calcium binding; proliferation
AHCY	2	9.259	7.176	5.324	Metabolism
PRDX6	2	16.07	9.375	9.375	Peroxidase
CFL1	2	27.71	21.08	15.06	Cell motility
ATP5B	2	10.96	4.159	4.159	ATP synthesis
ALDH1A2	2	5.019	3.668	3.668	Blood vessel development
TCP1	2	5.576	3.597	3.597	Cytosolic chaperone
UGDH	2	6.883	4.656	4.656	Carbohydrate metabolic process
RAB15	2	10.38	10.38	10.38	GTPase

Table 4.4: Major proteins that interact with AGR2 identified by mass spectrometry in OE33 cells with the presence of NEM.

Gene Name	Peptides (95%)	%Cov	%Cov (50)	%Cov (95)	GO Function
AGR2	7	33.71	29.71	29.71	Mucus secretion
KLK15	4	3.125	3.125	3.125	Protease
RANBP1	2	10.95	10.95	10.95	Intracellular transport
DLST	2	1.766	1.766	1.766	Generation of precursor metabolites and energy

4.4 AGR2 interacts with SQSTM1 in an alkylation dependant manner

AGR2 was shown to interact with SQSTM1 in OE19 cells in the absence of an alkylating agent (Table 1). SQSTM1 was not detected in the OE33 cells, nor in the OE19 cells lysates or IPs lysed in the presence of an alkylating agent (NEM). To validate the interaction, OE19 and 33 cells were lysed +/- NEM. The lysates were IPed with an AGR2 antibody and analysed with SDS-PAGE and western blotting against SQSTM1 (Figure 4.4). Although SQSTM1 was present in both the OE19 and OE33 cells, it only interacted with AGR2 in the non-NEM treated OE19 cell lysates. SQSTM1 is involved in binding to LC3 to enable degradation of ubiquitinated protein aggregates by autophagy (Pankiv, Clausen, Lamark, *et al.* 2007). SQSTM1 is also involved in the degradation of excess mucin granules present in the cell (Sweeter, Kudrna, Hunt, *et al.* 2021). Further work to investigate how AGR2 links with SQSTM1 would be required to see if it is also involved in these processes.

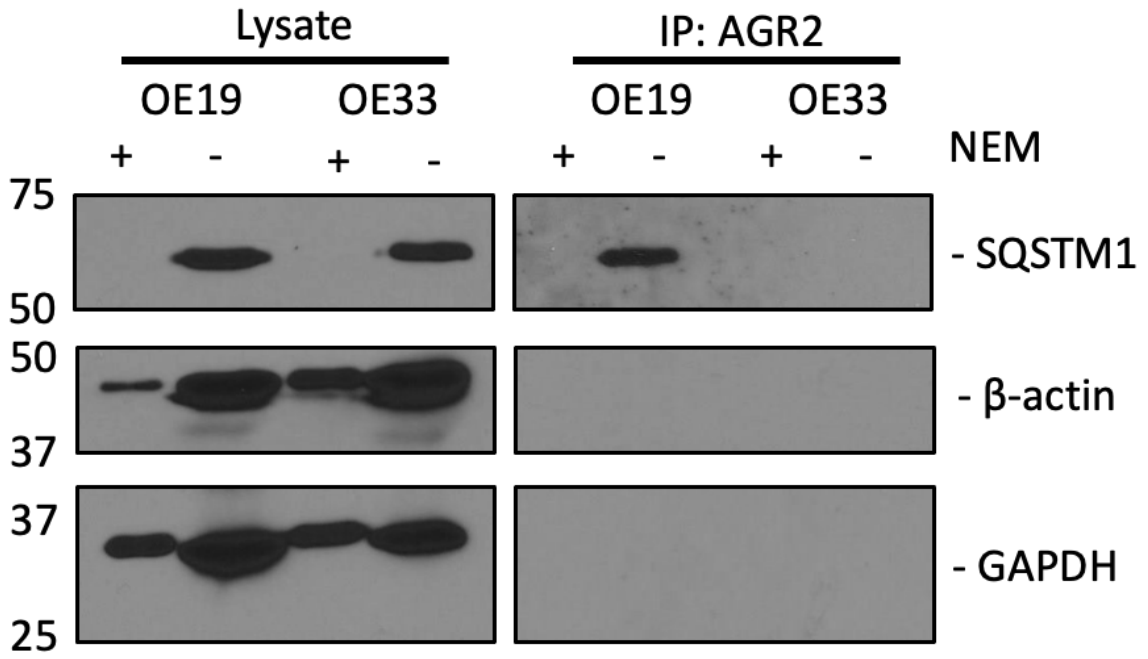

Figure 4.4: AGR2 interacts with SQSTM1 in OE19 cells. Lysates from OE19 cells and OE33 cells were analysed for the expression of SQSTM1 by WB +/- NEM. They were also subjected to IP with the AGR2 antibody (ab76473) prior to WB. SQSTM1 co-IPed with AGR2 in the OE19 cells but not the OE33 cells. β-actin and GAPDH were used as loading controls. Both loading controls were affected by the presence of NEM.

4.5 AGR2 co-localises with MUC5AC, ALDH3A1 and PrxIV in OE19 cells

As shown in the proteomics results (Table 1, 2, 3 and 4) and earlier studies (Worfolk, Bell, Simpson, *et al.* 2019), AGR2 interacts with a wide variety of proteins including clients such as MUC5AC, ER chaperones such as PDI and non-ER proteins such as ALDH3A1. AGR2 has been shown to be mainly intracellular (iAGR2) but it can be excreted as extracellular (eAGR2) in some cancers (Liu, Kanan, Radon, *et al.* 2019). To localise AGR2 in OE19 cells and to validate some of the MS findings with immunofluorescence colocalization, the cells were grown on coverslips. They were then fixed with PFA, permeabilised with Tx100 and then co-stained with various antibodies against the following proteins: AGR2 and PDI (Figure 4.5A), AGR2 and the

Golgi marker GM130 (Figure 4.5B), AGR2 and the interacting ER peroxiredoxin PrxIV (Figure 4.5C), AGR2 and the potentially interacting protein ALDH3A1 (Figure 4.5D) and AGR2 and one of the main clients, MUC5AC (Figure 4.5E). As expected, AGR2 co-localised with PDI showing that AGR2 is present in the ER of OE19 cells and was not present in the Golgi as there was no overlap with GM130. AGR2 also co-localised with MUC5AC and PrxIV in the ER where it most likely interacts with the client protein, and this further validates the MS results. Some AGR2 is present outside of the ER, most likely due to a leaky KTEL sequence, as there is some co-localisation with ALDH3A1. As a control to show that the fixing and staining process did not cause any artefactual cell rounding, PDI and tubulin (Figure 4.5F) staining was compared. The result showed that the cytoskeleton and ER were distinctly stained, highlighting that the majority of AGR2 is present in the ER with a small amount residing in the cytoplasm. Differential interference contrast microscopy was also used to show that the staining process did not cause any artefactual cell rounding.

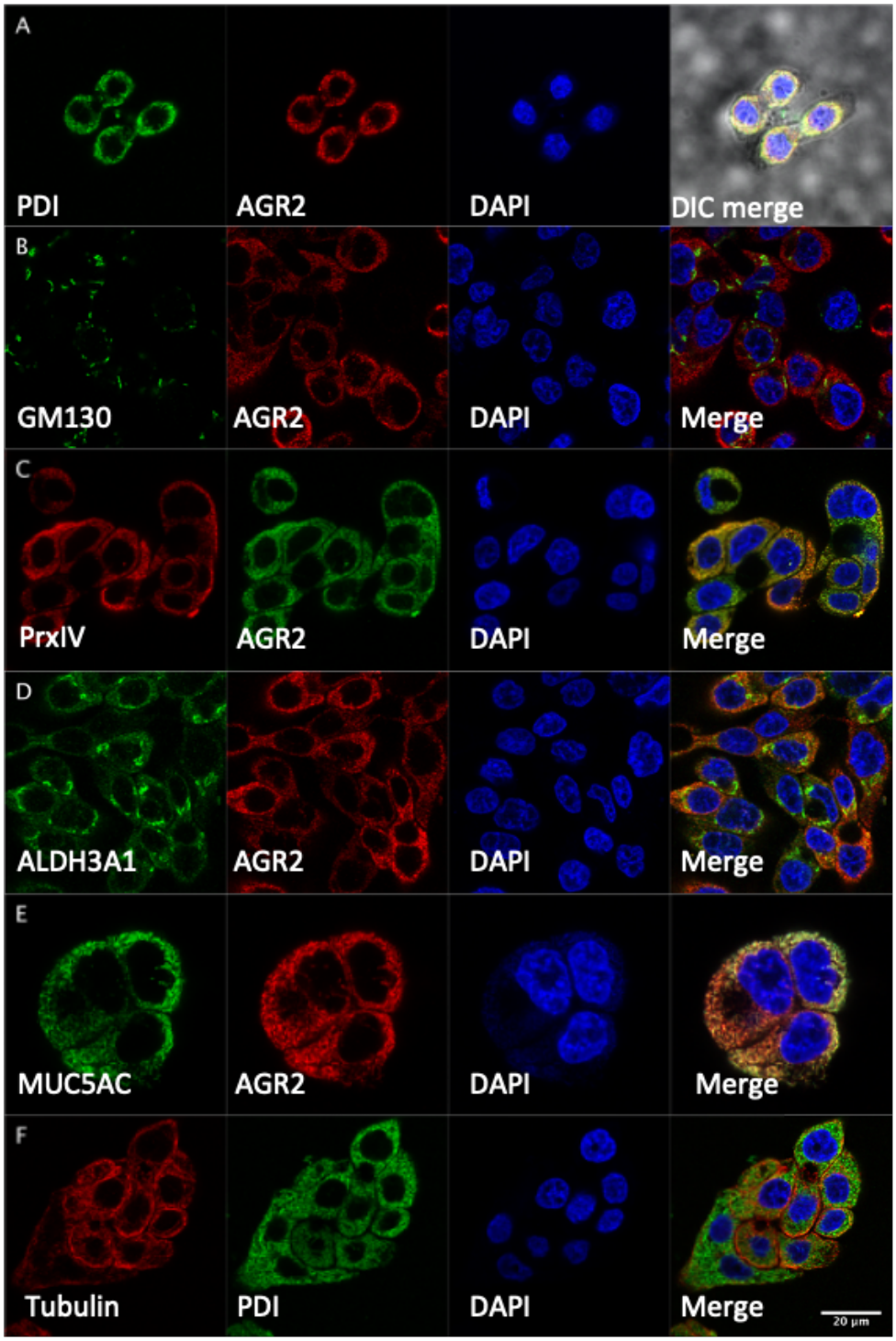

Figure 4.5: AGR2 co-localisation in OE19 cells. OE19 cells were grown on coverslips then fixed and stained for various antibodies to determine the cellular localisation of AGR2. ER localisation was shown with (A) PDI and AGR2; lack of Golgi localisation was shown with (B) GM130 and AGR2; (C) PrxIV and AGR2; (D) ALDH3A2 and AGR2; (E) MUC5AC and AGR2; (F) Tubulin and PDI was used to show the distinction between the ER and the cytoskeleton. DAPI was used to stain the nucleus and DIC was used to show general cell morphology. The images were taken on a Zeiss LSM 880 confocal microscope with Airyscan at 63x magnification.

4.6 AGR2 interacts with MUC5AC in oesophageal adenocarcinoma tissue

After exploring some of the targets observed in the MS data occurred in OE19 cells via western blot and immunofluorescence, the next step was to investigate whether this also occurred *in vivo* in tumour tissue. Oesophageal adenocarcinoma tissue lysates and normal tissue lysates from sites adjacent to the tumour were subject to IPed for AGR2. The samples were run on SDS-PAGE and analysed by western blotting against MUC5AC. In the adenocarcinoma lysate, there was a strong co-expression of AGR2 and MUC5AC (Figure 4.6A and B). This was not present in the normal epithelial lysate. In the AGR2 IP, MUC5AC was also detected in the tumour lysate and not the normal tissue lysate (Figure 4.6C and D), thus backing up the earlier proteomic results suggesting the usefulness of using cell line interactions to identify likely *in vivo* interactions in the disease state. Coomassie blue was used as a loading control as actin levels in the adenocarcinoma tissue were inconsistent. The presence of NEM in the lysis buffer did not affect the interaction of AGR2 and MUC5AC but when NEM was present the higher molecular weight forms of MUC5AC were visible in the blot (Figure 4.6C).

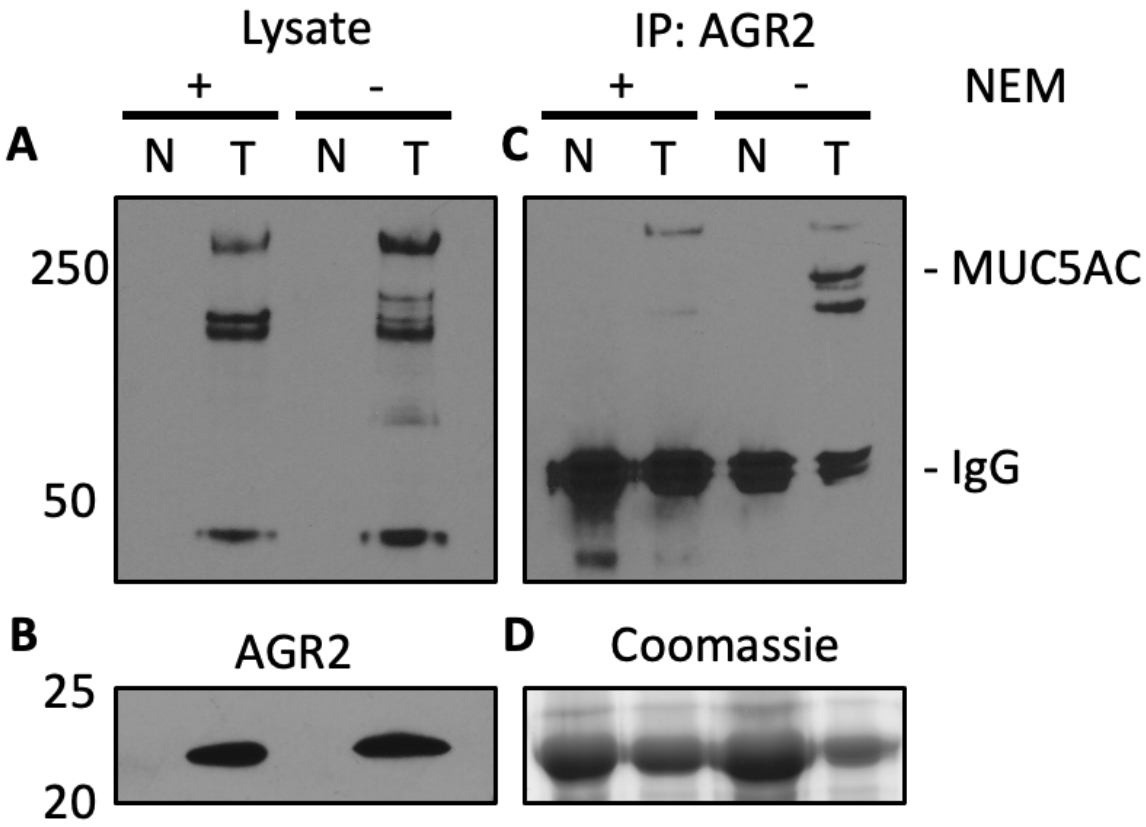

Figure 4.6: MUC5AC and AGR2 interact in human adenocarcinoma. Lysates (A, B) and an AGR2 IP (C) +/- NEM were run on SDS-PAGE and analysed with WB. AGR2 was only present in the adenocarcinoma tissue (B). MUC5AC was only present in the adenocarcinoma tissue (A) and the interaction with AGR2 only occurred in the adenocarcinoma tissue (C). A Coomassie gel was used as a loading control (D) due to the differences in β-actin and GAPDH levels between the normal and adenocarcinoma tissue.

4.7 AGR2 is co-expressed with MUC5AC, SQSTM1, PrxIV, ALDH3A1 and ERP44 in Barrett's and oesophageal adenocarcinoma tissue

When normal oesophageal tissue transitions to adenocarcinoma, it can be preceded by Barrett's oesophagus. This transition can involve changes in the cell morphology and an increase in mucin expression in the tissue. To observe if there were any visible changes in the general tissue structure, H&E staining was performed on normal, Barrett's and adenocarcinoma oesophageal tissue (Figure 4.7).

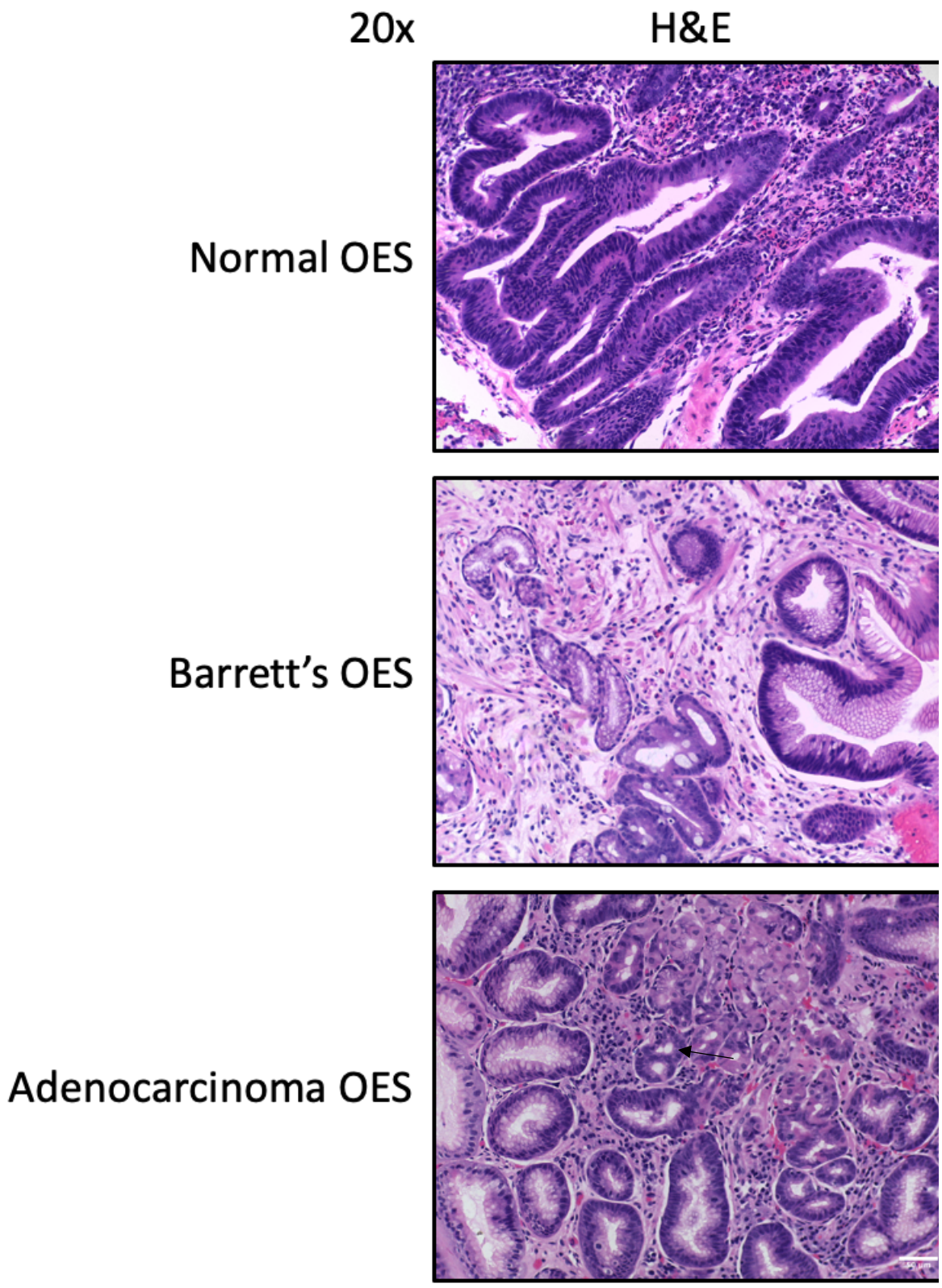

Figure 4.7: Control stains of OES tissue. Normal, Barrett's and adenocarcinoma OES were stained with H&E to see the structure of the tissue. Some of the key structures observed are gastric foveolar-type cells and intestinal-type goblet cells. In the Barrett's OES tissue section, the columnar epithelium in squamous mucosa are also visible. Arrow pointing to goblet cells.

To decipher if MUC5AC and some of the other proteins that were shown co-localise with AGR2 in human tissue, normal, Barrett's and adenocarcinoma oesophageal tissue were stained for AGR2, MUC5AC, ALDH3A1, ERP44, PrxIV and SQSTM1. To be able to compare localisation of the proteins, the same tissue blocks were used for each section with their matching negative control. AGR2, MUC5AC and ERP44 stained the goblet cells primarily and there was little staining in the surrounding epithelia (Figure 4.8A, 4.8C, 4.8D, 4.9A, 4.9C, 4.9D, 4.10A, 4.10C, 4.10D, 4.11A, 4.11C, 4.11D, 4.12A, 4.12C, 4.12D, 4.13A, 4.13C and 4.13D). The MUC5AC levels were lower in the normal oesophageal tissue when compared to the Barrett's and adenocarcinoma (Figure 4.8D, 4.9D, 4.10D, 4.11D, 4.12D and 4.13D). This observation agrees with previous work which suggests in some GI cancers that MUC5AC is over expressed (Krishn, Ganguly, Kaur, *et al.* 2018). The other proteins present (ALDH3A1, PrxIV and SQSTM1) also primarily stained the goblet cells but were also seen in the surrounding epithelia (Figure 4.8B, 4.8E, 4.8F, 4.9B, 4.9E, 4.9F, 4.10B, 4.10E, 4.10F, 4.11B, 4.11E, 4.11F, 4.12B, 4.12E, 4.12F, 4.13B, 4.13E and 4.13F). These results further validate using OE19 as an experimental model for identifying molecular interactions in oesophageal cancer.

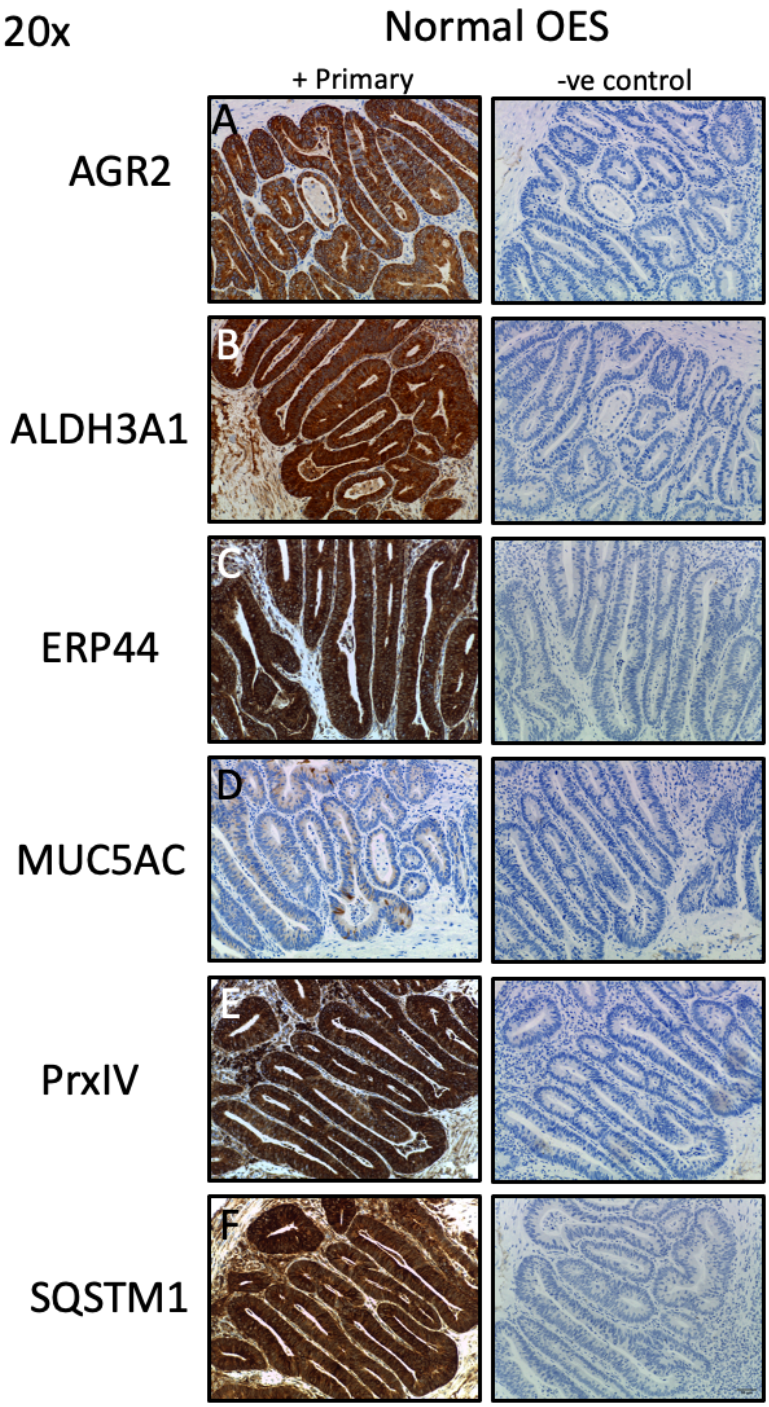

Figure 4.8: Expression of chaperone levels in normal OES tissue. Human tissue sections (4 µM) from normal tissue were immunohistochemically stained for (A) AGR2; (B) ALDH3A; (C) ERP44; (D) MUC5AC; (E) PrxIV; (F) SQSTM1. DAB (brown) was used to show the antibody staining and haematoxylin (blue) was used as a co-stain for the nuclei. Secondary antibody was only used as a negative control (column 2). All the sections were cut from the same block to keep consistent tissue structure for comparison. The goblet cells show strong staining with all the respective antibodies whereas some antibodies also show faint staining in the surrounding epithelia. These images were taken on the Leica ICC50 HD at 10x magnification.

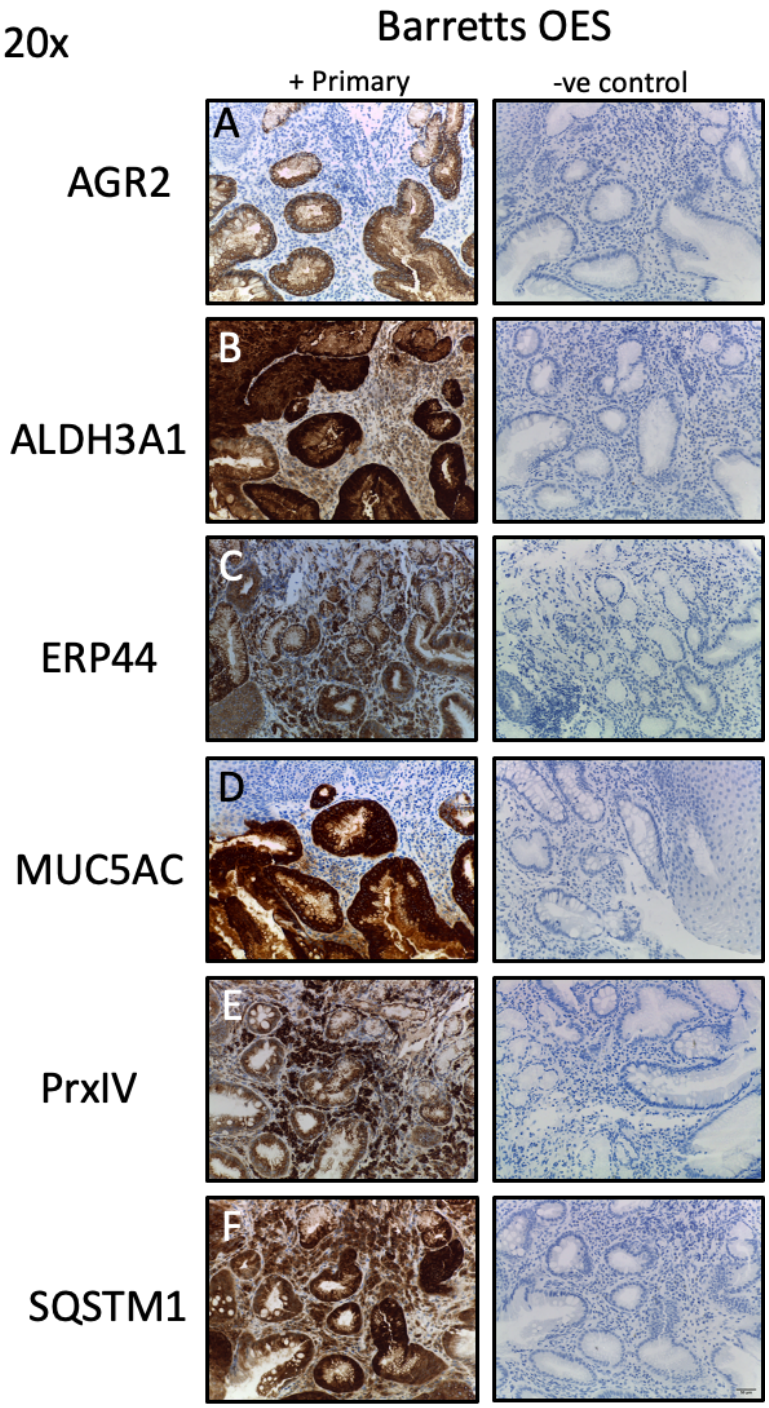

Figure 4.9: Expression of chaperone levels in, Barrett's oesophagus. Human tissue sections (4 µM) from Barrett's OES were immunohistochemically stained for (A) AGR2; (B) ALDH3A; (C) ERP44; (D) MUC5AC; (E) PrxIV; (F) SQSTM1. DAB (brown) was used to show the antibody staining and haematoxylin (blue) was used as a co-stain for the nuclei. Secondary antibody was only used as a negative control (column 2). All the sections were cut from the same block to keep consistent tissue structure for comparison. The goblet cells show strong staining with all the respective antibodies whereas some antibodies also show faint staining in the surrounding epithelia. These images were taken on the Leica ICC50 HD at 20x magnification.

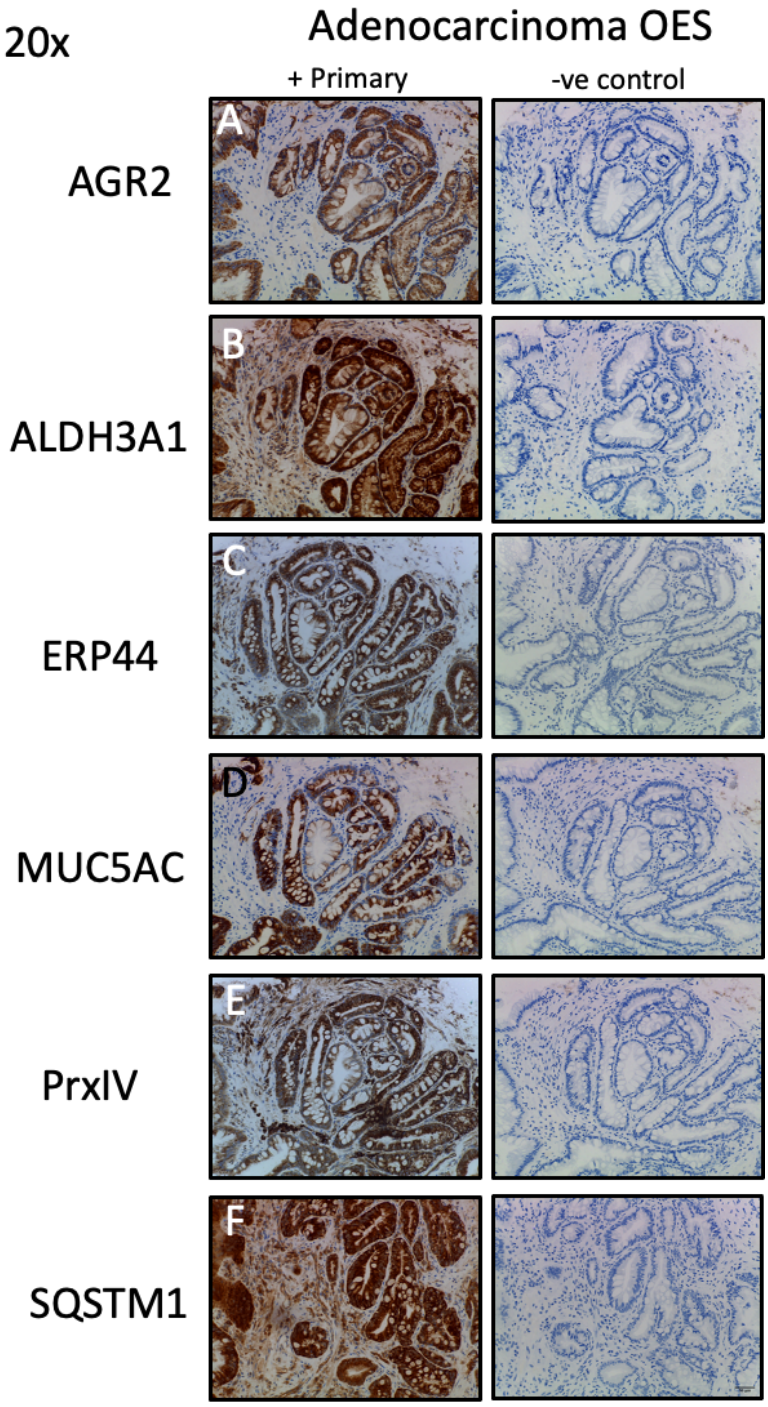

Figure 4.10: Expression of chaperone levels in adenocarcinoma OES tissue. Human tissue sections (4 µM) from adenocarcinoma OES were immunohistochemically stained for (A) AGR2; (B) ALDH3A; (C) ERP44; (D) MUC5AC; (E) PrxIV; (F) SQSTM1. DAB (brown) was used to show the antibody staining and haematoxylin (blue) was used as a co-stain for the nuclei. Secondary antibody was only used as a negative control (column 2). All the sections were cut from the same block to keep consistent tissue structure for comparison. The goblet cells show strong staining with all the respective antibodies whereas some antibodies also show faint staining in the surrounding epithelia. These images were taken on the Leica ICC50 HD at 20x magnification.

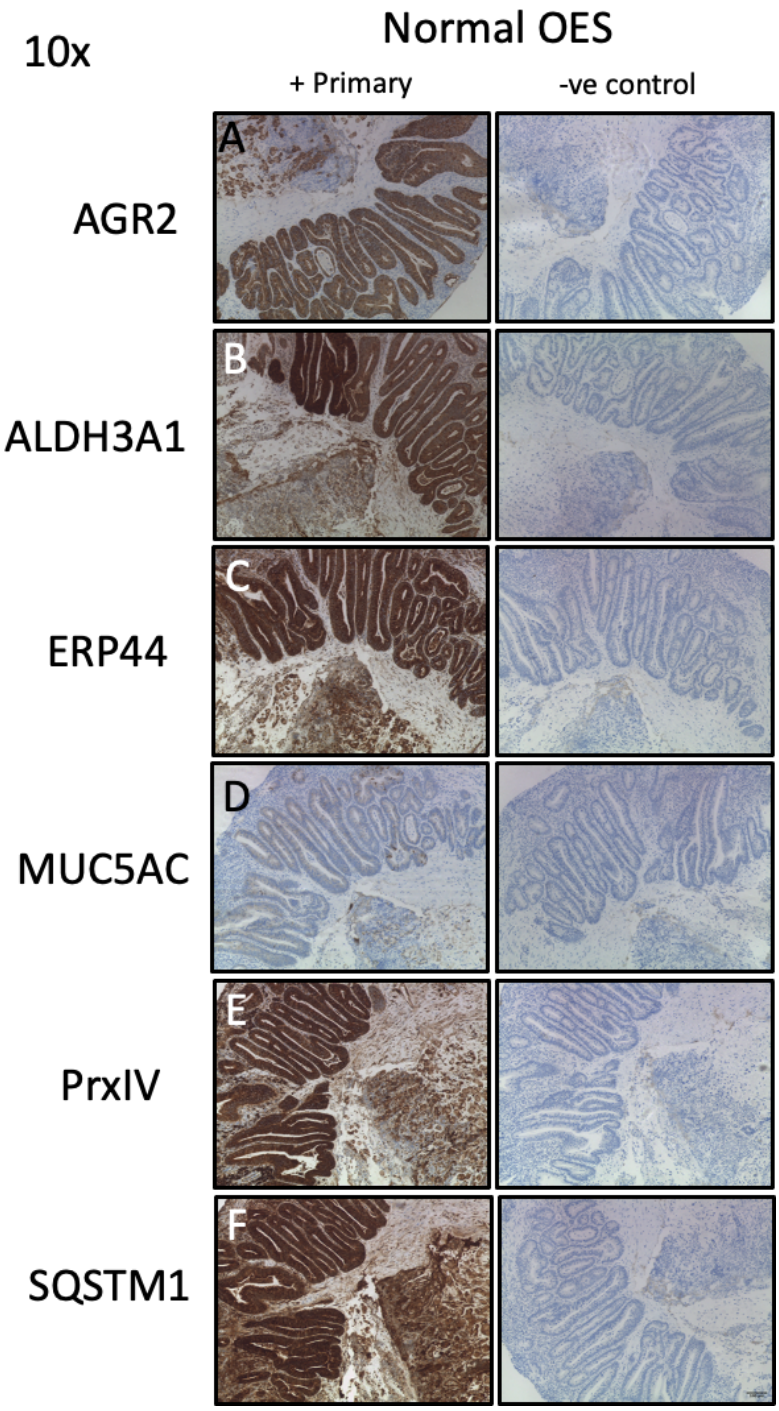

Figure 4.11: Expression of chaperone levels in normal OES tissue, Barrett's oesophagus, and adenocarcinoma. Human tissue sections (4 µM) from normal tissue (column 1, 2) Barrett's (column 3, 4) and adenocarcinoma (column 5, 6) were immunohistochemically stained for (A) AGR2; (B) ALDH3A; (C) ERP44; (D) MUC5AC; (E) PrxIV; (F) SQSTM1. DAB (brown) was used to show the antibody staining and haematoxylin (blue) was used as a co-stain for the nuclei. Secondary antibody only was used as a negative control (columns 2, 4 and 6). All the sections were cut from the same block to keep consistent tissue structure for comparison. The goblet cells show strong staining with all the respective antibodies where-as some antibodies also show faint staining in the surrounding epithelia. These images were taken on the Leica ICC50 HD at 10x magnification.

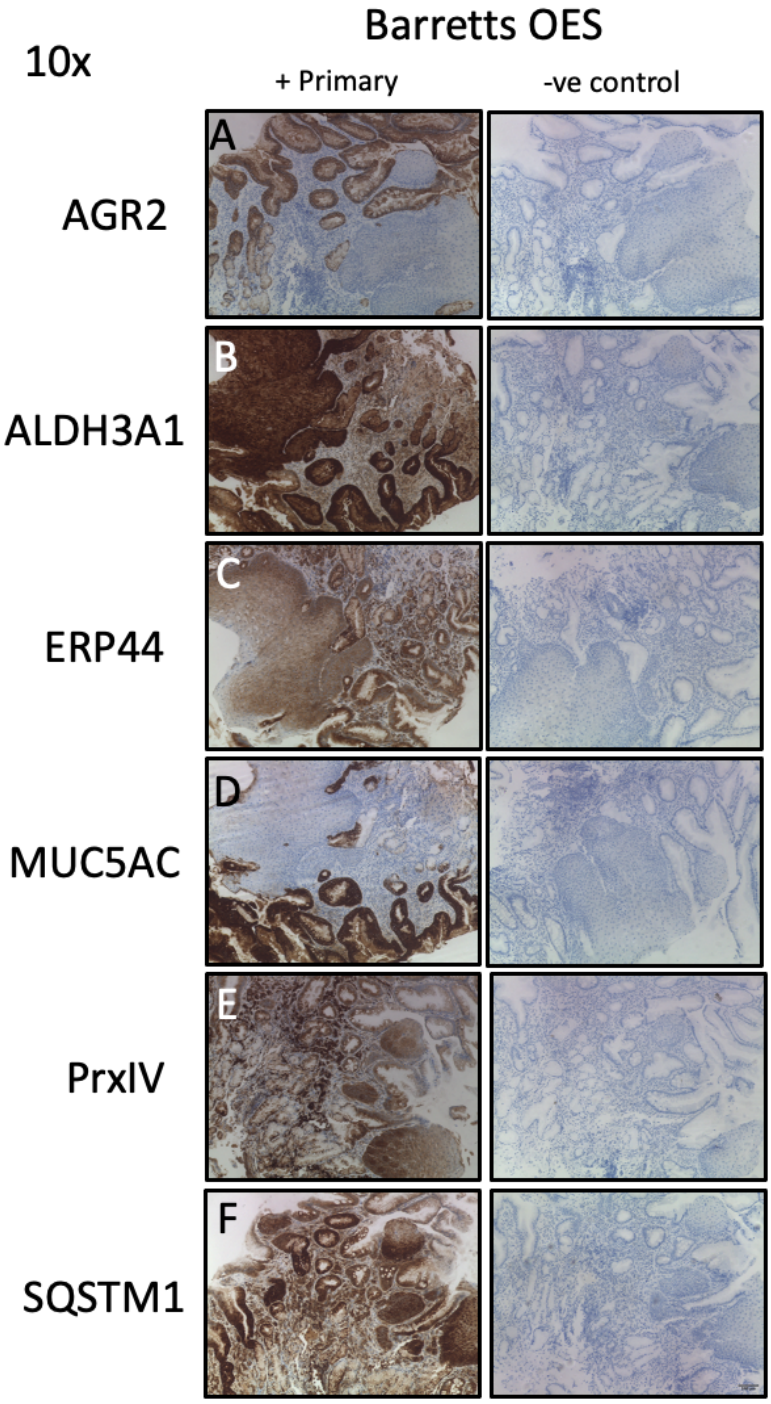

Figure 4.12: Expression of chaperone levels in, Barrett's oesophagus. Human tissue sections (4 µM) from Barrett's OES were immunohistochemically stained for (A) AGR2; (B) ALDH3A; (C) ERP44; (D) MUC5AC; (E) PrxIV; (F) SQSTM1. DAB (brown) was used to show the antibody staining and haematoxylin (blue) was used as a co-stain for the nuclei. Secondary antibody was only used as a negative control (column 2). All the sections were cut from the same block to keep consistent tissue structure for comparison. The goblet cells show strong staining with all the respective antibodies whereas some antibodies also show faint staining in the surrounding epithelia. These images were taken on the Leica ICC50 HD at 10x magnification.

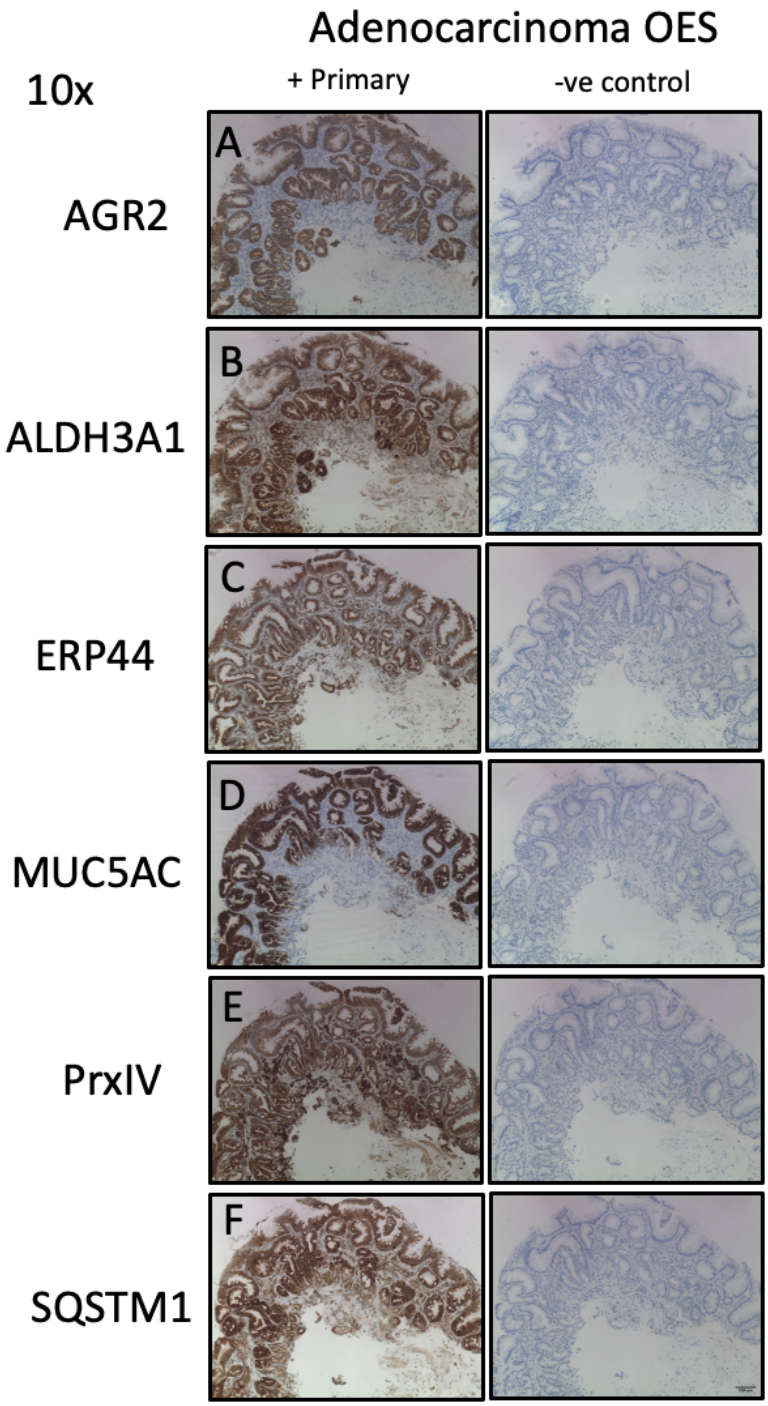

Figure 4.13: Expression of chaperone levels in adenocarcinoma OES tissue. Human tissue sections (4 µM) from adenocarcinoma OES were immunohistochemically stained for (A) AGR2; (B) ALDH3A; (C) ERP44; (D) MUC5AC; (E) PrxIV; (F) SQSTM1. DAB (brown) was used to show the antibody staining and haematoxylin (blue) was used as a co-stain for the nuclei. Secondary antibody was only used as a negative control (column 2). All the sections were cut from the same block to keep consistent tissue structure for comparison. The goblet cells show strong staining with all the respective antibodies whereas some antibodies also show faint staining in the surrounding epithelia. These images were taken on the Leica ICC50 HD at 10x magnification.

In summary this work has reinforced some of the more well-known interacting partners of AGR2 (MUC5AC, MUC5B) in oesophageal cell lines (OE19, OE33). It has also shown an alkylation sensitive novel interaction of AGR2 with SQSTM1, suggesting AGR2 may play a role in autophagy. AGR2 interacting with MUC5AC has also been shown in oesophageal adenocarcinoma tissue and this validates using cell lines as a method to discover protein interactions in disease. The pathways found may be used as targets for disease or biomarkers for the detection of oesophageal adenocarcinoma.

4.8 Discussion and conclusion

The work presented in this chapter explores new interacting partners of AGR2 in oesophageal cancer cell lines, such as MUC5AC and SQSTM1 proteins (Worfolk, Bell, Simpson, *et al.* 2019). AGR2 has been shown to be upregulated in cancers and it is also upregulated in the oesophageal cancer cell line OE19. In contrast, other chaperones such as PDI and ERP29 were not visibly overexpressed in OE19 cells (Figure 4.3). It is still unknown if AGR2 is able to act as an isomerase as it only contains one active cysteine in its CXXS motif unlike PDI which contains two cysteines (CGHC) in its CXXC motif. The interaction of AGR2 with MUC5AC and MUC5B most likely occurs through the single AGR2 active cysteine C81 and non-covalent interactions may occur through the N-terminal part of AGR2. As MUC5AC and MUC5B are large glycoproteins they will have exposed cysteine residues which could lead to misfolding of the mucin protein. AGR2 may stop these cysteines from being exposed and may help prevent misfolding of mucin. The interaction of AGR2 and mucin was further confirmed with immunofluorescence in OE19 cells (Figure 4.5) and in human tissue via WB and IHC (Figure 4.6, 4.9, 4.10, 4.11, 4.13). Both AGR2 and MUC5AC were shown to be expressed in the dysplastic mucosa of the Barrett's and oesophageal adenocarcinoma tissue.

Other AGR2 interactions were investigated with and without the presence of the chemical NEM in OE19 and OE33 cells. The NEM alkylates the disulphide bonds preventing their re-arrangement, but it can also impair detection by MS meaning some possible hits may be lost from the dataset (Table 4.1, 4.2, 4.3, and 4.4). As shown by looking at both the NEM treated and NEM untreated AGR2 IP there is a significant loss of AGR2 interacting partners in the NEM treated lysate as opposed to the non-NEM treated one (Table 4.1, 4.2). Even though there are potential interacting partners in the AGR2 IP +/- NEM in OE33 cells, these were not taken forward as the expression levels of AGR2 in the OE33 cell line is very small so these possible interactions may be false positives. A novel interaction was observed with AGR2 and SQSTM1 (Figure 4.4). SQSTM1 is an autophagosomal membrane binding protein. It is possible that AGR2 interacts with SQSTM1 and other proteins that are regulated post-ER. AGR2 is normally ER localised (but has been detected extracellularly), SQSTM1 is either cytoplasmic prior to sequestosome formation or can localise within the autophagic compartment post-sequestosome formation; so, an interaction was initially unexpected as both proteins appear to reside in different compartments. Research has been performed to show that in goblet cells autophagosomal proteins were required for secretion of mucin proteins; thus, it is possible that AGR2 also interacts with the autophagosomal machinery during mucin granule biogenesis (Patel, Miyoshi, Beatty, *et al.* 2013). In the results chapter, AGR2 has been shown to interact with ALDH3A1 in the OE19 cells (Figure 4.5), in oesophageal adenocarcinoma and Barrett's oesophagus tissue sections (Figure 4.9, 4.10, 4.12 and 4.13). Partial co-localisation of AGR2 with ALDH3A1 was also demonstrated in the OE19 cells (Figure 4.5D). A proteomic analysis of a goblet cell line synthesising mucin containing vesicles (using a nano LC-MS and MS/MS approach) found that purified granules contained AGR2, MUC5AC, BiP, ERp29, ERp57, ERp44, ERO1, PrxIV, SQSTM1, BCAP31, VAPA and aldehyde dehydrogenases such as ALDH3A1,

amongst other proteins (Rodríguez-Piñeiro, van der Post, Johansson, *et al.* 2012; Patel, Miyoshi, Beatty, *et al.* 2013). This shows the interaction between AGR2 and ALDH3A1 as well as PrxIV may occur in the vesicular granules in a non-cancer setting. Alternatively, the SQSTM1-AGR2 interaction may also occur in the cytoplasm of the cell, as AGR2 possess a weaker KTEL ER retention sequence instead of the KDEL sequence possessed by other PDI family members (Gupta, Dong & Lowe 2012). In such a scenario, AGR2 could be exported from the ER by retro-translocation or could be secreted and re-internalised by endocytosis. Further analysis of how AGR2 is able to interact with proteins in the mucin granules will be needed to work out when in mucin granule biogenesis AGR2 interacts with these proteins.

In conclusion, novel interacting partners of AGR2 have been observed via DDA MS. Further experiments could involve exploring how acid reflux and the transition of Barrett's oesophagus to oesophageal adenocarcinoma occurs by using quantitative proteomics to study the change in protein expression between these two tissue types. As MUC5AC is also overexpressed in chronic obstructive pulmonary disease (Kesimer, Ford, Ceppe, *et al.* 2017) and AGR2 is a key factor in MUC5AC production then using AGR2 as a drug target may reduce mucus secretion in chronic obstructive pulmonary disease (COPD) and other lung pathologies.

5 Proteomics of fibroblast cells subjected to PDGF and niacinamide

5.1 Introduction

In this chapter, the effect of protective agents such as PDGF and niacinamide on BJ fibroblast cells was investigated. The effect of PDGF on BJ fibroblasts follows previous data from the laboratory where the growth factor PDGF was found to increase the intracellular lamin A/C and phospho-lamin A/C levels. The work in the chapter also explored how lamin A/C is phosphorylated after PDGF treatment. Protection against oxidative stress was investigated by using niacinamide as a protective agent against hydrogen peroxide applied to fibroblasts. This was explored with SWATH proteomics to observe which proteins change after the addition of niacinamide.

Adult human skin contains multiple subpopulations of fibroblasts, the subpopulations occupy different niches in the environment of the dermis. Fibroblasts are an essential part of the skin and act to regulate skin physiology. An example of this is by producing and organising the ECM of the dermis. Two of the subpopulations of fibroblasts inhabit distinct dermal layers. The two subpopulations are the papillary fibroblasts, where the fibroblasts are more densely packed and the reticular where there are less cells present but more ECM (Sorrell & Caplan 2004). A third population of fibroblasts is linked with the hair follicles of the skin, they are present in the dermal papilla of the follicle and up the shaft of the follicle (Jahoda & Reynolds 1996). The fibroblasts in the skin are important for the secretion of various ECM components such as collagen and glycosaminoglycans (GAGs) which help maintain the structure and elasticity of skin (Thangapazham, Darling & Meyerle 2014). One of the main functions of the fibroblasts, is their role in wound healing.

During *in vitro* cell culture the two fibroblast populations (papillary and dermal fibroblasts) present with two morphologically distinct characteristics. Papillary fibroblasts

grow in a more spindle shape unlike reticular fibroblasts which grow as a more of a squarer cell (Janson, Saintigny, van Adrichem, *et al.* 2012). They also present with different characteristics when cultured *in vitro*: the papillary fibroblasts divide at a faster rate and grow to a higher cell density than their reticular counterparts. This is due to the fact that the papillary fibroblasts are not completely contact inhibited (Harper & Grove 1979; Schafer, Pandy, Ferguson, *et al.* 1985). Reticular fibroblasts are the primary producers of collagen and ECM in skin, they are one of the first cells recruited to a wound for healing. This explains why there is ECM rich scar tissue present after wound healing (Driskell, Lichtenberger, Hoste, *et al.* 2013).

Wound closure is facilitated by fibroblasts and is an important part of the work in this chapter. Wound healing starts with haemostasis, which can last from hours to weeks; after this event, neutrophil and monocyte invasion occurs. This is followed by granulation tissue formation, re-epithelialisation, formation of scar tissue and then further remodelling. The granulation tissue (new connective tissue and blood vessels that form during wound healing) is caused by the migration of fibroblasts to the wound site where they deposit ECM. This allows for further migration of fibroblasts and other cells to the wound. After the initial formation of the granulation tissue the fibroblasts produce further ECM which increases the tensile strength of the wound (Greaves, Ashcroft, Baguneid, *et al.* 2013). Fibroblasts are also capable of releasing cytokines, chemokines and growth factors which can recruit other cells to the site (Vistejnova, Safrankova, Nesporova, *et al.* 2014). Papillary fibroblasts are mainly involved in the immune response during wound closure, whereas reticular fibroblasts are involved in cytoskeletal organisation and cell motility (Janson, Saintigny, van Adrichem, *et al.* 2012). Fibroblasts originating from the reticular dermis compared to the papillary dermis are more predominant in the healing of human skin wounds (Woodley 2017).

One of the key growth factors studied in this chapter that has a large involvement in wound closing is platelet derived growth factor (PDGF). PDGF was first discovered in 1974 when Ross et al., noticed that smooth muscle cell proliferation occurred better in serum containing platelets compared to the plasma which contained few platelets (Ross, Glomset, Kariya, *et al.* 1974). There are four PDGF family members A, B, C and D with the latter two being the most recently discovered. PDGF proteins possess a cysteine knot motif which contains two disulphide bands, linking the antiparallel strands of the peptide chain. This forms a ring which is infiltrated by a third disulphide bridge (Vitt, Hsu & Hsueh 2001). PDGF can form homo or heterodimers due to the hydrophobic residues being exposed, these are PDGF-AA, PDGF-AB, PDGF-BB, PDGF-CC and PDGF-DD (Reigstad, Varhaug & Lillehaug 2005). In their monomeric forms the PDGF proteins are inactive, only becoming active upon dimerisation. Signalling occurs when dimeric PDGF binds to the protein tyrosine kinase receptors (PKR) -α and -β. After this the receptor dimerises creating homo or heterodimers which results in PDGFR-αα, -αβ or -ββ. Each PDGF dimer has a different affinity to each PDGF receptor and thus they bind to different receptors. PDGF-AA binds to PDGFR-αα, PDGF-AB binds to PDGFR-αα and-αβ, PDGF-BB can bind to all three receptors, PDGF-CC binds to PDGFR-αα and-αβ similarly to PDGF-AB and PDGF-DD binds to PDGFR-αβ with low affinity but it binds to -ββ at high affinity (Hart, Forstrom, Kelly, *et al.* 1988; Larochelle, Jeffers, Mcdonald, *et al.* 2001; Gilbertson, Duff, West, *et al.* 2001). PDGF signalling can be involved in the tissue development in the body with each receptor being involved in the development of different areas. PDGFRα is involved in neural crest development (Soriano 1997), the lung (Boström, Willetts, Pekny, *et al.* 1996) and intestinal villi (Karlsson, Lindahl, Heath, *et al.* 2000). PDGFRβ is involved in blood vessel and kidney development (Levéen, Pekny, Gebre-Medhin, *et al.* 1994; Soriano 1994). As well as developmental biology, PDGF is involved in wound healing. Pierce et al showed that

PDGF-BB treatment in incisional wounds amplified wound breaking strength by 50-70% over the first three weeks of the wound, in excisional wounds PDGF-BB treatment accelerated wound closure by 30%. It is thought to achieve this by causing a positive autocrine feedback loop, which causes cytokine synthesis during the inflammatory phase of wound repair. The PDGF-BB stimulated fibroblasts are activated by this cascade and produce increased levels of procollagen 1 which provides structure during the wound repair (Pierce, Mustoe, Altrock, et al. 1991).

The nuclear lamins have been shown to indirectly interact with PDGF and in the work presented in this thesis appear to influence lamin phosphorylation. The nuclear lamins are a key part of the nuclear cytoskeleton. They are part of the intermediate filament (IF) family of proteins. In mammals there are two types of lamins, A and B. The *LMNA* gene encodes lamin A, lamin C, lamin AΔ10 and lamin C2. The *LMNB1* and *LMNB2* gene encodes lamin B1 and lamin B2 (Dechat, Pfleghaar, Sengupta, *et al.* 2008). Lamin A is involved in co-ordinating nuclear shape and nuclear stiffness (Simon & Wilson 2013). Lamin A is able to directly and indirectly bind to DNA, affecting epigenetic regulation, chromatin organisation and DNA regulation plus transcription (Dechat, Pfleghaar, Sengupta, *et al.* 2008). The most common post-translational modification of the lamins is phosphorylation. Lamin phosphorylation is involved in cell survival, growth, differentiation, cell death and migration. Mutations of the *LMNA* gene causes diseases known as laminopathies. The laminopathies can affect skeletal, cardiac muscle, ageing and metabolism (Worman, Fong, Muchir, *et al.* 2009). Lamin phosphorylation occurs during the cell cycle, this includes interphase and mitosis. During mitosis lamin A and B are phosphorylated by cyclin dependant kinase 1 (Cdk1), disassembly occurs after lamin A/C N-terminal S22 and C-terminal S392. In B-type lamins, the phosphorylation occurs on mitotic sites (Peter, Nakagawa, Dorée, *et al.* 1990). During

interphase lamin A is phosphorylated at three regions, Torvaldson et al., used western blotting with an antibody against S22 to show that S22 is phosphorylated during interphase but at a lower rate than during mitosis (Torvaldson, Kochin & Eriksson 2015). In other physiological roles lamins can act as mechanosensors; cells growing on a soft substrate have a softer nucleus whereas cells grown on a hard substrate have a harder nucleus. Lamin A levels and lamin A phosphorylation was shown to be affected by the substrate the cells were grown on (Swift, Ivanovska, Buxboim, *et al.* 2013). One of the scenarios which is reliant on nuclear stiffness is cancer metastasis. Cells with high levels of lamin A have stiffer nuclei, whilst cells with lower levels of lamin A have softer nuclei. The stiffer nuclei will hinder migration as the nucleus cannot be deformed easily, whereas the softer nuclei can squeeze through smaller spaces, but their nuclei are prone to being sheered which causes cell death (Harada, Swift, Irianto, et al. 2014). Although there isn't a great deal known about lamin A phosphorylation in cancer cells during migration, it has been thought that the phosphorylation of lamin makes the lamin more mobile which increases nuclear softness. Lamins have been shown to be up and down regulated in cancers; this could allow for cellular migration through promoting cell cycle kinase activity (Foster, Przyborski, Wilson, *et al.* 2010). There may be many other roles of lamin A phosphorylation which have yet to be discovered.

Another protective agent of the skin is niacinamide (Figure 5.1). It is also known as nicotinamide and is an amide form of vitamin B3. It is present in many foods but is also synthesised from tryptophan metabolism (Damian 2017). Niacinamide is a precursor of nicotinamide adenine dinucleotide (NAD^+) which is a required precursor for ATP synthesis.

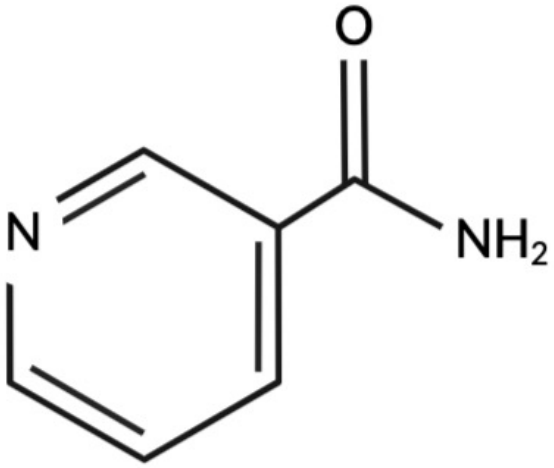

Figure 5.1: Structural form of niacinamide.

Niacinamide is required for cellular energy due to the fact that it contributes to ATP production. After the skin is exposed to UV radiation DNA damage occurs, this needs to be repaired but it is an energy intensive process. UV damage can also block glycolysis and depletes ATP which further reduces the cells energy pool. UV damage can also activate poly-ADP-ribose polymerase (PARP) which is an enzyme that is involved in DNA repair. As NAD^+ is the substrate for PARP activation, UV damage can quickly deplete the cells store of NAD^+ (Surjana, Halliday & Damian 2010). Niacinamide treatment can prevent the excess loss of NAD^+ as in keratinocytes it has been shown to prevent the UV damage blocking glycolysis and has been shown to inhibit PARP which further restores energy to the cells (Birkmayer, Vrecko, Volc, *et al.* 1993; Park, Halliday, Surjana, *et al.* 2010). Tan et al., found that niacinamide can protect against senescence caused by UVB radiation and H_2O_2 treatment, suggesting that niacinamide is also able to offer protective affects against these stressors (Tan, Tan, Chin, *et al.* 2021). Similarly to PDGF, niacinamide has been shown to be effective in wound healing. Topical niacinamide applied to full thickness wounds increased the rate of healing, by increasing the proliferation of fibroblasts, the production of collagen and revascularisation. It

also reduced inflammation at the site of the wound and increased epithelisation which improved wound closure rate (Esfahani, Khoshneviszadeh, Namazi, *et al.* 2015). Further experiments to elucidate how exactly niacinamide achieves its wound helping capabilities and if there is any risk of long-term application are needed.

This chapter will explore further the effect of PDGF on BJ fibroblasts and will harness explore previous mass spectrometry work performed by this laboratory by investigating the relationship between PDGF and lamin A/C phosphorylation. It will also look at the BJ fibroblast proteome after treatment with niacinamide and H_2O_2 by using DIA mass spectrometry and SWATH analysis to identify any key proteins which are up and down regulated.

5.2 PDGF treated BJ fibroblasts exhibit lamin-A upregulation

The response of fibroblasts to PDGF is well understood and is one of the major factors that contribute to wound healing. The response fibroblasts to reductive stress and PDGF treatment is not understood as well. The work in this chapter builds upon previous studies which aimed to understand the response of skin cells to stress and growth factors (Carne, Bell, Brown, *et al.* 2019). PDGF stimulates the PDGFR to become dimerised and autophosphorylated; this recruits signal transduction molecules, including PI3K which in turn activate STAT transcription factors (Deuel, Silverman & Kawahara 1988). PDGF proteins are disulphide bonded growth factors which occur in various forms (PDGF-AA, AB, BB, CC and DD). PDGF-BB was used in this study as it can bind to the PDGFR-αβ that is present on BJF, the cell line of choice for these experiments (Bergsten, Uutela, Li, *et al.* 2001). Previous experiments performed in this laboratory investigated the effect of PDGF-BB treatment on BJF. This involved treating BJF cells in serum free media +/- 10 $ngml^{-1}$ PDGF-BB for 24 hr, after the treatment the cells were lysed and analysed with DIA-MS. From this analysis, there were 10

significant proteins with a fold change of 2 or more (FDR adjusted $P<0.05$). Of the 10 significant proteins identified 4 were upregulated and 6 downregulated (Figure 5.2). This work was used as a starting point for the experiments performed in the rest of this chapter.

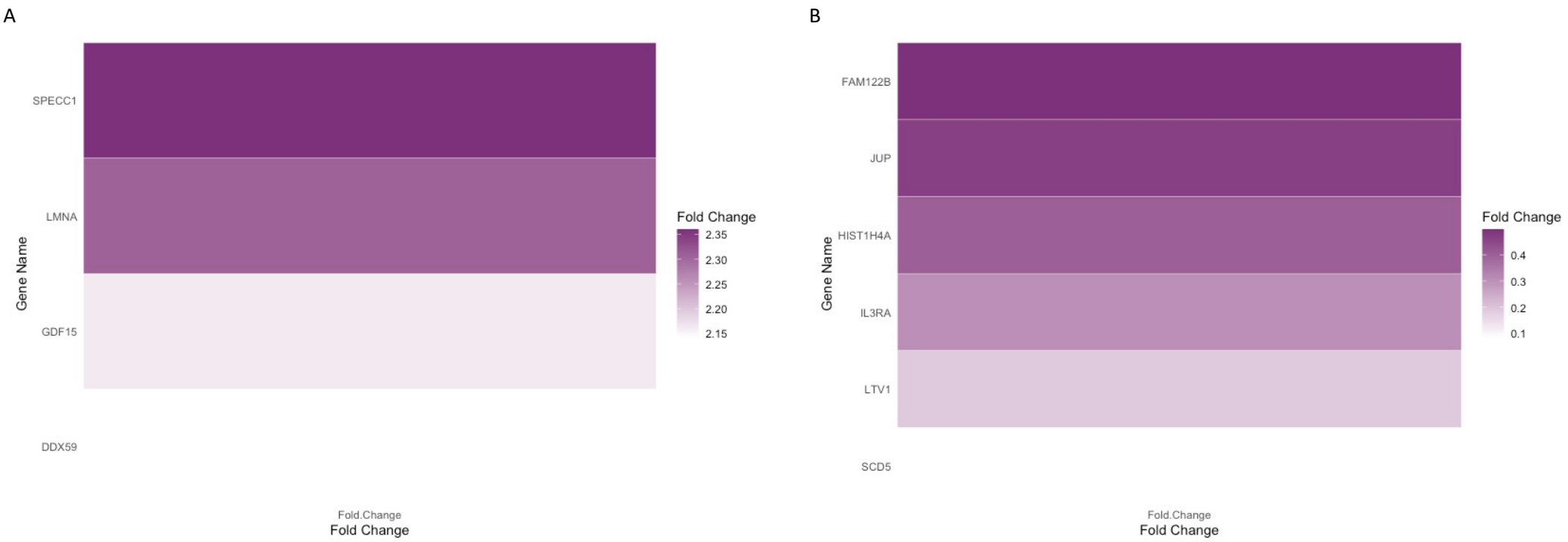

Figure 5.2: Visualising the changes in proteins that are affected in both the untreated vs PDGF treated. Heatmaps were used to show how the fold change of the proteins either increased (A) and decreased (B) (data adapted from (Carne 2018).

To ensure that the PDGF treatment alone did not cause ER stress, the BJF were incubated in SFM for 24 hr and then were either left untreated, treated with 10 $ngml^{-1}$ PDGF-BB at 18 h for a 6 hr treatment, treated with 5 mM DTT at 18 hr for a 6 hr treatment or treated with both 10 $ngml^{-1}$ PDGF-BB and 5 mM DTT for the last 6 hr. DTT was used as it is a known inducer of reductive stress, and the results could be compared against the PDGF treatment. The cells were then fixed and stained with PDI, an ER marker and DAPI. From the immunofluorescence data, there is evidence the cells remained viable and adherent, with no cell rounding or observable death (Figure 5.3).

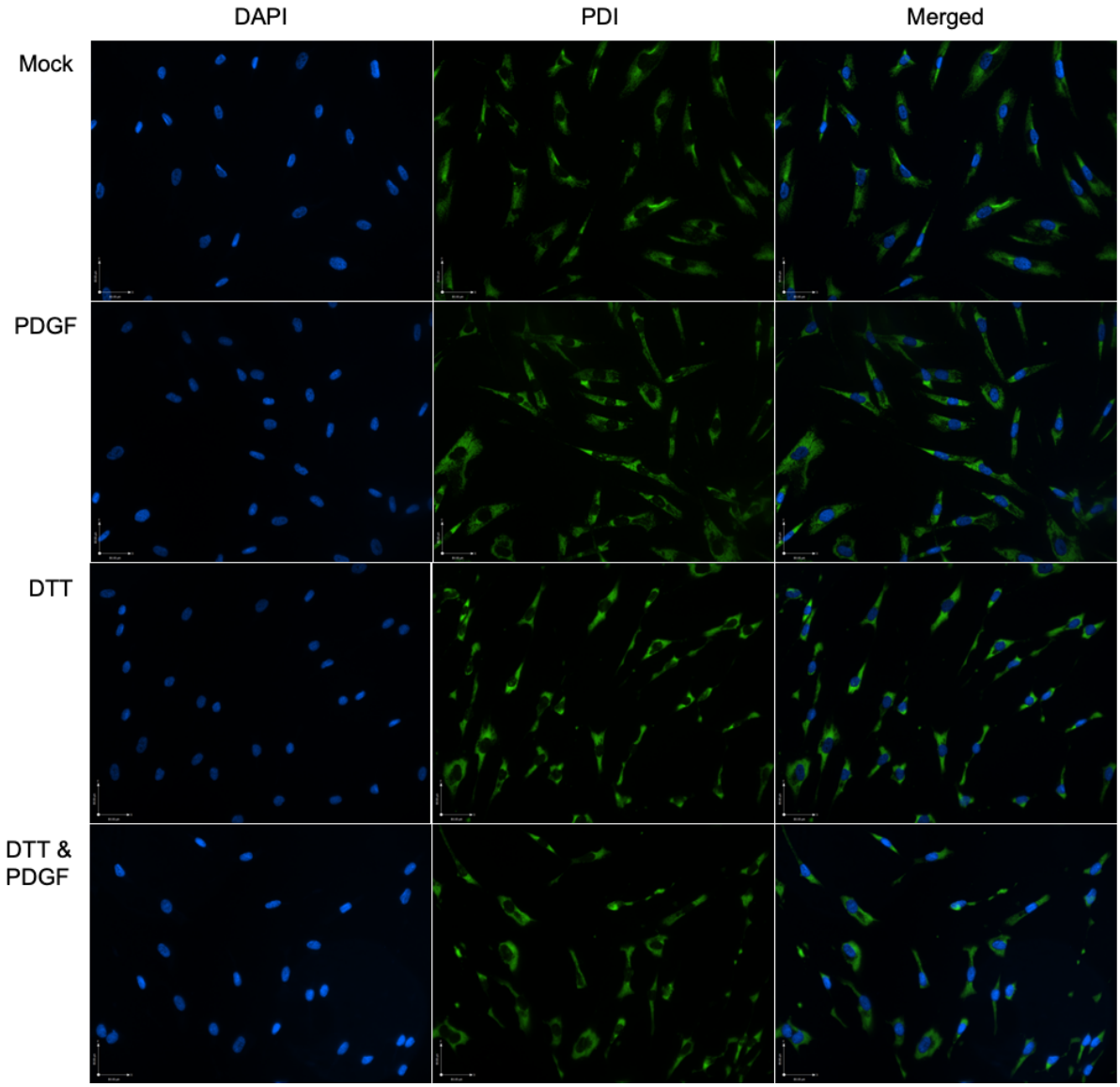

Figure 5.3: Treatment of BJ fibroblasts with PDGF and/or DTT does not alter the gross morphology of fibroblasts. Cells were incubated in serum free media for 24 hr with (A) no additional treatment, (B) 6 hr 10 ng/ml PDGF-BB beginning at t = 18 hr, (C) 6 hr 5 mM DTT beginning at t = 18 hr, or (D) 6 hr 10 ng/ml PDGF-BB and 5 mM DTT beginning at t = 18 hr before fixing and staining for DAPI and PDI. Stained cells were then imaged at 20x magnification with a brightfield fluorescent microscope. Scale bar represents 10 µM.

5.3 PDGF and DTT help stimulate BJ fibroblast migration

Previous work has shown that PDGF-BB is capable of accelerating wound healing (Pierce, Mustoe, Altrock, et al. 1991). DTT was used to investigate if the further addition of a reducing agent enhances the accelerated wound closing, observed with just PDGF. BJF were serum starved for 24 hr and were then scratched with a pipette tip. The BJF were either untreated or treated with 10 $ngml^{-1}$ and +/- 5 mM DTT. The BJF were imaged for 10 hr on a cell observer microscope (Figure 5.4A). The addition of DTT caused 62% of the BJF to migrate into the wound site compared to only 45% when DTT was not present (Figure 5.4C).

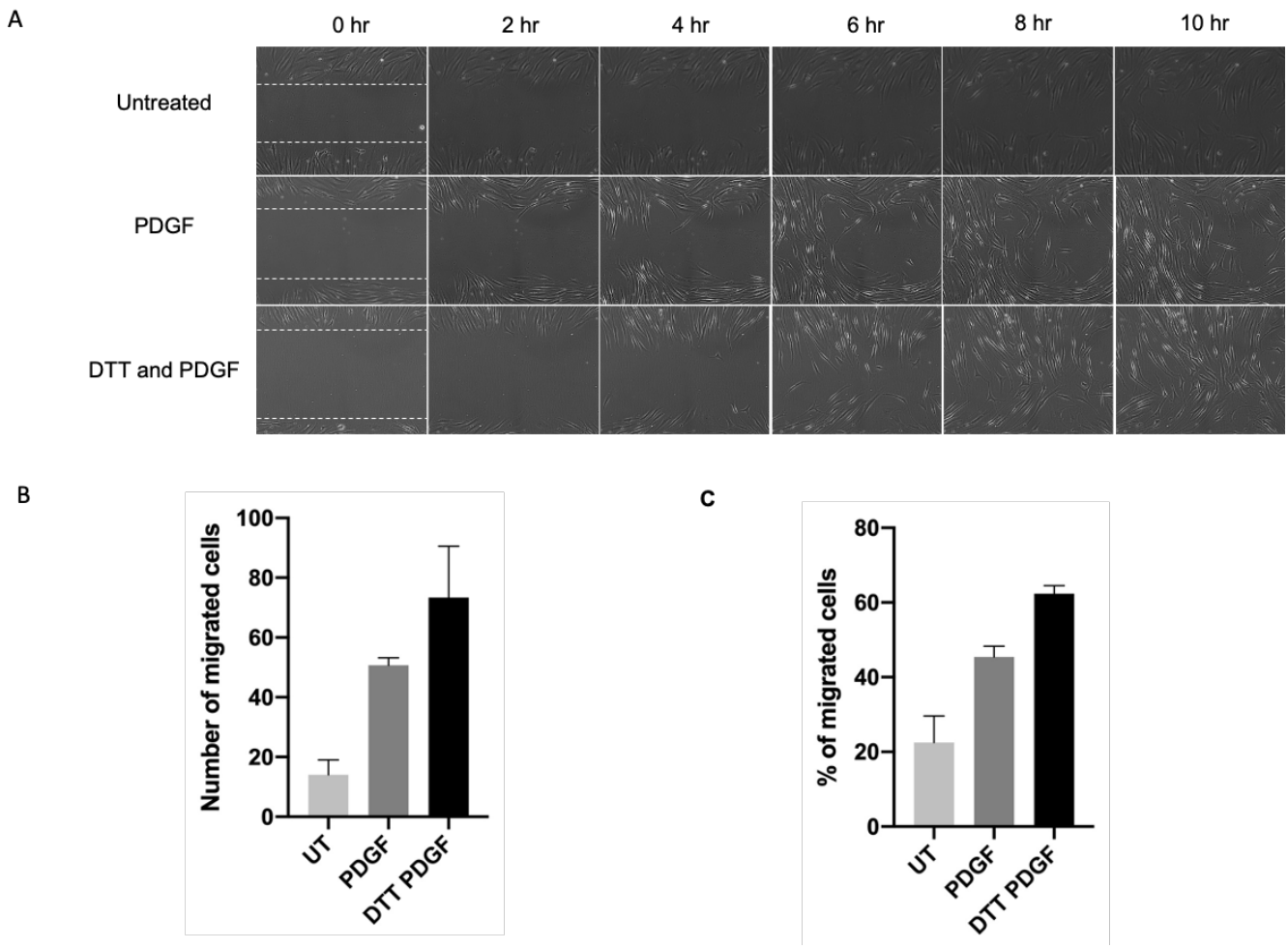

Figure 5.4: Treating BJ fibroblasts with DTT causes an increased amount of wound closure. (A) Time lapse images of BJ fibroblasts, representative images showing the effects of the various reducing agents on the migration/wound closure of the fibroblasts. (B) Quantitative analysis of the number of cells that pass a reference point after 10 hr (mean ± SD, n=3, P=0.0013). (C) Quantitative analysis of the percentage of cells that pass a reference point after 10 hr (mean ± SD, n=3, P=0.0001).

5.4 P-lamin A/C levels are affected by PDGF treatment

The work previously performed by the laboratory found an increase in LMNA steady state levels after BJF have been treated with PDGF-BB (Figure 5.2A) (Carne 2018). BJF were grown in serum containing media for 24 hr, SFM for 24 hr or SFM for 24 hr with 10 $ngml^{-1}$ PDGF added for the last 6 hr. The cells were then lysed and analysed with SDS-PAGE and western blotting. Antibodies against P-lamin A/C, lamin A/C (Jol2) and β-actin were used. When analysing the levels of protein expression, there was a higher lamin A/C expression and Lamin A/C phosphorylation in the BJF treated with PDGF as opposed to those just grown in SFM (Figure 5.5). This confirmed the results that were found in the proteomics, where the addition of PDGF to BJF increased the expression of lamin A/C and in turn appeared to increase phosphorylation at serine 22 (Ser22). Other sites on lamin A/C may be phosphorylated; other published work has shown that serine 404 (Ser404) can also become phosphorylated on lamin A/C (Cenni, Bertacchini, Beretti, et al. 2008). As the only commercially available lamin A/C phospho antibody can only detects Ser22 phosphorylation some sites may be missed, resulting in a weaker western blot signal than would be obtained for an antibody that recognises multiple phosphorylation sites.

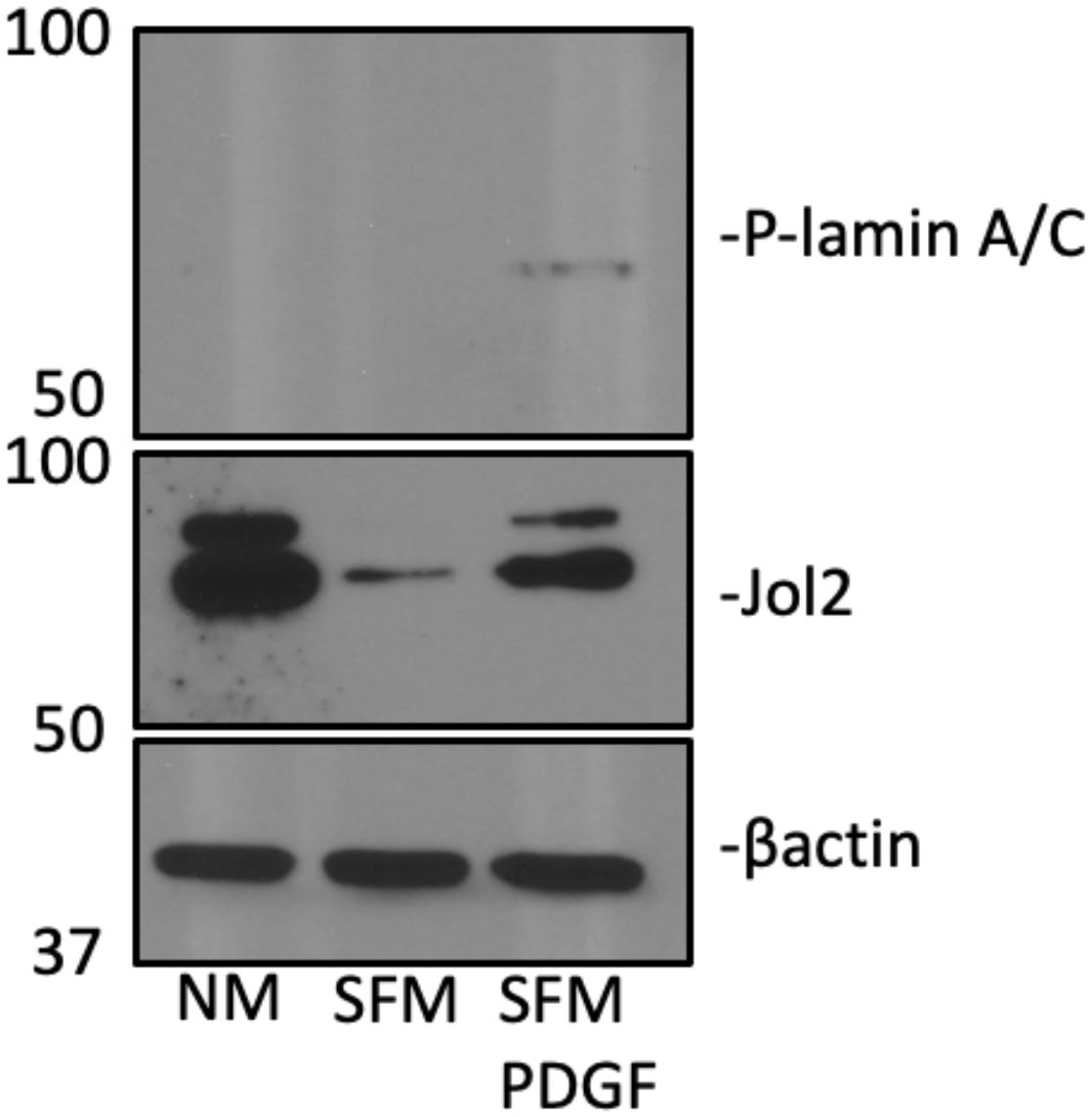

Figure 5.5: P-lamin A/C levels are increased after serum starvation and treatment with PDGF. BJF cells were either grown in serum containing media for 24 hr, SFM for 24 hr or serum free media for 24 hr with 10 ng ml^{-1} PDGF added for the final 6 hr. These cells were then lysed and analysed by SDS-PAGE and WB. Antibodies P-lamin A/C and lamin A/C were used. β-actin was used as a loading control.

To visualise the effect of PDGF treatment on BJ fibroblast cells, IF was performed. The BJ fibroblast cells were grown in serum containing media for 24 hr, SFM for 24 hr or SFM for 24 hr with 10 $ngml^{-1}$ PDGF added for the last 6 hr. These BJF cells were then fixed and stained with antibodies against PDI, P-lamin A/C and DAPI. The P-lamin A/C intensity was analysed in ImageJ and plotted in Prism 9 (Figure 5.6). Similarly to the western blot results, there is a higher P-lamin A/C intensity in the BJF treated with PDGF for 6 hr as opposed to those grown in the SFM exclusively. This further backs up the initial proteomics data, confirming that after PDGF treatment there is an increase in lamin A/C phosphorylation.

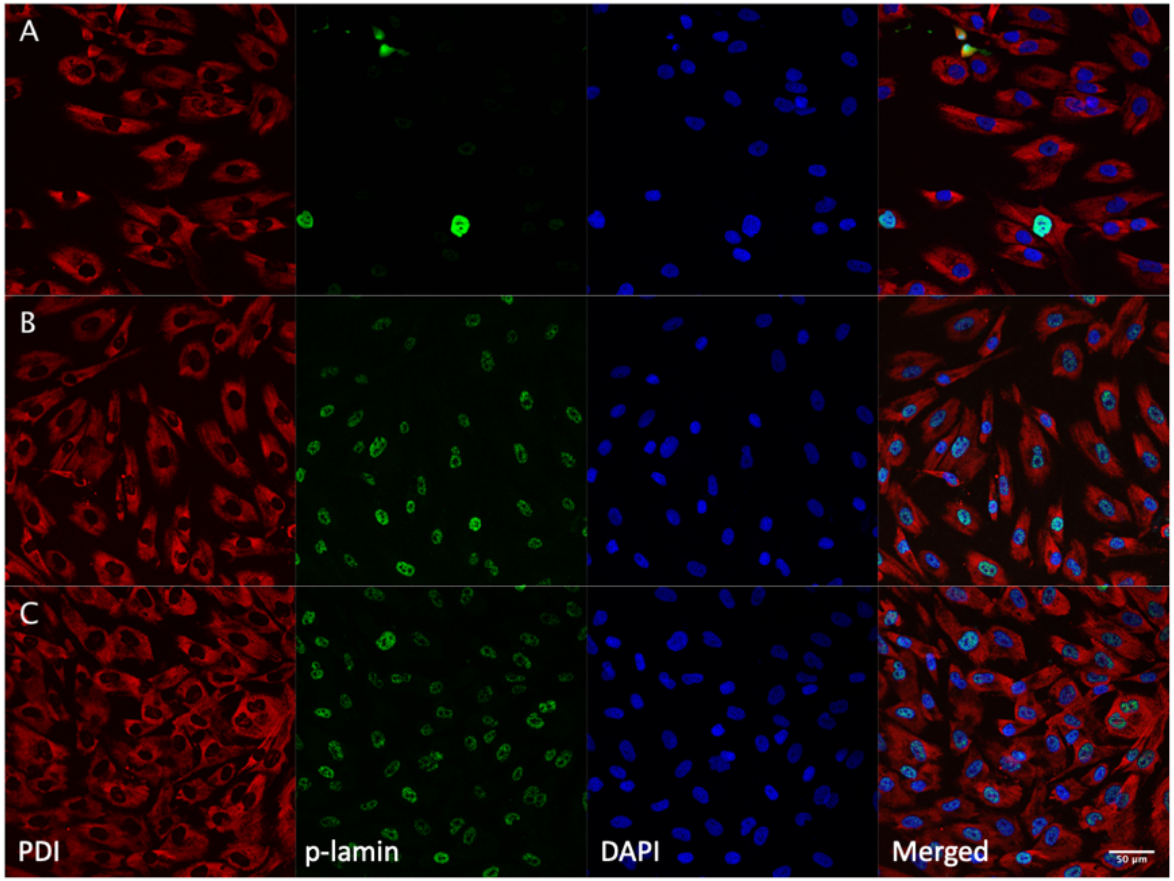

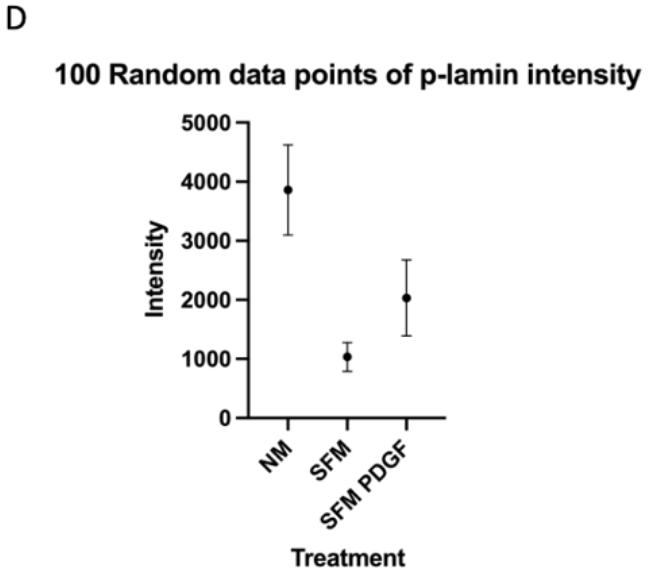

Figure 5.6: The intensity of P-lamin A/C staining in IF is increased in PDGF containing SFM as opposed to that without. BJF were grown on coverslips in serum containing media for 24 hr, SFM for 24 hr or SFM for 24 hr with 10 ng ml^{-1} PDGF added for the final 6 hr. The cells were fixed and stained for P-lamin A/C. P-lamin intensity from (A) normal media, (B) SFM and (C) SFM with PDGF were measured in ImageJ and then plotted in Prism 9 (D). DAPI was used to stain the DNA and the images were taken on a Zeiss 800 confocal microscope with Airyscan at 63x.

To observe if physical insult, namely a pipette tip to scratch the BJF cell lawn, had any effect on P-lamin A/C expression in the BJF. A wound closing assay was performed on BJF grown in serum containing media for 24 hr, SFM for 24 hr or SFM for 24 hr with 10 $ngml^{-1}$ PDGF added for the last 6 hr. The cells were fixed and stained with antibodies against PDI, P-lamin A/C and DAPI. ImageJ was used to measure the intensity of cells present in the wound vs. those present in the periphery. The BJF grown only in SFM had a higher percentage of P-lamin A/C stained cells present in the wound compared to those grown in SFM with the addition of PDGF (Figure 5.7). There appeared to be more BJF present in the centre of the wound of the BJF grown in SFM and PDGF compared to that present in just SFM. This result was similar to the wound closing assay performed previously (Figure 5.4), suggesting that PDGF is once again exerting its wound closing capabilities.

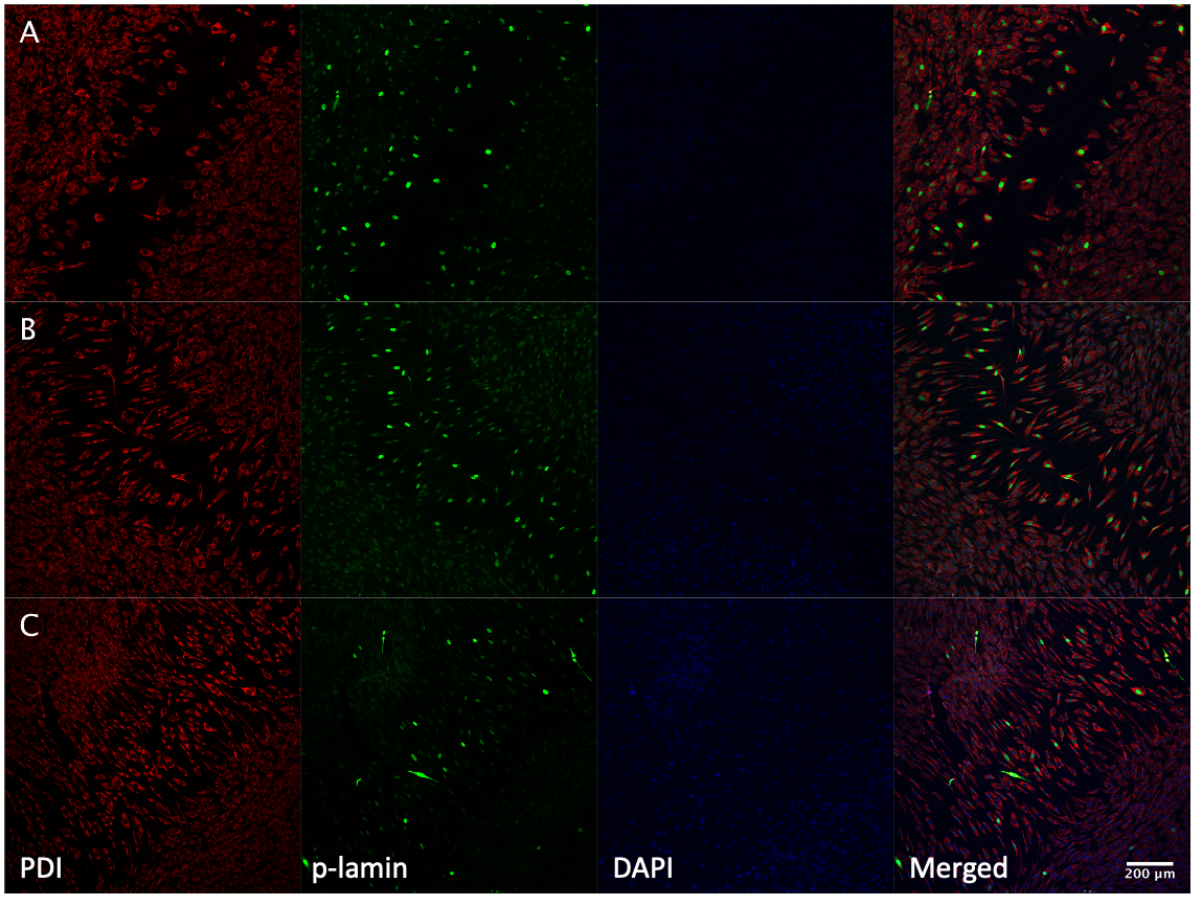

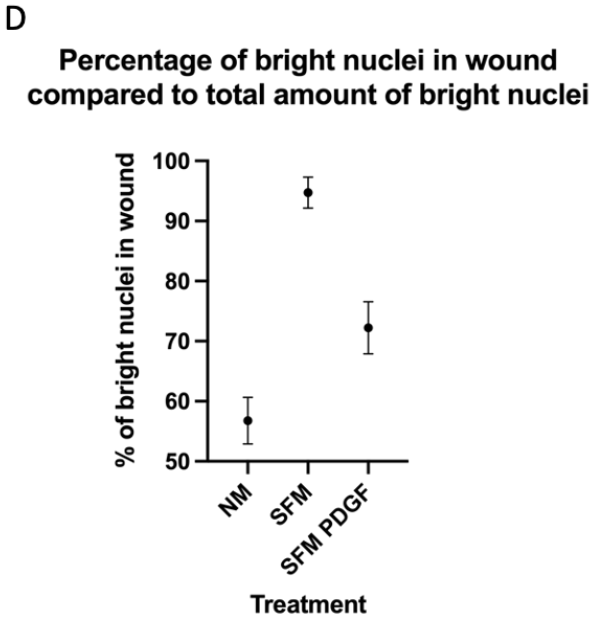

Figure 5.7: The proportion of P-lamin A/C staining is higher in the wound site of cells grown in SFM. A wound closing assay was performed on BJF grown on coverslips in serum containing media for 24 hr, SFM for 24 hr or SFM for 24 hr with 10 ng ml^{-1} PDGF added for the final 6 hr. The cells were fixed and stained for P-lamin A/C. The number of cells that were stained at a higher intensity were measured in (A) serum containing media, (B) SFM and (C) SFM with PDGF. The cells which had stained more intensely were counted in ImageJ and plotted using Prism 9 (D). DAPI was used to stain the nucleus and the images were taken on a Zeiss 800 confocal microscope at 10x.

To compare how detergents affect lamin and P-lamin recovery from cell lysis, BJF were grown in serum containing media for 24 hr, SFM for 24 hr or SFM for 24 hr with 10 $ngml^{-1}$ PDGF added for the last 6 hr. The cells were then lysed in either, RIPA buffer, MNT buffer containing Tx100 or MNT buffer containing NP40. Each of the lysis buffers contained a different detergent which were able to extract differing parts of the cells, SDS in the RIPA buffer is a strong lysis agent, Tx100 in the MNT buffer is mild and non-denaturing and NP40 is also non-denaturing and mild although it is better at isolating cytoplasmic proteins and not nuclear (Walker 2002). Similarly, to the previous P-lamin expression experiment (Figure 5.5) the expression of P-lamin A/C is increased in SFM with PDGF as opposed to that without, validating the previous results (Figure 5.8). There does not appear to be any discernible difference in the amount of lamin or P-lamin expression between the different lysis buffers, but as shown earlier (Figure 5.5) even with the different detergents there appears to be higher expression of both the lamin A and lamin C bands and P-lamin A/C bands. The experiment was a preliminary analysis (n=1), hence further repeats would be required to determine statistical significance.

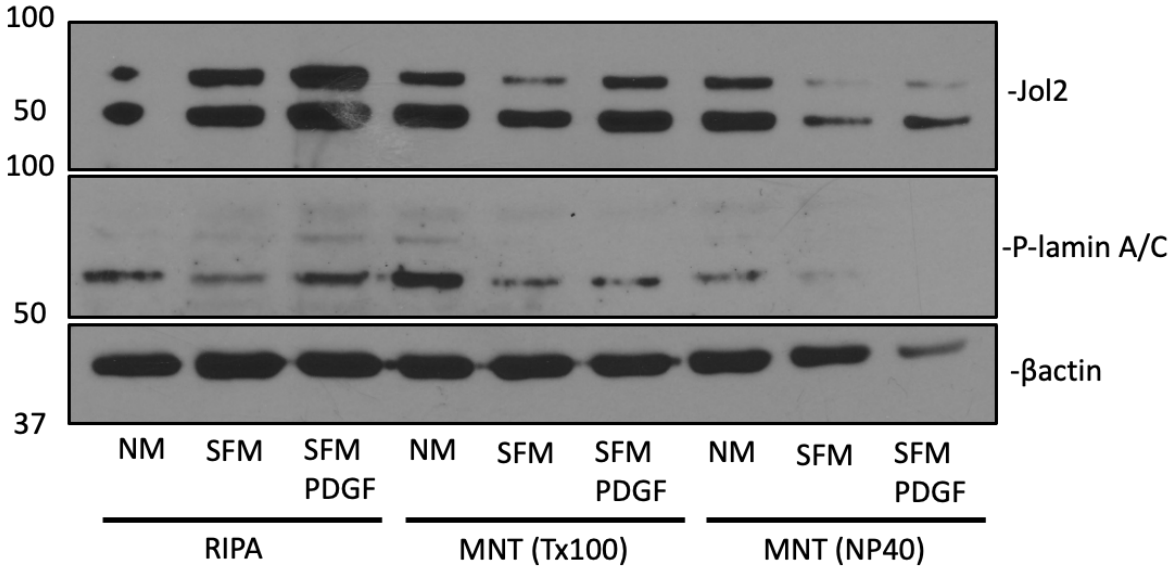

Figure 5.8: Lamin recovery appears to be unaffected by the detergent used for cell lysis. BJF were either grown in serum containing media for 24 hr, serum free media for 24 hr or serum free media for 24 hr with 10 ng ml^{-1} PDGF added for the final 6 hr. They were then either lysed with RIPA buffer, MNT containing Tx100 or MNT containing NP40. The lysates were analysed by reducing SDS-PAGE and WB. Antibodies against P-lamin A/C and lamin A/C were used. β-actin was used as a loading control. n=1

5.5 Proteomic analysis of BJ fibroblasts treated with H_2O_2 and niacinamide

As shown previously in the wound closing assays (Figure 5.4), PDGF can promote cell growth and proliferation of BJF cells. This exposure to a growth factor will have an impact on the rate of wound closure (Figure 5.4). Another chemical which offers cellular protective properties is niacinamide. Niacinamide has been shown to also help with wound closing *in vitro* by promoting fibroblast proliferation and upregulate NAD+ and NADPH which help maintain cellular redox balance (Wessels, Pretorius, Smith, *et al.* 2014; Magni, Amici, Emanuelli, *et al.* 2004). To observe if a similar protective effect of niacinamide occurred with BJF, they were grown in SFM for 24 hr and untreated, treated with 1 mM H_2O_2 for 6 hr or treated with 500 µM Niacinamide for 24 hr with 6 hr of H_2O_2. 500 µM of Niacinamide was used as this was a concentration previously optimised by Proctor and Gamble (P&G) who were involved in the

niacinamide work. The cells were lysed and analysed with DIA MS. Approximately 4600 proteins were identified from the 3 biological repeats and 3 technical repeats from untreated vs 1 mM H_2O_2 and the same from untreated vs 1 mM H_2O_2 with 500 µM Niacinamide (Figure 5.9). Of these two groups, the untreated vs 1 mM H_2O_2 had 216 significant proteins (FDR adjusted $P<0.05$) identified (Figure 5.10A) and the untreated vs 1 mM H_2O_2 with 500 µM Niacinamide had 187 significant proteins (FDR adjusted $P<0.05$) identified (Figure 5.10B).

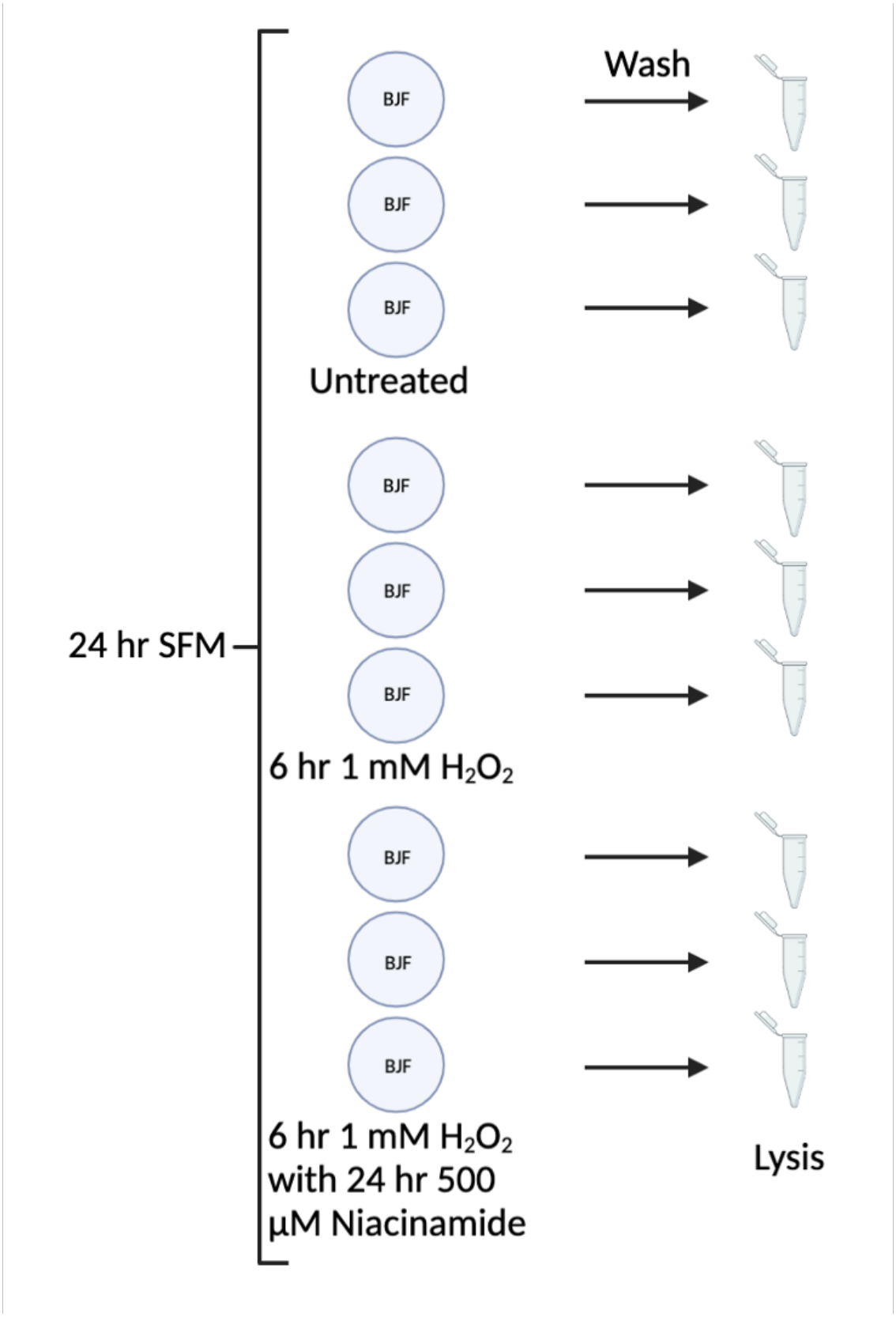

Figure 5.9: DIA proteomic analysis of BJF cells subjected to H_2O_2 and niacinamide. Schematic. Lysates from 3 biological repeats for each state were trypsinised and used for MS analysis with 3 technical injections for each.

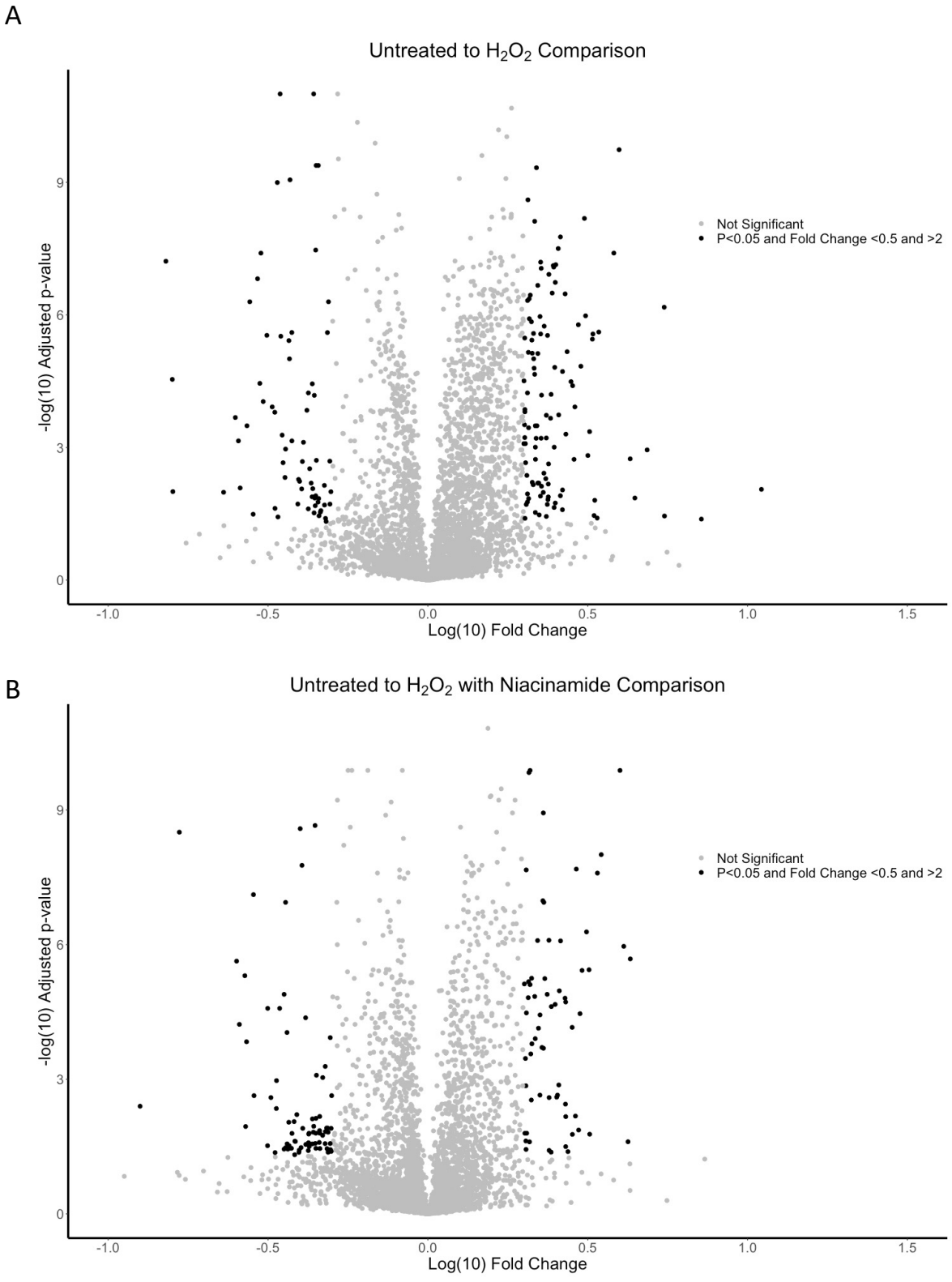

Figure 5.10: DIA proteomic analysis of BJF cells subjected to H_2O_2 and Niacinamide. Cells were untreated, treated with 1 mM H_2O_2 for 6 hr or treated with 500 µM Niacinamide for 24 hr. Protein identification and relative quantification was achieved using SWATH acquisition on a TripleTOF 6600 (SCIEX). Proteins with a significant (FDR-adjusted p<0.05) and fold change > 2 are marked on the volcano plot. (A) Untreated vs 1 mM H_2O_2 comparison and (B) untreated vs 1 mM H_2O_2 with 500 µM Niacinamide. Figures represent 3 biological repeats and 3 technical repeats.

To compare the differences in the proteins in those exposed to just 1 mM H_2O_2 vs those exposed to 1 mM H_2O_2 and 500 µM Niacinamide, the significant proteins from each data set were extracted and inputted into R. A Venn diagram was created which showed that of all the significant proteins only 64 overlapped (Figure 5.11).

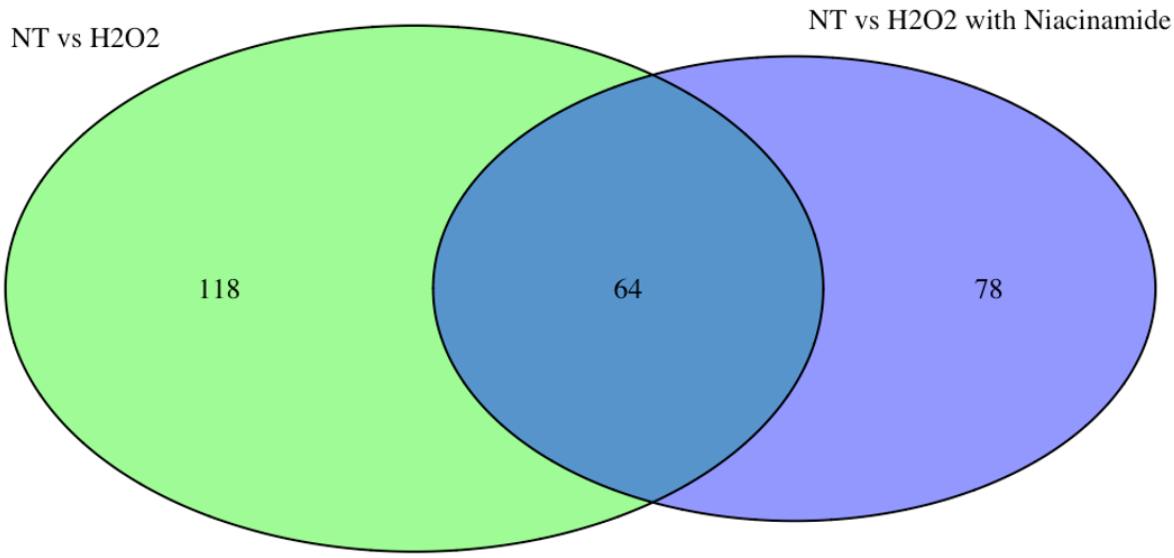

Figure 5.11: Differences in protein changes when BJF cells were treated with H_2O_2 and Niacinamide. A Venn diagram was used to visualise the differences in individual protein changes with the different treatments. Untreated vs H_2O_2 was compared with untreated vs H_2O_2 and Niacinamide.

To investigate if the levels of the proteins that change in both untreated vs H_2O_2 and untreated vs H_2O_2 with niacinamide, the data was analysed in R. Heatmaps were generated which showed how the fold change either increased (Figure 5.12A) or decreased (Figure 5.12B) when niacinamide was added. One of the key proteins identified was glutathione peroxidase-1 (GPX1) an enzyme which detoxifies H_2O_2 and is an antioxidant enzyme (NCBI 2022). In the experiment where the BJF are treated with just H_2O_2, GPX1 fold change was 3.11

when compared to the untreated BJF, in a separate experiment the fold change of GPX1 drops to 1.7 after the addition of niacinamide when compared to the untreated sample. If the niacinamide is causing the protective effects, then lower GPX1 expression is to be expected. Another gene which sees a significant change after the addition of niacinamide is super oxide dismutase 2 (SOD2). This enzyme clears ROS in the mitochondria and protects against apoptosis (Pias, Ekshyyan, Rhoads, *et al.* 2003). The fold change of SOD2 increases from 0.34 when compared to untreated, to 0.25 after the addition of niacinamide when compared to the untreated sample. The addition of niacinamide may be stimulating the BJF cells to produce more SOD2 to protect the cell against the increased ROS generated by the H_2O_2 treatment.

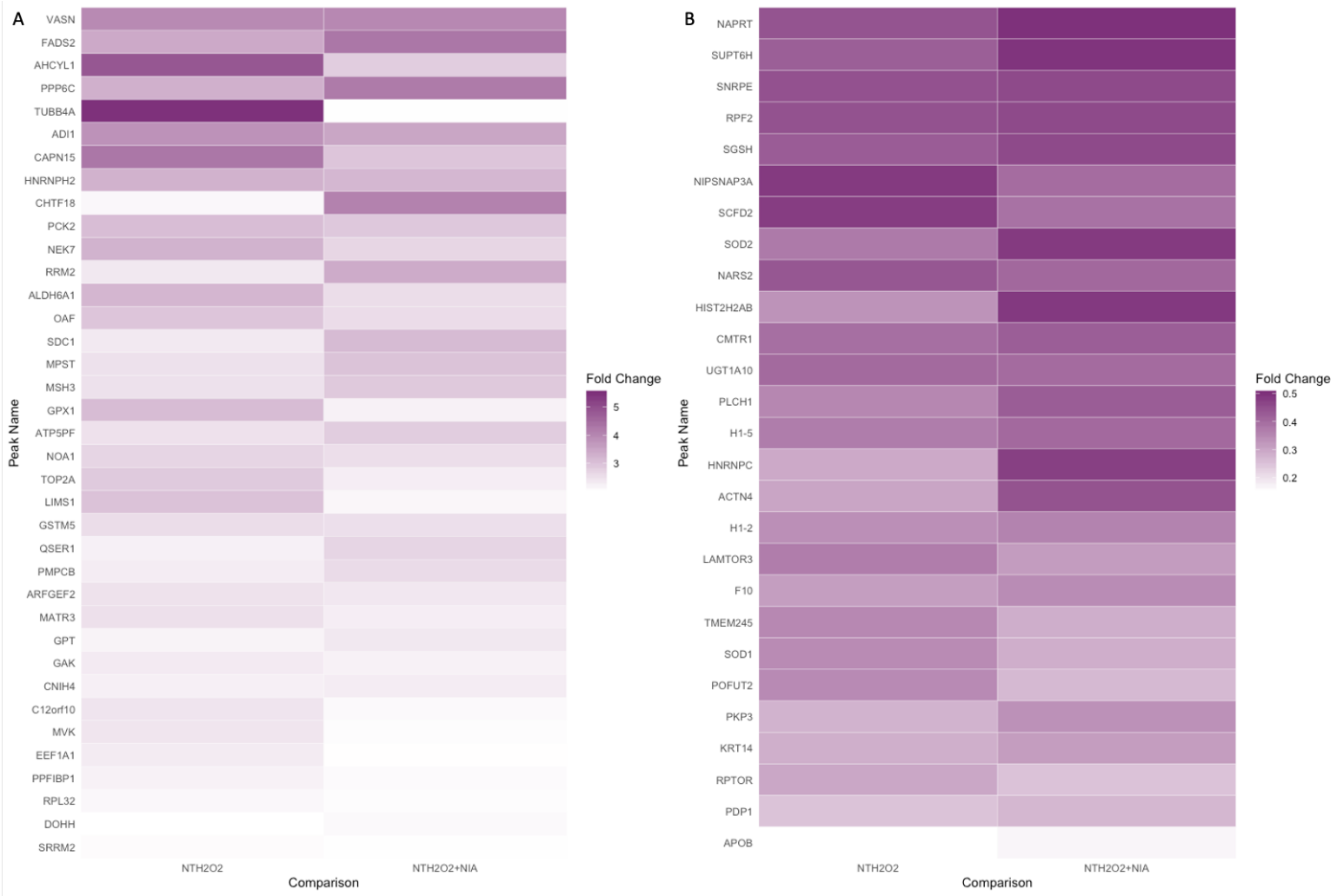

Figure 5.12: Visualising the changes in individual proteins that are affected in both the untreated vs H_2O_2 and the untreated vs H_2O_2 with Niacinamide. Heatmaps were used to show how the fold change of the proteins either increased (A) or decreased (B).

To observe how the intracellular distribution of the proteins affected by both untreated vs H_2O_2 and untreated vs H_2O_2 with niacinamide the data was inputted into R and the gene names were replaced by their GO values. The GO values were then sorted based on their biological processes, cellular compartment, or molecular function (Figure 5.13). One of the molecular functions that changes occur in is the antioxidant activity and detoxification in the biological processes. These are proteins which have been identified by GO analysis to be involved in antioxidant activity and detoxification in the cell. This suggests that the niacinamide was influencing these processes, but it is not known how. It is possible that the presence of niacinamide reduces the amount of ROS present in the cell or it may upregulate protective proteins which affects antioxidant activity in the cell. Future experiments could involve identifying which proteins fall under the antioxidant activity and detoxification. These proteins could be validated in western blotting and may be targets for increasing antioxidant activity in the skin.

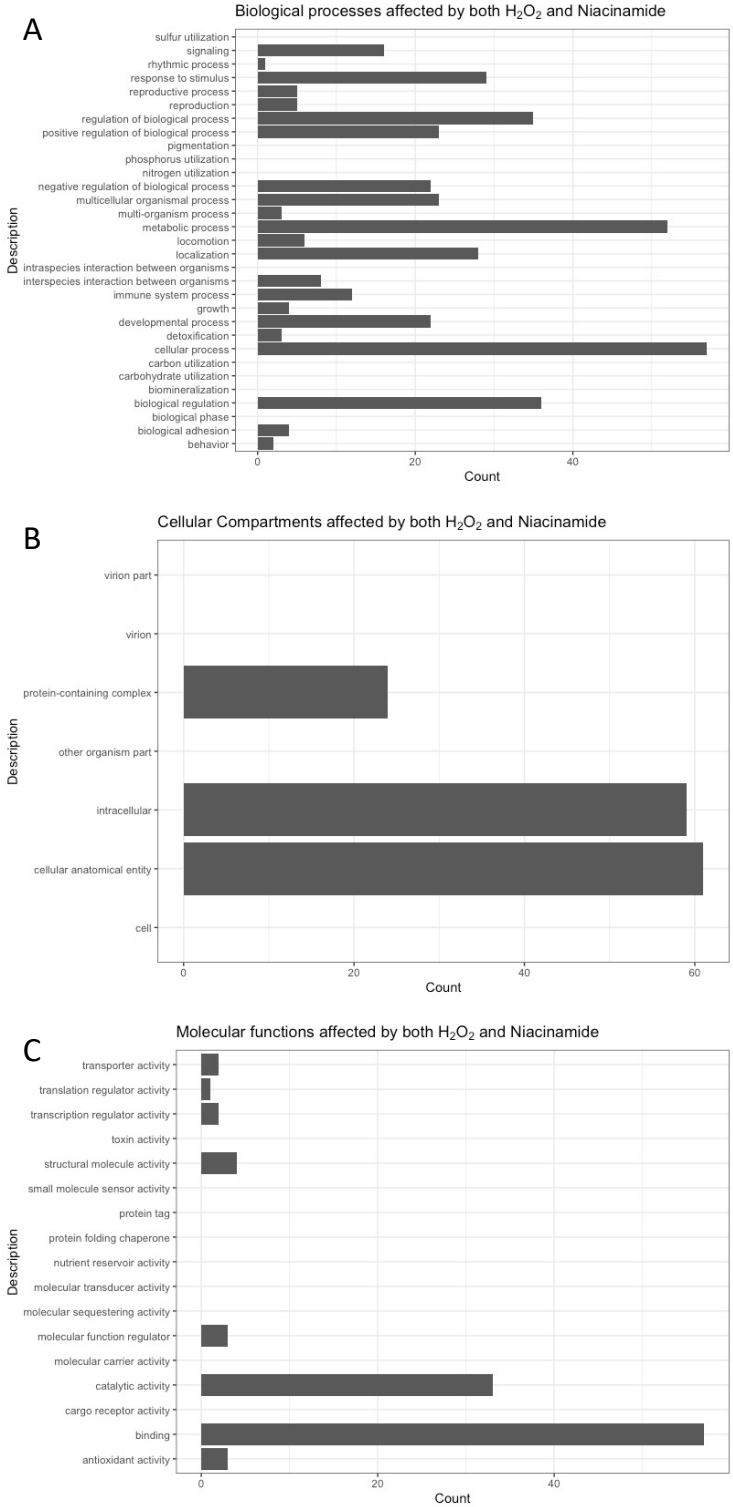

Figure 5.13: GO analysis of proteomic data from SWATH of BJF treated with 1 mM H_2O_2 and 500 µM Niacinamide. The proteins affected by both the untreated vs H_2O_2 and the untreated vs H_2O_2 with Niacinamide were analysed. The significant (FDR-adjusted $p<0.05$) SWATH data with a fold change > 2 was converted to GO terms in R, these were then plotted based on (A) biological processes, (B) molecular function and (C) cellular compartment.

In summary, PDGF and niacinamide both offer protective effects *in vitro* wound closing assays on BJF. PDGF has been found to mainly affect Lamin A/C and its phosphorylation, offering a previously underappreciated sensitivity of lamins to signalling from growth factors in skin cells. In contrast niacinamide appears to offer protective function in the form of protecting against H_2O_2, this has also been shown by Tan et al who observed that niacinamide restored the energy metabolism of human primary keratinocytes after it was lost due to oxidative stress (Tan, Tan, Chin, *et al.* 2021). Further experiments could be performed to validate the proteomics results from the niacinamide data such as treating cells with H_2O_2 +/- niacinamide and observing if there is an increase or decrease of some of the identified proteins such as GPX1 and SOD2. Another experiment could involve using a wound closing assay to observe if niacinamide has any protective effects on the wound closure of the BJF cells.

5.6 Discussion and conclusion

The results in this chapter relate to the protective functions of PDGF and niacinamide in response to reductive and oxidative stress on BJ fibroblasts. The work also highlights a novel observation of increased P-lamin A/C phosphorylation after stimulation by PDGF. Previous work performed in this laboratory showed that after treating BJ fibroblasts previously grown in SFM with 10 $ngml^{-1}$ PDGF-BB for 24 hr there was an upregulation of lamin A/C expression (Figure 5.2) (Carne 2018). To validate this work and to ensure the upregulation was due directly to the PDGF treatment IF was performed which showed that there was no cell rounding or death after PDGF treatment (Figure 5.3). Similarly to work performed by Pierce et al., the addition of PDGF caused an increase in the rate of wound closure. This was most likely due to an autocrine feedback loop being created which increases the amount of PDGF

released and other growth factors which contribute to wound closure (Pierce, Mustoe, Altrock, et al. 1991).

As lamin A/C levels were shown to increase in previous proteomics data performed by this laboratory, this work was validated by WB (Figure 5.5). Lamin A/C levels did increase after the addition of PDGF as expected but the levels of lamin A/C phosphorylation also increased. The antibody used in this work only identifies phosphorylation at the site Ser22, but other studies have shown that lamin A/C can be phosphorylated on multiple sites, such including high turnover sites. Some of these sites are Ser390, Ser392 and Ser404. These sites can be phosphorylated by different kinases such as Cdk, PKC and Akt (Kochin, Shimi, Torvaldson, et al. 2014; Cenni, Bertacchini, Beretti, et al. 2008). The higher intensity of P-lamin A/C staining after the addition of PDGF may be due to the growth factor effects of PDGF causing the cells to prepare for cell division by increasing lamin A/C phosphorylation (Figure 5.6). Multiple studies have shown that PDGF treatment enhances the proliferation of fibroblasts through mechanisms such as downregulating programmed cell death 4 (PDCD4) (Lee, Yun, Paik, *et al.* 2016). Kochin et al., showed that lamin A/C is hyper phosphorylated on two interphase sites in mitotic cells; one of these sites is an N-terminal Ser22, and this is the same site as detected by the antibody used in IF. Phosphorylation on this site contributes to lamin A/C disassembly in preparation for mitotic division (Kochin, Shimi, Torvaldson, *et al.* 2014). It is possible that the PDGF treatment is causing more division in the BJ fibroblasts, and this indirectly causes an increase in lamin A/C phosphorylation as the cells undergo mitotic division. Future experiments could involve using a live cell imaging method with a dye or transfected cells to target Ser22 in lamin A/C to observe if there is increase in cell division after PDGF treatment. Conversely there appears to be more nuclei staining with P-lamin A/C in the SFM media as opposed to the SFM with PDGF in the wound closing assay (Figure 5.7) this differs from what

was previously observed in this chapter (Figure 5). Lamin levels have been shown to change in relation to nuclear stiffness and this can affect migration in cells as stiffer nuclei may impair cell migration (Harada, Swift, Irianto, et al. 2014). Lamin A/C phosphorylation has been purported to be also involved in cell migration as cells grown on a softer surface appear to have softer nuclei most likely due to the lamin A/C phosphorylation causing solubilisation of lamin A/C (Buxboim, Swift, Irianto, *et al.* 2014). The decreased levels of lamin A/C phosphorylation observed by IF in the wound closing assay (Figure 5.7) are likely due to the fact there appears to be more cells present in the middle of the wound. The increase in the number of cells may have meant there was less movement at the time the cells were fixed so the cells may have had a stiffer nucleus and thus less lamin phosphorylation occurred. Live cell imaging of the wound closing with tagged lamin A/C would allow for the observation of the point where lamin A/C becomes solubilised in a wound closing scenario.

Niacinamide, like PDGF, can offer protective functions to skin cells. To quantify this, DIA MS was used to study how niacinamide can protect cells after the addition of an oxidising agent such as H_2O_2. ALDH6A1 is an enzyme which is involved in the valine (an amino acid) catabolic pathways and pyrimidine (a nitrogenous base found in DNA) catabolic pathways. After H_2O_2 treatment ALDH6A1 expression levels are increased but when comparing +/- niacinamide treatment ALDH6A1 fold change decreases from 3.21 to 2.57. ALDH6A1 has been shown to be involved in the valine, leucine, and isoleucine degradation pathway; this generates succinyl-CoA by promoting valine metabolism. ALDH6A1 is also involved in propanoate metabolism pathway and generates acetyl-CoA. Where both pathways lead to increased energy levels in the cell. This increased energy in the cell may allow leucine to counteract H_2O_2 induced damage in the cell (Wu, Liu, Cheng, *et al.* 2022). The decrease of ALDH6A1 expression after the addition of niacinamide suggests that niacinamide may itself

be exerting protective effects against H_2O_2, meaning less ALDH6A1 is required to generate energy to protect the cell. Another protein which shows a change after the addition of niacinamide is nicotintinate phosphoribosyltransferase (NAPRT); this enzyme is involved in the first step of the biosynthesis of NAD from niacinamide. The fold change decreased from 0.44 to 0.50. The presence of NAD/NADPH in the cell are critical for reduction of oxidative stress, in this case H_2O_2 as NADPH is a reducing agent which can remove ROS (Audrito, Messana & Deaglio 2020). The reduction of NAPRT expression after the addition of niacinamide may be unexpected as it is involved in the first step of the biosynthesis of NAD, but niacinamide itself may have antioxidant properties meaning the cells do not need to upregulate the expression of NAPRT. Future experiments would involve using WB to validate the results observed from the proteomics data, followed by functional analysis of the relevant metabolic pathways.

In conclusion, the work in this chapter has shown that PDGF affects lamin A/C phosphorylation indirectly and this work could be used to investigate degenerative disorders such as progeria as lamin A/C Ser22 phosphorylation binding sites are lost in this ageing disease (Ikegami, Secchia, Almakki, et al. 2020). The work also shows that niacinamide can alter protein homeostasis in cells undergoing oxidative stress. UV damage on skin can cause oxidative stress so further work into how niacinamide is able to help protect or prevent UV damage using proteomics could be performed.

6 Optimising collagen imaging and processing in HT1080 cells for skin ageing

6.1 Introduction

In this chapter, the optimisation of collagen imaging in HT1080 cells was explored. Collagen is an important PDI client but tagging collagen can interfere with its post-translational processing which has proven difficult in the field. Thus, the processing of a novel mNeonGreen collagen reporter construct was analysed in transfected cells by IP and mass spectrometry. This was to observe if collagen is being correctly processed with the correct post-translational modifications.

The skin is the largest organ in the body. It acts as a barrier against pathogen invasion and prevents dehydration. It is made up of three layers; the epidermis, dermis, and subcutaneous tissue. Also present in the skin are hair follicles, sweat and sebaceous glands. The epidermis or outer layer of the skin contains keratinocytes and melanocytes. In contrast, the dermis is thicker and sits below the epidermis, it contains blood vessels and the nerves which are supported by a collagen matrix (the ECM) (Calleja-Agius, Muscat-Baron & Brincat 2007). The two are joined by the dermal epidermal junction (DEJ) which is where the basal epidermal keratinocytes are attached to a type IV collagen containing basement membrane via hemidesmosomes. The dermis is attached to the DEJ via collagen VII and fibrillin rich microfibre bundles. As described in chapter 3, the dermal fibroblasts form the collagen and other key ECM proteins (Naylor, Watson & Sherratt 2011).

As we age the skin is exposed to UV radiation, which causes photo-ageing of the skin. The quality of the skin also deteriorates due to chronological ageing, hormonal effects, and other environmental factors. These factors can be referred to as intrinsic or extrinsic ageing. Intrinsic ageing occurs as time passes whereas extrinsic ageing is usually due to UV radiation

exposure. Due to ageing, skin becomes wrinkled, stiffer and is unable to recoil as well. However, these processes do occur faster and are more severe in skin which has been exposed to more UV radiation (Escoffier, de Rigal, Rochefort, *et al.* 1989; Warren, Gartstein, Kligman, *et al.* 1991). The skin primarily contains type I and type III collagen (Bahar, Bauer, Tredget, *et al.* 2004). Fibroblasts synthesise collagen from procollagen. The procollagen undergoes PTMs such as hydroxylation which improve the collagens stability and tensile strength. Collagen in young people is present in uniform fibrillar units. Ageing causes the skin becomes thinner; its structure and function also changes. Clumps of collagen form from the basophilic area which can be due to collagen degradation (Waller & Maibach 2005). As we age the quality of the collagen diminishes, due to the fact there are less enzymes such as lysyl oxide present which deal with collagen PTM (Calleja-Agius, Muscat-Baron & Brincat 2007).

Collagen is mainly present in the dermis of the skin. Around 85-90% of collagen in the dermis is type I collagen and around 10-15% is type III collagen. Collagen is mainly synthesised by dermal fibroblasts which create precursor polypeptide chain procollagen molecules (Smith, Holbrook & Madri 1986). Collagen in the skin is affected by chronological ageing and environmental ageing from UV irradiation. UV irradiation has been shown to activate protein kinase signalling pathways roughly 1 hour after exposure to UV. Several kinases become phosphorylated with the maximum effect occurring after 4 hours of exposure. This then upregulates AP-1 which then leads to the upregulation of gene transcription for various matrix degradation proteins such as matrix metalloproteinase 1 (MMP-1), MMP-3 and MMP-9 (Angel, Szabowski & Schorpp-Kistner 2001; Cobb 1999; Fisher, Talwar, Lin, *et al.* 1998). Type I and III collagen are cleaved first by MMP-1, this targets the central triple helix at a single site. After this, MMP-3 and MMP-9 can cleave more of the remaining collagen present (Sternlicht & Werb 2001). As UV irradiation occurs, the structural integrity of collagen in the dermis is

impaired, this is because with each exposure to UV the collagen damage from MMPs accumulates. UV irradiation also causes the downregulation of type I and III collagen by decreasing the amount of procollagen transcription (Fisher, Datta, Wang, *et al.* 2000). The increased AP-1 expression from UV radiation also blocks transforming growth factor β (TGF-β), this cytokine is a potent inducer of collagen deposition (Chung, Agarwal, Uitto, *et al.* 1996; Verrecchia, Tacheau, Schorpp-Kistner, *et al.* 2001). Quan et al., also showed that UV irradiation downregulated the expression of the type II TGF-β receptor, which decreased the cells responsiveness to TGF-β which downregulated the expression of type I procollagen genes (Quan, He, Voorhees, *et al.* 2001). In aged skin fragmented collagen, decreased cell-collagen interactions and a reduction in total collagen were observed. *In vitro* fibroblasts obtained from young adults vs. those obtained from older individuals showed a reduction of collagen synthesis in the fibroblasts from the older individuals. This, combined with the fact that aged skin contains less fibroblasts, further decreases collagen production (Varani, Warner, Gharaee-Kermani, *et al.* 2000). The decrease in collagen in the skin causes a reduction in mechanical tension applied to fibroblasts. There are links between mechanical tension on fibroblasts and the production of collagen and other ECM components (Geesin, Brown, Gordon, *et al.* 1993; Lambert, Soudant, Nusgens, *et al.* 1992). Therefore, a decrease in collagen and a reduction of mechanical tension in older skin will further cause a decrease in collagen production (Varani, Dame, Rittie, *et al.* 2006).

Two of the key chaperones which are involved in collagen folding are prolyl 4-hydroxylase (P4HA) and P4HB which is also known as PDI. P4H is an $\alpha_2\beta_2$ tetrameric α-ketoglutarate (α-KG)-dioxygenase and it catalyses the 4-hydroxylation of proline to promote collagen triple helix formation (Gorres & Raines 2010). The α subunit of P4H is responsible for binding to peptides and for the catalytic activity of the protein. There are three isoforms

present in cells with P4HA1 being the most common of these and it is the primary contributor to protein hydroxylation. The hydroxylation of proline residues on individual pro-collagen strands are catalysed by P4HA in the Yaa position of the Xaa-Yaa-Gly triplets (Cardinale & Udenfriend 1974; Hutton, Kaplan & Udenfriend 1967; Berg & Prockop 1973a). The two β subunits of P4H (P4HB/PDI) are discussed in detail in chapter 1 (section 1). The full function of the P4HB subunit is unknown but it is required to keep P4H in the ER as P4HB contains a KDEL sequence. P4HB also prevents the α unit from aggregating (Vuori, Pihlajaniemi, Marttila, *et al.* 1992; Vuori, Pihlajaniemi, Myllyla, *et al.* 1992). A missense mutation in P4HB that occurs in Cole-Carpenters (CC) syndrome causes bone fragility (Rauch, Fahiminiya, Majewski, *et al.* 2015). This is likely due to the fact collagen formation is impeded and this may affect the assembly or deposition of ECM. This mutation does not seem to affect collagen production elsewhere e.g., in the skin (Balasubramanian, Padidela, Pollitt, *et al.* 2018).

To mimic a possible ageing phenotype in cells with regards to collagen formation the preliminary work presented in this chapter observed how PDI inhibitor treatment affected cell viability and how it affected the PDI interactome. The PDI inhibitors used were PACMA31 and 16F16; both are small molecule irreversible inhibitors of PDI. The first inhibitor, 16F16, was published in 2010 by Hoffstrom et al., who were using drug screening to find small molecules suitable for inhibiting the toxicity of mutant Huntington exon1 and Aβ peptides. Using MS, it was found that 16F16 binds to PDIA1 and PDIA3 (Hoffstrom, Kaplan, Letso, *et al.* 2010). PACMA31 was discovered in 2012 by Xu et al., who were looking for small molecules to inhibit PDI for treatment of ovarian cancers (Xu, Butkevich, Yamada, *et al.* 2012). PACMA31 was shown to covalently bind to PDI; MS found that PACMA31 binds either Cys397 or Cys400, but this modification does not occur simultaneously due to steric hinderance caused by the binding of PACMA31. They also found that the secondary structure of PDI changed after

PACMA31 binding by using circular dichroism spectrometry. The change in the secondary structure may affect the protein activity of PDI and using an insulin reduction assay it appeared that 100 µM PACMA31 was able to stop the reductase activity of PDI (Xu, Butkevich, Yamada, *et al.* 2012). Due to these factors, the two PDI inhibitors were chosen for experiments described in this chapter of the thesis.

This chapter will further explore intracellular collagen processing. Optimisation of mNeonGreen (mNG) imaging and the transfection of HT1080 cells with a mNG tagged collagen 1α (col1α) construct will be described. The initial work of using PDI inhibitors PACMA31 and 16F16 on the viability and PDI interactome will also be discussed. The interactome and inhibitor work can be used in future research to understand how cells such as fibroblasts age and to investigate how this affects collagen formation in health and disease.

6.2 Optimisation of mNeonGreen (mNG) imaging

Collagen production is important to understand as studies have shown collagen production decreases as we age (Varani, Dame, Rittie, *et al.* 2006). To monitor the localisation and trafficking of collagen, a construct of mNG attached to col1α was created in the laboratory to monitor the assembly and release of collagen in various cell types (Casey, Brown, Benham, Hawkins, unpublished data). mNG is the brightest monomeric green or yellow fluorescent protein currently, which makes it advantageous for imaging. It also does not share sequence identity with other fluorescent proteins, so antibodies developed against it are specific and as shown later in the chapter, it is a suitable target for co-IP (Shaner, Lambert, Chammas, *et al.* 2013). To first optimise the fixative method for detecting mNG in transfected HT1080 cells, cells stably expressing an mNG tagged Lifeact construct were used (Benham and Hawkins, unpublished data). Lifeact is a 17 amino acid peptide which stains filamentous actin (F-actin) in eukaryotic cells (Riedl, Crevenna, Kessenbrock, *et al.* 2008). The Lifeact-mNG fusion protein

that was stably expressed in the HT1080 cells was attached to mNG, this allowed the suitability of mNG in fixation and its ability to stain small filamentous structures to be tested. The HT1080 cells were grown on coverslips and fixed with 4% PFA and the cytoskeleton fix (composition described in the section 2.8) +/- Tx100 permeabilisation. The cells were then stained with DAPI and imaged on the Zeiss 800 confocal microscope with Airyscan. There was no observable difference in the cells fixed in 4% PFA (Figure 6.1A, 6.1B) vs those fixed with the cytoskeleton fix (Figure 6.1C, 6.1D). The addition of Tx100 for permeabilisation (Figure 6.1A, 6.1C) did not affect the quality of the Lifeact images; this suggests that permeabilisation did not cause any of the Lifeact-mNG to leak as any soluble mNG would result in a dimmer image.

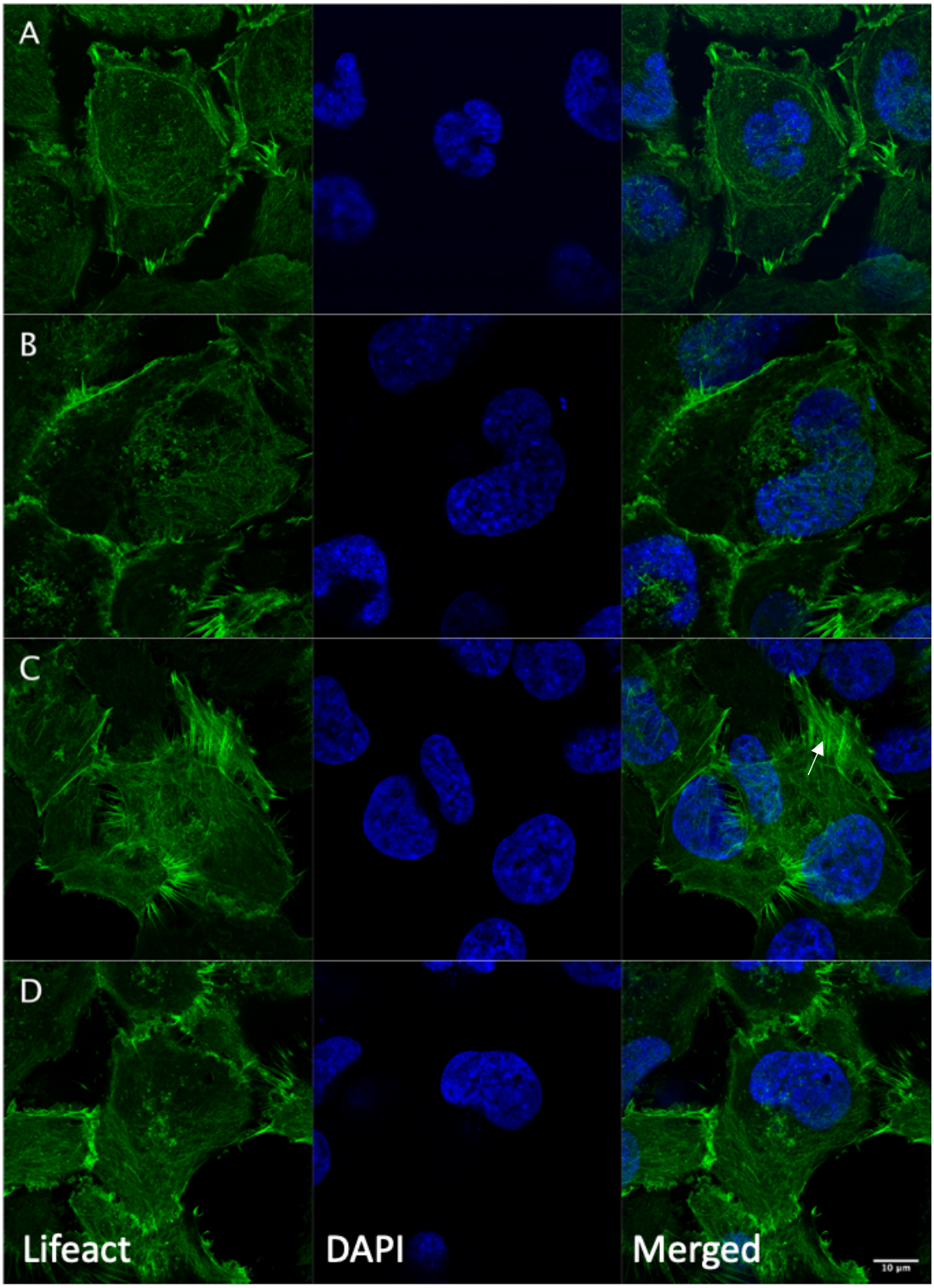

Figure 6.1: Different fixative methods do not appear to make a large difference to fixing Lifeact transfected HT1080 cells. HT1080 cells expressing a stable Lifeact construct were fixed with varying fixatives to see if there were any advantages of using one over another. The fixatives (A) 4% PFA with 0.1% Tx100; (B) 4% PFA without 0.1% Tx100; (C) cytoskeleton fix with 0.1% Tx100 and (D) cytoskeleton fix without Tx100, were all left on the cells for 10 min. DAPI was used for nuclear staining. The images were taken on a Zeiss LSM 800 confocal microscope with Airyscan at 63x magnification. Arrow indicates a representative actin filament.

Next, to assess the suitability of the fixatives for mNG col1α fixation, HT1080 cells were transfected with the col1α construct (Figure 6.2). These cells were then once again fixed with a range of fixatives and +/- Tx100, stained with DAPI and imaged on the Zeiss 800 with Airyscan. There was not a discernible difference in the appearance of mNG-col1α between 4% PFA (Figure 6.3A, 6.3B) or the cytoskeleton fix (Figure 6.3C, 6.3D). The addition of Tx100 (Figure 6.3A, 6.3C) did not affect the localisation or appearance of the mNG-col1α. The fusion protein appears to have perinuclear staining which was expected as this is where the majority of collagen processing occurs. As there was no major difference observed in the fixatives 4% PFA was used as the fixative going forward. 4% PFA was chosen as it was compatible for co-staining with other proteins of interest.

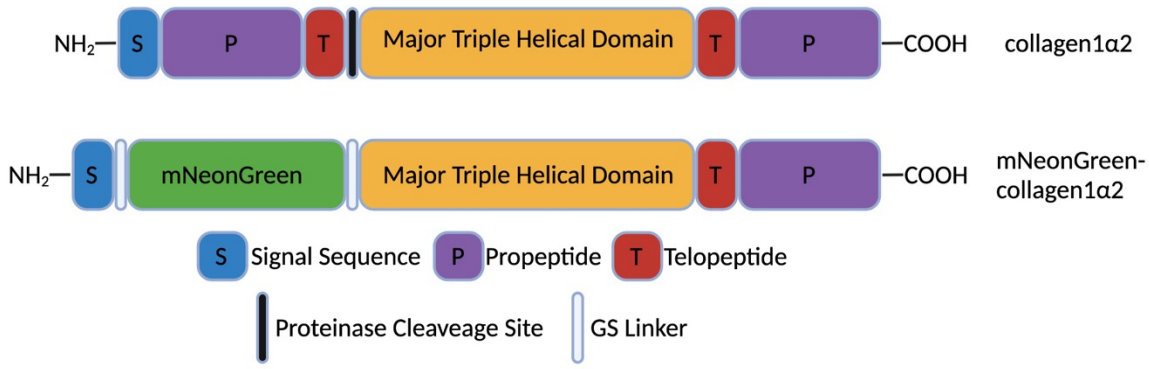

Figure 6.2: Diagram of collagen1α2 and the mNeonGreen collagen1α2 construct displaying the key sites of the protein.

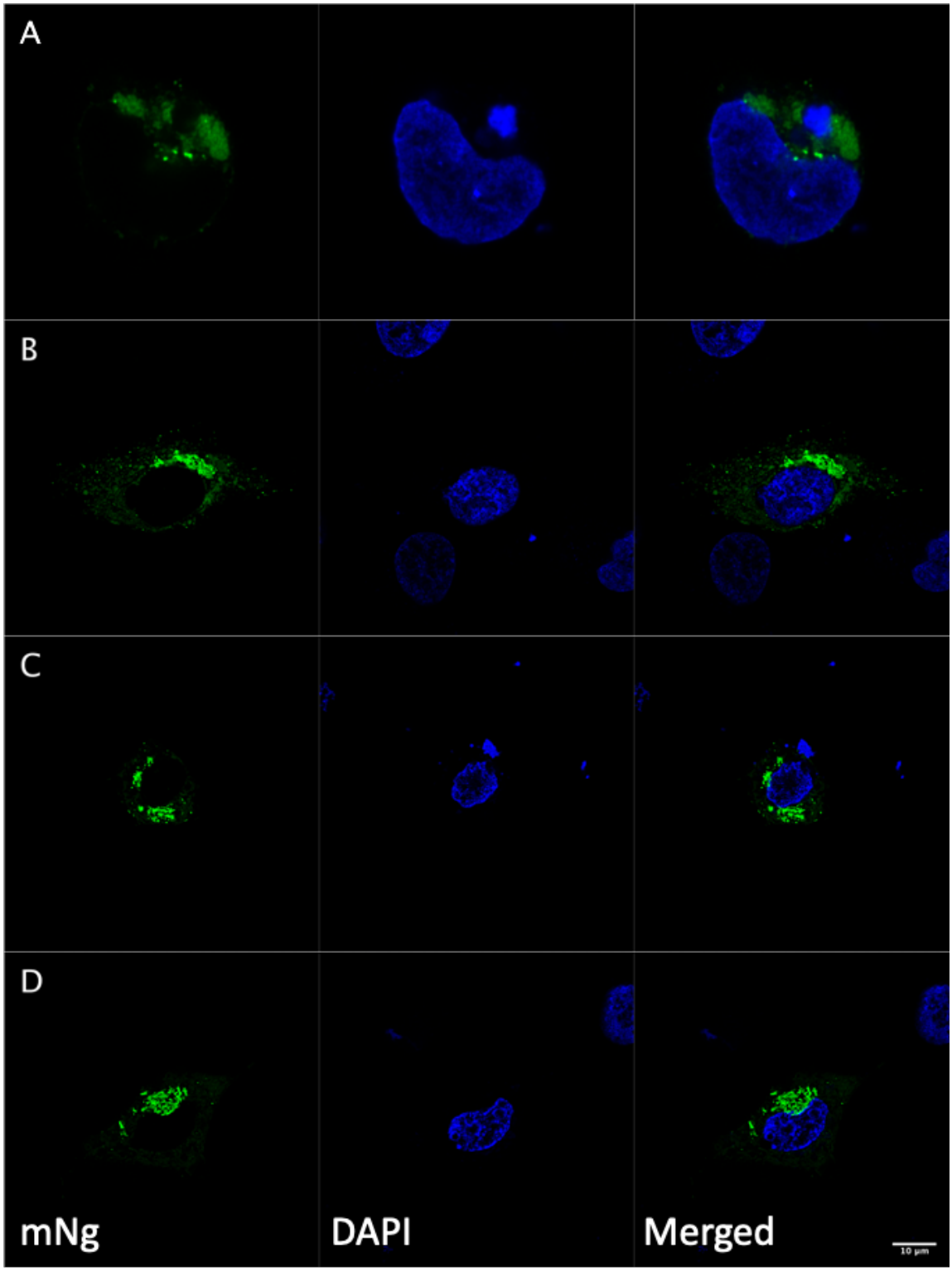

Figure 6.3: Different fixative methods do not appear to make a large structural difference to fixing mNG-col1α transfected HT1080 cells. HT1080s transfected with an mNG-col1α construct were fixed with varying fixatives to see if there were any advantages of using one over another. The fixatives (A) 4% PFA with 0.1% Tx100; (B) 4% PFA without 0.1% Tx100; (C) cytoskeleton fix with 0.1% Tx100 and (D) cytoskeleton fix without Tx100, were all left on the cells for 10 min. DAPI was used for nuclear staining. The images were taken on a Zeiss LSM 800 confocal microscope with Airyscan at 63x magnification.

6.3 Localisation of the mNG construct in HT1080 cells

To observe where the mNG-col1α fusion protein localises in the HT1080 cells, the transfected cells were fixed, permeabilised and stained with various antibodies against proteins such as collagen 1, the ER-Golgi compartment (ERGIC), the collagen folding subunits P4HA and the ER localised protein PDI (which is also known as P4HB, a component of the P4H complex). The cells were stained with DAPI and imaged on the Zeiss 800 with Airyscan. As expected, mNG-col1α co-localised with the col1 antibody showing that the collagen is likely to be folded and processed enough in the cells to be recognised by the antibody. mNG-col1α also co-localised with the two subunits which help fold and hydroxylate pro-collagen, P4HA and P4HB, which suggests that the mNG-col1α construct localises to the ER. Procollagen has been shown to be transported from the ER to the Golgi in coat protein complex II (COPII) vesicles for processing (Matsui, Hirata, Wada, *et al.* 2020). In the immunofluorescence data (Figure 6.4C, 6.4D) the localisation of the fusion protein with PDI and P4HA suggests that the col1α was being correctly processed by the HT1080 cells.

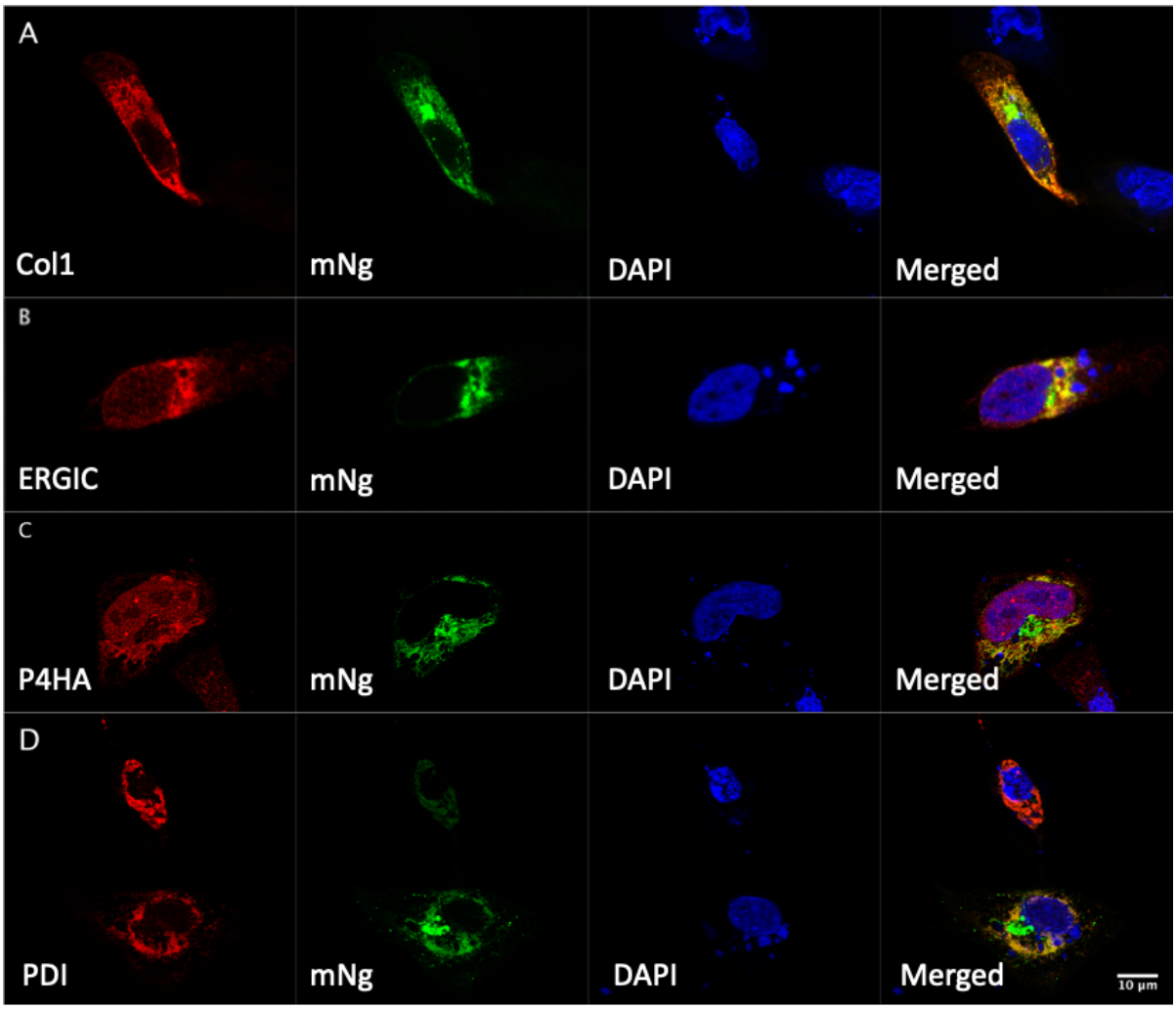

Figure 6.4: mNG-col1α construct localisation in HT1080 cells. HT1080 cells were grown on coverslips, transfected with the mNG-col1α construct then fixed and stained for various antibodies to determine the cellular localisation of the mNG-col1α fusion protein. Localisation with collagen was shown with (A) Collagen 1. ER localisation was shown with (B) ERGIC; (C) P4HA and (D) PDI. DAPI was used for nuclear staining. The images were taken on a Zeiss LSM 800 confocal microscope with Airyscan at 63x magnification.

6.4 Using proteomics to further investigate collagen processing

To establish if the transfected collagen was being correctly processed and post-translationally modified by the HT1080 cells, IP followed by MS was used. Proline hydroxylation is a key post translational modification in procollagen as it helps keep the triple helix structure of collagen stable (Rappu, Salo, Myllyharju, *et al.* 2019). HT1080 cells were transfected with the mNG-col1α construct, lysed and then an IP against mNG was performed. The mNG lysate which had not been IP'd and the lysates which had been IP'd were analysed with DDA MS. The data

obtained showed that the mNG collagen interacted with some key processing proteins (supplementary table 10.1, 10.2, 10.3) such as P4HA and P4HB (PDI), which are the two subunits key in catalysing the 4-hydroxylation of collagen to promote the collagen triple helix formation. To further verify if the collagen in the IPs performed was becoming hydroxylated, the post-translational modifications of the mNG-col1α fusion protein were analysed. The proteins were found to be becoming hydroxylated on certain sites (Figure 6.5), suggesting that the fusion protein was being correctly processed inside the HT1080 cells. The fact that col1α is detectable in the IP suggests that the fusion protein remained intact inside the HT1080 cells.

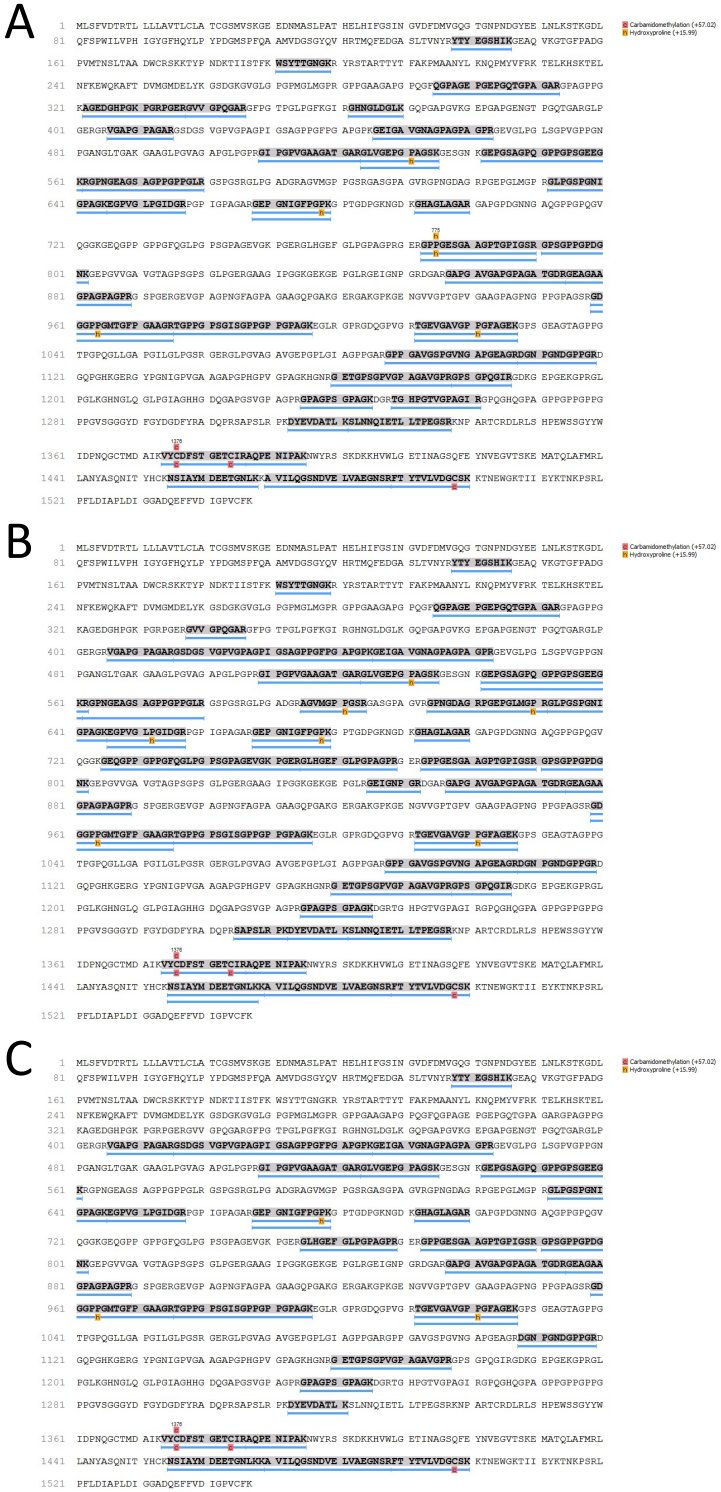

Figure 6.5: mNG-col1α construct has had its prolines hydroxylated when transfected into HT1080 cells. HT1080 cells were transfected with an mNG-col1α construct and lysed. The three sets of lysates (A), (B) and (C) were subjected to a mNG IP and MS was performed. The highlighted rows are peptides recovered and the h are the hydroxylprolinated sites. The red box represents Carbamidomethylation, and the orange box represents a hydroxyproline post-translational modification (PTM).

6.5 Viability of HT1080 cells treated with PDI and Ero1α

PDI is a key protein in the formation of folded collagen. It has been shown to independently associate with the C-propeptide of procollagen, directing the formation of the heterotrimeric molecules and forming disulphide bonds within the collagen protein (Wilson, Lees & Bulleid 1998). To understand how PDI influences collagen folding and quality control, PDI was inhibited in HT1080 cells with two different inhibitors PACMA31 and 16F16. This was carried out with the aim of applying it to cells which expressed mNG-col1α construct to observe how PDI inhibition affected collagen localisation and trafficking. First, an optimal inhibitor concentration was established. HT1080 and BJF cells were seeded in two separate 96 well plates, grown to confluency and then treated with 1-100 µM PACMA31, 1-100 µM 16F16, 1-100 µM EN460, 1 µl DMSO (as a control), 100 µM DTBA and 100 µM DTT. These treatments were performed in triplicate. The treatments were left on the cells for 2 hr and after 1 hr, 10 µl of Orangu dye was added. The Orangu viability assay uses WST-8 a tetrazolium salt; this salt is reduced to an orange formazan dye when in the presence of an electron moderator. The amount of dye generated is proportional to the number of viable cells. The plates were read at 450 nm in a standard microplate reader and the results were plotted in Prism 9. The HT1080 cells viability did not seem to be as negatively affected by the addition of the inhibitors (Figure 6.6A) when comparing the results to the BJF cells, as the HT1080 cells have higher absorbance values than the corresponding BJF cells treatments (Figure 6.6B) suggesting there are more viable HT1080 cells present in all of the treatments. In the experiments going forward 10 µM of inhibitor was used as this concentration was shown to be an effective concentration in the corresponding papers where the inhibitors were used to judge the activity of the inhibitors in cancer cells whilst also limiting the effect on surrounding

non-cancerous cells viability (Xu, Butkevich, Yamada, *et al.* 2012; Blais, Chin, Zito, *et al.* 2010; Li, Liu, Ding, *et al.* 2020).

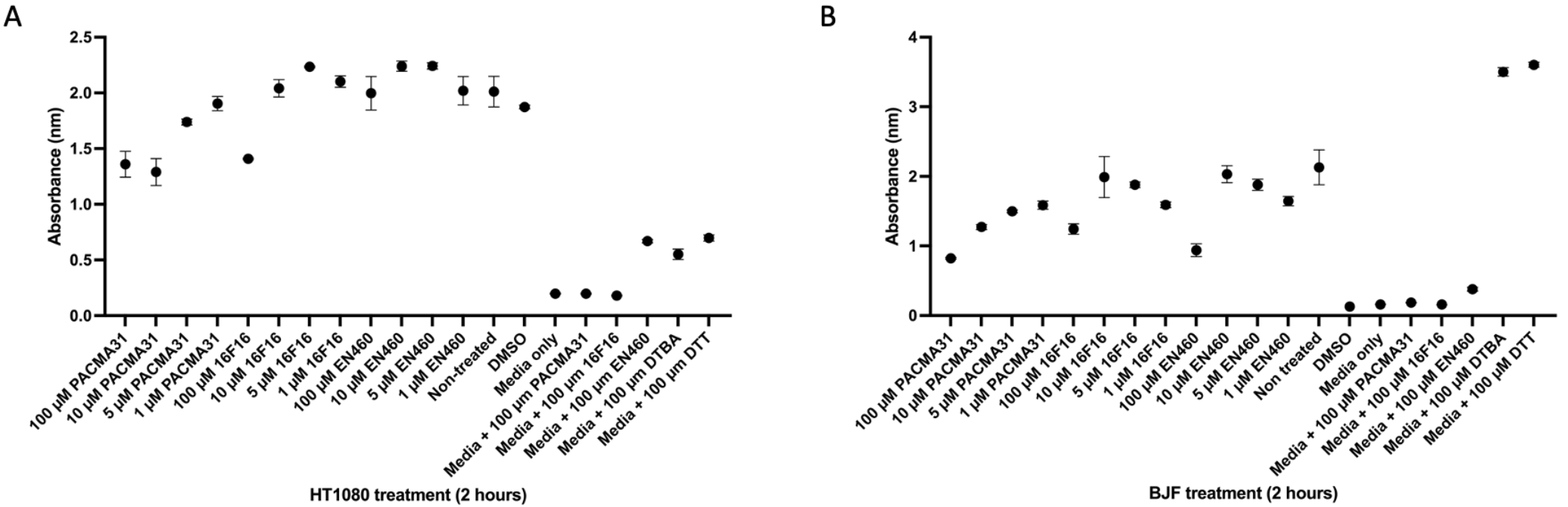

Figure 6.6: Viability assay of treatment with PDI and Ero1α inhibitors. HT1080 (A) and BJF cells (B) were grown in a 96 well plate and treated with various PDI and Ero1α inhibitors at varying concentrations for 2 hr (n=3 $P<0.05$). Orangu cell dye was added after 1 hr of the treatments. The plate was read at 450 nm on a plate reader after 2 hr total (BioTek ELX800).

6.6 Proteomic analysis of HT1080 cells treated with PDI inhibitors

As the transfection of the mNG-col1α construct was performed in HT1080 cells the proteomics was performed on these cells. To investigate if there are any differences in PDI binding partners when inhibitors are added, HT1080 cells were treated with 10 µM of the various inhibitors (PACMA31, 16F16 and EN460). These cells were lysed, IP'd with a polyclonal PDI antibody, eluted, trypsin digested and then analysed with DDA MS to identify co-IPing proteins. The significant proteins (more than two unique peptide hits with $P<0.05$) that were identified are presented (Table 6.1, 6.2, 6.3 and 6.4 - see discussion for further expansion). The non-specific binding partners were removed by comparison to a database containing common non-specific proteins. The identified proteins present were deemed to be significant when Mascot and ProteinPilot analysis showed that there were two or more peptide matches at a 95% confidence interval. Some of the key proteins which were present in all the treatments include both P4HA subunits (1 & 2) and the disulphide bond donor Ero1α. Although DDA MS was unable to specify the amount of protein present, it does suggest that the inhibitor treatments of 10 µM does not completely inhibit PDI-partner interactions as there was still evidence of P4HA and Ero1α interacting with PDI. This may mean that collagen production, even in the presence of PDI inhibitors, could still occur. A useful future experiment could involve treating mNG col1α expressing cells with the inhibitors and using IF and WB to quantitate the trafficking and secretion of collagen.

Table 6.1: Major proteins that interact with PDI identified by MS in untreated HT1080 cells.

Gene Name	Peptides (95%)	%Cov	GO Function
PDIA1	33	53	Protein folding
FIBB	18	26	Cell adhesion
FIBG	18	25	Cell-matrix adhesion
FINC	12	6	Cell adhesion
P4HA1	11	24	Collagen fibril organisation
P4HA2	10	20	Peptidyl-proline hydroxylation to 4-hydroxy-L-proline
ERO1A	9	21	Protein folding
TGM2	6	9	Peptide cross-linking
RO52	6	13	Protein ubiquitination
CO4A	5	3	Complement activation
ANXA2	5	14	Collagen fibril organisation
PSA4	5	16	Proteasomal ubiquitin-independent protein catabolic process
PSB1	4	19	Proteasomal ubiquitin-independent protein catabolic process
PSA6	4	17	Proteasomal ubiquitin-independent protein catabolic process
CO3	4	2	Complement activation
PSA3	4	15	Proteasomal ubiquitin-independent protein catabolic process
PSA1	4	14	Proteasomal ubiquitin-independent protein catabolic process
PSB5	3	13	Proteolysis
ANT3	3	5	Blood coagulation
PSA5	2	10	Proteasomal ubiquitin-independent protein catabolic process
HSP7C	2	4	Protein folding
PSB2	2	9	Proteasomal ubiquitin-independent protein catabolic process
MYH9	2	1	Actin cytoskeleton reorganisation
PSB6	2	8	Proteasomal ubiquitin-independent protein catabolic process
FIBA	2	2	Cell-matrix adhesion
PSA7	2	8	Proteasomal ubiquitin-independent protein catabolic process
EF1A1	2	4	Translation
EF1A2	2	4	Translation
PSB7	2	6	Proteasomal ubiquitin-independent protein catabolic process

Table 6.2: Major proteins that interact with PDI identified by MS in HT1080 cells treated with 10 µM PACMA31 for 2 hr.

Gene Name	Peptides (95%)	%Cov	GO Function
PDIA1	30	51	Protein folding
FINC	24	11	Cell adhesion
FIBB	22	24	Cell adhesion
FIBG	22	30	Cell-matrix adhesion
P4HA1	10	21	Collagen fibril organisation
ERO1A	9	21	Protein folding
TGM2	9	14	Peptide cross-linking
P4HA2	7	16	Peptidyl-proline hydroxylation to 4-hydroxy-L-proline
CO4A	5	3	Complement activation
FIBA	5	3	Cell-matrix adhesion
PSA5	4	22	Proteasomal ubiquitin-independent protein catabolic process
CO3	4	2	Complement activation
PSA4	4	14	Proteasomal ubiquitin-independent protein catabolic process
PSA7	4	15	Proteasomal ubiquitin-independent protein catabolic process
PSB1	3	13	Proteasomal ubiquitin-independent protein catabolic process
PSA6	2	10	Proteasomal ubiquitin-independent protein catabolic process
HSP7C	2	4	Protein folding
PSB5	2	8	Proteolysis
PSA3	2	7	Proteasomal ubiquitin-independent protein catabolic process
A2MG	2	1	Negative regulation of complement activation, lectin pathway
DCD	2	20	Defence response to bacteria
RO52	2	4	Innate immune response

Table 6.3: Major proteins that interact with PDI identified by MS in HT1080 cells treated with 10 µM 16F16 for 2 hr.

Gene Name	Peptides (95%)	%Cov	GO Function
PDIA1	32	53	Protein folding
FIBB	14	24	Cell adhesion
FIBG	14	23	Cell-matrix adhesion
FINC	10	5	Cell adhesion
P4HA2	10	22	Peptidyl-proline hydroxylation to 4-hydroxy-L-proline
ERO1A	10	22	Protein folding
P4HA1	8	18	Collagen fibril organisation
TGM2	7	11	Peptide cross-linking
ANXA2	6	18	Collagen fibril organisation
CO4A	5	3	Complement activation
RO52	4	8	Innate immune response
PSB5	3	13	Proteolysis
CO3	3	2	Complement activation
PSA6	3	13	Proteasomal ubiquitin-independent protein catabolic process
PSA5	3	14	Proteasomal ubiquitin-independent protein catabolic process
HSP7C	3	5	Protein folding
PSA1	3	11	Proteasomal ubiquitin-independent protein catabolic process
PSA3	3	11	Proteasomal ubiquitin-independent protein catabolic process
PSB1	3	13	Proteasomal ubiquitin-independent protein catabolic process
PSA4	3	10	Proteasomal ubiquitin-independent protein catabolic process
FIBA	3	3	Cell-matrix adhesion
PSA7	2	8	Proteasomal ubiquitin-independent protein catabolic process
PSB6	2	8	Proteasomal ubiquitin-independent protein catabolic process

Table 6.4: Major proteins that interact with PDI identified by MS in HT1080 cells treated with 10 µM EN460 for 2 hr.

Gene Name	Peptides (95%)	%Cov	GO Function
PDIA1	29	51	Protein folding
FIBB	25	30	Cell adhesion
FINC	23	11	Cell adhesion
FIBG	21	28	Cell-matrix adhesion
ERO1A	9	21	Protein folding
MYH9	7	4	Actin cytoskeleton reorganisation
CO4A	6	4	Complement activation
P4HA1	6	14	Collagen fibril organisation
TGM2	6	10	Peptide cross-linking
CO3	5	3	Complement activation
FIBA	5	3	Cell-matrix adhesion
PSA6	3	14	Proteasomal ubiquitin-independent protein catabolic process
PSB6	3	13	Proteasomal ubiquitin-independent protein catabolic process
PSA7	3	12	Proteasomal ubiquitin-independent protein catabolic process
ANT3	3	5	Blood coagulation
P4HA2	2	5	Peptidyl-proline hydroxylation to 4-hydroxy-L-proline
MYL6	2	16	Muscle filament sliding
MYL6B	2	12	Muscle filament sliding
A2MG	2	1	Negative regulation of complement activation, lectin pathway
PSA1	2	8	Proteasomal ubiquitin-independent protein catabolic process
PSA4	2	7	Proteasomal ubiquitin-independent protein catabolic process
APOE	2	5	Cytoskeleton organisation

To establish if different inhibitor treatments affected the protein-protein interactions with PDI in various ways the significant proteins in the untreated, 10 µM PACMA31, 10 µM 16F16 and 10 µM EN460 were taken from Excel and analysed with an R script which takes the gene name and finds the GO ID for the respective protein (Figure 6.7, 6.8, 6.9, 6.10). This data was then plotted on graphs which display the biological processes (Figure 6.7A, 6.8A, 6.9A, 6.10A), the molecular function (Figure 6.7B, 6.8B, 6.9B, 6.10B) and cellular compartment (Figure 6.7C, 6.8C, 6.9C, 6.10C). The inhibitor treated IP's were compared with the non-treated PDI IP and plotted onto a Venn diagram (Figure 6.11) there is quite a lot of overlapping proteins meaning some of these interactions may be translational proteins or artefactual ones such as the IgG protein from the PDI antibody. An example of protein interactions that were gained on inhibition is alpha-2-macroglobulin which is an extracellular protease inhibitor, this interaction was gained after PACMA31 and EN460 inhibition. An interaction lost after treatment with the inhibitors was elongation factor 1-alpha 1 which was observed after treatment with all three inhibitors. When comparing the different treatments there were not large differences between the data, this suggests that both the PDI inhibitors (PACMA31, 16F16) and the Ero1α inhibitor (EN460) do not exert large effects on the PDI interactome at the concentration and time points used.

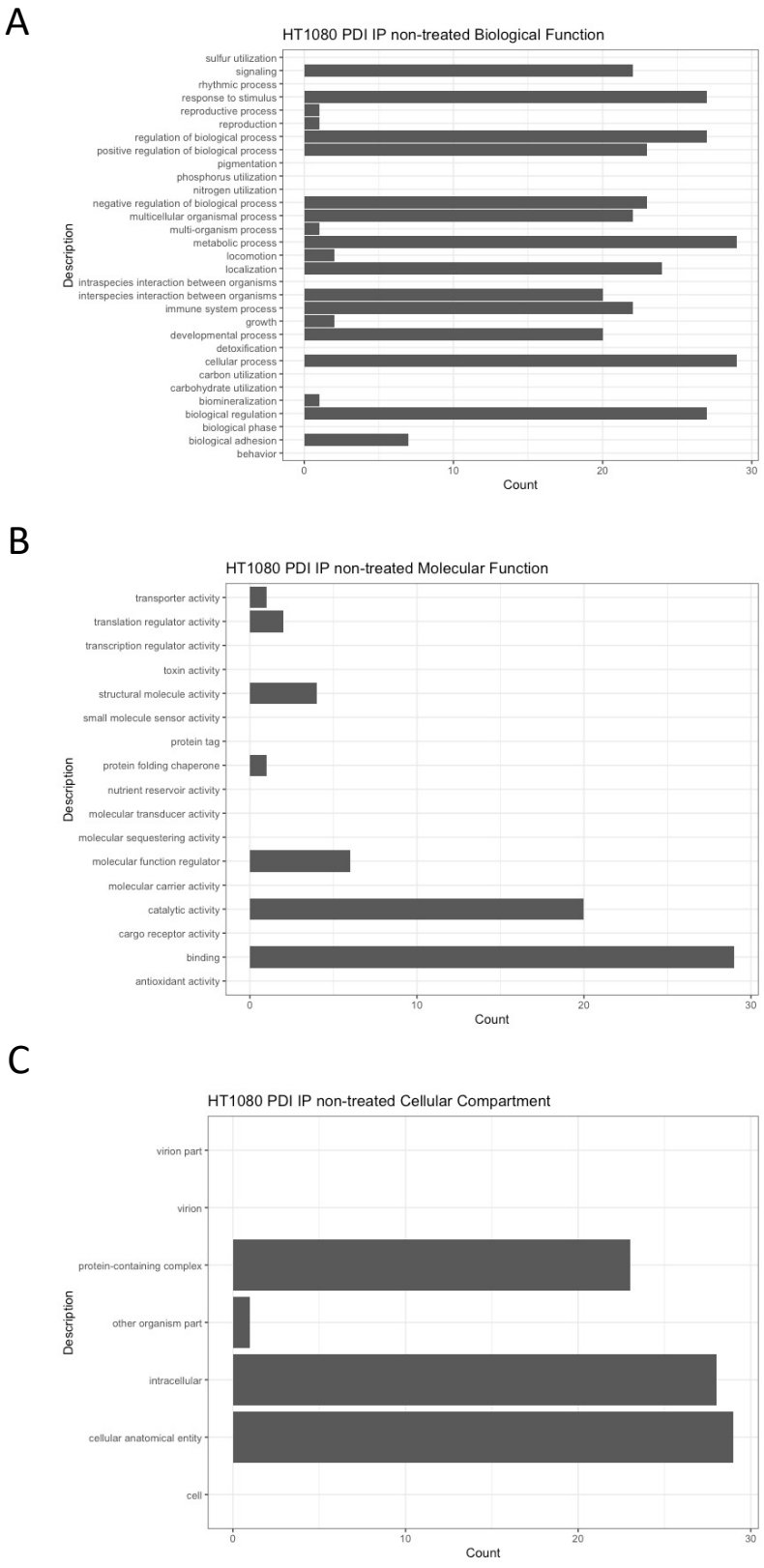

Figure 6.7: GO analysis of proteomic data from PDI IP of untreated HT1080 cells. The proteins that interacted with PDI were converted to GO terms in R, these were then plotted based on (A) biological processes, (B) molecular function and (C) cellular compartment.

A

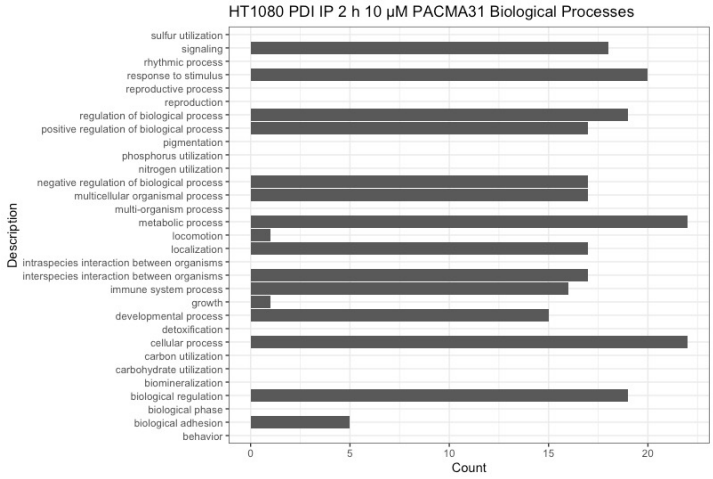

B

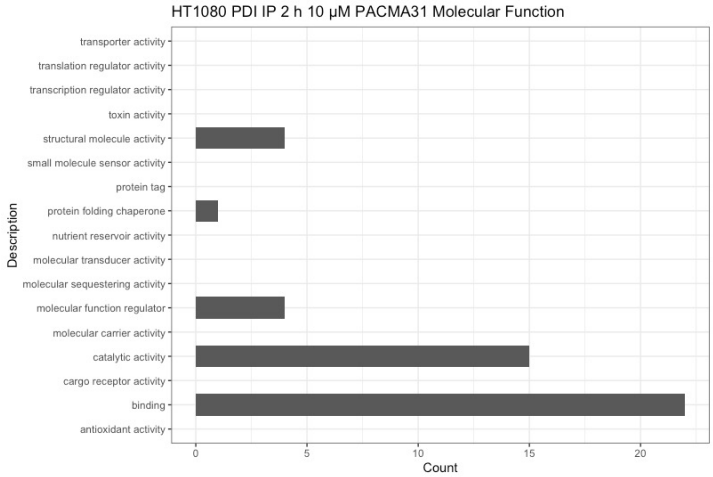

C

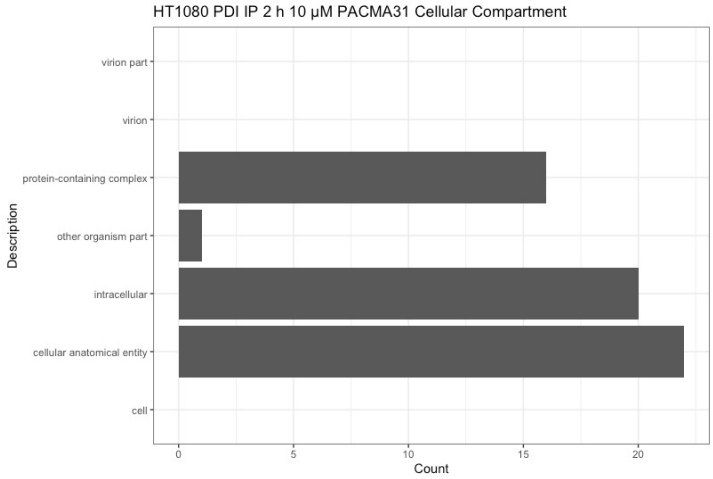

Figure 6.8: GO analysis of proteomic data from PDI IP of HT1080 cells treated with 10 µM PAMCA31 for 2 hr. The proteins that interacted with PDI were converted to GO terms in R, these were then plotted based on (A) biological processes, (B) molecular function and (C) cellular compartment.

A

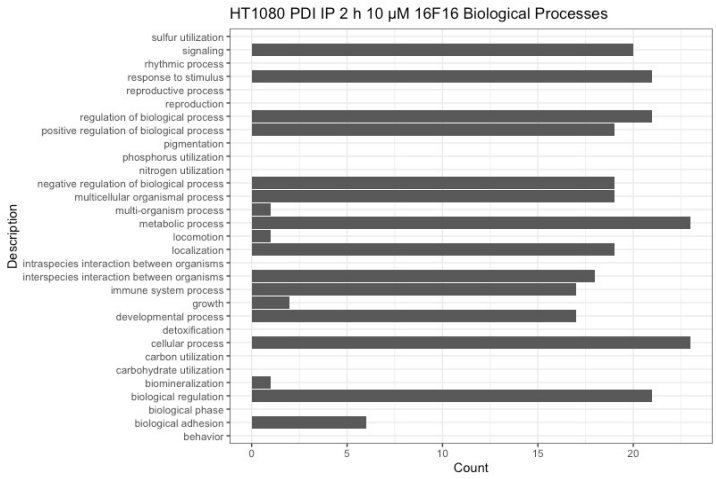

B

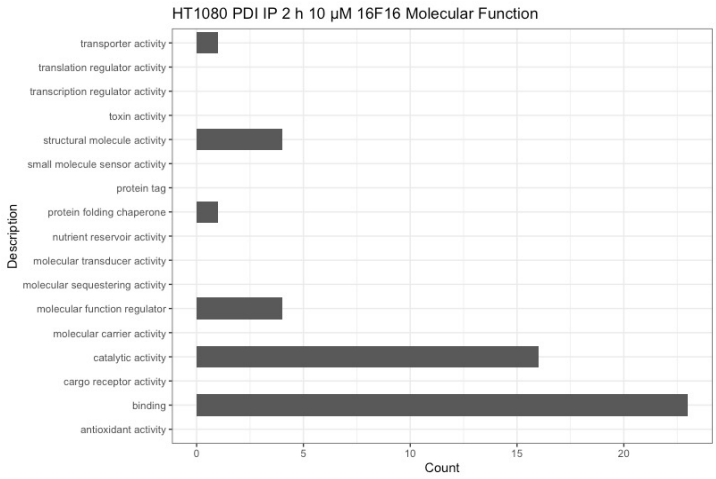

C

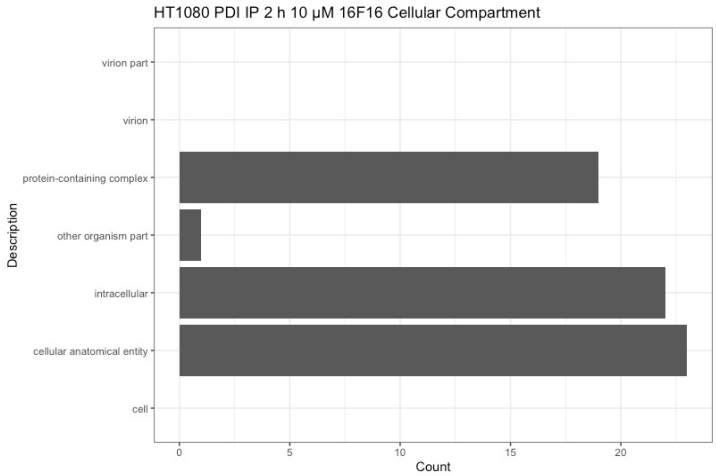

Figure 6.9: GO analysis of proteomic data from PDI IP of HT1080 cells treated with 10 µM 16F16 for 2 hr. The proteins that interacted with PDI were converted to GO terms in R, these were then plotted based on (A) biological processes, (B) molecular function and (C) cellular compartment.

A

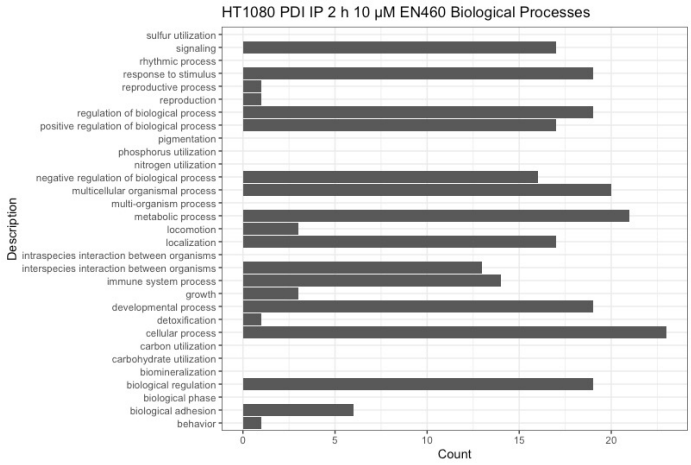

B

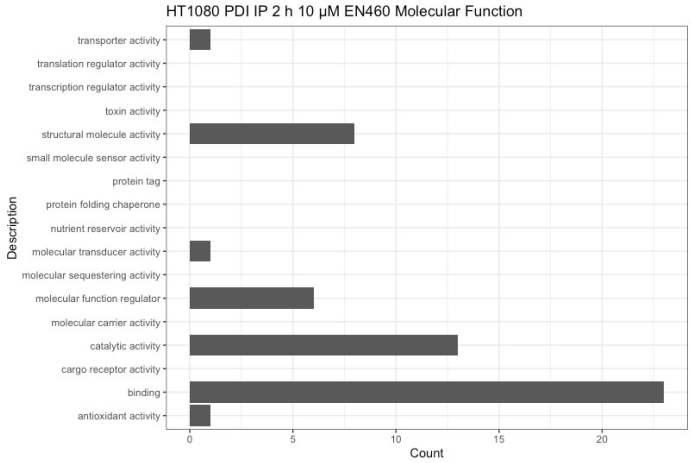

C

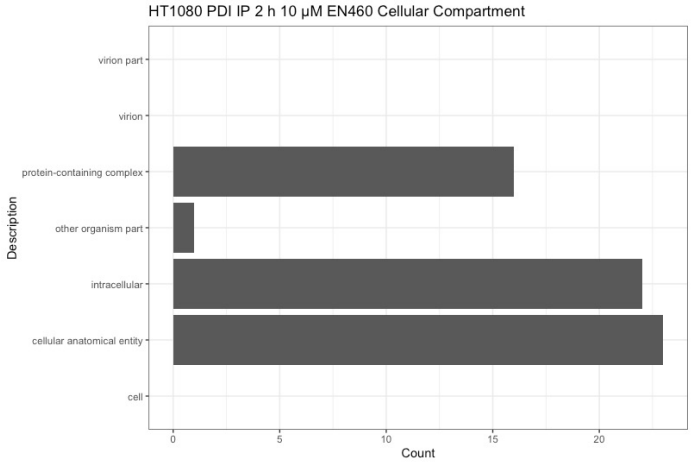

Figure 6.10: GO analysis of proteomic data from PDI IP of HT1080 cells treated with 10 µM EN460 for 2 hr. The proteins that interacted with PDI were converted to GO terms in R, these were then plotted based on (A) biological processes, (B) molecular function and (C) cellular compartment.

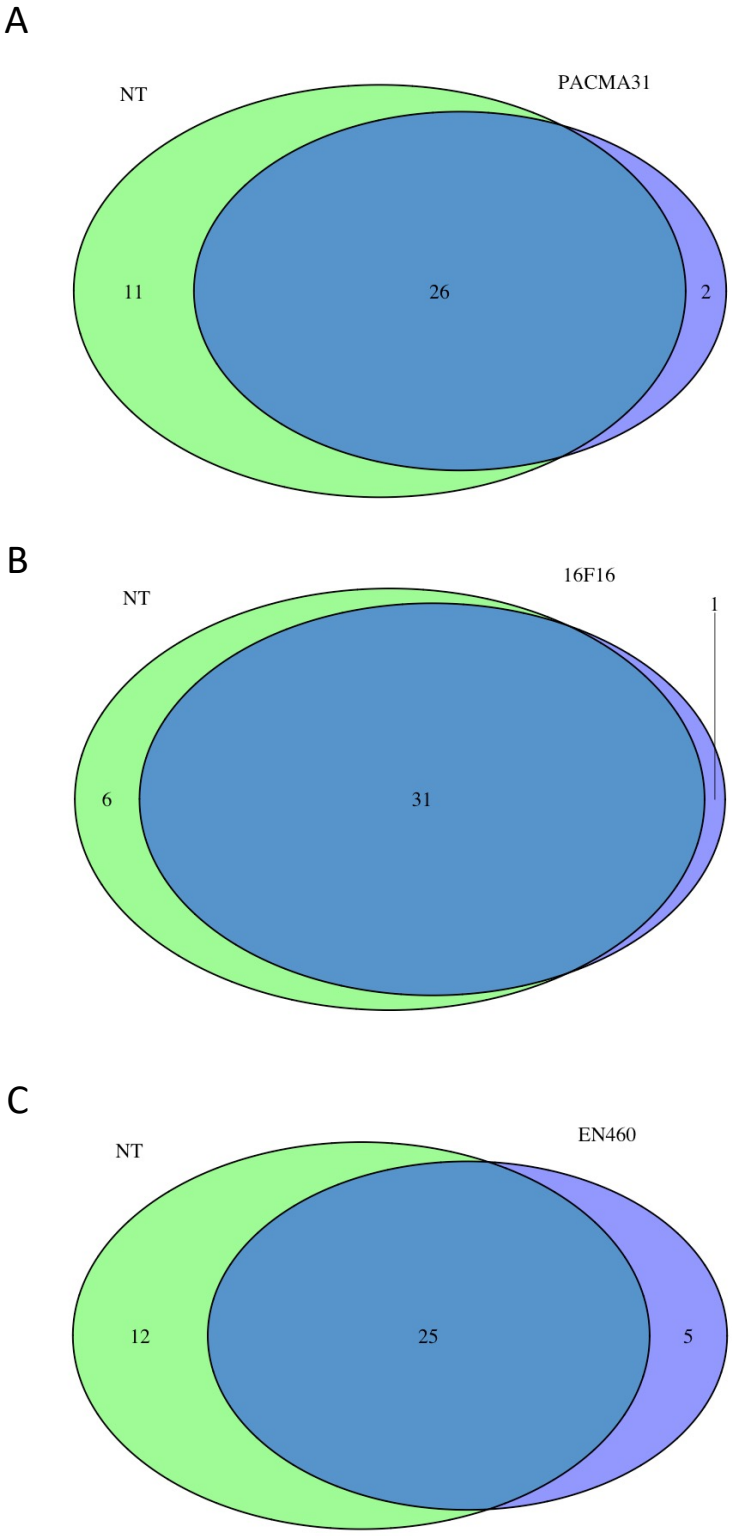

Figure 6.11: Differences in protein changes when HT1080 cells were treated with various inhibitors and a PDI IP was performed. A Venn diagram was used to visualise the differences in individual protein changes with the different treatments. (A) non-treated was compared with 10 µM 2 hr PACMA31 treatment, (B) non-treated was compared with 10 µM 2 hr 16F16 treatment, (C) non-treated was compared with 10 µM 2 hr EN460.

In summary, an optimised fixation and imaging method has been evaluated for mNG imaging. The optimised fixation and imaging method has been used for the co-localisation study of the mNG-col1α construct in HT1080 cells. PDI inhibitor experiments have been conducted in HT1080 cells with proteomics to discover how the PDI interactome is affected by these inhibitors. Future experiments could involve interactome studies on professional collagen secreting cells e.g., BJ fibroblast cells treated with the PDI inhibitors to see if there is any difference compared to the HT1080 cells, which support quality control but do not produce endogenous type 1 collagen. Transfecting cells with the mNG-col1α construct and then treating with the PDI inhibitors will allow for the discovery of the effect of the inhibitors on collagen formation.

6.7 Discussion and conclusion

The results in this chapter identify optimised fixation and imaging methods to best visualise the trafficking of collagen. An mNG-col1α fusion protein has been developed by the laboratory. This chapter also identifies that processing of mNG-col1α is occurring correctly by using proteomics to identify post-translational hydroxyl modifications on proline and lysine groups. In both the stably expressing mNG-Lifeact HT1080 cells and the transiently transfected with the mNG-col1α HT1080 cells bright and clear images were obtained where the actin strands were visible (Figure 6.1), XAand the accumulation of collagen and likely collagen-carrying vesicles were shown (Figure 6.2). A paper has also successfully used 4% PFA to fix mNG in mitochondria showing that it is a suitable fluorescent protein for both live and fixed cell imaging of multiple organelles and parts of the cell (Tanida-Miyake, Koike, Uchiyama, *et al.* 2018). The co-localisation IF work showed that the mNG-col1α protein is localised to the expected areas in the HT1080 cells, even though they do not natively produce

col1α. Procollagen has been shown to be recruited to the ERGIC via TANGO1 recruiting ERGIC membranes to the ER. This is also shown in the co-localisation IF performed in this results chapter as the mNG col1α protein co-localises with the ERGIC (Figure 4B). The enzyme P4H is essential for collagen biosynthesis, and it is made up of α_2 (P4HA) and β_2 (P4HB/PDI) (Myllyharju 2003). The IF in this chapter shows these subunits co-localising (Figure 6.4C, 6.4D) with the mNG-col1α suggesting that correct processing of collagen is occurring. As IF on its own was not enough to prove that collagen processing occurred, DDA MS was used. The post-translational modifications of collagen were analysed in the MS software and hydroxylation was present on the proline residues of the collagen fusion protein (Figure 6.5). Hydroxyproline stabilises the triple helix of collagen and is required for collagen processing - without it, the collagen molecule is not stable (Berg & Prockop 1973b). The co-localisation from the IF as well as the collagen fusion protein being recovered from the IP with hydroxyprolinated residues suggests that the transfected HT1080 cells are correctly processing the non-native collagen 1. Future experiments could involve using live cell imaging and the mNG-col1α construct to observe collagen trafficking and release as this will help identify if the events post-processing is occurring correctly.

To mimic the loss of collagen deposition as we age, PDI inhibitors were used to treat HT1080 and BJ fibroblast cells. One possibility is that PDI inhibitors prevent subunits of P4H working together correctly and this may cause a decrease in collagen processing and in turn deposition. As DDA MS was performed on the PDI IP it was not possible to quantify the number of proteins interacting with PDI and if these interactions decreased after the treatment of the PDI inhibitors PACMA31 and 16F16. This is because DDA MS can only detect the peptides and as such the proteins which are interacting with the immunoprecipitated protein, and it cannot quantify the amount present. The identification of P4HA suggests that

PDI inhibition does not result in the loss of P4HA from P4HB and that the interaction does not depend on the active site of PDI.

One of the PDI interactions observed in the non-treated and 16F16 treated HT1080 cells was annexin A2 (ANXA2). ANXA2 is involved in cell motility and is a calcium-dependent phospholipid-binding protein which assists in exocytosis of intracellular proteins (Table 6.1, 6.3). This includes the exocytosis of collagen as ANXA2 knockdowns have been shown to affect collagen secretion in the lungs (Dassah, Almeida, Hahn, *et al.* 2014). PDI may interact with ANXA2 and assist in the delivery of procollagen into the vesicles to be exocytosed. This interaction of ANXA2 is lost after treatment with PACMA31 suggesting that PACMA31 may be inhibiting the interaction of PDI and ANXA2 which could reduce the amount of collagen transported to the vesicles and because of this less collagen deposition may occur. Further work to validate these interactions with WB or IF could be performed in follow upstudies.

In conclusion, the data presented in this chapter shows that collagen export competent HT1080 cells are able to express the mNG col1α protein and process it correctly. The PDI inhibition experiments show that both HT1080 and BJ firbroblast cells are able to be treated with 10 µM of the PDI inhibitors without it becoming toxic to the cells. There is also a change in interactions after the treatment of the inhibitors as shown in the DDA MS data from a PDI IP (Figure 6.11). The data in this chapter opens up a wide scope for future experiments such as using BJ fibroblast cell lines which natively produce col1α and seeing if they also produce and process the mNG col1α fusion protein correctly. Another future experiment could involve treating mNG-col1α HT1080 cells with the PDI inhibitors and using WB or live cell imaging to observe the effect on the production or trafficking of the mNG-col1α fusion protein. Finally, the work in this chapter could be used for future studies into artificially

inducing some ageing phenotypes such as reduced collagen deposition and could be used to study drug targets which could reverse this process.

7 Discussion

This thesis explored what happened to the cellular redox balance when various cells were exposed to reducing stress and bioactive compounds. A lot of research has already been performed on oxidative stress and the ER as one of the main contributors to oxidative stress is from UV exposure which can cause photo-ageing (de Jager, Cockrell & du Plessis 2017). Not as much work has been performed on reducing stress especially in the context of ageing. There has been less work into reductive stress and the ER, for example, the human αB-crystalline mutation causes reductive stress which leads to protein aggregation related cardiomyopathy in mice (Rajasekaran, Connell, Christians, *et al.* 2007). Reductive stress has also been found to disrupt collagen homeostasis in fibroblast cells, suggesting that reductive stress as well as oxidative stress will impact skin ageing (Carne, Bell, Brown, *et al.* 2019). This thesis successfully used proteomics and bio-imaging to measure the effect of reductive stress on HT1080 cells and a system was used which allowed the process of collagen maturation and trafficking to be monitored. Taking these two techniques, reductive stress could be applied to the HT1080 or fibroblast cells expressing the mNG-col1α and this would allow for further mechanistic study of how reductive stress affects collagen homeostasis. Protective bioagents such as niacinamide have been used and shown to protect cells from oxidative stress caused by UV exposure and particulate matter by inhibiting ROS generation and glycolysis (Zhen, Piao, Kang, *et al.* 2019; Rovito & Oblong 2013). The work in this thesis has studied the change at the proteome level in fibroblasts after niacinamide is applied to the cells undergoing oxidative stress and it allowed the study of how the niacinamide affects

the cells to up or downregulate proteins to protect itself from the stress. Future experiments could involve treating cells with niacinamide after the cells been exposed to reducing stress such as from DTT and then observing how the proteome is affected. This work could allow for new anti-ageing creams to be developed which target the proteins that were observed to protect the cells most.

This thesis has used various analytical techniques such as western blotting and proteomics to elucidate the response of various cell lines to reductive stress and protective bioactive compounds. The work has revealed how the HT1080 cells proteome changes in response to varying levels of reductive stress, as shown by the changes in levels of proteins involved in vesicle transport and sorting (Chapter 1). Proteomics was also used to study the interactome of AGR2. The AGR2 interactome has been further expanded upon with MUC5AC and the novel interaction of SQSTM1 coming up as a main client. This suggests that AGR2 is most likely involved in autophagy as goblet cells delivering mucin granules have been shown to contain autophagosomal proteins which AGR2 may interact with (Patel, Miyoshi, Beatty, *et al.* 2013). AGR2 is also involved in protein folding (Chapter 2) (Park, Zhen, Verhaeghe, et al. 2009). Work in this thesis has expanded upon previous data from this laboratory between novel interaction of PDGF and lamin A/C upregulation and phosphorylation (Chapter 3). This only occurred after the treatment of PDGF suggesting that this growth factors involvement helped the fibroblasts nucleus become more pliable to enable movement. Finally, the first steps into optimising mNG-col1α imaging and setting up an ageing phenotype were undertaken. Proteomics was used to study how PDI inhibitors cause changes in the PDI interactome. The results obtained from this chapter suggests that the PDI inhibitors may cause a loss of collagen deposition, which makes them useful to create an ageing phenotype in the cell for further study (Chapter 4).

7.1 Future directions

The results presented in this thesis open a wide range of opportunities for future study.

1. Further mechanistic investigation could be carried out on the HT1080 proteome after treatment with the reducing agent DTBA, including knockdown or mutagenesis of genes involved in protein trafficking, cytoskeletal maintenance, and ECM turnover. The work could be extended into other cell types, validated in primary cells, and further examined in co-cultures and organoids.
2. SWATH-MS could be used to study how the proteome of normal oesophageal tissue changes due to environmental stress, or endogenous factors such as acid reflux, which is a risk factor for gastrointestinal cancer. The proteome could be compared with the tissue from Barrett's oesophagus at an adjacent site to the normal tissue. Viewing how the proteome is affected by acid reflux, studies have shown that the tight junction protein Zonula occludens-1 has significantly disrupted expression in the lower oesophagus after GERD (Okimoto, Arai, Ishigami, *et al.* 2018). One of the main drugs already in use for treating GERD are proton pump inhibitors (PPIs), they prevent gastric acid secretion by inhibiting the proton pump (Robinson 2004). The study of the change in the proteome may allow for drugs to be developed which could target upregulated proteins that cause these changes and prevent them possibly reducing the cases of Barrett's and the development of oesophageal adenocarcinoma.
3. The fixed cell imaging in chapter 3 shows how the expression of P-lamin A/C is affected by PDGF treatment. Prelamin A has a CaaX motif on the tail of the protein which is farnesylated at the C in the CaaX motif, this modification increases the hydrophobicity of the protein allowing it to be targeted to the nuclear envelope

(Reddy & Comai 2012). Future experiments could involve utilising a tagged lamin A/C construct and using live cell imaging to observe the dynamics of lamin after PDGF treatment, such as less lamin A/C appearing around the edge of the nucleus in cells which are mobile. Performing SWATH-MS on tissue from patients with age accelerating diseases such as progeria would allow for the investigation into how lamin A/C phosphorylation is affected in premature ageing. Tracking the temporal dynamics of the phosphoproteome in Hutchinson-Gifford Syndrome (progeria), the ageing disease caused by mutations in Lamin A/C, may lead to the identification of new drug targets. Indeed, a recent paper in Developmental Cell has shown that P-Ser22 lamin A/C binding sites were lost and new binding sites emerged, which increased histone acetylation, c-Jun binding and upregulated genes which are connected with progeria pathophysiology (Ikegami, Secchia, Almakki, et al. 2020).

4. The data presented in chapter 4 opens up scope for a wide range of experiments, such as expressing the mNG-col1α fusion protein in fibroblasts and using live cell imaging/IF and proteomics to analyse the trafficking secretion and deposition of collagen in *bona fide* collagen type 1 producing skin cells. The PDI inhibition work can be expanded to fibroblasts and other secretory cell types also to see if the PDI interactome is significantly altered after treatment in different cells. Setting up a suitable PDI inhibition experiment and employing the mNG-col1α fusion protein will allow for the study of collagen deposition in circumstances where the ER redox balance is compromised. Mock ageing scenario scenarios could also be established using cells aged by passaging in culture, or in fibroblast cells compromised by exposure to UV light This system could then be used to develop drugs which are able to reduce this process and help reduce the effects of ageing.

8 Bibliography

Aberger, F., Weidinger, G., Grunz, H. and Richter, K. (1998) Anterior specification of embryonic ectoderm: the role of the Xenopus cement gland-specific gene XAG-2. *Mechanisms of Development*. [Online] 72 (1–2), 115–130. Available at: doi:10.1016/S0925-4773(98)00021-5

Adamczyk, J., Bal, W. and Krężel, A. (2015) Coordination properties of dithiobutylamine (DTBA), a newly introduced protein disulfide reducing agent. *Inorganic Chemistry*. [Online] 54 (2), 596–606. Available at: doi:10.1021/ic5025026

Alberti, S., Esser, C. and Höhfeld, J. (2003) BAG-1—a nucleotide exchange factor of Hsc70 with multiple cellular functions. *Cell Stress & Chaperones*. [Online] 8 (3), 225. Available at: doi:10.1379/1466-1268(2003)008<0225:bnefoh>2.0.co;2

Alder, N.N., Shen, Y., Brodsky, J.L., Hendershot, L.M., et al. (2005) The molecular mechanisms underlying BiP-mediated gating of the Sec61 translocon of the endoplasmic reticulum. *The Journal of Cell Biology*. [Online] 168 (3), 389. Available at: doi:10.1083/JCB.200409174

Anfinsen, C.B. (1973) Principles that govern the folding of protein chains. *Science*. [Online] 181 (4096), 223–230. Available at: doi:10.1126/SCIENCE.181.4096.223/ASSET/1A648F0F-E322-4108-98DD-B0857103738D/ASSETS/SCIENCE.181.4096.223.FP.PNG

Angel, P., Szabowski, A. and Schorpp-Kistner, M. (2001) Function and regulation of AP-1 subunits in skin physiology and pathology. *Oncogene 2001 20:19*. [Online] 20 (19), 2413–2423. Available at: doi:10.1038/sj.onc.1204380

Antonino Fava, B., Iliceto, A., Camera, E., Reinboldt, H., et al. (1957) Kinetics of the Thiol-Disulfide Exchange. *Journal of the American Chemical Society*. [Online] 79 (4), 833–838. Available at: doi:10.1021/JA01561A014

Appenzeller-Herzog, C., Riemer, J., Christensen, B., Sørensen, E.S., et al. (2008) A novel disulphide switch mechanism in Ero1α balances ER oxidation in human cells. *The EMBO Journal*. [Online] 27 (22), 2977–2987. Available at: doi:10.1038/EMBOJ.2008.202

Audrito, V., Messana, V.G. and Deaglio, S. (2020) NAMPT and NAPRT: Two Metabolic Enzymes With Key Roles in Inflammation. *Frontiers in Oncology*. [Online] 10358. Available at: doi:10.3389/FONC.2020.00358/BIBTEX

Aviram, N., Ast, T., Costa, E.A., Arakel, E.C., et al. (2016) The SND proteins constitute an alternative targeting route to the endoplasmic reticulum. *Nature 2016 540:7631*. [Online] 540 (7631), 134–138. Available at: doi:10.1038/nature20169

Bahar, M.A., Bauer, B., Tredget, E.E. and Ghahary, A. (2004) Dermal fibroblasts from different layers of human skin are heterogeneous in expression of collagenase and types I and III procollagen mRNA. *Wound Repair and Regeneration*. [Online] 12 (2), 175–182. Available at: doi:10.1111/J.1067-1927.2004.012110.X

Balasubramanian, M., Padidela, R., Pollitt, R.C., Bishop, N.J., et al. (2018) P4HB recurrent missense mutation causing Cole-Carpenter syndrome. *Journal of Medical Genetics*. [Online] 55 (3), 158–165. Available at: doi:10.1136/jmedgenet-2017-104899

Battle, D.M., Gunasekara, S.D., Watson, G.R., Ahmed, E.M., et al. (2013) Expression of the endoplasmic reticulum oxidoreductase ero1α in gastro-intestinal cancer reveals a link between homocysteine and oxidative protein folding. *Antioxidants & redox signaling*. [Online] 19 (1), 24–35. Available at: doi:10.1089/ars.2012.4651.

Benesch, R.E. and Benesch, R. (2002) The Acid Strength of the -SH Group in Cysteine and Related Compounds. *Journal of the American Chemical Society*. [Online] 77 (22), 5877–5881. Available at: doi:10.1021/JA01627A030

Benham, A.M. (2012) The Protein Disulfide Isomerase Family: Key Players in Health and Disease. *Antioxidants & Redox Signaling*. [Online] 16 (8), 781–789. Available at: doi:10.1089/ars.2011.4439

Benham, A.M., van Lith, M., Sitia, R. and Braakman, I. (2013) Ero1-PDI interactions, the response to redox flux and the implications for disulfide bond formation in the mammalian endoplasmic reticulum. *Philosophical transactions of the Royal Society of London. Series B, Biological sciences*. [Online] 368 (1617), 20110403. Available at: doi:10.1098/rstb.2011.0403.

Berg, J.M., Tymoczko, J.L., Gatto, G.J. and Stryer, L. (2019) *Biochemistry*. 9th edition. New York, Macmillan International Higher Education.

Berg, R.A. and Prockop, D.J. (1973a) Purification of (14C) protocollagen and its hydroxylation by prolyl-hydroxylase. *Biochemistry*. [Online] 12 (18), 3395–3401. Available at: doi:10.1021/BI00742A005

Berg, R.A. and Prockop, D.J. (1973b) The thermal transition of a non-hydroxylated form of collagen. Evidence for a role for hydroxyproline in stabilizing the triple-helix of collagen. *Biochemical and Biophysical Research Communications*. [Online] 52 (1), 115–120. Available at: doi:10.1016/0006-291X(73)90961-3

Bergsten, E., Uutela, M., Li, X., Pietras, K., et al. (2001) PDGF-D is a specific, protease-activated ligand for the PDGF β-receptor. *Nature Cell Biology 2001 3:5*. [Online] 3 (5), 512–516. Available at: doi:10.1038/35074588

Bickel, P.E., Scherer, P.E., Schnitzer, J.E., Oh, P., et al. (1997) Flotillin and Epidermal Surface Antigen Define a New Family of Caveolae-associated Integral Membrane Proteins. *Journal of Biological Chemistry*. [Online] 272 (21), 13793–13802. Available at: doi:10.1074/JBC.272.21.13793

Birkmayer, J.G.D., Vrecko, C., Volc, D. and Birkmayer, W. (1993) Nicotinamide adenine dinucleotide (NADH)--a new therapeutic approach to Parkinson's disease. Comparison of oral and parenteral application. *Acta Neurologica Scandinavica. Supplementum*. [Online] 146 (146), 32–35. Available at: https://europepmc.org/article/med/8101414

Blais, J.D., Chin, K.T., Zito, E., Zhang, Y., et al. (2010) A small molecule inhibitor of Endoplasmic Reticulum Oxidation 1 (ERO1) with selectively reversible thiol reactivity. *Journal of Biological Chemistry*. [Online] 285 (27), 20993–21003. Available at: doi:10.1074/jbc.M110.126599.

Boström, H., Willetts, K., Pekny, M., Levéen, P., et al. (1996) PDGF-A Signaling Is a Critical Event in Lung Alveolar Myofibroblast Development and Alveogenesis. *Cell*. [Online] 85 (6), 863–873. Available at: doi:10.1016/S0092-8674(00)81270-2

Breen, G.A. and Draper, R.K. (2008) Organelle Structure and Function. *Medical Cell Biology: Third Edition*. [Online] 101–148. Available at: doi:10.1016/B978-0-12-370458-0.50009-8

Bulleid, N.J. (2012) Disulfide Bond Formation in the Mammalian Endoplasmic Reticulum. *Cold Spring Harbor Perspectives in Biology*. [Online] 4 (11). Available at: doi:10.1101/CSHPERSPECT.A013219

Buxboim, A., Swift, J., Irianto, J., Spinler, K.R., et al. (2014) Matrix elasticity regulates lamin-A,C phosphorylation and turnover with feedback to actomyosin. *Current biology : CB*. [Online] 24 (16), 1909. Available at: doi:10.1016/J.CUB.2014.07.001

Cabibbo, A., Pagani, M., Fabbri, M., Rocchi, M., et al. (2000) ERO1-L, a Human Protein That Favors Disulfide Bond Formation in the Endoplasmic Reticulum. *Journal of Biological Chemistry*. [Online] 275 (7), 4827–4833. Available at: doi:10.1074/JBC.275.7.4827

Cabral, C.M., Liu, Y., Moremen, K.W. and Sifers, R.N. (2002) Organizational diversity among distinct glycoprotein endoplasmic reticulum-associated degradation programs. *Molecular Biology of the Cell*. [Online] 13 (8), 2639–2650. Available at: doi:10.1091/MBC.E02-02-0068/ASSET/IMAGES/LARGE/MK0821915007.JPEG

Cai, H., Wang, C.C. and Tsou, C.L. (1994) Chaperone-like activity of protein disulfide isomerase in the refolding of a protein with no disulfide bonds. *Journal of Biological Chemistry*. [Online] 269 (40), 24550–24552. Available at: doi:10.1016/S0021-9258(17)31426-6

Calderwood, S.K. and Murshid, A. (2017) Molecular Chaperone Accumulation in Cancer and Decrease in Alzheimer's Disease: The Potential Roles of HSF1. *Frontiers in Neuroscience*. [Online] 11 (APR), 192. Available at: doi:10.3389/FNINS.2017.00192

Calleja-Agius, J., Muscat-Baron, Y. and Brincat, M.P. (2007) Skin ageing. *Menopause International*. [Online] 13 (2), 60–64. Available at: doi:10.1258/175404507780796325

Cardinale, G.J. and Udenfriend, S. (1974) Prolyl hydroxylase. *Advances in enzymology and related areas of molecular biology*. [Online] 41 (0), 245–300. Available at: doi:10.1002/9780470122860.CH6

Carne, N.A. (2018) *The Effect of Endoplasmic Reticulum and Reducing Stress on the Human Dermal Fibroblast Proteome*.

Carne, N.A., Bell, S., Brown, A.P., Määttä, A., et al. (2019) Reductive stress selectively disrupts collagen homeostasis and modifies growth factor-independent signalling through the MAPK/Akt pathway in human dermal fibroblasts. *Molecular & Cellular Proteomics*. [Online] mcp.RA118.001140. Available at: doi:10.1074/mcp.RA118.001140

Casson, J., McKenna, M., Haßdenteufel, S., Aviram, N., et al. (2017) Multiple pathways facilitate the biogenesis of mammalian tail-anchored proteins. *Journal of Cell Science*. [Online] 130 (22), 3851. Available at: doi:10.1242/JCS.207829

Cenni, V., Bertacchini, J., Beretti, F., Lattanzi, G., et al. (2008) Lamin A Ser404 Is a nuclear target of akt phosphorylation in C2C12 cells. *Journal of Proteome Research*. [Online] 7 (11), 4727–4735. Available at: doi:10.1021/PR800262G/ASSET/IMAGES/LARGE/PR-2008-00262G_0005.JPEG

Chakravarthi, S., Jessop, C.E. and Bulleid, N.J. (2006) The role of glutathione in disulphide bond formation and endoplasmic-reticulum-generated oxidative stress. *EMBO Reports*. [Online] 7 (3), 271. Available at: doi:10.1038/SJ.EMBOR.7400645

Cheetham, M.E. and Caplan, A.J. (1998) Structure, function and evolution of DnaJ: conservation and adaptation of chaperone function. *Cell Stress & Chaperones*. [Online] 3 (1), 28. Available at: doi:10.1379/1466-1268(1998)003<0028:sfaeod>2.3.co;2

Chen, M.X., Zhang, Y., Fernie, A.R., Liu, Y.G., et al. (2021) SWATH-MS-Based Proteomics: Strategies and Applications in Plants. *Trends in Biotechnology*. [Online] 39 (5), 433–437. Available at: doi:10.1016/J.TIBTECH.2020.09.002 (Accessed: 7 July 2022).

Chen, X. and Cubillos-Ruiz, J.R. (2020) Endoplasmic reticulum stress signals in the tumour and its microenvironment. *Nature Reviews Cancer 2020 21:2*. [Online] 21 (2), 71–88. Available at: doi:10.1038/s41568-020-00312-2

Chung, K.Y., Agarwal, A., Uitto, J. and Mauviel, A. (1996) An AP-1 Binding Sequence Is Essential for Regulation of the Human α2(I) Collagen (COL1A2) Promoter Activity by Transforming Growth Factor-β. *Journal of Biological Chemistry*. [Online] 271 (6), 3272–3278. Available at: doi:10.1074/JBC.271.6.3272

Cleland, W.W. (1963) Dithiothreitol, a New Protective Reagent for SH Groups. *Biochemistry*. [Online] 3 (4), 480–482. Available at: doi:10.1021/BI00892A002

Cobb, M.H. (1999) MAP kinase pathways. *Progress in Biophysics and Molecular Biology*. [Online] 71 (3–4), 479–500. Available at: doi:10.1016/S0079-6107(98)00056-X

Couto, N., Malys, N., Gaskell, S.J. and Barber, J. (2013) Partition and turnover of glutathione reductase from saccharomyces cerevisiae: A proteomic approach. *Journal of Proteome Research*. [Online] 12 (6), 2885–2894. Available at: doi:10.1021/PR4001948/SUPPL_FILE/PR4001948_SI_001.PDF

Damian, D.L. (2017) Nicotinamide for skin cancer chemoprevention. *Australasian Journal of Dermatology*. [Online] 58 (3), 174–180. Available at: doi:10.1111/AJD.12631

Dassah, M.A., Almeida, D., Hahn, R., Bonaldo, P., et al. (2014) Annexin A2 mediates secretion of collagen VI, pulmonary elasticity and apoptosis of bronchial epithelial cells. *Journal of Cell Science*. [Online] 127 (4), 828–844. Available at: doi:10.1242/JCS.137802/-/DC1

Dechat, T., Pfleghaar, K., Sengupta, K., Shimi, T., et al. (2008) Nuclear lamins: major factors in the structural organization and function of the nucleus and chromatin. *Genes & Development*. [Online] 22 (7), 832. Available at: doi:10.1101/GAD.1652708

Delom, F., Mohtar, M.A., Hupp, T. and Fessart, D. (2020) The anterior gradient-2 interactome. *American Journal of Physiology-Cell Physiology*. [Online] 318 (1), C40–C47. Available at: doi:10.1152/ajpcell.00532.2018

Denisov, A.Y., Määttänen, P., Dabrowski, C., Kozlov, G., et al. (2009) Solution structure of the bb' domains of human protein disulfide isomerase. *The FEBS Journal*. [Online] 276 (5), 1440–1449. Available at: doi:10.1111/J.1742-4658.2009.06884.X

Deuel, T.F., Silverman, N.J. and Kawahara, R.S. (1988) Platelet-derived growth factor: a multifunctional regulator of normal and abnormal cell growth. *Biofactors (Oxford, England)*. [Online] 1 (3), 213–217. Available at: https://europepmc.org/article/med/2855705

Dill, K.A., Ozkan, S.B., Shell, M.S. and Weikl, T.R. (2008) The Protein Folding Problem. *Annual review of biophysics*. [Online] 37289. Available at: doi:10.1146/ANNUREV.BIOPHYS.37.092707.153558

Dobson, C.M. (2003) Protein folding and misfolding. *Nature 2003 426:6968*. [Online] 426 (6968), 884–890. Available at: doi:10.1038/nature02261

Dong, A., Gupta, A., Pai, R.K., Tun, M., et al. (2011) The Human Adenocarcinoma-associated Gene, AGR2, Induces Expression of Amphiregulin through Hippo Pathway Co-activator YAP1 Activation. *The Journal of Biological Chemistry*. [Online] 286 (20), 18301. Available at: doi:10.1074/JBC.M110.215707

Driskell, R.R., Lichtenberger, B.M., Hoste, E., Kretzschmar, K., et al. (2013) Distinct fibroblast lineages determine dermal architecture in skin development and repair. *Nature 2013 504:7479*. [Online] 504 (7479), 277–281. Available at: doi:10.1038/nature12783

Dyson, H.J., Wright, P.E. and Scheraga, H.A. (2006) The role of hydrophobic interactions in initiation and propagation of protein folding. *Proceedings of the National Academy of Sciences of the United States of America*. [Online] 103 (35), 13057. Available at: doi:10.1073/PNAS.0605504103

Eccles, S.A., Massey, A., Raynaud, F.I., Sharp, S.Y., et al. (2008) NVP-AUY922: A Novel Heat Shock Protein 90 Inhibitor Active against Xenograft Tumor Growth, Angiogenesis, and Metastasis. *Cancer Research*. [Online] 68 (8), 2850–2860. Available at: doi:10.1158/0008-5472.CAN-07-5256

Ellgaard, L. (2004) Catalysis of disulphide bond formation in the endoplasmic reticulum. *Biochemical Society Transactions*. [Online] 32 (5), 663–667. Available at: doi:10.1042/BST0320663

Escoffier, C., de Rigal, J., Rochefort, A., Vasselet, R., et al. (1989) Age-related mechanical properties of human skin: An in vivo study. *Journal of Investigative Dermatology*. [Online] 93 (3), 353–357. Available at: doi:10.1016/0022-202X(89)90058-4

Esfahani, S.A., Khoshneviszadeh, M., Namazi, M.R., Noorafshan, A., et al. (2015) Topical Nicotinamide Improves Tissue Regeneration in Excisional Full-Thickness Skin Wounds: A Stereological and Pathological Study. *Trauma Monthly*. [Online] 20 (4), 18193. Available at: doi:10.5812/TRAUMAMON.18193

Evans, C.M., Raclawska, D.S., Ttofali, F., Liptzin, D.R., et al. (2015) The polymeric mucin Muc5ac is required for allergic airway hyperreactivity. *Nature communications*. [Online] 66281. Available at: doi:10.1038/NCOMMS7281

Fabio Falsone, S., Leptihn, S., Osterauer, A., Haslbeck, M., et al. (2004) Oncogenic Mutations Reduce the Stability of Src Kinase. *Journal of Molecular Biology*. [Online] 344 (1), 281–291. Available at: doi:10.1016/J.JMB.2004.08.091

Fagerberg, L., Hallstrom, B.M., Oksvold, P., Kampf, C., et al. (2014) Analysis of the Human Tissue-specific Expression by Genome-wide Integration of Transcriptomics and Antibody-based Proteomics. *Molecular & Cellular Proteomics : MCP*. [Online] 13 (2), 397. Available at: doi:10.1074/MCP.M113.035600

Fagone, P. and Jackowski, S. (2009) Membrane phospholipid synthesis and endoplasmic reticulum function. *Journal of Lipid Research*. [Online] 50 (Suppl), S311. Available at: doi:10.1194/JLR.R800049-JLR200

Favaloro, V., Spasic, M., Schwappach, B. and Dobberstein, B. (2008) Distinct targeting pathways for the membrane insertion of tail-anchored (TA) proteins. *Journal of cell science*. [Online] 121 (Pt 11), 1832. Available at: doi:10.1242/JCS.020321

Fenn, J.B., Mann, M., Meng, C.K., Wong, S.F., et al. (1989) Electrospray Ionization for Mass Spectrometry of Large Biomolecules. *Science*. [Online] 246 (4926), 64–71. Available at: doi:10.1126/SCIENCE.2675315

Fessart, D., de Barbeyrac, C., Boutin, I., Grenier, T., et al. (2021) Extracellular AGR2 triggers lung tumour cell proliferation through repression of p21CIP1. *Biochimica et Biophysica Acta (BBA) - Molecular Cell Research*. [Online] 1868 (3), 118920. Available at: doi:10.1016/J.BBAMCR.2020.118920

Fessart, D., Domblides, C., Avril, T., Eriksson, L.A., et al. (2016) Secretion of protein disulphide isomerase AGR2 confers tumorigenic properties. *eLife*. [Online] 5 (MAY2016). Available at: doi:10.7554/ELIFE.13887

Finley, D. (2009) Recognition and Processing of Ubiquitin-Protein Conjugates by the Proteasome. *Annual review of biochemistry*. [Online] 78477. Available at: doi:10.1146/ANNUREV.BIOCHEM.78.081507.101607

Fisher, G.J., Datta, S., Wang, Z.Q., Li, X.Y., et al. (2000) c-Jun–dependent inhibition of cutaneous procollagen transcription following ultraviolet irradiation is reversed by all-trans retinoic acid. *Journal of Clinical Investigation*. [Online] 106 (5), 663. Available at: doi:10.1172/JCI9362

Fisher, G.J., Talwar, H.S., Lin, J., Lin, P., et al. (1998) Retinoic acid inhibits induction of c-Jun protein by ultraviolet radiation that occurs subsequent to activation of mitogen-activated protein kinase pathways in human skin in vivo. *Journal of Clinical Investigation*. [Online] 101 (6), 1432. Available at: doi:10.1172/JCI2153

Foresti, O., Ruggiano, A., Hannibal-Bach, H.K., Ejsing, C.S., et al. (2013) Sterol homeostasis requires regulated degradation of squalene monooxygenase by the ubiquitin ligase Doa10/Teb4. *eLife*. [Online] 2 (2), 953. Available at: doi:10.7554/ELIFE.00953

Forrester, A., Leonibus, C. de, Grumati, P., Fasana, E., et al. (2019) A selective ER-phagy exerts procollagen quality control via a Calnexin-FAM134B complex. *The EMBO Journal*. [Online] 38 (2), e99847. Available at: doi:10.15252/EMBJ.201899847

Foster, C.R., Przyborski, S.A., Wilson, R.G. and Hutchison, C.J. (2010) Lamins as cancer biomarkers. *Biochemical Society Transactions*. [Online] 38 (1), 297–300. Available at: doi:10.1042/BST0380297

Frand, A.R. and Kaiser, C.A. (1998) The ERO1 Gene of Yeast Is Required for Oxidation of Protein Dithiols in the Endoplasmic Reticulum. *Molecular Cell*. [Online] 1 (2), 161–170. Available at: doi:10.1016/S1097-2765(00)80017-9

Fritzsche, F.R., Dahl, E., Dankof, A., Burkhardt, M., et al. (2007) Expression of AGR2 in non small cell lung cancer. *Histology and histopathology*. [Online] 22 (7), 703–708. Available at: doi:10.14670/HH-22.703

Fritzsche, F.R., Dahl, E., Pahl, S., Burkhardt, M., et al. (2006) Prognostic Relevance of AGR2 Expression in Breast Cancer. *Clinical Cancer Research*. [Online] 12 (6), 1728–1734. Available at: doi:10.1158/1078-0432.CCR-05-2057

Fuchs, S., de Lorenzo, F. and Anfinsen, C.B. (1967) Studies on the mechanism of the enzymic catalysis of disulfide interchange in proteins. *Journal of Biological Chemistry*. 242 (3), 398–402.

Fukuda, Y., Aguilar-Bryan, L., Vaxillaire, M., Dechaume, A., et al. (2011) Conserved Intramolecular Disulfide Bond Is Critical to Trafficking and Fate of ATP-binding Cassette (ABC) Transporters ABCB6 and Sulfonylurea Receptor 1 (SUR1)/ABCC8. *The Journal of Biological Chemistry*. [Online] 286 (10), 8481. Available at: doi:10.1074/JBC.M110.174516

Gao, X., Carroni, M., Nussbaum-Krammer, C., Mogk, A., et al. (2015) Human Hsp70 Disaggregase Reverses Parkinson's-Linked α-Synuclein Amyloid Fibrils. *Molecular cell*. [Online] 59 (5), 781. Available at: doi:10.1016/J.MOLCEL.2015.07.012

Gao, Y., Wang, X., Sang, Z., Li, Z., et al. (2017) Quantitative proteomics by SWATH-MS reveals sophisticated metabolic reprogramming in hepatocellular carcinoma tissues. *Scientific Reports*. [Online] 7. Available at: doi:10.1038/SREP45913

Geesin, J.C., Brown, L.J., Gordon, J.S. and Berg, R.A. (1993) Regulation of Collagen Synthesis in Human Dermal Fibroblasts in Contracted Collagen Gels by Ascorbic Acid, Growth Factors, and Inhibitors of Lipid Peroxidation. *Experimental Cell Research*. [Online] 206 (2), 283–290. Available at: doi:10.1006/EXCR.1993.1148

Gilbertson, D.G., Duff, M.E., West, J.W., Kelly, J.D., et al. (2001) Platelet-derived Growth Factor C (PDGF-C), a Novel Growth Factor That Binds to PDGF α and β Receptor. *Journal of Biological Chemistry*. [Online] 276 (29), 27406–27414. Available at: doi:10.1074/JBC.M101056200

Goldberger, R.F., Epstein, C.J. and Anfinsen, C.B. (1963) Acceleration of Reactivation of Reduced Bovine Pancreatic Ribonuclease by a Microsomal System from Rat Liver. *Journal of Biological Chemistry*. [Online] 238 (2), 628–635. Available at: doi:10.1016/S0021-9258(18)81309-6

Gorres, K.L. and Raines, R.T. (2010) Prolyl 4-hydroxylase. *Critical reviews in biochemistry and molecular biology*. [Online] 45 (2), 106. Available at: doi:10.3109/10409231003627991

Gray, T.A., Murray, E., Nowicki, M.W., Remnant, L., et al. (2013) Development of a fluorescent monoclonal antibody-based assay to measure the allosteric effects of synthetic peptides on self-oligomerization of AGR2 protein. *Protein Science : A Publication of the Protein Society*. [Online] 22 (9), 1266. Available at: doi:10.1002/PRO.2299

Greaves, N.S., Ashcroft, K.J., Baguneid, M. and Bayat, A. (2013) Current understanding of molecular and cellular mechanisms in fibroplasia and angiogenesis during acute wound healing. *Journal of Dermatological Science*. [Online] 72 (3), 206–217. Available at: doi:10.1016/J.JDERMSCI.2013.07.008

Gundry, R.L., White, M.Y., Murray, C.I., Kane, L.A., et al. (2009) Preparation of Proteins and Peptides for Mass Spectrometry Analysis in a Bottom-Up Proteomics Workflow. *Current protocols in molecular biology / edited by Frederick M. Ausubel ... [et al.]*. [Online] CHAPTER (SUPPL. 88), Unit10.25. Available at: doi:10.1002/0471142727.MB1025S88

Gupta, A., Dong, A. and Lowe, A.W. (2012) AGR2 Gene Function Requires a Unique Endoplasmic Reticulum Localization Motif. *The Journal of Biological Chemistry*. [Online] 287 (7), 4773. Available at: doi:10.1074/JBC.M111.301531

Gupta, A., Wodziak, D., Tun, M., Bouley, D.M., et al. (2013) Loss of Anterior Gradient 2 (Agr2) Expression Results in Hyperplasia and Defective Lineage Maturation in the Murine Stomach. *The Journal of Biological Chemistry*. [Online] 288 (6), 4321. Available at: doi:10.1074/JBC.M112.433086

Haas, I.G. and Wabl, M. (1983) Immunoglobulin heavy chain binding protein. *Nature 1983 306:5941*. [Online] 306 (5941), 387–389. Available at: doi:10.1038/306387a0

Han, X., Aslanian, A. and Yates, J.R. (2008) Mass Spectrometry for Proteomics. *Current opinion in chemical biology*. [Online] 12 (5), 483. Available at: doi:10.1016/J.CBPA.2008.07.024

Hanson, S.R., Culyba, E.K., Hsu, T.L., Wong, C.H., et al. (2009) The core trisaccharide of an N-linked glycoprotein intrinsically accelerates folding and enhances stability. *Proceedings of the National Academy of Sciences of the United States of America*. [Online] 106 (9), 3131. Available at: doi:10.1073/PNAS.0810318105

Harada, T., Swift, J., Irianto, J., Shin, J.W., et al. (2014) Nuclear lamin stiffness is a barrier to 3D migration, but softness can limit survival. *The Journal of Cell Biology*. [Online] 204 (5), 669. Available at: doi:10.1083/JCB.201308029

Harding, H.P., Zhang, Y. and Ron, D. (1999) Protein translation and folding are coupled by an endoplasmic-reticulum-resident kinase. *Nature 1999 397:6716*. [Online] 397 (6716), 271–274. Available at: doi:10.1038/16729

Hardman, G., Perkins, S., Brownridge, P.J., Clarke, C.J., et al. (2019) Strong anion exchange-mediated phosphoproteomics reveals extensive human non-canonical phosphorylation. *The EMBO Journal*. [Online] 38 (21), e100847. Available at: doi:10.15252/EMBJ.2018100847

Harper, R.A. and Grove, G. (1979) Human Skin Fibroblasts Derived from Papillary and Reticular Dermis: Differences in Growth Potential in Vitro. *Science*. [Online] 204 (4392), 526–527. Available at: doi:10.1126/SCIENCE.432659

Hart, C.E., Forstrom, J.W., Kelly, J.D., Seifert, R.A., et al. (1988) Two classes of PDGF receptor recognize different isoforms of PDGF. *Science*. [Online] 240 (4858), 1529–1531. Available at: doi:10.1126/SCIENCE.2836952

Hatahet, F. and Ruddock, L.W. (2009) Protein disulfide isomerase: A critical evaluation of its function in disulfide bond formation. *Antioxidants and Redox Signaling*. [Online] 11 (11), 2807–2850. Available at: doi:10.1089/ARS.2009.2466/ASSET/IMAGES/LARGE/FIG-22.JPEG

Hegde, R.S. and Bernstein, H.D. (2006) The surprising complexity of signal sequences. *Trends in Biochemical Sciences*. [Online] 31 (10), 563–571. Available at: doi:10.1016/J.TIBS.2006.08.004

Hegde, R.S. and Keenan, R.J. (2011) Tail-anchored membrane protein insertion into the endoplasmic reticulum. *Nature reviews. Molecular cell biology*. [Online] 12 (12), 787. Available at: doi:10.1038/NRM3226

Higa, A., Mulot, A., Delom, F., Bouchecareilh, M., et al. (2011) Role of Pro-oncogenic Protein Disulfide Isomerase (PDI) Family Member Anterior Gradient 2 (AGR2) in the Control of Endoplasmic Reticulum Homeostasis. *The Journal of Biological Chemistry*. [Online] 286 (52), 44855. Available at: doi:10.1074/JBC.M111.275529

Hirata, T., Fujita, M., Nakamura, S., Gotoh, K., et al. (2015) Post-Golgi anterograde transport requires GARP-dependent endosome-to-TGN retrograde transport. *Molecular Biology of the Cell*. [Online] 26 (17), 3071. Available at: doi:10.1091/MBC.E14-11-1568

Hoffstrom, B.G., Kaplan, A., Letso, R., Schmid, R.S., et al. (2010) Inhibitors of protein disulfide isomerase suppress apoptosis induced by misfolded proteins. *Nature chemical biology*. [Online] 6 (12), 900. Available at: doi:10.1038/NCHEMBIO.467

Holmgren, A. (1979) Thioredoxin catalyzes the reduction of insulin disulfides by dithiothreitol and dihydrolipoamide. *Journal of Biological Chemistry*. [Online] 254 (19), 9627–9632. Available at: doi:10.1016/S0021-9258(19)83562-7

Hutton, J.J., Kaplan, A. and Udenfriend, S. (1967) Conversion of the amino acid sequence Gly-Pro-Pro in protein to Gly-Pro-Hyp by collagen proline hydroxylase. *Archives of Biochemistry and Biophysics*. [Online] 121 (2), 384–391. Available at: doi:10.1016/0003-9861(67)90091-4

Ikegami, K., Secchia, S., Almakki, O., Lieb, J.D., et al. (2020) Phosphorylated Lamin A/C in the Nuclear Interior Binds Active Enhancers Associated with Abnormal Transcription in Progeria. *Developmental Cell*. [Online] 52 (6), 699-713.e11. Available at: doi:10.1016/J.DEVCEL.2020.02.011

Inaba, K., Masui, S., Iida, H., Vavassori, S., et al. (2010) Crystal structures of human Ero1α reveal the mechanisms of regulated and targeted oxidation of PDI. *The EMBO Journal*. [Online] 29 (19), 3330–3343. Available at: doi:10.1038/EMBOJ.2010.222

Ishida, Y., Yamamoto, A., Kitamura, A., Lamandé, S.R., et al. (2009) Autophagic elimination of misfolded procollagen aggregates in the endoplasmic reticulum as a means of cell protection. *Molecular Biology of the Cell*. [Online] 20 (11), 2744–2754. Available at: doi:10.1091/MBC.E08-11-1092/ASSET/IMAGES/LARGE/ZMK0110990660009.JPEG

Ivanova, A.S., Tereshina, M.B., Ermakova, G. v., Belousov, V. v., et al. (2013) Agr genes, missing in amniotes, are involved in the body appendages regeneration in frog tadpoles. *Scientific Reports*. [Online] 3. Available at: doi:10.1038/SREP01279

Jackson, R.C. and Blobel, G. (1977) Post-translational cleavage of presecretory proteins with an extract of rough microsomes from dog pancreas containing signal peptidase activity. *Proceedings of the National Academy of Sciences of the United States of America*. [Online] 74 (12), 5598. Available at: doi:10.1073/PNAS.74.12.5598

de Jager, T.L., Cockrell, A.E. and du Plessis, S.S. (2017) Ultraviolet light induced generation of reactive oxygen species. *Advances in Experimental Medicine and Biology*. [Online] 99615–23. Available at: doi:10.1007/978-3-319-56017-5_2/COVER/

Jahoda, C.A.B. and Reynolds, A.J. (1996) DERMAL-EPIDERMAL INTERACTIONS: Adult Follicle-Derived Cell Populations and Hair Growth. *Dermatologic Clinics*. [Online] 14 (4), 573–583. Available at: doi:10.1016/S0733-8635(05)70385-5

Jansens, A., van Duijn, E. and Braakman, I. (2002) Coordinated nonvectorial folding in a newly synthesized multidomain protein. *Science*. [Online] 298 (5602), 2401–2403. Available at: doi:10.1126/SCIENCE.1078376/SUPPL_FILE/JANSENS.SOM.PDF

Janson, D.G., Saintigny, G., van Adrichem, A., Mahé, C., et al. (2012) Different gene expression patterns in human papillary and reticular fibroblasts. *Journal of Investigative Dermatology*. [Online] 132 (11), 2565–2572. Available at: doi:10.1038/JID.2012.192/ATTACHMENT/BB3574F9-D639-4D3B-AE58-9B09DA1E9C3B/MMC1.PDF

Jeung-Hoi, H. and McKay, D.B. (1994) ATPase kinetics of recombinant bovine 70 kDa heat shock cognate protein and its amino-terminal ATPase domain. *Biochemistry*. [Online] 33 (48), 14625–14635. Available at: doi:10.1021/BI00252A031

Jocelyn, P.C. (1987) Chemical reduction of disulfides. *Methods in Enzymology*. [Online] 143 (C), 246–256. Available at: doi:10.1016/0076-6879(87)43048-6

Jordan, R. and McMacken, R. (1995) Modulation of the ATPase Activity of the Molecular Chaperone DnaK by Peptides and the DnaJ and GrpE Heat Shock Proteins. *Journal of Biological Chemistry*. [Online] 270 (9), 4563–4569. Available at: doi:10.1074/JBC.270.9.4563

Karas, M. and Hillenkamp, F. (1988) Laser desorption ionization of proteins with molecular masses exceeding 10,000 daltons. *Analytical chemistry*. [Online] 60 (20), 2299–2301. Available at: doi:10.1021/AC00171A028

Karlsson, L., Lindahl, P., Heath, J.K. and Betsholtz, C. (2000) Abnormal gastrointestinal development in PDGF-A and PDGFR-(alpha) deficient mice implicates a novel mesenchymal structure with putative instructive properties in villus morphogenesis. *Development*. [Online] 127 (16), 3457–3466. Available at: doi:10.1242/DEV.127.16.3457

Kemmink, J., Darby, N.J., Dijkstrat, K., Nilges, M., et al. (1997) The folding catalyst protein disulfide isomerase is constructed of active and inactive thioredoxin modules. *Current Biology*. [Online] 7 (4), 239–245. Available at: doi:10.1016/S0960-9822(06)00119-9

Kesimer, M., Ford, A.A., Ceppe, A., Radicioni, G., et al. (2017) Airway Mucin Concentration as a Marker of Chronic Bronchitis. *New England Journal of Medicine*. [Online] 377 (10), 911–922. Available at: doi:10.1056/NEJMOA1701632/SUPPL_FILE/NEJMOA1701632_DISCLOSURES.PDF

Kim, S., Sideris, D.P., Sevier, C.S. and Kaiser, C.A. (2012) Balanced Ero1 activation and inactivation establishes ER redox homeostasis. *Journal of Cell Biology*. [Online] 196 (6), 713–725. Available at: doi:10.1083/JCB.201110090

Kim, S.M., Kwon, C.H., Shin, N., Park, D.Y., et al. (2014) Decreased Muc5AC expression is associated with poor prognosis in gastric cancer. *International Journal of Cancer*. [Online] 134 (1), 114–124. Available at: doi:10.1002/IJC.28345

Kim, Y.E., Hipp, M.S., Bracher, A., Hayer-Hartl, M., et al. (2013) Molecular Chaperone Functions in Protein Folding and Proteostasis. *http://dx.doi.org/10.1146/annurev-biochem-060208-092442*. [Online] 82323–355. Available at: doi:10.1146/ANNUREV-BIOCHEM-060208-092442

Klappa, P., Ruddock, L.W., Darby, N.J. and Freedman, R.B. (1998) The b' domain provides the principal peptide-binding site of protein disulfide isomerase but all domains contribute to binding of misfolded proteins. *The EMBO Journal*. [Online] 17 (4), 927–935. Available at: doi:10.1093/EMBOJ/17.4.927

Kochin, V., Shimi, T., Torvaldson, E., Adam, S.A., et al. (2014) Interphase phosphorylation of lamin A. *Journal of Cell Science*. [Online] 127 (12), 2683–2696. Available at: doi:10.1242/JCS.141820/-/DC1

Kojer, K. and Riemer, J. (2014) Balancing oxidative protein folding: The influences of reducing pathways on disulfide bond formation. *Biochimica et Biophysica Acta (BBA) - Proteins and Proteomics*. [Online] 1844 (8), 1383–1390. Available at: doi:10.1016/J.BBAPAP.2014.02.004

Komiya, T., Tanigawa, Y. and Hirohashi, S. (1999) Cloning of the gene gob-4, which is expressed in intestinal goblet cells in mice. *Biochimica et Biophysica Acta (BBA) - Gene Structure and Expression*. [Online] 1444 (3), 434–438. Available at: doi:10.1016/S0167-4781(99)00010-X

Kozutsumi, Y., Segal, M., Normington, K., Gething, M.J., et al. (1988) The presence of malfolded proteins in the endoplasmic reticulum signals the induction of glucose-regulated proteins. *Nature 1988 332:6163*. [Online] 332 (6163), 462–464. Available at: doi:10.1038/332462a0

Krishn, S.R., Ganguly, K., Kaur, S. and Batra, S.K. (2018) Ramifications of secreted mucin MUC5AC in malignant journey: a holistic view. *Carcinogenesis*. [Online] 39 (5), 633–651. Available at: doi:10.1093/CARCIN/BGY019

Labbadia, J., Novoselov, S.S., Bett, J.S., Weiss, A., et al. (2012) Suppression of protein aggregation by chaperone modification of high molecular weight complexes. *Brain*. [Online] 135 (4), 1180. Available at: doi:10.1093/BRAIN/AWS022
\
Lakkaraju, A.K.K., Mary, C., Scherrer, A., Johnson, A.E., et al. (2008) SRP maintains nascent chains translocation-competent by slowing translation rates to match limiting numbers of targeting sites. *Cell*. [Online] 133 (3), 440. Available at: doi:10.1016/J.CELL.2008.02.049

Lambert, C.A., Soudant, E.P., Nusgens, B. v. and Lapiere, C.M. (1992) Pretranslational regulation of extracellular matrix macromolecules and collagenase expression in fibroblasts by mechanical forces. *Laboratory Investigation; a Journal of Technical Methods and Pathology*. [Online] 66 (4), 444–451. Available at: https://europepmc.org/article/med/1316527

Larochelle, W.J., Jeffers, M., Mcdonald, W.F., Chillakuru, R.A., et al. (2001) PDGF-D, a new protease-activated growth factor. *Nature Cell Biology 2001 3:5*. [Online] 3 (5), 517–521. Available at: doi:10.1038/35074593

Lee, J.Y., Yun, M., Paik, J.S., Lee, S.B., et al. (2016) PDGF-BB Enhances the Proliferation of Cells in Human Orbital Fibroblasts by Suppressing PDCD4 Expression Via Up-Regulation of microRNA-21. *Investigative Ophthalmology & Visual Science*. [Online] 57 (3), 908–913. Available at: doi:10.1167/IOVS.15-18157

Levéen, P., Pekny, M., Gebre-Medhin, S., Swolin, B., et al. (1994) Mice deficient for PDGF B show renal, cardiovascular, and hematological abnormalities. *Genes & development*. [Online] 8 (16), 1875–1887. Available at: doi:10.1101/GAD.8.16.1875

Li, L., Liu, J., Ding, Y., Shi, Z., et al. (2020) Design, synthesis and evaluation of protein disulfide isomerase inhibitors with nitric oxide releasing activity. *Bioorganic and Medicinal Chemistry Letters*. [Online] 30 (3). Available at: doi:10.1016/j.bmcl.2019.126898

Li, Z., Zhu, Q., Hu, L., Chen, H., et al. (2015) Anterior gradient 2 is a binding stabilizer of hypoxia inducible factor-1α that enhances CoCl2-induced doxorubicin resistance in breast cancer cells. *Cancer Science*. [Online] 106 (8), 1041. Available at: doi:10.1111/CAS.12714

Lièvremont, J.P., Rizzuto, R., Hendershot, L. and Meldolesi, J. (1997) BiP, a Major Chaperone Protein of the Endoplasmic Reticulum Lumen, Plays a Direct and Important Role in the Storage of the Rapidly Exchanging Pool of Ca2+. *Journal of Biological Chemistry*. [Online] 272 (49), 30873–30879. Available at: doi:10.1074/JBC.272.49.30873

Lillehoj, E.P., Kato, K., Lu, W. and Kim, K.C. (2013) Cellular and Molecular Biology of Airway Mucins. *International Review of Cell and Molecular Biology*. [Online] 303139–202. Available at: doi:10.1016/B978-0-12-407697-6.00004-0

Lim, J. and Yue, Z. (2015) Neuronal aggregates: formation, clearance and spreading. *Developmental cell*. [Online] 32 (4), 491. Available at: doi:10.1016/J.DEVCEL.2015.02.002

Liou, G.Y. and Storz, P. (2010) Reactive oxygen species in cancer. *Free radical research*. [Online] 44 (5), 479–496. Available at: doi:10.3109/10715761003667554

Liu, A.Y., Kanan, A.D., Radon, T.P., Shah, S., et al. (2019) AGR2, a unique tumor-associated antigen, is a promising candidate for antibody targeting. *Oncotarget*. [Online] 10 (42), 4276. Available at: doi:10.18632/ONCOTARGET.26945

Liu, Y., Borel, C., Li, L., Müller, T., et al. (2017) Systematic proteome and proteostasis profiling in human Trisomy 21 fibroblast cells. *Nature Communications 2017 8:1*. [Online] 8 (1), 1–15. Available at: doi:10.1038/s41467-017-01422-6

Lodish, H.F. and Kong, N. (1993) The secretory pathway is normal in dithiothreitol-treated cells, but disulfide-bonded proteins are reduced and reversibly retained in the endoplasmic reticulum. *Journal of Biological Chemistry*. [Online] 268 (27), 20598–20605. Available at: doi:10.1016/S0021-9258(20)80767-4

Lovric, J. (2011) *Introducing Proteomics*. Wiley-Blackwell.

Ludwig, C., Gillet, L., Rosenberger, G., Amon, S., et al. (2018) Data-independent acquisition-based SWATH-MS for quantitative proteomics: a tutorial. *Molecular Systems Biology*. [Online] 14 (8), e8126. Available at: doi:10.15252/MSB.20178126

Lukesh, J.C., Palte, M.J. and Raines, R.T. (2012) A potent, versatile disulfide-reducing agent from aspartic acid. *Journal of the American Chemical Society*. [Online] 134 (9), 4057–4059. Available at: doi:10.1021/ja211931f

Lukesh, J.C., Wallin, K.K. and Raines, R.T. (2014) Pyrazine-derived disulfide-reducing agent for chemical biology. *Chemical Communications*. [Online] 50 (67), 9591–9594. Available at: doi:10.1039/C4CC04491F

Magni, G., Amici, A., Emanuelli, M., Orsomando, G., et al. (2004) Enzymology of NAD+ homeostasis in man. *Cellular and Molecular Life Sciences CMLS 2004 61:1*. [Online] 61 (1), 19–34. Available at: doi:10.1007/S00018-003-3161-1

Maley, C.C. and Rustgi, A.K. (2006) Barrett's Esophagus and Its Progression to Adenocarcinoma. *Journal of the National Comprehensive Cancer Network*. [Online] 4 (4), 367–374. Available at: doi:10.6004/JNCCN.2006.0031

Marciniak, S.J., Yun, C.Y., Oyadomari, S., Novoa, I., et al. (2004) CHOP induces death by promoting protein synthesis and oxidation in the stressed endoplasmic reticulum. *Genes & Development*. [Online] 18 (24), 3066. Available at: doi:10.1101/GAD.1250704

Martins-Marques, T., Anjo, S.I., Pereira, P., Manadas, B., et al. (2015) Interacting Network of the Gap Junction (GJ) Protein Connexin43 (Cx43) is Modulated by Ischemia and Reperfusion in the Heart. *Molecular & Cellular Proteomics*. [Online] 14 (11), 3040–3055. Available at: doi:10.1074/MCP.M115.052894

Marzec, M., Eletto, D. and Argon, Y. (2012) GRP94: an HSP90-like protein specialized for protein folding and quality control in the Endoplasmic Reticulum. *Biochimica et biophysica acta*. [Online] 1823 (3), 774. Available at: doi:10.1016/J.BBAMCR.2011.10.013

Matlack, K.E.S., Misselwitz, B., Plath, K. and Rapoport, T.A. (1999) BiP Acts as a Molecular Ratchet during Posttranslational Transport of Prepro-α Factor across the ER Membrane. *Cell*. [Online] 97 (5), 553–564. Available at: doi:10.1016/S0092-8674(00)80767-9

Matsui, Y., Hirata, Y., Wada, I. and Hosokawa, N. (2020) Visualization of Procollagen IV Reveals ER-to-Golgi Transport by ERGIC-independent Carriers. *Cell Structure and Function*. [Online] 45 (2), 107–119. Available at: doi:10.1247/CSF.20025

Maurel, M., Obacz, J., Avril, T., Ding, Y., et al. (2019) Control of anterior GRadient 2 (AGR2) dimerization links endoplasmic reticulum proteostasis to inflammation. *EMBO Molecular Medicine*. [Online] 11 (6). Available at: doi:10.15252/EMMM.201810120

Mayer, M.P., Schröder, H., Rüdiger, S., Paal, K., et al. (2000) Multistep mechanism of substrate binding determines chaperone activity of Hsp70. *Nature structural biology*. [Online] 7 (7), 586–593. Available at: doi:10.1038/76819

McDonagh, B. (2017) Detection of ROS Induced Proteomic Signatures by Mass Spectrometry. *Frontiers in Physiology*. [Online] 8 (JUL), 470. Available at: doi:10.3389/FPHYS.2017.00470

Meldolesi, J. and Pozzan, T. (1998) The endoplasmic reticulum Ca2+ store: a view from the lumen. *Trends in Biochemical Sciences*. [Online] 23 (1), 10–14. Available at: doi:10.1016/S0968-0004(97)01143-2

Messina, M.S., O'Riordan, T.G. and Smaldone, G.C. (1991) Changes in Mucociliary Clearance during Acute Exacerbations of Asthma. *https://doi.org/10.1164/ajrccm/143.5_Pt_1.993*. [Online] 143 (5 I), 993–997. Available at: doi:10.1164/AJRCCM/143.5_PT_1.993

Michalak, M., Parker, J.M.R. and Opas, M. (2002) Ca2+ signaling and calcium binding chaperones of the endoplasmic reticulum. *Cell Calcium*. [Online] 32 (5–6), 269–278. Available at: doi:10.1016/S0143416002001884

Molinari, M. and Helenius, A. (1999) Glycoproteins form mixed disulphides with oxidoreductases during folding in living cells. *Nature 1999 402:6757*. [Online] 402 (6757), 90–93. Available at: doi:10.1038/47062

Mónico, A., Duarte, S., Pajares, M.A. and Pérez-Sala, D. (2019) Vimentin disruption by lipoxidation and electrophiles: Role of the cysteine residue and filament dynamics. *Redox Biology*. [Online] 23101098. Available at: doi:10.1016/J.REDOX.2019.101098

Montero, D., Tachibana, C., Rahr Winther, J. and Appenzeller-Herzog, C. (2013) Intracellular glutathione pools are heterogeneously concentrated. *Redox Biology*. [Online] 1 (1), 508. Available at: doi:10.1016/J.REDOX.2013.10.005

Moore, L., Chen, T., Knapp, H.R. and Landon, E.J. (1975) Energy-dependent Calcium Sequestration Activity in Rat Liver Microsomes. *Journal of Biological Chemistry*. [Online] 250 (12), 4562–4568. Available at: doi:10.1016/S0021-9258(19)41338-0

Murray, J.I., Whitfield, M.L., Trinklein, N.D., Myers, R.M., et al. (2004) Diverse and Specific Gene Expression Responses to Stresses in Cultured Human Cells. *Molecular Biology of the Cell*. [Online] 15 (5), 2361. Available at: doi:10.1091/MBC.E03-11-0799

Myllyharju, J. (2003) Prolyl 4-hydroxylases, the key enzymes of collagen biosynthesis. *Matrix Biology*. [Online] 22 (1), 15–24. Available at: doi:10.1016/S0945-053X(03)00006-4

Naylor, E.C., Watson, R.E.B. and Sherratt, M.J. (2011) Molecular aspects of skin ageing *Maturitas*. [Online]. 69 (3) pp.249–256. Available at: doi:10.1016/j.maturitas.2011.04.011

NCBI (2022) *GPX1 glutathione peroxidase 1 [Homo sapiens (human)] - Gene - NCBI*. [Online]. 2022. Available at: https://www.ncbi.nlm.nih.gov/gene?Db=gene&Cmd=ShowDetailView&TermToSearch=2876

Nesvizhskii, A. (2015) *Welcome to CRAPome 2.0 | CRAPome*. [Online]. 2015. Available at: https://reprint-apms.org/?q=chooseworkflow

Netzer, W.J. and Hartl, F.U. (1997) Recombination of protein domains facilitated by co-translational folding in eukaryotes. *Nature 1997 388:6640*. [Online] 388 (6640), 343–349. Available at: doi:10.1038/41024

Nguyen, V.D., Wallis, K., Howard, M.J., Haapalainen, A.M., et al. (2008) Alternative Conformations of the x Region of Human Protein Disulphide-Isomerase Modulate Exposure of the Substrate Binding b' Domain. *Journal of Molecular Biology*. [Online] 383 (5), 1144–1155. Available at: doi:10.1016/J.JMB.2008.08.085

Okimoto, K., Arai, M., Ishigami, H., Saito, K., et al. (2018) A Prospective Study of Eosinophilic Esophagitis and the Expression of Tight Junction Proteins in Patients with Gastroesophageal Reflux Disease Symptoms. *Gut and Liver*. [Online] 12 (1), 30–37. Available at: doi:10.5009/GNL16600

Pagani, M., Fabbri, M., Benedetti, C., Fassio, A., et al. (2000) Endoplasmic Reticulum Oxidoreductin 1-Lβ (ERO1-Lβ), a Human Gene Induced in the Course of the Unfolded Protein Response. *Journal of Biological Chemistry*. [Online] 275 (31), 23685–23692. Available at: doi:10.1074/JBC.M003061200

Pakula, T.M., Laxell, M., Huuskonen, A., Uusitalo, J., et al. (2003) The Effects of Drugs Inhibiting Protein Secretion in the Filamentous Fungus Trichoderma reesei: EVIDENCE FOR DOWN-REGULATION OF GENES THAT ENCODE SECRETED PROTEINS IN THE STRESSED CELLS. *Journal of Biological Chemistry*. [Online] 278 (45), 45011–45020. Available at: doi:10.1074/JBC.M302372200

Pankiv, S., Clausen, T.H., Lamark, T., Brech, A., et al. (2007) p62/SQSTM1 Binds Directly to Atg8/LC3 to Facilitate Degradation of Ubiquitinated Protein Aggregates by Autophagy. *Journal of Biological Chemistry*. [Online] 282 (33), 24131–24145. Available at: doi:10.1074/JBC.M702824200

Park, J., Halliday, G.M., Surjana, D. and Damian, D.L. (2010) Nicotinamide prevents ultraviolet radiation-induced cellular energy loss. *Photochemistry and Photobiology*. [Online] 86 (4), 942–948. Available at: doi:10.1111/J.1751-1097.2010.00746.X

Park, S.W., Zhen, G., Verhaeghe, C., Nakagami, Y., et al. (2009) The protein disulfide isomerase AGR2 is essential for production of intestinal mucus. *Proceedings of the National Academy of Sciences of the United States of America*. [Online] 106 (17), 6950–6955. Available at: doi:10.1073/PNAS.0808722106/SUPPL_FILE/0808722106SI.PDF

Parodi, A.J. (2003) Protein Glucosylation and Its Role in Protein Folding. *http://dx.doi.org/10.1146/annurev.biochem.69.1.69*. [Online] 6969–93. Available at: doi:10.1146/ANNUREV.BIOCHEM.69.1.69

Patel, K.K., Miyoshi, H., Beatty, W.L., Head, R.D., et al. (2013) Autophagy proteins control goblet cell function by potentiating reactive oxygen species production. *The EMBO Journal*. [Online] 32 (24), 3130. Available at: doi:10.1038/EMBOJ.2013.233

Patel, P., Clarke, C., Barraclough, D.L., Jowitt, T.A., et al. (2013b) Metastasis-Promoting Anterior Gradient 2 Protein Has a Dimeric Thioredoxin Fold Structure and a Role in Cell Adhesion. *Journal of Molecular Biology*. [Online] 425 (5), 929–943. Available at: doi:10.1016/J.JMB.2012.12.009

Pérez-Sala, D., Oeste, C.L., Martínez, A.E., Carrasco, M.J., et al. (2015) Vimentin filament organization and stress sensing depend on its single cysteine residue and zinc binding. *Nature Communications 2015 6:1*. [Online] 6 (1), 1–17. Available at: doi:10.1038/ncomms8287

Peter, M., Nakagawa, J., Dorée, M., Labbé, J.C., et al. (1990) In vitro disassembly of the nuclear lamina and M phase-specific phosphorylation of lamins by cdc2 kinase. *Cell*. [Online] 61 (4), 591–602. Available at: doi:10.1016/0092-8674(90)90471-P

Petersen, C.M., Nielsent, M.S., Nykjaer, A., Jacobsen, L., et al. (1997) Molecular Identification of a Novel Candidate Sorting Receptor Purified from Human Brain by Receptor-associated Protein Affinity Chromatography. *Journal of Biological Chemistry*. [Online] 272 (6), 3599–3605. Available at: doi:10.1074/JBC.272.6.3599

Petersen, T.N., Brunak, S., von Heijne, G. and Nielsen, H. (2011) SignalP 4.0: discriminating signal peptides from transmembrane regions. *Nature Methods 2011 8:10*. [Online] 8 (10), 785–786. Available at: doi:10.1038/nmeth.1701

Pias, E.K., Ekshyyan, O.Y., Rhoads, C.A., Fuseler, J., et al. (2003) Differential Effects of Superoxide Dismutase Isoform Expression on Hydroperoxide-induced Apoptosis in PC-12 Cells. *Journal of Biological Chemistry*. [Online] 278 (15), 13294–13301. Available at: doi:10.1074/JBC.M208670200

Pierce, G.F., Mustoe, T.A., Altrock, B.W., Deuel, T.F., et al. (1991b) Role of platelet-derived growth factor in wound healing. *Journal of Cellular Biochemistry*. [Online] 45 (4), 319–326. Available at: doi:10.1002/JCB.240450403

Pohler, E., Craig, A.L., Cotton, J., Lawrie, L., et al. (2004) The Barrett's Antigen Anterior Gradient-2 Silences the p53 Transcriptional Response to DNA Damage *. *Molecular & Cellular Proteomics*. [Online] 3 (6), 534–547. Available at: doi:10.1074/MCP.M300089-MCP200

Pollard, M.G., Travers, K.J. and Weissman, J.S. (1998) Ero1p: A Novel and Ubiquitous Protein with an Essential Role in Oxidative Protein Folding in the Endoplasmic Reticulum. *Molecular Cell*. [Online] 1 (2), 171–182. Available at: doi:10.1016/S1097-2765(00)80018-0

Porchet, N., Pigny, P., Buisine, M.P., Debailleul, V., et al. (1995) Human mucin genes: genomic organization and expression of MUC4, MUC5AC and MUC5B. *Biochemical Society Transactions*. [Online] 23 (4), 800–805. Available at: doi:10.1042/BST0230800

Puig, A. and Gilbert, H.F. (1994) Anti-chaperone behavior of BiP during the protein disulfide isomerase-catalyzed refolding of reduced denatured lysozyme. *Journal of Biological Chemistry*. [Online] 269 (41), 25889–25896. Available at: doi:10.1016/S0021-9258(18)47329-2

Quan, T., He, T., Voorhees, J.J. and Fisher, G.J. (2001) Ultraviolet Irradiation Blocks Cellular Responses to Transforming Growth Factor-β by Down-regulating Its Type-II Receptor and Inducing Smad7. *Journal of Biological Chemistry*. [Online] 276 (28), 26349–26356. Available at: doi:10.1074/JBC.M010835200

Rabinovich, E., Kerem, A., Fröhlich, K.-U., Diamant, N., et al. (2002) AAA-ATPase p97/Cdc48p, a Cytosolic Chaperone Required for Endoplasmic Reticulum-Associated Protein Degradation. *Molecular and Cellular Biology*. [Online] 22 (2), 626. Available at: doi:10.1128/MCB.22.2.626-634.2002

Rajasekaran, N.S., Connell, P., Christians, E.S., Yan, L.J., et al. (2007) Human αB-Crystallin Mutation Causes Oxido-Reductive Stress and Protein Aggregation Cardiomyopathy in Mice. *Cell*. [Online] 130 (3), 427–439. Available at: doi:10.1016/J.CELL.2007.06.044

Rand, J.D. and Grant, C.M. (2006) The Thioredoxin System Protects Ribosomes against Stress-induced Aggregation. *Molecular Biology of the Cell*. [Online] 17 (1), 387. Available at: doi:10.1091/MBC.E05-06-0520

Rappu, P., Salo, A.M., Myllyharju, J. and Heino, J. (2019) Role of prolyl hydroxylation in the molecular interactions of collagens. *Essays in Biochemistry*. [Online] 63 (3), 325. Available at: doi:10.1042/EBC20180053

Rauch, F., Fahiminiya, S., Majewski, J., Carrot-Zhang, J., et al. (2015) Cole-Carpenter Syndrome Is Caused by a Heterozygous Missense Mutation in P4HB. *American Journal of Human Genetics*. [Online] 96 (3), 425. Available at: doi:10.1016/J.AJHG.2014.12.027

Reddy, S. and Comai, L. (2012) Lamin A, farnesylation and aging. *Experimental cell research*. [Online] 318 (1), 1. Available at: doi:10.1016/J.YEXCR.2011.08.009

Reigstad, L.J., Varhaug, J.E. and Lillehaug, J.R. (2005) Structural and functional specificities of PDGF-C and PDGF-D, the novel members of the platelet-derived growth factors family. *The FEBS Journal*. [Online] 272 (22), 5723–5741. Available at: doi:10.1111/J.1742-4658.2005.04989.X

Riedl, J., Crevenna, A.H., Kessenbrock, K., Yu, J.H., et al. (2008) Lifeact: a versatile marker to visualize F-actin. *Nature methods*. [Online] 5 (7), 605. Available at: doi:10.1038/NMETH.1220

Rivera-Monroy, J., Musiol, L., Unthan-Fechner, K., Farkas, Á., et al. (2016) Mice lacking WRB reveal differential biogenesis requirements of tail-anchored proteins in vivo. *Scientific Reports*. [Online] 6. Available at: doi:10.1038/SREP39464

Robinson, M. (2004) Review article: the pharmacodynamics and pharmacokinetics of proton pump inhibitors – overview and clinical implications. *Alimentary Pharmacology & Therapeutics*. [Online] 20 (6), 1–10. Available at: doi:10.1111/J.1365-2036.2004.02160.X

Rockett, J.C., Larkin, K., Darnton, S.J., Morris, A.G., et al. (1997) Five newly established oesophageal carcinoma cell lines: phenotypic and immunological characterization. *British Journal of Cancer*. [Online] 75 (2), 258. Available at: doi:10.1038/BJC.1997.42

Rodríguez-Piñeiro, A.M., van der Post, S., Johansson, M.E.V., Thomsson, K.A., et al. (2012) Proteomic Study of the Mucin Granulae in an Intestinal Goblet Cell Model. *Journal of Proteome Research*. [Online] 11 (3), 1879. Available at: doi:10.1021/PR2010988

Rohner, N., Jarosz, D.F., Kowalko, J.E., Yoshizawa, M., et al. (2013) Cryptic variation in morphological evolution: HSP90 as a capacitor for loss of eyes in cavefish. *Science*. [Online] 342 (6164), 1372–1375. Available at: doi:10.1126/SCIENCE.1240276/SUPPL_FILE/ROHNER-SM.PDF

Ron, D. and Walter, P. (2007) Signal integration in the endoplasmic reticulum unfolded protein response. *Nature Reviews Molecular Cell Biology 2007 8:7*. [Online] 8 (7), 519–529. Available at: doi:10.1038/nrm2199

Rooman, M., Dehouck, Y., Kwasigroch, J.M., Biot, C., et al. (2012) What is Paradoxical about Levinthal Paradox? *http://dx.doi.org/10.1080/07391102.2002.10506850*. [Online] 20 (3), 327–329. Available at: doi:10.1080/07391102.2002.10506850

Rose, M.C. and Voynow, J.A. (2006) Respiratory tract mucin genes and mucin glycoproteins in health and disease. *Physiological Reviews*. [Online] 86 (1), 245–278. Available at: doi:10.1152/PHYSREV.00010.2005/ASSET/IMAGES/LARGE/Z9J0010623871006.JPEG

Rosenberger, G., Koh, C.C., Guo, T., Röst, H.L., et al. (2014) A repository of assays to quantify 10,000 human proteins by SWATH-MS. *Scientific Data 2014 1:1*. [Online] 1 (1), 1–15. Available at: doi:10.1038/sdata.2014.31

Ross, R., Glomset, J., Kariya, B. and Harker, L. (1974) A Platelet-Dependent Serum Factor That Stimulates the Proliferation of Arterial Smooth Muscle Cells In Vitro. *Proceedings of the National Academy of Sciences of the United States of America*. [Online] 71 (4), 1207. Available at: doi:10.1073/PNAS.71.4.1207

Rovito, H.A. and Oblong, J.E. (2013) Nicotinamide preferentially protects glycolysis in dermal fibroblasts under oxidative stress conditions. *British Journal of Dermatology*. [Online] 169 (SUPPL.2), 15–24. Available at: doi:10.1111/BJD.12365

Roy, M.G., Livraghi-Butrico, A., Fletcher, A.A., McElwee, M.M., et al. (2014) Muc5b Is Required for Airway Defense. *Nature*. [Online] 505 (7483), 412. Available at: doi:10.1038/NATURE12807

Russell, R., Karzai, A.W., Mehl, A.F. and McMacken, R. (1999) DnaJ dramatically stimulates ATP hydrolysis by DnaK: Insight into targeting of Hsp70 proteins to polypeptide substrates. *Biochemistry*. [Online] 38 (13), 4165–4176. Available at: doi:10.1021/BI9824036/ASSET/IMAGES/LARGE/BI9824036F00006.JPEG

Ryu, J., Park, S.G., Lee, P.Y., Cho, S., et al. (2013) Dimerization of pro-oncogenic protein Anterior Gradient 2 is required for the interaction with BiP/GRP78. *Biochemical and Biophysical Research Communications*. [Online] 430 (2), 610–615. Available at: doi:10.1016/J.BBRC.2012.11.105

Salmans, M.L., Zhao, F. and Andersen, B. (2013) The estrogen-regulated anterior gradient 2 (AGR2) protein in breast cancer: a potential drug target and biomarker. *Breast Cancer Research : BCR*. [Online] 15 (2), 204. Available at: doi:10.1186/BCR3408

Saraogi, I. and Shan, S. ou (2011) Molecular Mechanism of Co-translational Protein Targeting by the Signal Recognition Particle. *Traffic*. [Online] 12 (5), 535–542. Available at: doi:10.1111/J.1600-0854.2011.01171.X

Schafer, I.A., Pandy, M., Ferguson, R. and Davis, B.R. (1985) Comparative observation of fibroblasts derived from the papillary and reticular dermis of infants and adults: Growth kinetics, packing density at confluence and surface morphology. *Mechanisms of Ageing and Development*. [Online] 31 (3), 275–293. Available at: doi:10.1016/0047-6374(85)90095-8

Shaner, N.C., Lambert, G.G., Chammas, A., Ni, Y., et al. (2013) A bright monomeric green fluorescent protein derived from Branchiostoma lanceolatum. *Nature methods*. [Online] 10 (5), 407. Available at: doi:10.1038/NMETH.2413

Simon, D.N. and Wilson, K.L. (2013) Partners and post-translational modifications of nuclear lamins. *Chromosoma*. [Online] 122 (0), 13. Available at: doi:10.1007/S00412-013-0399-8

Simpson, R.J. (2006) Fragmentation of Protein Using Trypsin. *Cold Spring Harbor Protocols*. [Online] 2006 (5), pdb.prot4550. Available at: doi:10.1101/PDB.PROT4550

Singh, R. and Whitesides, G.M. (1990) Comparisons of rate constants for thiolate-disulfide interchange in water and in polar aprotic solvents using dynamic proton NMR line shape analysis. *Journal of the American Chemical Society*. [Online] 112 (3), 1190–1197. Available at: doi:10.1021/JA00159A046

Singh, R. and Whitesides, G.M. (1993) *The Chemistry of Sulfur-Containing Functional Groups*. London, J. Wiley and Sons, Ltd.

Smith, L.T., Holbrook, K.A. and Madri, J.A. (1986) Collagen types I, III, and V in human embryonic and fetal skin. *The American journal of anatomy*. [Online] 175 (4), 507–521. Available at: doi:10.1002/AJA.1001750409

Soriano, P. (1994) Abnormal kidney development and hematological disorders in PDGF beta-receptor mutant mice. *Genes & development*. [Online] 8 (16), 1888–1896. Available at: doi:10.1101/GAD.8.16.1888

Soriano, P. (1997) The PDGF alpha receptor is required for neural crest cell development and for normal patterning of the somites. *Development*. [Online] 124 (14), 2691–2700. Available at: doi:10.1242/DEV.124.14.2691

Sorrell, J.M. and Caplan, A.I. (2004) Fibroblast heterogeneity: more than skin deep. *Journal of Cell Science*. [Online] 117 (5), 667–675. Available at: doi:10.1242/JCS.01005

Sousa, M.C., Ferrero-Garcia, M.A. and Parodi, A.J. (1992) Recognition of the oligosaccharide and protein moieties of glycoproteins by the UDP-Glc:glycoprotein glucosyltransferase. *Biochemistry*. [Online] 31 (1), 97–105. Available at: doi:10.1021/BI00116A015

Sousa, R. and Lafer, E.M. (2006) Keep the Traffic Moving: Mechanism of the Hsp70 Motor. *Traffic (Copenhagen, Denmark)*. [Online] 7 (12), 1596. Available at: doi:10.1111/J.1600-0854.2006.00497.X

Stankewich, M.C., Tse, W.T., Peters, L.L., Ch'ng, Y., et al. (1998) A widely expressed βIII spectrin associated with Golgi and cytoplasmic vesicles. *Proceedings of the National Academy of Sciences of the United States of America*. [Online] 95 (24), 14158. Available at: doi:10.1073/PNAS.95.24.14158

Sternlicht, M.D. and Werb, Z. (2001) How Matrix Metalloproteinases Regulate Cell Behaviour. *Annual review of cell and developmental biology*. [Online] 17463. Available at: doi:10.1146/ANNUREV.CELLBIO.17.1.463

Stevens, R., Stevens, L. and Price, N. (1983) The stabilities of various thiol compounds used in protein purifications. *Biochemical Education*. [Online] 11 (2), 70–70. Available at: doi:10.1016/0307-4412(83)90048-1

Surjana, D., Halliday, G.M. and Damian, D.L. (2010) Role of Nicotinamide in DNA Damage, Mutagenesis, and DNA Repair. *Journal of Nucleic Acids*. [Online] 201013. Available at: doi:10.4061/2010/157591

Sweeter, J.M., Kudrna, K., Hunt, K., Thomes, P., et al. (2021) Autophagy of mucin granules contributes to resolution of airway mucous metaplasia. *Scientific Reports 2021 11:1*. [Online] 11 (1), 1–19. Available at: doi:10.1038/s41598-021-91932-7

Swift, J., Ivanovska, I.L., Buxboim, A., Harada, T., et al. (2013) Nuclear lamin-A scales with tissue stiffness and enhances matrix-directed differentiation. *Science*. [Online] 341 (6149). Available at: doi:10.1126/SCIENCE.1240104/SUPPL_FILE/SWIFT.SM.PDF

Tan, C.Y.R., Tan, C.L., Chin, T., Morenc, M., et al. (2021) Nicotinamide Prevents UVB- and Oxidative Stress–Induced Photoaging in Human Primary Keratinocytes. *Journal of Investigative Dermatology*. [Online] Available at: doi:10.1016/J.JID.2021.10.021

Tanida-Miyake, E., Koike, M., Uchiyama, Y. and Tanida, I. (2018) Optimization of mNeonGreen for Homo sapiens increases its fluorescent intensity in mammalian cells. *PLOS ONE*. [Online] 13 (1), e0191108. Available at: doi:10.1371/JOURNAL.PONE.0191108

Tavender, T.J., Springate, J.J. and Bulleid, N.J. (2010) Recycling of peroxiredoxin IV provides a novel pathway for disulphide formation in the endoplasmic reticulum. *The EMBO Journal*. [Online] 29 (24), 4185–4197. Available at: doi:10.1038/EMBOJ.2010.273

Taylor, S.C., Thibault, P., Tessier, D.C., Bergeron, J.J.M., et al. (2003) Glycopeptide specificity of the secretory protein folding sensor UDP–glucose glycoprotein:glucosyltransferase. *EMBO Reports*. [Online] 4 (4), 405. Available at: doi:10.1038/SJ.EMBOR.EMBOR797

Thangapazham, R.L., Darling, T.N. and Meyerle, J. (2014) Alteration of Skin Properties with Autologous Dermal Fibroblasts. *International Journal of Molecular Sciences*. [Online] 15 (5), 8407. Available at: doi:10.3390/IJMS15058407

Thornton, D.J. and Sheehan, J.K. (2004) From mucins to mucus: toward a more coherent understanding of this essential barrier. *Proceedings of the American Thoracic Society*. [Online] 1 (1), 54–61. Available at: doi:10.1513/PATS.2306016

Tian, G., Xiang, S., Noiva, R., Lennarz, W.J., et al. (2006) The Crystal Structure of Yeast Protein Disulfide Isomerase Suggests Cooperativity between Its Active Sites. *Cell*. [Online] 124 (1), 61–73. Available at: doi:10.1016/J.CELL.2005.10.044

Torvaldson, E., Kochin, V. and Eriksson, J.E. (2015) Phosphorylation of lamins determine their structural properties and signaling functions. *Nucleus*. [Online] 6 (3), 166. Available at: doi:10.1080/19491034.2015.1017167

Tsaytler, P., Harding, H.P., Ron, D. and Bertolotti, A. (2011) Selective inhibition of a regulatory subunit of protein phosphatase 1 restores proteostasis. *Science*. [Online] 332 (6025), 91–94. Available at: doi:10.1126/SCIENCE.1201396/SUPPL_FILE/TSAYTLER.SOM.PDF

Tsunoda, S., Avezov, E., Zyryanova, A., Konno, T., et al. (2014) Intact protein folding in the glutathione-depleted endoplasmic reticulum implicates alternative protein thiol reductants. *eLife*. [Online] 3. Available at: doi:10.7554/ELIFE.03421

Tu, B.P. and Weissman, J.S. (2002) The FAD- and O2-Dependent Reaction Cycle of Ero1-Mediated Oxidative Protein Folding in the Endoplasmic Reticulum. *Molecular Cell*. [Online] 10 (5), 983–994. Available at: doi:10.1016/S1097-2765(02)00696-2

Ushioda, R., Hoseki, J., Araki, K., Jansen, G., et al. (2008) ERdj5 is required as a disulfide reductase for degradation of misfolded proteins in the ER. *Science*. [Online] 321 (5888), 569–572. Available at: doi:10.1126/SCIENCE.1159293/SUPPL_FILE/USHIODA.SOM.PDF

Varani, J., Dame, M.K., Rittie, L., Fligiel, S.E.G., et al. (2006) Decreased Collagen Production in Chronologically Aged Skin : Roles of Age-Dependent Alteration in Fibroblast Function and Defective Mechanical Stimulation. *The American Journal of Pathology*. [Online] 168 (6), 1861. Available at: doi:10.2353/AJPATH.2006.051302

Varani, J., Warner, R.L., Gharaee-Kermani, M., Phan, S.H., et al. (2000) Vitamin A Antagonizes Decreased Cell Growth and Elevated Collagen-Degrading Matrix Metalloproteinases and Stimulates Collagen Accumulation in Naturally Aged Human Skin1. *Journal of Investigative Dermatology*. [Online] 114 (3), 480–486. Available at: doi:10.1046/J.1523-1747.2000.00902.X

Venetianer, P. and Straub, F.B. (1963) The enzymic reactivation of reduced ribonuclease. *Biochimica et biophysica acta*. [Online] 67 (C), 166–168. Available at: doi:10.1016/0006-3002(63)91812-2

Verrecchia, F., Tacheau, C., Schorpp-Kistner, M., Angel, P., et al. (2001) Induction of the AP-1 members c-Jun and JunB by TGF-β/Smad suppresses early Smad-driven gene activation. *Oncogene 2001 20:18*. [Online] 20 (18), 2205–2211. Available at: doi:10.1038/sj.onc.1204347

Vistejnova, L., Safrankova, B., Nesporova, K., Slavkovsky, R., et al. (2014) Low molecular weight hyaluronan mediated CD44 dependent induction of IL-6 and chemokines in human dermal fibroblasts potentiates innate immune response. *Cytokine*. [Online] 70 (2), 97–103. Available at: doi:10.1016/J.CYTO.2014.07.006

Vitt, U.A., Hsu, S.Y. and Hsueh, A.J.W. (2001) Evolution and Classification of Cystine Knot-Containing Hormones and Related Extracellular Signaling Molecules. *Molecular Endocrinology*. [Online] 15 (5), 681–694. Available at: doi:10.1210/MEND.15.5.0639

Vuori, K., Pihlajaniemi, T., Marttila, M. and Kivirikko, K.I. (1992) Characterization of the human prolyl 4-hydroxylase tetramer and its multifunctional protein disulfide-isomerase subunit synthesized in a baculovirus expression system. *Proceedings of the National Academy of Sciences of the United States of America*. [Online] 89 (16), 7467–7470. Available at: doi:10.1073/PNAS.89.16.7467

Vuori, K., Pihlajaniemi, T., Myllyla, R. and Kivirikko, K.I. (1992) Site-directed mutagenesis of human protein disulphide isomerase: effect on the assembly, activity and endoplasmic reticulum retention of human prolyl 4-hydroxylase in Spodoptera frugiperda insect cells. *The EMBO Journal*. [Online] 11 (11), 4213–4217. Available at: doi:10.1002/J.1460-2075.1992.TB05515.X

Walch, A.K., Zitzelsberger, H.F., Bink, K., Hutzler, P., et al. (2000) Molecular Genetic Changes in Metastatic Primary Barrett's Adenocarcinoma and Related Lymph Node Metastases: Comparison with Nonmetastatic Barrett's Adenocarcinoma. *Modern Pathology 2000 13:7*. [Online] 13 (7), 814–824. Available at: doi:10.1038/modpathol.3880143

Walker, J.M. (2002) Protein Protocols Handbook, The. *Protein Protocols Handbook, The*. [Online] Available at: doi:10.1385/1592591698

Waller, J.M. and Maibach, H.I. (2005) Age and skin structure and function, a quantitative approach (I): blood flow, pH, thickness, and ultrasound echogenicity. *Skin Research and Technology*. [Online] 11 (4), 221–235. Available at: doi:10.1111/J.0909-725X.2005.00151.X

Walter, P. and Blobel, G. (1982) Signal recognition particle contains a 7S RNA essential for protein translocation across the endoplasmic reticulum. *Nature 1982 299:5885*. [Online] 299 (5885), 691–698. Available at: doi:10.1038/299691a0

Walter, P. and Ron, D. (2011) The unfolded protein response: From stress pathway to homeostatic regulation. *Science*. [Online] 334 (6059), 1081–1086. Available at: doi:10.1126/SCIENCE.1209038/ASSET/238BD530-CE66-4C19-BA32-FC13641E3646/ASSETS/GRAPHIC/334_1081_F3.JPEG

Wang, C., Chen, S., Wang, X., Wang, L., et al. (2010) Plasticity of Human Protein Disulfide Isomerase: EVIDENCE FOR MOBILITY AROUND THE X-LINKER REGION AND ITS FUNCTIONAL SIGNIFICANCE. *Journal of Biological Chemistry*. [Online] 285 (35), 26788–26797. Available at: doi:10.1074/JBC.M110.107839

Wang, C., Li, W., Ren, J., Fang, J., et al. (2013) Structural Insights into the Redox-Regulated Dynamic Conformations of Human Protein Disulfide Isomerase. *https://home.liebertpub.com/ars*. [Online] 19 (1), 44–53. Available at: doi:10.1089/ARS.2012.4630

Wang, Z., Hao, Y. and Lowe, A.W. (2008) The Adenocarcinoma-Associated Antigen, AGR2, Promotes Tumor Growth, Cell Migration, and Cellular Transformation. *Cancer Research*. [Online] 68 (2), 492–497. Available at: doi:10.1158/0008-5472.CAN-07-2930

Warren, R., Gartstein, V., Kligman, A.M., Montagna, W., et al. (1991) Age, sunlight, and facial skin: A histologic and quantitative study. *Journal of the American Academy of Dermatology*. [Online] 25 (5), 751–760. Available at: doi:10.1016/S0190-9622(08)80964-4

Wessels, Q., Pretorius, E., Smith, C.M. and Nel, H. (2014) The potential of a niacinamide dominated cosmeceutical formulation on fibroblast activity and wound healing in vitro. *International Wound Journal*. [Online] 11 (2), 152. Available at: doi:10.1111/J.1742-481X.2012.01052.X

Westrate, L.M., Lee, J.E., Prinz, W.A. and Voeltz, G.K. (2015) Form Follows Function: The Importance of Endoplasmic Reticulum Shape. *http://dx.doi.org/10.1146/annurev-biochem-072711-163501*. [Online] 84791–811. Available at: doi:10.1146/ANNUREV-BIOCHEM-072711-163501

Whitesell, L. and Lindquist, S.L. (2005) HSP90 and the chaperoning of cancer. *Nature Reviews Cancer 2005 5:10*. [Online] 5 (10), 761–772. Available at: doi:10.1038/nrc1716

Wilson, R., Lees, J.F. and Bulleid, N.J. (1998) Protein disulfide isomerase acts as a molecular chaperone during the assembly of procollagen. *The Journal of biological chemistry*. [Online] 273 (16), 9637–9643. Available at: doi:10.1074/JBC.273.16.9637

Wingfield, P.T. (2001) Use of Protein Folding Reagents. *Current protocols in protein science / editorial board, John E. Coligan ... [et al.]*. [Online] APPENDIX 3 (1), Appendix. Available at: doi:10.1002/0471140864.PSA03AS00

Woodley, D.T. (2017) Distinct Fibroblasts in the Papillary and Reticular Dermis: Implications for Wound Healing. *Dermatologic Clinics*. [Online] 35 (1), 95–100. Available at: doi:10.1016/J.DET.2016.07.004

Worfolk, J.C., Bell, S., Simpson, L.D., Carne, N.A., et al. (2019) Elucidation of the AGR2 Interactome in Esophageal Adenocarcinoma Cells Identifies a Redox-Sensitive Chaperone Hub for the Quality Control of MUC-5AC. *Antioxidants & Redox Signaling*. [Online] 1–47. Available at: doi:10.1089/ars.2018.7647.

Worman, H.J., Fong, L.G., Muchir, A. and Young, S.G. (2009) Laminopathies and the long strange trip from basic cell biology to therapy. *The Journal of Clinical Investigation*. [Online] 119 (7), 1825. Available at: doi:10.1172/JCI37679

Wu, S., Liu, X., Cheng, L., Wang, D., et al. (2022) Protective Mechanism of Leucine and Isoleucine against H2O2-Induced Oxidative Damage in Bovine Mammary Epithelial Cells. *Oxidative Medicine and Cellular Longevity*. [Online] 2022. Available at: doi:10.1155/2022/4013575

Xiao, W., Duan, X., Lin, Y., Cao, Q., et al. (2018) Distinct Proteome Remodeling of Industrial Saccharomyces cerevisiae in Response to Prolonged Thermal Stress or Transient Heat Shock. *Journal of Proteome Research*. [Online] 17 (5), 1812–1825. Available at: doi:10.1021/ACS.JPROTEOME.7B00842/ASSET/IMAGES/LARGE/PR-2017-008427_0005.JPEG

Xu, S., Butkevich, A.N., Yamada, R., Zhou, Y., et al. (2012) Discovery of an orally active small-molecule irreversible inhibitor of protein disulfide isomerase for ovarian cancer treatment. *Proceedings of the National Academy of Sciences of the United States of America*. [Online] 109 (40), 16348–16353. Available at: doi:10.1073/PNAS.1205226109/-/DCSUPPLEMENTAL

Ye, J., Rawson, R.B., Komuro, R., Chen, X., et al. (2000) ER Stress Induces Cleavage of Membrane-Bound ATF6 by the Same Proteases that Process SREBPs. *Molecular Cell*. [Online] 6 (6), 1355–1364. Available at: doi:10.1016/S1097-2765(00)00133-7

Yoshida, H., Matsui, T., Yamamoto, A., Okada, T., et al. (2001) XBP1 mRNA Is Induced by ATF6 and Spliced by IRE1 in Response to ER Stress to Produce a Highly Active Transcription Factor. *Cell*. [Online] 107 (7), 881–891. Available at: doi:10.1016/S0092-8674(01)00611-0

Yoshimori, T., Semba, T., Takemoto, H., Akagi, S., et al. (1990) Protein disulfide-isomerase in rat exocrine pancreatic cells is exported from the endoplasmic reticulum despite possessing the retention signal. *Journal of Biological Chemistry*. [Online] 265 (26), 15984–15990. Available at: doi:10.1016/S0021-9258(18)55494-6

Zhang, Y., Li, T., Zhang, L., Shangguan, F., et al. (2019) Targeting the functional interplay between endoplasmic reticulum oxidoreductin-1α and protein disulfide isomerase suppresses the progression of cervical cancer. *EBioMedicine*. [Online] 41408. Available at: doi:10.1016/J.EBIOM.2019.02.041

Zhao, R. and Houry, W.A. (2011) Hsp90: a chaperone for protein folding and gene regulation. *https://doi.org/10.1139/o05-158*. [Online] 83 (6), 703–710. Available at: doi:10.1139/O05-158

Zhen, A.X., Piao, M.J., Kang, K.A., Fernando, P.D.S.M., et al. (2019) Niacinamide Protects Skin Cells from Oxidative Stress Induced by Particulate Matter. *Biomolecules & Therapeutics*. [Online] 27 (6), 562. Available at: doi:10.4062/BIOMOLTHER.2019.061

Zito, E., Melo, E.P., Yang, Y., Wahlander, Å., et al. (2010) Oxidative Protein Folding by an Endoplasmic Reticulum-Localized Peroxiredoxin. *Molecular Cell*. [Online] 40 (5), 787–797. Available at: doi:10.1016/J.MOLCEL.2010.11.010

Zünkler, B.J., Wos-Maganga, M. and Panten, U. (2004) Fluorescence microscopy studies with a fluorescent glibenclamide derivative, a high-affinity blocker of pancreatic β-cell ATP-sensitive K+ currents. *Biochemical Pharmacology*. [Online] 67 (8), 1437–1444. Available at: doi:10.1016/J.BCP.2003.12.011

9 R scripts

9.1 P-value adjustment

```
#set working directory to local folder
setwd("~/Documents/PhD/Year 3/R")

#Have R read your data file, must be saved as a .csv
p.values <- read.csv("111219 BJF 1mM H2O2 6h vs 24h 500um niacinamide and
1mM H2O2 6h SWATH comparison.csv")

#This tells R to add a new column which has your new p adjusted data.
p.values can be changed to whatever the name of your column containing
your P values is called.
p.values$p.adjusted <- (p.adjust(p.values$p, method = "fdr"))

#Creates a new file with the adjusted p values in
write.csv(p.values, "111219 BJF 1mM H2O2 6h vs 24h 500um niacinamide and
1mM H2O2 6h SWATH comparison adjusted.csv")
```

9.2 GO analysis

```
#set working directory to local folder
setwd("~/Documents/PhD/Year 4/Data/Proteomics/R")
library(clusterProfiler)
library(org.Hs.eg.db)
library(ggplot2)

#import data from excel and create a character vector
GenenameNTDTBA <- read.csv("020621 100um DTBA HT1080 Ov NT vs Ov DTBA
adjusted 2 fold change and P<0.05 entrezID.csv")
GenenameNTDTBA$EntrezID <- as.character(GenenameNTDTBA$EntrezID)
Genes <- c(GenenameNTDTBA$EntrezID)

#converts IDs from entrezid to GO terms BP = biological process MF =
molecular function CC = cellular compartment
GenesGOBP <-groupGO(Genes, OrgDb = "org.Hs.eg.db", ont = "BP", level =
2,readable = FALSE)
barplot(GenesGOBP, drop=TRUE, showCategory=12)
GenesGOMF <-groupGO(Genes, OrgDb = "org.Hs.eg.db", ont = "MF", level =
2,readable = FALSE)
barplot(GenesGOMF, drop=TRUE, showCategory=12)
GenesGOCC <-groupGO(Genes, OrgDb = "org.Hs.eg.db", ont = "CC", level =
2,readable = FALSE)
barplot(GenesGOCC, drop=TRUE, showCategory=12)

#plot GO term graph
ggplot(GenesGOBP@result,
       aes(x = Count,
           y = Description)) +
  geom_bar(stat="identity") +          # basic bar chart
  ylab("Description") +
  xlab("Count") +
```

```
  ggtitle("Ov NT vs Ov 100 µm DTBA Biological Processes") +
  theme_bw()
```

9.3 Volcano plots

```
#set working directory to local folder
setwd("~/Documents/PhD/Year 4/Data/Proteomics/R")
library(org.Hs.eg.db)
library(clusterProfiler)
library(dplyr)
library(ggplot2)
library(ggrepel)

#read .csv file and import it
NTDTBA <- read.csv("020621 100um DTBA HT1080 1h NT vs 1h DTBA
adjusted.csv")

#add csv which is just key Transport proteins to label the graph with
NTDTBA2FS <- read.csv("020621 100um DTBA HT1080 1h NT vs 1h DTBA adjusted
2 fold change and P<0.05.csv")

#adjust columns in the .csv file
NTDTBA$p.adjusted = as.numeric(as.character(NTDTBA$p.adjusted))
NTDTBA$logp.adjusted = -log10(NTDTBA$p.adjusted)
NTDTBAsub <- subset(NTDTBA, NTDTBA$p.adjusted<0.05 &
(NTDTBA$Log.Fold.Change>0.3|NTDTBA$Log.Fold.Change<(-0.3)))

#adjust columns in the .csv file
NTDTBA2FS$p.adjusted = as.numeric(as.character(NTDTBA2FS$p.adjusted))
NTDTBA2FS$logp.adjusted = -log10(NTDTBA2FS$p.adjusted)

#Make a new table with significant column
NTDTBAlogs = mutate(NTDTBA, sig=ifelse(NTDTBA$logp.adjusted>1.3 &
(NTDTBA$Log.Fold.Change>0.3|NTDTBA$Log.Fold.Change<(-0.3)), "P<0.05 and
Fold Change>2", "Not Significant"))

#plot and display volcano plot
vNTDTBA = ggplot(NTDTBAlogs,
aes(Log.Fold.Change, (logp.adjusted))) +
  geom_point(aes(col=sig), size=2) +
  scale_color_manual(values=c("grey", "black")) +
  theme_classic() +
  xlab("Log(10) Fold Change") +
  ylab("-log(10) Adjusted p-value") +
  ggtitle("100 µm 1 h DTBA to 1 h Untreated Comparison")+
  theme(plot.title = element_text(hjust = 0.5))+
  theme(legend.title = element_blank())+
  theme(text = element_text(size=20)) +
  theme(axis.line = element_line(size=1.25)) +
  theme(plot.margin=unit(c(0.5,0.5,1,0.5),"cm")) +
  theme(legend.justification = c(1,1), legend.position = c(1,0.75)) +
  xlim(-1,1.5) +
  geom_text_repel(data = NTDTBA2FS, aes(label = Gene.Name), nudge_y = 0.1,
```

```
hjust = 1, size = 7, min.segment.length = 0, fontface = "plain")
```

9.4 Heatmaps

```
#set working directory to local folder
setwd("~/Documents/PhD/Year 4/Data/Proteomics/R")
library(ggplot2)
library(reshape2)

#import data from excel and create vectors
NTvsDTBA1h <- read.csv("020621 100um DTBA HT1080 1h NT vs 1h DTBA adjusted
2 fold change and P<0.05 gene name.csv")
names(NTvsDTBA1h)[1:2] <- c("Fold.Change", "test")
heatmapNTvsDTBA1h <- melt(NTvsDTBA1h, id.vars = "test")

#plot heatmap
ggplot(heatmapNTvsDTBA1h, aes(x=variable, y=reorder(test, value, median, o
rder=TRUE))) +
  geom_tile(aes(fill = value), color = "white") +
  scale_fill_gradient(low = "white", high = "#7E317B", na.value = "black")
+
  ylab("Peak Name") +
  xlab("Comparison") +
  theme(legend.title = element_text(size = 10),
        legend.text = element_text(size = 12),
        plot.title = element_text(size=16),
        axis.title=element_text(size=14,face="bold"),
        axis.text.x = element_text(angle = 90, hjust = 1)) +
  labs(fill = "Fold Change") + theme_minimal() +
  theme(panel.grid.major = element_blank(), panel.grid.minor = element_bla
nk()) +
  scale_x_discrete(expand = c(0, 0)) + scale_y_discrete(expand = c(0, 0))
+
  theme(axis.ticks = element_blank())
```

9.5 Venn diagrams

```
#set working directory to local folder
setwd("~/Documents/PhD/Year 4/Data/Proteomics/R")
library(org.Hs.eg.db)
library(clusterProfiler)
library(dplyr)
library(ggplot2)
library(ggrepel)
library(VennDiagram)

#import data from excel
NT <- read.csv("260121 HT1080 NT PDI IP.csv")
F16 <- read.csv("260121 HT1080 10um 16F16 2h PDI IP.csv")

#create overlaps and unique
overlap <- intersect(NT$Peak.Name, F16$Peak.Name)
NT.unique <- setdiff(NT$Peak.Name, F16$Peak.Name)
F16.unique <- setdiff(F16$Peak.Name, NT$Peak.Name)
```

```
full.list <- unique(c(NT$Peak.Name, F16$Peak.Name))

#plot venn diagram
grid.newpage()
venn.plot <- draw.pairwise.venn(area1 = length(NT$Peak.Name),#no MCP set
                                area2 = length(F16$Peak.Name),#no JPR set
                                cross.area = length(overlap),
                                expression("NT", "16F16"), scaled = TRUE,
                                fill = c("green", "blue"),
                                cex = 1.5,
                                cat.cex = 1.5,
```

10 Supplementary figures

Table 10.1 Major proteins that interact with mNG col1α identified by MS in HT1080 cells repeat 1.

Gene Name	Peptides (95%)	%Cov	GO function
mNeonGreen_Col_1A2	37	33	Collagen fusion protein
EF2	13	15	Translation
FLNA	9	5	Angiogenesis
PDIA1	9	20	Protein folding
PRDX1	7	41	Removal of superoxide radicals
SDHA	7	14	Tricarboxylic acid cycle
GRP78	6	13	Protein folding
LDHA	6	23	Glycolytic process
PDIA6	6	20	Protein folding
P4HA1	6	12	Collagen fibril organisation
ALDOA	5	15	Glycolytic process
TGM2	5	8	Peptide cross-linking
LASP1	5	18	Ion transport
RAN	5	25	Cell division
MIF	5	32	Cell ageing
SPB3	5	13	Autocrine signalling
CH60	4	7	Protein folding
SAHH	4	11	S-adenosylmethionine cycle
PPIA	4	22	Apoptotic process
LEG1	4	33	Apoptotic process
TXND5	4	10	Apoptotic cell clearance
DCD	4	33	Defence response to bacteria
CASPE	4	17	Epidermis development
ATPA	3	7	Ageing
HNRPK	3	6	RNA processing
PRDX2	3	23	Cell redox homeostatsis
6PGD	3	8	D-gluconate catabolic process
CBR1	3	13	Cyclooxygenase pathway
SDHB	3	10	Aerobic respiration
DEST	3	24	Cell motility
IFIT3	3	7	Innate immune response
S10A9	3	25	Autophagy
LEG7	3	29	Apoptotic process
AHNK	2	0	Positive regulation of plasma membrane repair
GRP75	2	3	Protein refolding
TBB5	2	23	Cell division
PLST	2	4	Actin filament network formation
EFTU	2	5	Mitochondrial translational elongation
IF4A1	2	5	Translational initiation
VDAC1	2	8	Apoptotic process
PFKAP	2	3	Canonical glycolysis
TAGL2	2	13	Epithelial cell differentiation
TPM4	2	7	Actin filament organisation
TPM3	2	6	Actin filament organisation
PAIRB	2	6	Regulation of mRNA stability
1433T	2	14	Protein targeting
RS3	2	11	Apoptotic process
CLIC1	2	10	Regulation of cell cycle
NDKB	2	14	Cell adhesion
G6PD	2	4	Cellular response to oxidative stress
PCBP1	2	10	Regulation of gene expression
NDKA	2	14	Cell differentiation
GUAA	2	4	Glutamine metabolic process
RS5	2	9	Translation
EF1B	2	12	Translational elongation
RL40	2	20	Translation
RS27A	2	16	Translation
UBB	2	11	Energy homeostasis
UBC	2	4	Protein ubiquitination
GLRX3	2	8	Cell redox homeostatsis
IF5A1	2	8	Protein transport
TEBP	2	13	Cyclooxygenase pathway
K2C6B	2	46	Ectoderm development
SKP1	2	15	Protein ubiquitination
SC61B	2	26	Ubiquitin-dependent ERAD pathway
IF5AL	2	8	mRNA transport
MT1X	2	33	Response to metal ion
MT2	2	33	Negative regulation of growth
MT1G	2	32	Negative regulation of growth
ARPC3	2	13	Regulation of actin filament polymerisation
K2C6A	2	45	Cell differentiation
ARGI1	2	6	Adaptive immune response
TGM3	2	3	Cell envelope orginisation
CALL5	2	16	Epidermis development
S10A7	2	23	Innate immune response
LYSC	2	14	Cytolysis
HSPB1	2	12	Chaperone-mediated protein folding
S10A8	2	20	Apoptotic process

Table 10.2 Major proteins that interact with mNG col1α identified by MS in HT1080 cells repeat 2.

Gene Name	Peptides (95%)	%Cov	GO function
mNeonGreen_Col_1A2	42	37	Collagen fusion protein
PDIA1	10	22	Protein folding
P4HA1	8	18	Collagen fibril organisation
TGM2	5	8	Peptide cross-linking
1433T	5	21	Protein targeting
S10A9	5	39	Autophagy
G6PD	4	6	Cellular response to oxidative stress
FILA	4	1	Establishment of skin barrier
HNRPK	3	6	RNA processing
IF4A1	3	8	Translational initiation
6PGD	3	8	D-gluconate catabolic process
SDHB	3	10	Aerobic respiration
DEST	3	19	Cell motility
IFIT3	3	7	Innate immune response
ARGI1	3	8	Adaptive immune response
SPB3	3	7	Autocrine signalling
PIP	3	31	Proteolysis
MYH9	2	1	Angiogenesis
GRP75	2	3	Protein refolding
PLST	2	4	Actin filament network formation
TCPH	2	4	Protein folding
CALX	2	3	Protein folding
PFKAP	2	3	Canonical glycolysis
PHB	2	8	Protein stabilisation
RS3	2	11	Apoptotic process
SERPH	2	6	Protein matuation
RS5	2	8	Translation
PSME3	2	7	Apoptotic process
CBR1	2	8	Cyclooxygenase pathway
EF1B	2	10	Translational elongation
CATD	2	4	Proteolysis
VDAC2	2	9	Anion transport
2ABA	2	5	Protein dephosphorylation
GSTM3	2	11	Glutathione metabolic process
CAN2	2	4	Proteolysis
TEBP	2	13	Cyclooxygenase pathway
RS20	2	19	Translation
RL30	2	21	Translation
FABP5	2	15	Glucose homeostatsis
DSC1	2	3	Cell-cel adhesion
HSPB1	2	12	Chaperone-mediated protein folding
S10A8	2	20	Apoptotic process
CYTB	2	21	Negative regulation of proteolysis
PLAK	2	3	Cell migration
GSDMA	2	4	Apoptotic process
TGM1	2	2	Peptide cross-linking

Table 10.3 Major proteins that interact with mNG col1α identified by MS in HT1080 cells repeat 3.

Gene Name	Peptides (95%)	%Cov	GO function
mNeonGreen_Col_1A2	28	26	Collagen fusion protein
PDIA1	6	15	Protein folding
P4HA1	4	10	Collagen fibril organisation
LASP1	2	9	Ion transport
K2C6A	2	39	Cell differentiation
LYSC	2	14	Cytolysis